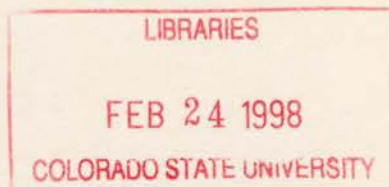


Cloud Chemical Heterogeneity and Its Influence
On Aqueous Sulfur (IV) Oxidation

Xin Rao
Jeffrey L. Collett, Jr.



Research Supported by the University of Illinois Campus Research Board, the Department of the Navy, Office of the Chief of Naval Research, the Midwestern Regional Center of the National Institute for Global Environmental Change, National Science Foundation (ATM-9509596), the U.S. Environmental Protection Agency and the San Joaquin Valleywide Air Pollution Study Agency.

**Colorado
State
University**

**DEPARTMENT OF
ATMOSPHERIC SCIENCE**

PAPER NO. 641

Cloud chemical heterogeneity and its influence
on aqueous sulfur (IV) oxidation

by

Xin Rao
Jeffrey L. Collett, Jr.

Department of Atmospheric Science
Colorado State University
Ft. Collins, Colorado 80523

June, 1997



018401 5990951

QC
852
1C6
no. 644
ATMOS

ABSTRACT

Differences in chemical composition among cloud and fog drops of diverse sizes were investigated at several locations across the United States. Chemical species including acidity, sulfur (IV), hydrogen peroxide, formaldehyde, hydroxymethanesulfonate (HMS) and trace metals iron and manganese were measured. The study examined coastal stratus and stratocumulus clouds in southern California and northern Oregon, frontal and orographic clouds at Mt. Mitchell, North Carolina and Whiteface Mountain, New York, and radiation fogs in California's San Joaquin Valley. Samples were collected with three cloud samplers capable of partitioning the cloud drop size spectrum into two or three independent drop size fractions.

Measurements of pH variations within natural cloud drop populations reveal that small drops are often more acidic than large drops. Differences between small and large cloud drop acidities as large as two pH units were observed, although differences were generally below one pH unit. The chemical heterogeneity can significantly enhance oxidation of sulfur dioxide to sulfate within clouds, relative to oxidation rates predicted from the average cloudwater composition.

Trace metal concentrations were found to vary with drop size in clouds and fogs sampled at a variety of U.S. locations. Significantly higher concentrations of total iron and manganese were found in large drops in clouds sampled at Mt. Mitchell, North Carolina, and along the southern California coast, while small drops were often enriched in concentrations of iron and manganese in fogs sampled in California's San Joaquin Valley and coastal clouds

sampled at Angora Pk., Oregon. Iron speciation measurements in San Joaquin Valley fogs revealed that dissolved iron in small fog drops was present almost entirely as Fe(III). The observed size dependence of trace metal concentrations in cloud and fog drops is expected to influence in-cloud S(IV) oxidation rates as well.

Effects of chemical heterogeneity on overall in-cloud S(IV) oxidation rates will largely depend on contributions of the different oxidation paths. Errors in predicting sulfur oxidation rates based on average cloud drop compositions are smallest when abundant hydrogen peroxide is present, for example in the summer clouds at La Jolla Pk., California and at Mt. Mitchell, North Carolina. About 84 percent of the samples are calculated to experience little enhancement in S(IV) oxidation, due to the dominance of the H_2O_2 path. Approximately 9 percent of the samples are calculated to experience oxidation rate enhancement between 10 and 30%, while 7 percent of the samples are calculated to experience oxidation rate enhancement of 30% or more. Effects of chemical heterogeneity on enhancements in sulfur oxidation rates are likely to be strong when (1) hydrogen peroxide concentrations are low, for example the radiation fog in California's San Joaquin Valley, where the calculated enhancement factors range from 1.10 to 1.65, or (2) the droplet pH is high enough to support rapid S(IV) oxidation by ozone and metal-catalyzed S(IV) autooxidation, for example in relatively pristine environments like Angora Pk., Oregon, where the calculated enhancement factors range from 1.02 to 2.0. We expect real clouds to contain more than two chemically distinct drop populations. A wide distribution of drop compositions can support even faster sulfur oxidation rates.

ACKNOWLEDGMENTS

We would like to express our sincere thanks to Aaron Bator, Belay Demoz, Ralph Iovinelli, Srinivas Devulapalli, Pete Van Rens, Erika Walke, Anne Sautman, David Eli Sherman, Oliver Graf, Betsy Andrews, Gang Xu, and Lynn Raponi for their assistance in conducting the field campaigns and analyzing the samples collected. We are also grateful to Prof. Susan Larson, Prof. Richard Larson and Prof. Zhuangjie Li of the University of Illinois at Urbana who offered constructive recommendations to this work. We are also grateful to the numerous individuals and organizations who provided access to the numerous cloud sampling sites used in this work.

This work benefited from financial support provided by a number of sponsors including the University of Illinois Campus Research Board, the Department of the Navy, Office of the Chief of Naval Research, the Midwestern Regional Center of the National Institute for Global Environmental Change, the National Science Foundation (ATM-9509596), the U.S Environmental Protection Agency and the San Joaquin Valleywide Air Pollution Study Agency.

TABLE OF CONTENTS

1. INTRODUCTION	1
1.1. Sulfur (IV) related chemical reactions in cloudwater	3
1.1.1. S(IV) oxidation by H_2O_2	3
1.1.2. S(IV) oxidation by ozone	5
1.1.3. S(IV) autooxidation catalyzed by iron (III) and manganese (II)	8
1.1.4. S(IV) complexation with formaldehyde	12
1.1.5. In-cloud photochemical reactions involving iron species	14
1.2. Cloud drop size dependent chemical composition and its effect on in-cloud S(IV) oxidation	19
1.3. Research goals and approach	26
2. EXPERIMENTAL METHODS	28
2.1. Cloud/fogwater sampling	28
2.2. Chemical preservation and analyses	34
2.3. Laboratory experiments on photochemical reactions of authentic cloudwater and Fe(III)-oxalate solutions	39
3. RESULTS AND DISCUSSION	42
3.1. Drop size-dependent cloud/fogwater chemical composition	42
3.1.1. Cloud/fogwater pH	42
3.1.2. Sulfur (IV), formaldehyde and their complex, HMS	44
3.1.3. Hydrogen peroxide	48
3.1.4. Iron and manganese	55
3.1.5. Iron speciation	58
3.2. Drop size dependence of S(IV) oxidation	60
3.3. Field observations of S(IV) complexation with formaldehyde and its competition with S(IV) oxidation	70

3.3.1. S(IV) complexation and oxidation	70
3.3.2. Case studies on the relative importance of reactions of S(IV) with H ₂ O ₂ , O ₃ and HCHO	77
3.4. Enhancement of S(IV) oxidation in the chemically heterogeneous clouds	81
3.4.1. Effect of chemical heterogeneity on S(IV) oxidation by H ₂ O ₂	81
3.4.2. Effect of chemical heterogeneity on S(IV) oxidation by O ₃	82
3.4.3. Effect of chemical heterogeneity on S(IV) autooxidation catalyzed by trace metals	83
3.4.4. Enhancement of S(IV) oxidation by the non-uniform distribution of chemical species in cloud and fog drop populations	93
3.5. Case studies of S(IV) oxidation in chemically heterogeneous clouds/fog	98
3.5.1. The radiation fog in California's San Joaquin Valley	98
3.5.1.1. Fogwater chemical heterogeneity and enhancements in S(IV) oxidation rates	98
3.5.1.2. Comparison of enhancements in S(IV) oxidation rates obtained from the two-stage size-fractionating CASCC and the three-stage size-fractionating IESL	104
3.5.1.3. Fogwater acid buffer capacity and its effect on enhancements in sulfate production	115
3.5.2. Coastal stratus clouds at Angora Pk., Oregon	139
3.5.2.1. Cloud water chemical heterogeneity and enhancements in S(IV) oxidation rates ...	139
3.5.2.2. Photochemical reactions in the authentic cloud water and prepared solutions and their influence on S(IV) oxidation	146
4. CONCLUSIONS	158
5. RECOMMENDATIONS FOR FUTURE WORK	163
REFERENCES	168
APPENDICES	182
Appendix A. Sample preservation	182
Appendix B. Analyses of total S(IV) and HMS in cloudwater	190
Appendix C. Analysis of hydroperoxides in cloudwater	199
Appendix D. Analysis of formaldehyde in cloudwater	208

Appendix E. Analyses of Fe(II) and Fe(III) in cloudwater	213
Appendix F. Mass transport consideration for formaldehyde gas-liquid equilibrium	221
Appendix G. Calculation of liquid-water-content weighted average chemical composition	226

LIST OF TABLES

Table 1.1. Rate expressions for Fe(III) catalyzed S(IV) autooxidation	9
Table 1.2. Rate laws determined for manganese (II) catalyzed autooxidation of S(IV) in aqueous solution	10
Table 1.3. Daytime sinks for Fe(II) in atmospheric water drops (pH < 5)	16
Table 1.4. Sinks for HO ₂ /O ₂ ⁻ in atmospheric water drops	17
Table 2.1. Summary of chemical preservation and analyses	35
Table 3.1. Chemical compositions of cloud/fogwater collected by the size fractionating CASCC	46
Table 3.2. Fe(III) and Fe(II) concentrations in the San Joaquin Valley fog droplets	59
Table 3.3. Fe(III) concentrations in filtered and unfiltered fogwater samples	59
Table 3.4. Gaseous SO ₂ and O ₃ concentrations used in the calculations	60
Table 3.5. Thermodynamic data: Henry's law and aqueous-phase equilibrium constants	75
Table 3.6. Kinetic data of S(IV) related reactions	76
Table 3.7. Fractions of S(IV) oxidation through the different paths and enhancement in S(IV) oxidation rate	96
Table 3.8. Contributions of various chemical components to the initial acid buffer intensities at the sample pH	124
Table 3.9. Effects of external and internal buffer on sulfate production over the four hour simulation	137
Table 3.10. Contributions of different S(IV) oxidation pathways in the small and large drops	142
Table 3.11. Contributions of different S(IV) oxidation pathways in chemically homogeneous and heterogeneous clouds	143
Table 3.12. Total S(IV) oxidation rates in the clouds of Angora Pk., Oregon	144
Table 3.13. Influence of the ozone concentration on contributions of the different S(IV) oxidation paths in the chemically heterogeneous cloud	145
Table 3.14. Influence of the catalytically active iron fraction on contributions of the different S(IV) oxidation paths in the chemically heterogeneous clouds	146

Table 4.1. Summary of the size-dependent cloud/fog chemical composition at various locations	159
Table B.1. Analysis precision and accuracy for S(IV) and HMS	196
Table C.1. Analysis precision and accuracy for peroxides	203
Table D.1. Analysis precision and accuracy for formaldehyde	212
Table F.1. Characteristic times for droplet growth, formaldehyde mass transport and chemical reaction	222

LIST OF FIGURES

Figure 2.1. Caltech Active Strand Cloudwater Collector 2	29
Figure 2.2. Caltech Active Strand Cloudwater Collector with a size-fractionating inlet	31
Figure 2.3. ETH cloud impactor	32
Figure 2.4. IESL cloud impactor	33
Figure 3.1. pH values in cloud/fog drops of small and large drop fractions collected at various locations	43
Figure 3.2. Comparison of total S(IV) and HMS concentrations in cloudwater collected by the sf-CASCC at several locations	49
Figure 3.3. Aqueous hydrogen peroxide concentrations in bulk cloudwater	50
Figure 3.4. Corresponding pH values for the bulk cloud samples in Figure 3.3	50
Figure 3.5. Comparison of total S(IV) and hydrogen peroxide concentrations in bulk cloudwater collected by the CASCC2 at several locations	52
Figure 3.6. Comparison of hydrogen peroxide concentrations in small and large drops collected at several locations	54
Figure 3.7. Total iron concentrations in small and large drop fractions at several locations	56
Figure 3.8. Total manganese concentrations in small and large drop fractions at several locations	57
Figure 3.9. Dependence of the oxidation rates for the different paths on pH	62
Figure 3.10. Rates of S(IV) oxidation by hydrogen peroxide in cloud/fog drops of small and large drop fractions collected by the sf-CASCC at various locations	63
Figure 3.11. Rates of S(IV) oxidation by ozone in cloud/fog drops of small and large drop fractions collected by the sf-CASCC at various locations	65
Figure 3.12. Rates of S(IV) autooxidation catalyzed by both Fe(III) and Mn(II) in cloud/fog drops of small and large drop fractions collected by the sf-CASCC at various locations	67
Figure 3.13. Total S(IV) oxidation rates in cloud/fog drops of small and large drop fractions collected by the sf-CASCC at various locations	68
Figure 3.14. A comparison of the characteristic times for S(IV) complexation and	

oxidation	74
Figure 3.15. Calculated enhancement of sulfur oxidation by ozone due to the presence of chemical heterogeneity within the cloud	84
Figure 3.16. Calculated enhancement of sulfur oxidation by ozone as a function of the observed pH difference between large and small drops	85
Figure 3.17. Calculated enhancement of sulfur oxidation for different catalyzed S(IV) autooxidation pathways due to the presence of chemical heterogeneity within the clouds	88
Figure 3.18. Calculated enhancement of sulfur oxidation for the Fe(III)-Mn(II) synergistic catalysis pathway as functions of chemical heterogeneity within the clouds	90
Figure 3.19. Calculated enhancement of S(IV) oxidation for ozone and Fe(III)-Mn(II) synergistic catalysis pathways due to the presence of chemical heterogeneity within the clouds	91
Figure 3.20. Comparison of S(IV) oxidation enhancement factors among the different oxidation paths	94
Figure 3.21. Chemical composition of fog drops collected by the size-fractionating CASCC at Bakersfield, CA 1/15/1994	99
Figure 3.22. S(IV) oxidation rate by the different pathways for the fog event of January 15, 1994 at Bakersfield, CA	101
Figure 3.23. Calculated sulfur oxidation rates in small and large drop fractions and in bulk fogwater with averaged fog drop compositions	103
Figure 3.24. Fogwater pH values as functions of drop size for IESL and sf-CASCC samples	105
Figure 3.25. The S(IV) oxidation rates in size-fractionated drops and bulk fogwater	106
Figure 3.26. Comparison of bulk cloud/fog pH values calculated from the sf-CASCC samples and measured in the CASCC2 bulk fog samples	108
Figure 3.27. S(IV) oxidation rates in drops of the four size fractions derived from the IESL impactor	111
Figure 3.28. S(IV) oxidation rates in drops of the four size fractions derived from the IESL	113

Figure 3.29. Acid titration curves for fog samples collected with the sf-CASCC at Bakersfield, CA on 1/15/94	117
Figure 3.30. Acid titration curves for four bulk fog samples collected with a CASCC2 at Bakersfield, CA on December 10, 1995	119
Figure 3.31. Acid buffer intensities of fog samples measured at pH values observed immediately after collection in the field	121
Figure 3.32. Acid buffer intensities measured as a function of pH during acid titration of three fog samples collected at Bakersfield, California on January 15, 1994	122
Figure 3.33. Acid titration curves for small ($4 < d < 23 \mu\text{m}$) and large ($d > 23 \mu\text{m}$) drop fractions collected with the sf-CASCC at a rural site near the Kern Wildlife Refuge in California's San Joaquin Valley on January 1, 1996	127
Figure 3.34. Diagram of the model simulation	130
Figure 3.35. Mathematical equations employed in the simulation	131
Figure 3.36. (1a) - (3a) Profile of pH versus time. (1b) - (3b) Profile of S(IV) oxidation by ozone and S(IV) autooxidation versus time	136
Figure 3.37. The liquid water contents and chemical compositions of clouds at Angora Pk., Oregon, July 14-15, 1993	140
Figure 3.38. Ultraviolet-visible absorption spectra of filtered ($0.45 \mu\text{m}$) cloud samples measured by a Hitachi U-2000 UV/VIS spectrophotometer with 1.0 cm path length	148
Figure 3.39. Change of chemical composition of an authentic cloud water after irradiation with 313 nm light	150
Figure 3.40. Cloudwater pH change during irradiation with February sunlight (February 14, 1995)	151
Figure 3.41. Change of pH in the Fe(III)-oxalate solutions illuminated with July sunlight ...	154
Figure 3.42. Total hydrogen ion consumption, hydrogen peroxide formation and fraction of Fe(III) as functions of initial oxalate concentration	155
Figure B.1. Effect of formaldehyde concentration on method sensitivity	198
Figure B.2. Effect of formaldehyde concentration on color development	198
Figure E.1. Equipment set-up for DPKBH synthesis	220

Figure F.1. A comparison of the characteristic times of droplet growth and formaldehyde hydration with those for formaldehyde mass transport processes223

CHAPTER 1. INTRODUCTION

The issue of acid deposition, and its associated deleterious ecological impact, began to receive serious attention approximately twenty years ago. Since then numerous studies have been launched concerning related atmospheric chemistry and deposition processes (Calvert et al., 1985; Hough, 1988; Schwartz, 1987). Legislation has also been passed in the U.S. and elsewhere restricting emissions of precursors to atmospheric acids, including sulfur and nitrogen oxides. While oxidation of NO_x to nitric acid mainly occurs in the gas phase, oxidation of SO_2 to sulfuric acid can be much more rapid in the aqueous phase than in the gas phase (Seinfeld, 1986). More recently, studies showed that atmospheric sulfate particles produced by oxidation of sulfur dioxide can exert a climate cooling effect, directly by backscattering of solar radiation and indirectly by modifying cloud properties. Globally, 80 to 90 percent of SO_2 oxidation is thought to occur in clouds (Lelieveld and Heintzenberg, 1992). In-cloud oxidation of SO_2 into sulfate and subsequent release of the dry sulfate aerosol by cloud evaporation is believed to affect climate forcing more than sulfate particles formed through gas-phase SO_2 oxidation. This is because through clouds the sulfate is preferentially added to the particles in the size range associated with high scattering coefficients.

It has also been argued that in-cloud sulfate production can generate new cloud condensation nuclei (CCN); however, this argument may depend on the definition of CCN utilized. In-cloud SO_2 oxidation, by definition, adds sulfate to particles which have already served as CCN. Through the oxidation driven growth of these particles however, they will be more easily activated in the future at lower supersaturations (Langner et al., 1992; Kaufman

and Tanre, 1994). In order to develop an accurate understanding of the influence of aqueous phase sulfate prediction on radiative and cloud-forming properties of atmospheric aerosols, numerous physical and chemical processes need to be addressed, and it is crucial to determine changes of atmospheric particle size distributions and aerosol composition following cloud processing.

Model calculations show that sulfate production by in-cloud oxidation of sulfur dioxide is not uniformly distributed across all drop sizes. Non-uniform sulfate production can have a significant impact on the particle size distribution after cloud evaporation. In turn this affects resulting light-scattering efficiencies of the processed particles as well as their ability to nucleate cloud drops (Hegg et al., 1992; Yuen et al., 1994).

Seasonal variations in sulfate deposition in the eastern United States indicate that SO_2 oxidation rates in both the gas phase and liquid phase are highly dependent on photochemically generated oxidants such as $\cdot\text{OH}$ radical, O_3 , H_2O_2 and CH_3OOH (Calvert et al., 1985). Although substantial progress has been made in identifying dominant S(IV) oxidation pathways and describing rates of chemical reactions in clouds, many uncertainties remain. For example, in-cloud photochemical processes may provide an important source of oxidants to the aqueous phase in addition to oxidant uptake from the gas phase. Chemical inhomogeneities among CCN, reflected among cloud drops, can also significantly influence in-cloud sulfate production. Since very few measurements have been made of the amount of chemical heterogeneity present among cloud drop populations, there is a clear need for more field measurements to better understand its impacts on atmospheric sulfate production.

1.1. Sulfur (IV) related chemical reactions in cloudwater

Once gas phase sulfur dioxide is dissolved into atmospheric droplets, several reactions take place, including ionization, oxidation and complexation. The ionization process partitions dissolved SO_2 between $\text{SO}_2 \cdot \text{H}_2\text{O}$, HSO_3^- and SO_3^{2-} . Kinetic studies reveal that the three free S(IV) species have substantial differences in their reduction potentials towards oxidants. Several predominant pathways leading to S(IV) transformation have been identified. These pathways include reaction of aqueous S(IV) with H_2O_2 , O_3 , O_2 (catalyzed by Fe(III) and Mn(II)), OH , HNO_2 , CH_3OOH , $\text{CH}_3\text{CO}_3\text{H}$, PAN, $\text{HO}_2\cdot$, HCHO, and soot. Their thermodynamic and kinetic data have been compiled by Hoffmann and Calvert (1985). The potential importance of each reaction largely depends on pH. H_2O_2 is the most effective oxidant at low pH. At pH above 4 a number of pathways may become competitive to the reaction between S(IV) and H_2O_2 . Oxidation of S(IV) by ozone and Fe(III) and Mn(II) catalyzed autooxidation are major oxidation pathways, although OH , $\text{HO}_2\cdot$, and HNO_2 may contribute some portions to S(IV) oxidation in polluted daytime atmospheres (Hoffmann and Calvert, 1985). S(IV) complexation with formaldehyde is another important S(IV) transformation path at high pH. In the following sections the kinetics and mechanisms of these major S(IV) transformation reactions and their importance to atmospheric sulfate production will be discussed.

1.1.1. S(IV) oxidation by H_2O_2

S(IV) oxidation by H_2O_2 has been acknowledged as a major acid generation pathway in clouds largely due to the high solubility of H_2O_2 in cloud drops and its rapid reaction with

S(IV). Hoffmann and Edwards (1975) proposed that S(IV) oxidation by H_2O_2 to sulfuric acid proceeds via two steps. First is nucleophilic displacement of a water molecule by H_2O_2 from HSO_3^- (Equation (1.1)), and second is acid-catalyzed rearrangement of the peroxymonosulfurous acid intermediate (Equation (1.2)). The oxidation of S(IV) is acid-catalyzed since the second step is the rate determining reaction.



Using the pseudo-steady state approximation for $HOOSO_2^-$ the rate expression can be obtained

$$-d[S(IV)]/dt = k_{1f}k_2[H_2O_2][HSO_3^-][H^+]/(k_{1b} + k_2[H^+]) \quad (1.3)$$

where k_{1f} and k_{1b} are the rate constants of forward and backward reactions of Equation (1.1), respectively, and k_2 is the reaction rate constant of Equation (1.2). Rearranging Equation (1.3) gives

$$-d[S(IV)]/dt = k[H^+][H_2O_2][HSO_3^-]/(1+K[H^+]) \quad (1.4)$$

where $k = k_{1f}k_2/k_{1b}$ and $K = k_2/k_{1b}$.

Since S(IV) oxidation by H_2O_2 is the only oxidation pathway identified that is effective at low pH, H_2O_2 is the principal oxidant of S(IV) in many atmospheric aqueous systems (pH < 5). Kelly et al. (1989) evaluated the feasibility of detecting the occurrence of S(IV) oxidation

by H_2O_2 and O_3 and concluded that S(IV) oxidation by H_2O_2 should be detectable in a wide variety of cloud conditions, either through gas (SO_2 , H_2O_2) concentration decrease and/or aqueous product (sulfate) increase. It has been shown that gaseous H_2O_2 is present in the troposphere in sufficient quantity to be a major oxidant for S(IV) in cloudwater (Calvert et al., 1985). However, field measurements and model calculations also indicated that if H_2O_2 mixing ratios are lower than those of SO_2 , which appears to be a phenomenon typical for the polluted boundary layer, most of the available H_2O_2 would be consumed within a short time of cloud/fog formation and then other oxidants such as O_3 , Fe(III)/O_2 and $\cdot\text{OH}$ may play important roles (Klemm et al., 1992; Hough, 1987).

At present, a major uncertainty concerning oxidation of S(IV) by H_2O_2 is in-cloud photochemical production of H_2O_2 . Diurnal and seasonal variations of gas phase and aqueous H_2O_2 concentrations, with highest levels occurring in the afternoon and the summer, strongly suggest that gas phase photochemical processes are largely responsible for atmospheric levels of H_2O_2 (Kleinman, 1991; Sakugawa et al., 1990). Aqueous photochemical processes also contribute a significant amount of H_2O_2 (Zuo and Hoigne, 1993; Anastasio et al., 1994; Weinstein-Lloyd and Schwartz, 1991). As much as 30% of the H_2O_2 in droplets could be produced from aqueous phase free radical reactions, with the other 70% contributed from scavenging of gaseous H_2O_2 (Chameides, 1984). Neglecting aqueous photochemical formation of H_2O_2 may certainly lead to underestimates of sulfate production in daytime clouds.

1.1.2. S(IV) oxidation by ozone

Although H_2O_2 is believed to be the major oxidant for SO_2 in atmospheric water in many environments, S(IV) oxidation by other oxidants may become important under certain conditions. H_2O_2 can be depleted quickly due to the fast oxidation reaction if the SO_2 mixing ratio is larger than the H_2O_2 mixing ratio and may not be resupplied into the cloud. Under typical tropospheric conditions S(IV) oxidation by O_3 is relatively unimportant at low pH, but the oxidation rate increases dramatically with cloud pH (Seinfeld, 1986). As cloud pH approaches a value of approximately 5, the rate of S(IV) oxidation by O_3 is comparable to that by H_2O_2 for the conditions of 1 ppb H_2O_2 and 50 ppb O_3 .

Kinetic studies reveal that the rate of S(IV) oxidation by O_3 is inversely proportional to $[\text{H}^+]$ over a broad pH range of -0.3 to 7.0 (Erickson et al., 1977; Penkett et al., 1979; Maahs, 1983a and 1983b; Hoigne et al., 1985; Botha et al., 1994). A variety of empirical rate laws and observed rate constants were reported. Hoffmann (1986) analyzed the kinetic data obtained from five research groups and found that the reaction of S(IV) with O_3 in aqueous solution can be expressed in a generalized rate law (Equation (1.5))

$$-\text{d}[\text{S(IV)}]/\text{dt} = (k_0\alpha_0 + k_1\alpha_1 + k_2\alpha_2)[\text{S(IV)}][\text{O}_3] \quad (1.5)$$

where k_0 , k_1 , and k_2 are the reaction rate constants for oxidation of $\text{SO}_2\text{H}_2\text{O}$, HSO_3^- and SO_3^{2-} respectively, and α_0 , α_1 and α_2 represent the fractions of total free S(IV) present as $\text{SO}_2\text{H}_2\text{O}$, HSO_3^- and SO_3^{2-} . The rate expression fits the kinetic observations by the five investigators. Recommended values for k_0 , k_1 , and k_2 at 25°C are $2.4 \times 10^4 \text{ M}^{-1}\text{s}^{-1}$, $3.7 \times 10^5 \text{ M}^{-1}\text{s}^{-1}$, and $1.5 \times 10^9 \text{ M}^{-1}\text{s}^{-1}$, respectively.

Two mechanisms for aqueous S(IV) oxidation by O_3 have been proposed. One of them is a free radical mechanism which involves HO , HSO_3^{\cdot} and HSO_5^{\cdot} as primary radicals (Larson et al., 1978; Penkett et al., 1979; Botha et al., 1994). Another mechanism describes the S(IV) oxidation as polar reactions that proceed via an electrophilic attack of O_3 on the S(IV) center of $SO_2 \cdot H_2O$, HSO_3^- or SO_3^{2-} species (Erickson et al., 1977; Hoigne et al., 1985; Hoffmann, 1986). The latter mechanism is supported by isotopic labeling experiments (Espenson and Taube, 1965).

Field studies and model calculations reveal that high SO_2 to sulfate conversion through the O_3 pathway is at times associated with sea-salt particles (Hegg et al., 1992; Sievering et al., 1994). SO_2 oxidation rates higher than $30\% h^{-1}$ were observed in cloud-chamber experiments with sea salts as cloud nuclei (Miller et al., 1987). These rates are 5 - 10 times larger than the rates observed with buffering ions as CCN. Hegg et al. (1992) assessed the impact of an externally mixed, marine aerosol on the magnitude of in-cloud sulfate production and found that as much as 67% of sulfate production in the cloud can take place in the drops which form on sea-salt, although these drops constitute 6% or less of the drop number concentration and no more than 25% of the liquid water mass.

Since S(IV) oxidation by O_3 is an effective process only at high pH, it is estimated that the oxidation will be limited by the fact that as sulfur oxidation progresses, cloudwater pH falls and hence the reaction rate decreases rapidly (Seidl, 1989). However, in the presence of gaseous ammonia, sulfuric acid that is produced can be neutralized by cloudwater uptake of ammonia, enabling further sulfur dioxide to be oxidized. Neutralization may also be provided by chemical species inside cloudwater. If cloud/fog water itself contains hydrogen ion

absorbing materials which provide an internal capacity to buffer acid addition, S(IV) oxidation through the O_3 pathway may be more important for atmospheric sulfate production than previously thought.

1.1.3. S(IV) autooxidation catalyzed by iron (III) and manganese (II)

S(IV) autooxidation catalyzed by transition metals is of interest because it may contribute significantly to aqueous S(IV) oxidation under certain atmospheric conditions. Several rate expressions for the metal ion catalyzed autooxidation of S(IV) have been postulated (Martin, 1984; Hoffmann and Jacob, 1984; Brimblecombe and Spedding, 1974; Conklin and Hoffmann, 1988; Martin et al., 1991; Berglund et al., 1993; Berglund and Elding, 1995). However, substantial discrepancies exist in terms of reaction orders for S(IV), metal ion and hydrogen ion concentrations (Table 1.1). The disagreements among the rate expressions are probably due to their varied experimental conditions (e.g. concentrations of S(IV), metal ion and pH values employed).

Fe(III) exists in various forms in solution (e.g. Fe^{3+} , $FeOH^{2+}$, $FeOHSO_3$, $FeSO_3^+$, $Fe(SO_3)^-$), among which the predominant forms are determined by pH and concentrations of other components. Due to complexities of the catalysis mechanisms for each of the Fe(III) species, it is not surprising that the rate law expressions derived by the different investigators vary substantially. For aqueous solutions with chemical compositions comparable to atmospheric conditions and over a broad pH range, the kinetics of Fe(III)-catalyzed S(IV) oxidation were studied by Martin et al. (1991) and Ibusuki and Takeuchi (1987). Martin et al. (1991) proposed that S(IV) autooxidation follows various mechanisms in different pH

regimes. Thus the autooxidation has quite diverse rate expressions for the different pH regimes. It was explained that a second-order dependence on Fe(III) in the pH range of 4-5 is due to formation of $\text{Fe}_2(\text{OH})_4^{2+}$, and the appearance of a zero-order dependence on Fe(III) at high pH results from Fe(III) solubility limitation. Ibusuki and Takeuchi (1987) constructed a general rate expression which is first order with respect to both Fe(III) and S(IV), over a wide pH range of 2.6 to 6.5. However, the rate constant was determined to be a function of pH with a maximum value at pH 4.

Table 1.1. Rate expressions for Fe(III) catalyzed S(IV) autooxidation

pH	Buffer	[S(IV)] (μM)	[Fe(III)] (μM)	Rate Expression ($\text{M}^{-1}\text{s}^{-1}$)	Reference
0-3	HCl	500	50	$0.82[\text{H}^+]^{-1}[\text{Fe}^{3+}][\text{S(IV)}]$	Martin 1984
3-4	NaOH	100	0.1-5.0	$k[\text{Fe}^{3+}][\text{S(IV)}]$	Fuzzi 1978
5-8	NaOH	100	0.1-10	$k[\text{Fe}^{3+}][\text{S(IV)}]^2$	Fuzzi 1978
0-3	HCl	<10	0.3-10	$6.0[\text{H}^+]^{-1}[\text{Fe}^{3+}][\text{S(IV)}]$	Martin 1991
4-5	NaOH	10-200	0.01-1.0	$1.0 \times 10^9 [\text{Fe}^{3+}]^2 [\text{S(IV)}]$	Martin 1991
5-6	NaOH	10-200	1	$1.0 \times 10^{-3} [\text{S(IV)}]$	Martin 1991
7	NaOH	100	1	$1.0 \times 10^{-4} [\text{S(IV)}]$	Martin 1991
2.6-6.5		20	0.1-1.0	$k[\text{Fe}^{3+}][\text{S(IV)}]$	Ibusuki and Takeuchi 1987

Like Fe(III), Mn(II) is another important catalyst for autooxidation of S(IV). Because of reaction complexities and different experimental conditions, published reaction rate laws for this pathway are quite diverse as well (Table 1.2). However, there is general agreement between Martin (1984) and Ibusuki and Takeuchi (1987) that the rate of Mn(II)-catalyzed S(IV) autooxidation is inversely proportional to the hydrogen ion concentration at very low

cloud pH (pH < 3). At higher pH the rate is first-order in S(IV) and first-order in Mn(II) (Martin and Hill, 1987; Ibusuki and Takeuchi, 1987; Berglund and Elding, 1995). The first-order rate expression has been suggested for use in atmospheric model calculations (Berglund and Elding, 1995).

In atmospheric water both iron and manganese are present in concentrations high enough to effectively catalyze S(IV) oxidation. It has been found that the rate of S(IV) oxidation catalyzed by both Fe(III) and Mn(II) is faster than expected from the sum of the individually catalyzed rates (Ibusuki and Takeuchi, 1987; Martin and Good, 1991; Grgic et al., 1992).

Table 1.2. Rate laws determined for manganese (II) catalyzed autooxidation of S(IV) in aqueous solution (from Berglund and Elding, 1995)

pH	[Mn(II)] (μM)	[S(IV)] (μM)	Rate law (M s^{-1})	Reference
3-6	1.8-7	100	$k[\text{Mn(II)}][\text{S(IV)}]^{0.65}$	(1)
3-6	1-4	4-15	$5.1 \times 10^3 [\text{Mn(II)}][\text{S(IV)}]$	(2)
3-6	1-4	4-15	$1.7 \times 10^3 [\text{Mn(II)}][\text{S(IV)}]$	(3)
0-3	10-1000	<1	$25[\text{Mn(II)}][\text{S(IV)}]/[\text{H}^+]$	(4)
0-2	1-1000	50-4000	$k_1[\text{Mn(II)}]/[\text{H}^+] +$ $k_2[\text{Mn(II)}]^2/(1+k_3[\text{S(IV)}][\text{H}^+]) +$ $k_4[\text{Mn(II)}][\text{H}^+][\text{S(IV)}]/(1+k_5[\text{S(IV)}])$	(5)
2.4	1-1500	23	$k_{12b}[\text{Mn(II)}]C(\text{HSO}_3^-)([\text{Mn(II)}]_0 +$ $[\text{Fe(III)}]_0)/(\beta_1^{-1} + [\text{HSO}_3^-] + [\text{Mn(II)}])$	(6)
4	1-1500	23	$C[\text{HSO}_3^-](k[\text{Mn(II)}] + k'[\text{Mn(II)}]^2)/(A +$ $[\text{Mn(II)}])$	(6)

Reference: (1) Grgic et al. (1991); (2) Ibusuki and Barnes (1984); (3) Ibusuki and Takeuchi (1987); (4) Martin (1984); (5) Collins (1987); (6) Berglund et al. (1993).

Ibusuki and Takeuchi (1987) reported a 1.5-14 times increase of the S(IV) oxidation rate due to this synergistic effect. The S(IV) autooxidation catalyzed synergistically by Fe(III)

and Mn(II) was observed to be pH dependent with a maximal value around pH 4, decreasing sharply at lower and higher pH. The pH dependent pattern is very similar to the Fe(III) catalyzed S(IV) oxidation. Ibusuki and Takeuchi failed to explain the pH dependence of the synergistic effect, although other workers suggested it results from Fe(III) solubility limitation at high pH (Martin and Good, 1991). However, the solubility limitation will cause the Fe(III) concentration to decrease by several orders of magnitude for a one unit pH increase. This large change was not observed in the rate of S(IV) oxidation. Indeed, the S(IV) oxidation rate decreases no more than two fold for the pH increase from 4 to 6.

Ibusuki and Takeuchi (1987) postulated rate laws at conditions of micromolar concentrations of Fe(III), Mn(II) and S(IV) and for a pH range of 2.6-6.5, as follows:

$$\begin{aligned} \text{pH} \leq 4.2 \\ -d[\text{S(IV)}]/dt = k_s' [\text{H}^+]^{-0.74} [\text{Mn(II)}][\text{Fe(III)}][\text{S(IV)}] \quad (1.6) \\ (k_s' = 3.72 \times 10^7 \text{ at } 23.8^\circ\text{C}) \end{aligned}$$

$$\begin{aligned} \text{pH} \geq 4.2 \\ -d[\text{S(IV)}]/dt = k_s'' [\text{H}^+]^{0.67} [\text{Mn(II)}][\text{Fe(III)}][\text{S(IV)}] \quad (1.7) \\ (k_s'' = 2.51 \times 10^{13} \text{ at } 23.8^\circ\text{C}) \end{aligned}$$

Martin and Good (1991b) reexamined the Fe(III)-Mn(II) catalyzed S(IV) oxidation for typical atmospheric concentrations of Fe(III), Mn(II) and S(IV). Their rate law has the form of

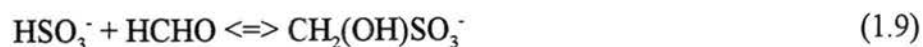
$$-d[\text{S(IV)}]/dt = (k_1[\text{Fe(III)}] + k_2[\text{Mn(II)}] + k_3[\text{Fe(III)}][\text{Mn(II)}])[\text{S(IV)}] \quad (1.8)$$

where k_1 , k_2 , and k_3 values are $2600 \text{ M}^{-1}\text{s}^{-1}$, $750 \text{ M}^{-1}\text{s}^{-1}$ and $1.0 \times 10^{10} \text{ M}^{-2}\text{s}^{-1}$ respectively at 25°C . The rate expression was obtained from measurements at pH 3 and 5. They found that the rate constant values from their measurements are in reasonable agreement with the work of Ibusuki and Takeuchi (1987).

It is noted that in the rate expressions by Ibusuki and Takeuchi (Equations (1.6) and (1.7)) S(IV) oxidation rates are proportional to the product of Fe(III) and Mn(II) concentrations. Also in the expression of Martin and Good (Equation (1.8)), the third term dominates for typical atmospheric conditions. This suggests that a small change in Fe(III) and Mn(II) concentrations will result in a substantial change in the S(IV) oxidation rate. This substantial change is not predicted from simply adding the rates of S(IV) autooxidation catalyzed by Fe(III) and Mn(II) individually. A synergistic effect increases the sensitivity of the S(IV) oxidation rate to concentrations of Fe(III) and Mn(II).

1.1.4. S(IV) complexation with formaldehyde.

Sulfite and bisulfite can form complexes with various aldehydes (Olson and Hoffmann, 1989). One important example is hydroxymethanesulfonate (HMS), an adduct of bisulfite or sulfite with formaldehyde, the most abundant aldehyde in the atmosphere (Munger et al., 1986; Facchini et al., 1992). Formation of HMS (Equations (1.9) and (1.10)) in clouds has received attention due to its ability to affect sulfate production rates (Olson and Hoffmann, 1989; Richards et al., 1983; Jacob and Hoffmann, 1983).



While formation of HMS can enhance overall SO_2 solubility and provide a reservoir for S(IV) in cloud drops, the S(IV)-aldehyde complexation may compete with S(IV) oxidation under certain atmospheric conditions. Formaldehyde itself may also compete with S(IV) for free radicals (e.g., OH radicals) (Adewuyi et al., 1984). However, the ability of formaldehyde to compete with oxidants for available free S(IV) remains open to discussion.

Rates of HMS formation and dissociation are dependent on cloud pH and concentrations of sulfite (or bisulfite) and formaldehyde. Kinetic studies reveal that HMS formation is favored at high pH. Studies of fogwater in the San Joaquin Valley (Munger et al., 1984; Jacob et al., 1989) also indicated that high concentrations of HMS are formed under conditions of high pH and P_{SO_2} .

Aqueous HCHO concentrations are usually calculated from HCHO gas/liquid partitioning equilibrium. Dixon (1992) critically evaluated atmospheric conditions at which assuming equilibrium is appropriate by considering HCHO mass transport from the gas phase to cloud drops. He found that HCHO concentrations in drops are expected to become limited by mass transport at relatively high pH ($\text{pH} > 5.5$), if sufficient SO_2 is present. The HCHO mass-transport limitation is most likely due to aqueous-phase diffusion. The limitation will be more significant for larger drops. The calculations also demonstrated that aqueous-phase HCHO and its hydrated form, $\text{CH}_2(\text{OH})_2$, can not be assumed to be in equilibrium with gas-phase HCHO if HCHO is being consumed quickly by chemical reactions, although

concentrations of HCHO and $\text{CH}_2(\text{OH})_2$ at the drop surface are in equilibrium with gaseous HCHO. At 10 ppb atmospheric SO_2 and cloud drop pH 7, the ratio of the average HCHO concentration to that at the droplet surface for a 10 μm diameter drop is 0.7, and the ratio is 0.3 for a 30 μm diameter drop. The results suggest that a decrease of the HCHO concentration from the droplet surface may occur, especially for large drops, due to the rapid chemical consumption at high SO_2 concentrations and high pH. The results imply a possible non-uniform distribution of HCHO concentrations among drops of different sizes. Field observations of large departures of HMS formation from theoretical predictions by assuming HCHO gas/liquid partitioning equilibrium supported the idea of HCHO mass-transport limitation, according to Facchini et al., 1992. In their measurements HMS concentrations were much less than expected from equilibrium considerations in samples with pH above 5, with even larger departures from equilibrium expectations when sample pH is higher.

1.1.5. In-cloud photochemical reactions involving iron species

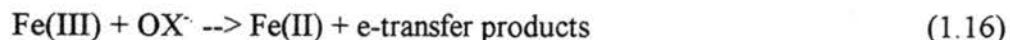
Recent studies of atmospheric iron chemistry show that Fe(III) species can initiate a series of radical reactions under irradiation (Faust and Hoigne, 1990; Faust, 1994; Allen and Faust, 1994; Zuo and Hoigne, 1992 and 1993). Photochemical reactions involving iron species produce oxidants, such as $\cdot\text{OH}$, HO_2/O_2^- and H_2O_2 , all of which are known to play important roles in oxidation of S(IV) in the atmosphere. Photolysis of $\text{Fe}(\text{OH})^{2+}$, a dominant form of Fe(III) between pH 2.5 and 5, produces $\cdot\text{OH}$ radicals at rates similar to calculated rates of $\cdot\text{OH}$ gas-to-droplet transfer in clouds (Faust and Hoigne, 1990). Major sinks for $\cdot\text{OH}$ in

atmospheric droplets may include reactions with bisulfite and soluble organic compounds such as formaldehyde and hydroxymethanesulfonate (HMS).

Another important photochemical process involving Fe(III) is photolysis of Fe(III)-polycarboxylates. Polycarboxylates are common constituents in atmospheric aerosols and the liquid phase (Grosjean et al., 1978; Satsumabayashi et al., 1990). Measured Fe concentrations in atmospheric water are often comparable in magnitude with polycarboxylate concentrations. Photolysis of Fe(III)-polycarboxylates is a potentially important source of O_2^-/HO_2^- , H_2O_2 and $\cdot OH$ in atmospheric water drops, while Fe(III) itself is reduced to Fe(II) in the reaction. Measurements of quantum yields of Fe(II) formation from several Fe(III)-polycarboxylates showed that values as high as 0.6-1.0 can be achieved for the Fe(III)-oxalate complex (Faust and Zepp, 1993). A mechanism of Fe(III)-oxalate photolysis has been postulated by Zuo (1992) (Equations (1.11) - (1.15)).



A critical step leading to H_2O_2 formation in the mechanism is the reaction of oxygen with oxalate radical (Equation (1.13)). The main species competing with oxygen for the oxalate radical is Fe(III) (Equation (1.16)).



The extent of competition will depend on the steady-state redox speciation between Fe(III) and Fe(II). Another critical step is the reaction of Fe(II) with peroxy radical (Equation (1.15)). To examine the potential importance of this reaction, several sink reactions for Fe(II) and peroxy radical are compared at atmospheric conditions (Tables 1.3 and 1.4). While Fe(II) is most likely oxidized by $\text{HO}_2^-/\text{O}_2^-$ and H_2O_2 in acidic atmospheric water (Table 1.3), reduction of $\text{HO}_2^-/\text{O}_2^-$ by Fe(II) competes with several O_2 -producing reactions (Table 1.4), among which the reaction of O_2^- with Fe(III) is a potentially important sink for $\text{HO}_2^-/\text{O}_2^-$. Therefore, the H_2O_2 yield will depend critically upon the speciation of Fe between Fe(II) and Fe(III) and upon the speciation of peroxy radical. While speciation between HO_2^- and O_2^- is largely dependent on cloud drop pH ($\text{pK}_a = 4.8$), steady-state concentrations of Fe(III) and Fe(II) will be controlled by photochemical reactions at daytime and by the thermal oxidation/reduction reactions at night.

Table 1.3. Daytime sinks for Fe(II) in atmospheric water drops (pH < 5)
(From Faust, 1994)

Oxidant	[Oxidant] _{ss} ^a (M)	$k_{\text{ox, Fe}^{2+}}$ ^b ($\text{M}^{-1}\text{s}^{-1}$)	$k_{\text{ox, Fe}^{2+}}[\text{Oxidant}]_{\text{ss}}$ ^c (s^{-1})
O_2^-	$1 \times 10^{-10} - 2 \times 10^{-9}$	1.0×10^7	$(1 - 20) \times 10^{-3}$ ^d
$\text{HO}_2^-/\text{RO}_2^-$	$1 \times 10^{-9} - 2 \times 10^{-8}$	$(1.2 - 1.7) \times 10^6$	$(1 - 30) \times 10^{-3}$
H_2O_2	$10^{-6} - 10^{-4}$	5.1×10^1	$(0.05 - 5) \times 10^{-3}$
O_3	1×10^{-9} ^e	8.3×10^5	$(0.8) \times 10^{-3}$
$\cdot\text{OH}$	$10^{-14} - 10^{-12}$	4×10^8	$(0.004 - 0.4) \times 10^{-3}$
$\text{O}_2(^1\Delta_g)$	$10^{-14} - 10^{-12}$	NA ^f	$(0.004 - 0.4) \times 10^{-3}$
O_2	2.7×10^{-4}	NA	$(0.000003) \times 10^{-3}$

- a. Typical steady-state concentration of oxidant in sunlit atmospheric water drops.
b. Bimolecular rate constant for the reaction $\text{Fe}^{2+} + \text{OXIDANT} \rightarrow \text{Fe(III)}$, Rate constants for reactions of Fe(II) complexes with H_2O_2 could be much larger than the value used here for Fe^{2+} .
c. Apparent first-order rate constant for the oxidation of Fe(II) in atmospheric water drops by the specified oxidant for a typical daytime steady-state concentration of the oxidant.
d. Assumes $[\text{O}_2^-]_{\text{ss}} = 0.1[\text{HO}_2^-]_{\text{ss}}$ (pH = 3.8); $\text{pK}_a(\text{HO}_2^-) = 4.8$.
e. Based on Henry's law equilibrium with 100 ppbv gas-phase O_3 .
f. Rate constant is unknown, and therefore, a value identical to that for $\cdot\text{OH}$ was used.

Table 1.4. Sinks for HO₂[·]/O₂^{·-} in atmospheric water drops, some of which form H₂O₂ (From Faust, 1994)

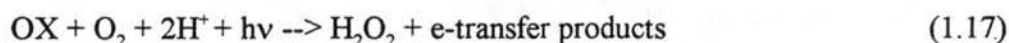
Reaction (A + B → Products)	k _{A,B} (M ⁻¹ s ⁻¹)	Rate = k _{A,B} [A][B] (Ms ⁻¹)
H ₂ O ₂ -forming reactions		
HO ₂ [·] + HO ₂ [·] → H ₂ O ₂ + O ₂	8.3 × 10 ⁵	0.057
HO ₂ [·] + O ₂ ^{·-} (+H ⁺) → H ₂ O ₂ + O ₂	9.7 × 10 ⁷	0.66
HO ₂ [·] + Fe(II) (+H ⁺) → H ₂ O ₂ + Fe(III)	1.2 × 10 ⁶	5.6
HO ₂ [·] + Cu(I) (+H ⁺) → H ₂ O ₂ + Cu(II)	1 × 10 ⁹	460
O ₂ ^{·-} + Fe(II) (+H ⁺) → H ₂ O ₂ + Fe(III)	1.0 × 10 ⁷	3.7
O ₂ ^{·-} + Cu(I) (+H ⁺) → H ₂ O ₂ + Cu(II)	1 × 10 ¹⁰	370
O ₂ -forming reactions		
HO ₂ [·] + Fe(III) → O ₂ + Fe(II) + H ⁺	< 10 ⁴	< 0.05
HO ₂ [·] + Cu(II) → O ₂ + Cu(I) + H ⁺	1 × 10 ⁸	46
O ₂ ^{·-} + Fe(III) → O ₂ + Fe(II)	1.5 × 10 ⁸	56
O ₂ ^{·-} + Cu(II) → O ₂ + Cu(I)	1 × 10 ¹⁰	370
O ₂ ^{·-} + O ₃ (aq) (+H ⁺) → 2O ₂ + OH	1.5 × 10 ⁹	1.1

Note: Assumed chemical composition in atmospheric water drops: pH = 3.7, [HO₂[·]] = 9.26 nM, [O₂^{·-}] = 0.74 nM, [Fe(III)] = [Fe(II)] = 0.5 μM, [Cu(II)] = [Cu(I)] = 50 nM, [O₃(aq)] = 1 nM (based on Henry's law equilibrium with 100 ppbv gas-phase O₃).

Both photoreduction of Fe(III) and oxidation of Fe(II) have been demonstrated to occur on time scales of minutes. Thus it is strongly suggested that during the daytime, dissolved iron in atmospheric water drops is rapidly cycling between Fe(III) and Fe(II).

Photoredox reactions of Fe can affect atmospheric aqueous S(IV) oxidation in several ways: (1) by forming oxidants (OH, HO₂/O₂^{·-} and H₂O₂) that oxidize S(IV) species; (2) by controlling the speciation of Fe (dynamic cycling of Fe(III) and Fe(II) controls the steady-state concentration of Fe(III) which is an effective catalyst for autooxidation of S(IV)), (3) by providing H⁺ sink reactions, which can increase cloud drop pH and hence rates of pH sensitive S(IV) oxidation (by O₃ and O₂ catalyzed by Fe(III) and Mn(II)).

According to the mechanism of Fe(III)-oxalate photolysis (Equations (1.11) - (1.15)), hydrogen ion can be consumed during photochemical cycling of Fe(III) and Fe(II). The net reaction for one photoredox cycle can be written as



While one molecule of H_2O_2 is produced, two molecules of hydrogen ion are consumed and oxalate is finally converted to CO_2 . The photoredox cycle can be continued until oxalate is depleted in the cloud drops. The photochemical consumption of H^+ could act as an 'acid buffer' to neutralize sulfuric acid produced through S(IV) oxidation, and therefore enhance the importance of pH sensitive S(IV) oxidation pathways.

Fractions of Fe(III) in aerosols and atmospheric water are of interest since it is well known that only Fe(III) can effectively catalyze S(IV) autooxidation and initiate photochemical reactions. Numerous studies have been conducted to speciate the oxidation state of iron in both aerosols (Hoffmann et al., 1996; Zhuang et al., 1992a and 1992b) and in the atmospheric aqueous phase (Behra and Sigg, 1990; Erel et al., 1993; Pehkonen, 1992; Sinner et al., 1994; Zhuang et al., 1995). However, effort has been focused on Fe(II) measurements by most of the investigators. It has been found that fractions of Fe(II) in atmospheric aqueous phase varied substantially from a few percent to as much as 90 percent. The wide range of Fe(II) fractions is obviously due to the different physical, chemical and photochemical properties of atmospheric water investigated. Therefore characterization of

both Fe(II) and Fe(III) in atmospheric water is important in determining its catalytic effect on S(IV) oxidation.

1.2 Cloud drop size dependent chemical composition and its effect on in-cloud S(IV) oxidation.

Traditional approaches to the study of sulfate production treated the cloud as being comprised of a chemically homogeneous distribution of drops. This approach was simpler from a modeling perspective and experimental studies of cloud and fog chemistry did little to refute the hypothesis, largely because sampling instruments were designed to collect bulk samples representative of the entire cloud drop spectrum. Several recently developed cloud chemistry models (Seidl, 1989; Twohy et al., 1989; Pandis and Seinfeld, 1990; Hegg and Larson, 1990; Roelofs, 1993) have been structured to identify distributions of chemical species across the evolving cloud drop size distribution. Their predictions suggest that substantial variations in drop chemistry occur across the drop size spectrum. The variations arise from a variety of sources including the chemically heterogeneous nature of the cloud condensation nuclei (CCN) population, differences in condensational growth rates for small and large drops, and differences in chemical reaction rates between drops of disparate composition.

The effects of size dependent chemical composition on S(IV) oxidation have been modeled for a variety of cloud types and environments including wintertime stratus cloud (Ayers and Larson, 1990), warm stratiform clouds (Lin and Chameides, 1991), hill cap and

cumulus clouds (Bower et al., 1991; Roelofs, 1992), and radiation and winter urban fogs (Bott and Carmichael, 1993; Pandis and Seinfeld, 1990). A V-shape size dependence of chemical composition has been predicted with a minimum solute concentration occurring for drops with diameter around 10 μm (Pandis and Seinfeld, 1990; Roelofs, 1992; Seidl, 1989). For small, unactivated drops, the concentration is predicted to decrease with increasing drop size. This occurs because lower solute concentrations are required to balance the decreased surface curvature in order to maintain equilibrium between the water vapor pressure above the drop surface and the ambient water vapor concentration. For the large, activated drops which are growing unstably by condensation, the concentration is predicted to increase with increasing drop size because the small drops grow (and hence dilute) more quickly due to their higher ratios of surface area to volume. Effects of chemical heterogeneity among cloud drop populations on sulfur oxidation can be substantial when a wide variety of droplet compositions are present and S(IV) autooxidation or oxidation by ozone contribute significantly to total sulfate production. A critical review of the processes controlling chemical heterogeneities among cloud droplets and their implications has been made by Ogren and Charlson (1992). Among other things, the chemical heterogeneity can affect in-cloud S(IV) oxidation rates due to variations of cloudwater pH, and S(IV), oxidants and catalyst concentrations across the drop size spectrum.

In the process of nucleation, cloud condensation nuclei (CCN) provide the initial solute in cloud droplets and often control droplet pH in the early stages of droplet growth. Thereafter, gas-to-liquid partitioning of trace gases and in-cloud chemical reactions may take over. It is clear that atmospheric aerosols acting as CCN are composed of coarse and fine

particles, which are chemically distinct. Fine particles, which are submicron in size, primarily contain chemical species produced through gas-to-particle conversion, while coarse (super-micron) particles are mainly produced mechanically and consist primarily of sea-salt and crustal material. Cloud droplets formed on an external mixture of coarse and fine particles are expected to retain a size-dependent chemical signature at least in the initial condensational step of cloud development. Field investigations of the dependence of chemical composition on droplet size confirm this expectation (Munger et al., 1989; Collett et al., 1993; Collett et al., 1994; Bator and Collett, 1997). For several types of clouds investigated, the small cloud drops typically contain higher concentrations of NO_3^- , SO_4^{2-} and NH_4^+ , while the large drops are often enriched in Na^+ , K^+ , Ca^{2+} , Mg^{2+} and Cl^- .

Due to the size dependence of the chemical composition, a distribution of drop acidities as a function of drop size can be expected and has been observed in field measurements (Collett et al., 1994; Munger et al., 1989). The existence of even a small number concentration of alkaline cloud drops can significantly enhance overall in-cloud sulfate production when pH is high or H_2O_2 is limited. In the case of oxidation by ozone, the enhancement arises from the high solubility of SO_2 and rapid S(IV) oxidation by O_3 in the high pH cloud drops (Bower et al., 1991; Lin and Chameides, 1991; Hegg et al., 1992). Because the increase in the oxidation rate changes non-linearly with drop acidity, predictions of the net oxidation rate in populations of chemically heterogeneous cloud drops from average cloud drop properties are generally too low. Hegg and Larson (1990) calculated in-cloud sulfate production using an explicit cloud chemistry model and compared it with the predictions by a bulk chemistry model. It was found that the sulfate production rate can be 3 to 30 times

higher when a non-uniform distribution of acidities among the cloud drops was considered than in the bulk model using an average chemical composition.

The chemically heterogeneous nature of cloud condensation nuclei is a source of not only acidity variation among drops of different size but also non-uniform distributions of catalyst concentrations with drop size. Measurements of trace metals in atmospheric aerosols reveal that they are predominantly found in coarse particles (1.0 - 2.5 μm) from crustal sources, although relatively high concentrations of Fe and Mn were also occasionally found in accumulation mode particles which were associated with trajectories from industrial regions (Hillamo et al., 1993; Jaffrezo et al., 1993). Noble and Prather (1996) recently performed measurements on the aerodynamic size and chemical composition of individual aerosol particles. It is found that transition metals are commonly associated with particles of two types. One type of particles has a size range of 0.5-2.3 μm and contains both transition metals and organic components. They are most likely formed in some combustion process. The second type of particles typically contain predominantly inorganic components, including transition metals, and they have relatively large size and most likely are derived from local soil. Based on observations of how other coarse mode aerosol species are distributed among cloud drops, it is expected that the trace metals will be preferentially found in larger drops in non-urban atmospheres.

A non-uniform distribution of trace metal ions across the cloud drop size spectrum can result in underprediction of S(IV) oxidation rates in clouds made using bulk cloud chemical composition. Rates of S(IV) oxidation catalyzed by iron and manganese are functions of both cloud drop acidities and catalyst concentrations, and the dependence of the oxidation rates on

acidity is non-linear. Field measurements have revealed that cloud drop acidities vary with drop size (Collett et al., 1994). Therefore using average cloud drop acidity can result in inaccurate estimation of in-cloud S(IV) oxidation through this pathway. Variations of iron and manganese concentrations across the drop size spectrum may magnify the effect of acidity variations on rates of S(IV) oxidation due to covariance of cloud drop pH and catalyst concentrations. Revelation of non-uniform distributions of trace metal concentrations among drop populations are also important in determining the effects of Fe on the chemistry of atmospheric waters. Faust and Hoigne (1990) compared the relative importance of gas-to-drop partitioning vs aqueous-phase photoformation as sources of a given oxidant (e.g. $\cdot\text{OH}$) to atmospheric water drops as a function of drop size. They argue that the gas-to-drop partitioning is less important with increasing drop size, although any size dependence of Fe species is not considered in their calculations. The uncertainty of the estimation due to using uniform Fe species concentrations across the drop size spectrum can be reduced as more information on Fe speciation and its drop size distribution in cloud drop populations becomes available.

Cloudwater chemical heterogeneity affecting in-cloud S(IV) oxidation could also result from drop size-dependent dissolution of reactive gases (e.g. SO_2 , H_2O_2 and O_3) into cloud drops. Gas dissolution to droplets involves three mass transport processes: gas diffusion to the drop surface, interfacial mass transport and aqueous diffusion throughout the drop. If the mass transport of the species between the bulk gas phase and solution is not sufficiently rapid to maintain a solubility equilibrium in the face of depletion of the dissolved gas by chemical reactions, or dilution by condensational droplet growth, concentration differences

might occur among drops of different sizes. This could in turn exert an influence on S(IV) oxidation rates. Schwartz (1988) examined mass-transport limitation to the rates of in-cloud oxidation of SO₂ by H₂O₂ and O₃. It was found that the mass transport processes are unlikely to inhibit the rate of reactive uptake of SO₂ into cloud droplets by either of these reactions under situations representative of non-urban industrialized regions. However, substantial O₃ aqueous-phase diffusion limitation is expected for the O₃-S(IV) reaction at high pH (pH > 5), indicating that although the O₃ concentration at the drop surface is at equilibrium with surrounding gaseous O₃, the concentration inside the drop may not reach equilibrium in extreme conditions (i.e. high pH and high SO₂ concentration). Due to the dependence of the aqueous phase diffusion time scale on drop size, the limitation will be more apparent in large drops than in small drops.

Examination of mass-transport limitation in the H₂O₂-S(IV) reaction showed that H₂O₂ limitation is absent for all three transport processes. The only H₂O₂ sink considered in this analysis was depletion of H₂O₂ by S(IV). Aqueous H₂O₂ can also be diluted through cloud drop condensational growth. It is quite possible that the time scale of H₂O₂ dilution by drop growth (Equation (1.18)) (Ogren and Charlson, 1992) is much shorter than the time scale for depletion by chemical reaction (Equation (1.19)).

$$\frac{1}{m_d} \frac{dm_d}{dt} = \frac{3(n_w - n_{rw})q_w D_w}{r_d^2 d_w} \quad (1.18)$$

where m_d is the mass of water, n_w and n_{rw} are the gas phase water molecule number concentrations far from the droplet and at the droplet surface, respectively, q_w is the mass of a

water molecule, D_w is the diffusion coefficient of water vapor, r_d is the droplet radius, and d_w is the density of water.

$$-\frac{d[H_2O_2]}{[H_2O_2]dt} = \frac{kK_{s1}P_{SO_2}H_{SO_2}}{1+k[H^+]} \quad (1.19)$$

In Equation (1.19) k and K represent the reaction constant ratios described for Equation (1.4), K_{s1} represents the first acid dissociation constant for dissolved SO_2 , and P_{SO_2} and H_{SO_2} represent the partial pressure and Henry's law constant of SO_2 . For example, under typical non-urban atmospheric conditions ($P_{SO_2} = 1$ ppb) the time scale of aqueous H_2O_2 depletion by oxidation of S(IV) is 840 seconds at 25 °C, while the time scale of dilution by condensational growth is 38 seconds for 10 μm diameter drops growing in response to a 0.2% supersaturation. According to Schwartz (1988) a time scale of minutes for H_2O_2 depletion cannot cause any mass transport limitation. However, droplet condensational growth can be fast enough to limit H_2O_2 transport from the bulk gas phase into cloud drops via interfacial mass transport. The mass transport limitation suggests that aqueous H_2O_2 concentrations will not always be in equilibrium with gas phase H_2O_2 . The departure from equilibrium concentrations was quantified by model simulation (Bower et al. (1991), and it was found that the equilibrium can be reached at least 80 seconds after cloud initiation at the modeled conditions. Therefore H_2O_2 concentrations in actively growing cloud droplets might be a function of drop size due to the size dependence of condensational growth rates.

1.3 Research goals and approach

In order to more accurately estimate the S(IV) oxidation rate in populations of chemically heterogeneous cloud drops it is essential to characterize the drop size dependence of concentrations of chemical species which are related to in-cloud S(IV) oxidation. In order to do this, field experiments have been carried out to measure chemical concentrations in cloud drops of two or three independent size ranges. These experiments have been conducted in a variety of cloud types and a variety of environments, from heavily polluted to pristine. The chemical species investigated include hydrogen ion, sulfur (IV), hydroxymethanesulfonate (HMS), hydrogen peroxide, formaldehyde, total iron, total manganese, iron (III) and iron (II).

By studying chemical heterogeneity across the cloud drop size spectrum we can investigate variations of S(IV) oxidation rates via the different pathways among drops of diverse sizes and characterize which drop size fractions contribute most to in-cloud sulfate production. This is of interest in providing more accurate estimates of net sulfate production rates in chemically heterogeneous clouds and in determining which aerosol particle sizes grow most through sulfate addition during cloud processing.

In-cloud S(IV) oxidation pathways considered in this study include oxidation by H_2O_2 , O_3 and O_2 (catalyzed by Fe(III) and Mn(II)). By using existing kinetic data and measured cloud chemical compositions in the different drop size ranges sampled, the size dependence of S(IV) oxidation rates will be calculated for each of the oxidation pathways, and the relative importance of the different S(IV) oxidation pathways can be identified for the different environments and cloud types studied. By comparing S(IV) oxidation rates

calculated from measured, chemically heterogeneous cloud compositions to those predicted from the average cloud drop properties, we can investigate under what conditions and through which oxidation pathways the size-dependent nature of cloud chemistry has a significant effect on overall sulfate production.

Effects of cloud chemical heterogeneity on overall in-cloud sulfate production will be evaluated by simple model simulations. Simulations will include S(IV) oxidation by H_2O_2 , O_3 and O_2 (synergistically catalyzed by Fe(III) and Mn(II)). Simulated clouds and fogs will be composed of two and three chemically distinct droplet size classes, with compositions reflecting those observed in our field measurements. Effects on sulfur oxidation rates in fogs containing four (hypothetical) chemically distinct drop size fractions will also be discussed.

Other chemical processes that exert an important influence on S(IV) oxidation will also be investigated. These processes include S(IV) complexation with formaldehyde, acid buffering processes and Fe(III) photochemical reactions.

CHAPTER 2. EXPERIMENTAL METHODS

2.1. Cloud/fogwater sampling

Ground-based sampling of clouds and fogs was conducted at a variety of sites between July 1993 and January 1996. Coastal stratus and stratocumulus clouds were sampled in June 1993 and 1994 at La Jolla Peak, California, situated near the southern end of the Santa Barbara Channel, and in July 1993 at Angora Peak, a remote site on the northern Oregon coast. Frontal clouds at Mt. Mitchell, North Carolina and Whiteface Mountain, New York were sampled during August and September 1993. Radiation fogs were sampled at several locations (Bakersfield, Woodland, Esparto, Fresno, and at a rural site near the Kern Wildlife Refuge (KWR)) in California's San Joaquin Valley during December 1992 - January 1993, January 1994 and December 1995 - January 1996.

Various combinations of cloudwater samplers were used at different sites. The collectors included a Caltech Active Strand Cloudwater Collector 2 (CASCC2), a Caltech Active Strand Cloudwater Collector with a size-fractionating inlet (sf-CASCC), a large IES cloud impactor constructed at the Institute for Environmental Studies (IESL) and the ETH cloud impactor designed at the Swiss Federal Institute of Technology (ETH).

The CASCC2 (Demoz et al., 1996) is an active cloud collector designed to collect droplets larger than 3.5 μm diameter at a flow rate of 5800 liters/minute, thereby providing a bulk sample of cloud or fogwater. Drops are collected by inertial impaction on banks of 508 micron diameter Teflon strands (Figure 2.1).

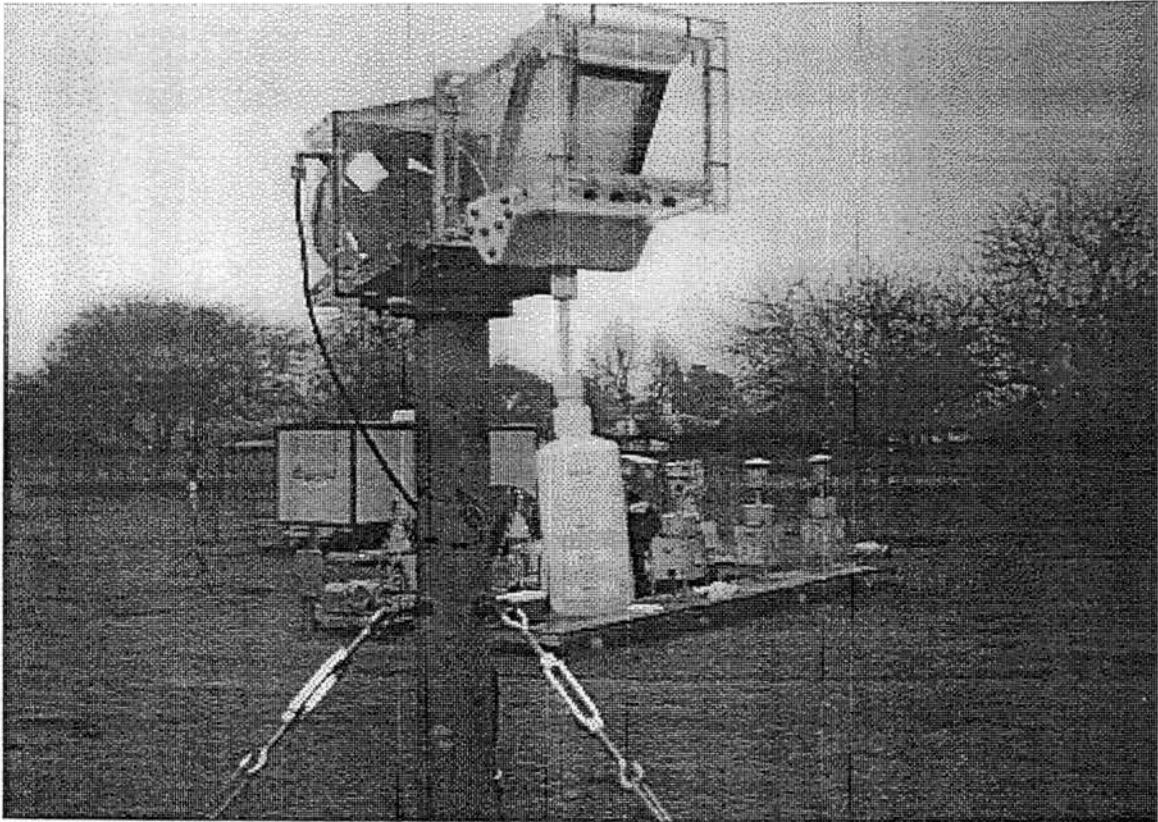


Figure 2.1 The Caltech Active Strand Cloudwater Collector 2 designed to collect droplets larger than $3.5 \mu\text{m}$ diameter.

The size-fractionating CASCC (Munger et al., 1989; Demoz et al., 1996) was used to collect two independent drop size fractions, one containing mainly drops larger than 23 μm diameter and one with drops mainly between 4 and 23 μm . The 23 μm theoretical size cut for the inlet, larger than the previously reported value of 16 μm , is based on velocity measurements in the CASCC made subsequent to the work of Munger et al. (1989). Like the CASCC2, the size-fractionating CASCC collects droplets by inertial impaction on cylinders. To obtain the size-fractionating capabilities, two banks of cylinders are arranged in series. The upstream bank uses larger cylinders to remove large droplets, while smaller droplets are collected in the second impaction bank downstream. The flow rate used in the sf-CASCC is 19,000 liters/minute (Figure 2.2).

The ETH cloud impactor (Collett et al., 1993; 1995) is a multiple-jet, two-stage cascade impactor designed to provide 50% lower size-cuts of 3 and 10 μm at a flow rate of 418 liters/minute. The impactor is constructed of Plexiglas but features Teflon impaction plates. Drops impact into shallow channels on the Teflon plates to facilitate sample removal. The ETH cloud impactor was used to collect two independent drop size fractions for analysis of pH and major ion concentrations (Figure 2.3).

The IESL impactor (Collett et al., 1995), a modified version of the ETH cloud impactor, is constructed primarily of Plexiglas with Teflon impaction plates. Two figures are significantly different from the ETH impactor. First, it is capable of simultaneously collecting three independent portions of the cloud drop size spectrum (Figure 2.4). The impaction plates are interchangeable with 50% lower size cuts of 3, 4, 10, 12, 15, 20, and 30 μm . Second, the flow rate of the IESL impactor (1500 liters/minute) was designed substantially higher than the

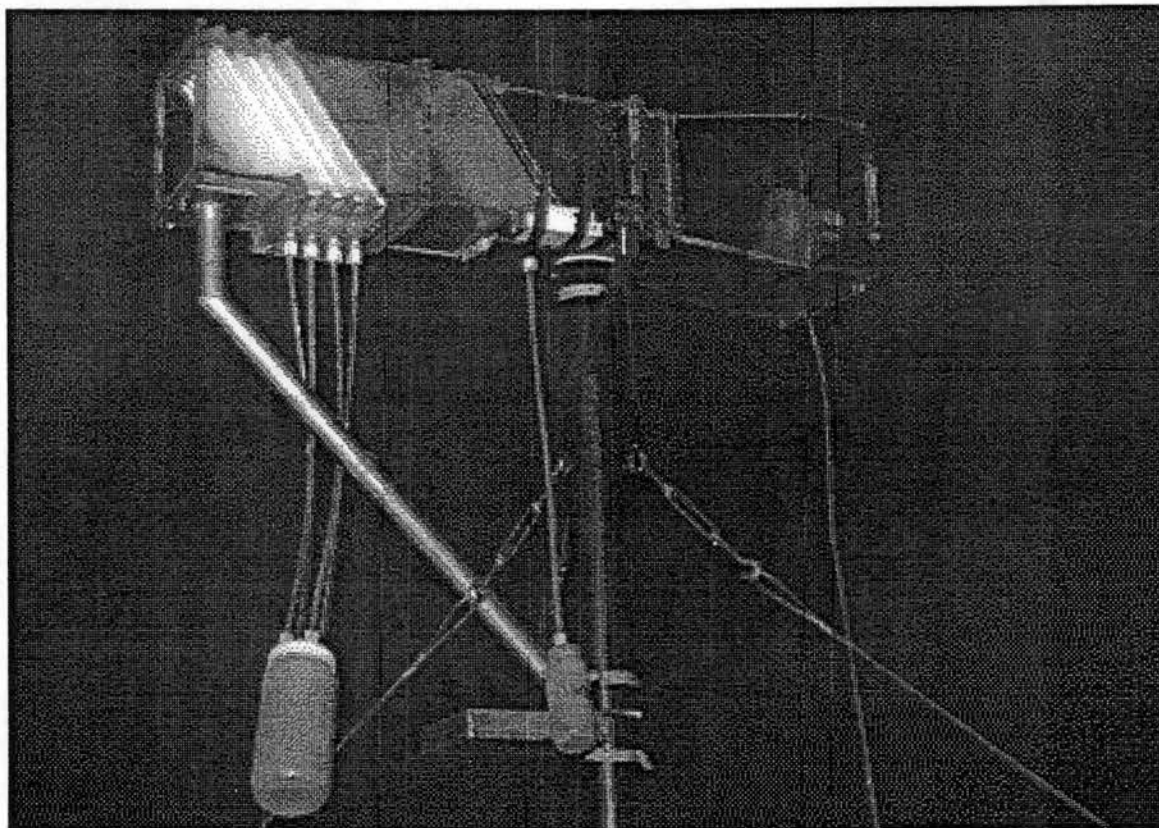


Figure 2.2. The Caltech Active Strand Cloudwater Collector with a size-fractioning inlet. The small drop fraction includes drops with diameters between 4 and 23 μm , while the large drop fraction contains drops larger than 23 μm .

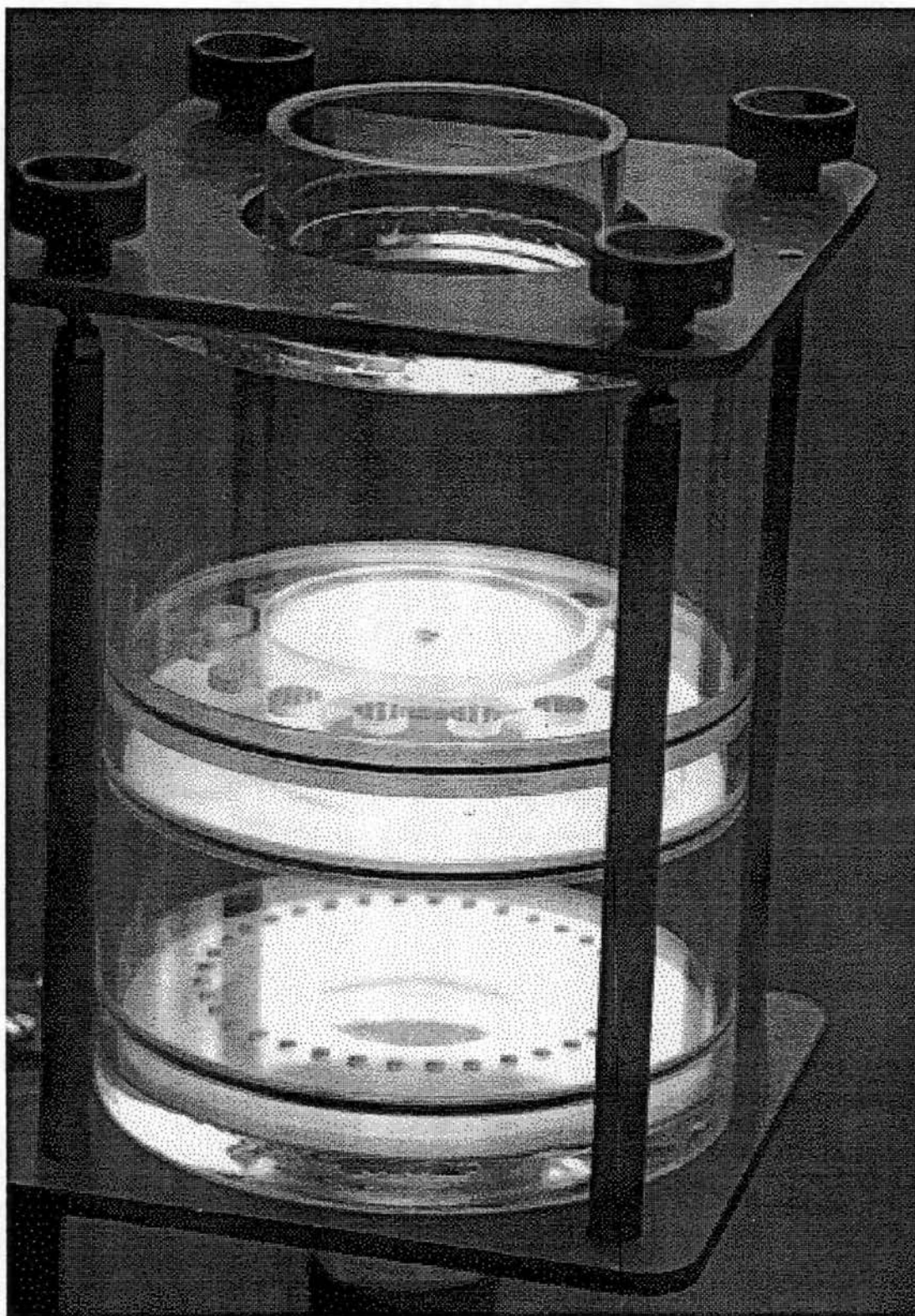


Figure 2.3. The ETH cloud impactor with 50% lower size-cuts of 3 and 10 μm .



Figure 2.4. The IESL cloud impactor. The impaction plates are interchangeable with 50% lower size-cuts of 3, 4, 10, 12, 15, 20, and 30 μm .

flow rate used in the ETH impactor (418 liters/minute). Both the ETH and IESL impactor are jet impactors and provide a sharper size cut between drop size fractions than is available with the size-fractionating CASCC. This advantage comes at the expense of a lower flow rate, meaning longer periods, generally exceeding one hour, are required to collect enough sample volume for trace chemical analysis.

In addition to the cloud collectors a Particle Measurement Systems CSASP-100-HV drop sizing probe was used to characterize the cloud drop size distribution. The drop size distribution is obtained from measurements of forward light scattered by drops when they are drawn across a focused laser beam.

Inorganic gases (SO_2 , HNO_3 and NH_3) were measured using glass annular denuders (Oberholzer et al., 1992). Two denuders were operated in parallel, one with KOH coating to capture SO_2 and HNO_3 and the other with H_3PO_4 coating to collect NH_3 . The denuders were operated at a flow rate of 17 liters/minute and with a time resolution of several hours. The denuders were extracted with 3.0 ml deionized water in the field immediately after sampling. The extract solutions were refrigerated for later analysis.

2.2. Chemical preservation and analyses

When sufficient sample volumes were available, aliquots of cloudwater were removed shortly after collection for pH analysis and for preservation of total S(IV), HMS, total formaldehyde, hydrogen peroxide and total metal iron and manganese (Appendix A). Speciation of Fe(II) and Fe(III) was measured at the sampling sites in the 1996 sampling campaign. Acid titration experiments were conducted in the laboratory for samples collected

in 1994 and at the sampling sites in the 1995/1996 sampling campaign. A summary of chemical preservation and analyses is listed in Table 2.1.

Table 2.1. Summary of chemical preservation and analyses

Analyte	Preserving Chemicals	Analytical Method	Instrumentation	Reference
Total S(IV)	HCHO CDTA NaOH Catalase	Schiff Reaction, Pararosaniline	Spectrophotometer	Dasgupta et al., 1980
HMS	HCHO CDTA NaOH Catalase	Schiff Reaction, Pararosaniline	Spectrophotometer	Dasgupta et al., 1980
Total Formaldehyde	NaHSO ₃ CDTA NaOH	DDL	Spectrofluorophotometer	Dong and Dasgupta, 1987
Hydroperoxides	POPFA KHPthalate Peroxidase EDTA	POPFA	Spectrofluorophotometer	Lazrus et al., 1989
Total Fe	HNO ₃	Atomic Absorption	Graphite Furnace Atomic Absorption Spectrophotometer	
Total Mn	HNO ₃	Atomic Absorption	Graphite Furnace Atomic Absorption Spectrophotometer	
Fe ²⁺ and Fe ³⁺	DPKBH NH ₄ Ac	DPKBH	Spectrophotometer	Pehkonen and Hoffmann, 1992

Measurement of sample pH was made using an Orion 250A portable pH meter equipped with a microelectrode (Model MI-710, Microelectrodes, Inc.) calibrated with pH 4 and 7 buffers. The microelectrode allows for analysis of small sample volumes (approximately 15 µl).

Total S(IV) was preserved by addition of a S(IV) preserving solution containing formaldehyde and Na₂CDTA and analyzed spectrophotometrically (Hitachi U-2000 UV/VIS spectrophotometer) according to the pararosaniline method (Dasgupta et al., 1980; Lodge 1989). S(IV) in samples was preserved in the form of HMS, a reaction product of S(IV) with formaldehyde. It should be noted that the amount of formaldehyde in the preservative solution is critical for method sensitivity (Appendix B), since formaldehyde not only acts as a preservative but is also involved in the chemical reactions leading to the color development. CDTA in the preservative solution prevents interference of trace metals in the analysis. A catalase solution is also added to the samples to destroy any H₂O₂ in cloud and fog samples. The detailed analysis procedure is described in Appendix B. The limit of detection (LOD, determined as three times the standard deviation for blank samples) is 0.25 μmole/l. The standard deviation ranged from 4.0% to 5.5% for analyses of 1.0 to 50 μM standard S(IV) solutions.

The HMS aliquot was processed first by addition of H₂O₂ for destroying free S(IV) followed by addition of catalase solution (activity of 24 σ unit/μl) to destroy excess H₂O₂. HMS remaining in this aliquot was preserved by addition of the S(IV) preserving solution described above and analyzed by the same method used for total S(IV). The LOD for HMS is 0.5 μmole/l.

The peroxide aliquot was stabilized by reacting the peroxides with parahydroxyphenylacetic acid (POPHA) to produce a stable dimer which could later be analyzed spectrofluorometrically (Perkin Elmer MPF-44B fluorescence spectrophotometer) in the laboratory (Lazrus et al., 1985). One molecular dimer is produced from one molecule of

hydroperoxide. The hydroperoxide concentrations in cloud and fog water can therefore be determined by measuring the dimer concentration. The technique measures total hydroperoxides including hydrogen peroxide and organic hydroperoxides. At typical atmospheric conditions organic hydroperoxides only contribute less than 1% of the total hydroperoxides in precipitation and cloud water samples (Lazrus et al., 1985). The measured hydroperoxide concentrations, therefore, are representative of hydrogen peroxide concentrations. The LOD for hydroperoxides is 0.1 $\mu\text{mole/l}$. The standard deviations are 1.2% and 2.4% for analyses of 1.6 μM and 8.0 μM standard H_2O_2 solutions, respectively. Detailed procedures for sample preservation, analysis and standard calibration are described in Appendix C.

The total formaldehyde aliquot was preserved in the form of HMS by addition of sodium bisulfite and Na_2CDTA . HMS can later be decomposed to formaldehyde and analyzed by a fluorometric method (Perkin Elmer MPF-44B fluorescence spectrophotometer) utilizing the Nash reaction (Dong and Dasgupta 1987). The measured total formaldehyde includes free and complexed formaldehyde present in cloud and fog water. The fluorometric method is only sensitive to formaldehyde; other aldehydes do not interfere with the analysis. The LOD for total formaldehyde is 0.4 $\mu\text{mole/l}$. The standard deviations are 12% and 5% for analyses of 4.1 μM and 20 μM standard formaldehyde solutions, respectively (Appendix D).

The total iron and manganese aliquot was preserved by addition of 9.7% HNO_3 and analyzed with a Varian SpectrAA-20 atomic absorption spectrometer equipped with a Varian GTA-96 graphite furnace and automatic injection accessories. Only a small sample volume (20 μl) is required by the autosampler, therefore replication is possible for the total Fe and Mn

analysis. Cloudwater samples for the total metal aliquot were not filtered before preservation, therefore measured iron and manganese concentrations represent the total of dissolved and particulate forms. The LOD for total iron is 0.18 μM . The standard deviation is less than 10% for low standard concentrations ($< 0.5 \mu\text{M}$) and less than 5% for high standard concentrations ($> 0.5 \mu\text{M}$). For 119 samples analyzed with three replicates 86.5% of the samples had standard deviations less than 5%, 11% of the samples had standard deviations between 5 and 10%, and 2.5% of the samples had standard deviations larger than 10%. The LOD for total Mn is 0.02 μM . The standard deviation is less than 2% for analyses of 0.09 to 0.36 μM of standard Mn solutions.

Speciation of Fe(II) and Fe(III) was performed spectrophotometrically (Pehkonen et al., 1992). This method allows for simultaneous measurement of dissolved Fe(II) and Fe(III). Dissolved Fe(II) and Fe(III) can both react with a chelating reagent, di-2-pyridyl ketone benzoylhydrazone (DPKBH). The complexed form of Fe(II) has two absorption peaks at 377 nm and 660 nm respectively, whereas the Fe(III)-DPKBH complex only has one absorption peak at 377 nm. Absorption at 660 nm permits Fe(II) to be quantified; absorption at 377 nm yields the amount of total dissolved Fe. Fe(III) can be determined by subtracting the amount of Fe(II) from the total Fe. The two oxidation states of Fe are interchangeable in cloudwater. Dynamic equilibrium between Fe(II) and Fe(III) depends on cloud conditions, for example types of oxidants in cloudwater and solar irradiation. Therefore Fe(II) and Fe(III) concentrations should be analyzed as quickly as possible after cloudwater is taken from collectors, and should be finished within minutes. During the fog events in California's San Joaquin Valley where iron speciation was measured sampling periods were usually a few

hours. Iron speciation was finished on site within 30 minutes after the samples were taken from the collectors. The long sampling periods may influence the Fe speciation, especially during daytime. Hence the measured Fe(II) and Fe(III) should be considered as thermal equilibrium concentrations. The detection limits for both Fe(II) and Fe(III) are 0.3 μM . The standard deviations for Fe(II) range from 3.9% to 24% at high concentrations and low concentrations, respectively, while the standard deviations for Fe(III) range from 6.9% to 60% at high and low concentrations, respectively (Appendix E).

Acid titrations were performed by sequential addition of 10 μl of sulfuric acid (1.0 or 10 millinormal) to 1.0 ml fog samples. After each acid addition, the sample was mixed and the pH was measured. The elapsed time between sample collection and titration ranged from a few minutes for some of the samples collected during 1995/96 to several months for the 1994 samples. Samples stored prior to titration were refrigerated at approximately 4 $^{\circ}\text{C}$.

2.3. Laboratory experiments on photochemical reactions of authentic cloudwater and Fe(III)-oxalate solutions

All chemicals were of reagent grade. Stock solutions and solutions for irradiation were freshly prepared using high purity (18 $\text{m}\Omega\text{-cm}$) water on the day of each experiment. Fe(III) and oxalate stock solutions were prepared from $\text{FeCl}_3 \cdot 6\text{H}_2\text{O}$ and $\text{Na}_2\text{C}_2\text{O}_4$. Irradiation solutions were prepared in the absence of light and light was totally excluded before irradiation by wrapping the tubes with aluminum foil. Buffers were not used in the experiments in order to measure pH changes during irradiation.

Ultraviolet-visible spectra of authentic cloudwater were measured with a Hitachi U-2000 UV/VIS spectrophotometer using a 1.0 cm quartz cuvette. A spectrum of pure water was subtracted from the spectra of cloudwater to exclude any contributions from water itself.

Indoor photochemical experiments were conducted in a quartz cuvette with dimensions of 1-cm L x 0.5-cm W x 4.5-cm H. Authentic cloud waters were irradiated with 313 nm light from a xenon lamp (150 W) in a Shimadzu RF-1510 spectrofluorophotometer. Cloudwater pH values were recorded at intervals of several minutes using a portable pH meter equipped with a microelectrode calibrated with pH 4.01 and 7.00 buffers. Hydrogen peroxide in the solutions was preserved immediately upon the completion of photolysis and analyzed spectrofluorometrically (Lazrus et al., 1985) as described above. Fe(II) and Fe(III) were preserved immediately after the completion of photolysis by addition of DPKBH and analyzed within 30 minutes.

Sunlight photochemical experiments were carried out in two kinds of quartz vessels. Irradiation of authentic cloud waters was performed in a quartz cuvette (1-cm L x 0.5-cm W x 4.5-cm H). Irradiation of Fe(III)-oxalate solutions was performed in quartz tubes (11-mm i.d. x 100-mm). Fe(III)-oxalate solutions (20 ml) were irradiated simultaneously in July sunlight from 10:30 to 11:00 am at Colorado State University in Fort Collins, Colorado. The ambient temperature was 32-35 °C. The samples were placed on a black, non-reflective background inclined at approximately 30° from the horizontal with the upper end pointing due north. After pH values of the solutions were stabilized in the outdoor environment in the absence of light, photolysis was initiated. Solution pH values were recorded at intervals of several minutes. Hydrogen peroxide in the solutions was preserved immediately upon the completion of

photolysis and analyzed spectrofluorometrically. Fe(II) and Fe(III) were preserved immediately after the completion of photolysis by addition of DPKBH and analyzed within 30 minutes.

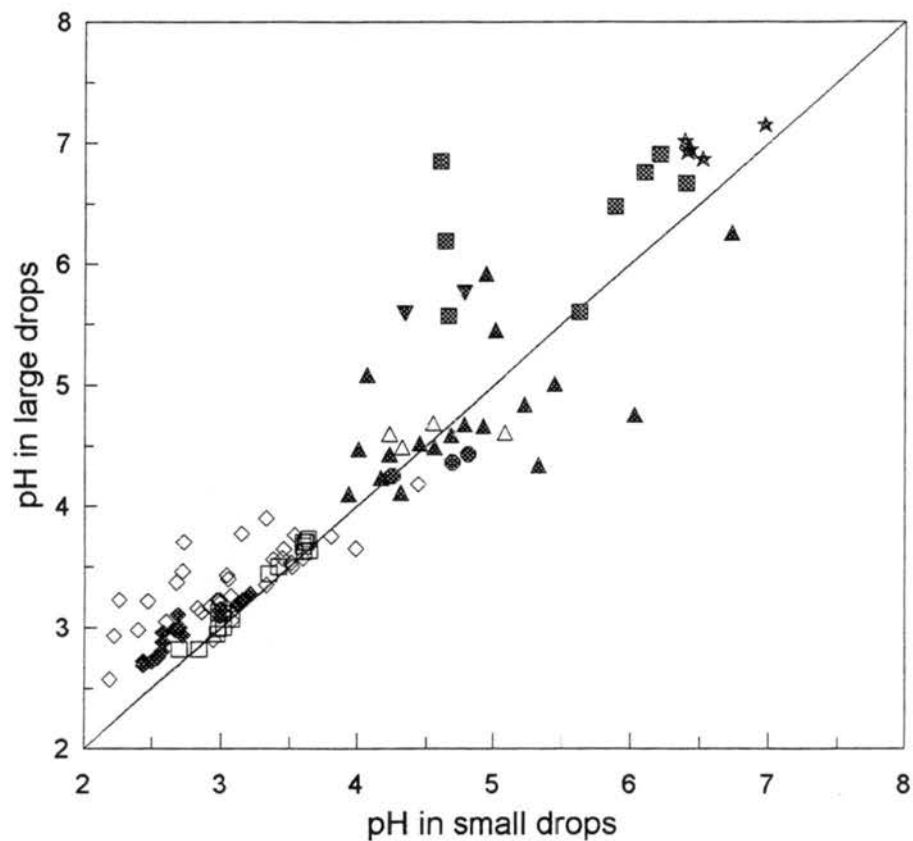
CHAPTER 3. RESULTS AND DISCUSSION

3.1. Drop size dependent cloud/fogwater chemical composition

3.1.1. cloud/fogwater pH

Figure 3.1 compares pH values in the small and large cloud (fog) drop fractions collected at several sites. Most of our measurements of the dependence of cloudwater pH on drop size to date reveal that the small drop fraction tends to be more acidic than the large drop fraction, although in less polluted clouds the reverse is sometimes observed. In several instances differences between small and large drop pH values were substantial, often several tenths of a pH unit or more. This is consistent with the observations of enrichment of strong acid anions (e.g. Cl^- , NO_3^- , SO_4^{2-}) and deficit of base cations (e.g. Na^+ , K^+ , Ca^{2+} , Mg^{2+}) in the small drop fraction (Bator and Collett, 1997). In the Oregon clouds we observed higher pH values in the small drop fraction for some of the samples. In these samples all major ions are enriched in the small drop fraction.

Differences in droplet acidity are expected to affect the oxidation rate of S(IV) in clouds. Although S(IV) oxidation by hydrogen peroxide is largely independent of pH in typical atmospheric conditions, oxidation by ozone, and by oxygen (catalyzed by Fe(III) and Mn(II)), is highly pH dependent. The H^+ dependence of the oxidation rates is nonlinear, hence predictions of aqueous phase S(IV) oxidation rates based on average cloud acidity values would be inaccurate.



- Bakersfield, CA 01/93 and 01/94 □ La Jolla Pk, CA 06/94
- ◇ La Jolla Pk., CA 07/93 ★ KWR, CA 12/95
- Esparto, CA 12/92 ◆ Mt. Mitchell, NC 08/93
- ▼ Woodland Airport, CA 12/92 △ Whiteface Mt., NY 09/93
- ▲ Angora Pk, OR 07/93 - one to one line

Figure 3.1. pH values in cloud/fog drops of small and large drop fractions collected at various locations. Small drop fraction includes drops with diameters between 4 and 23 μm , while large drop fraction contains drops larger than 23 μm .

3.1.2. S(IV), formaldehyde and their complex, HMS

Differences in pH values between small and large drops could also affect S(IV) complexation with formaldehyde. The complexation rate increases with pH and may be competitive with rates of S(IV) oxidation at high pH values. Therefore it is expected that the amount of S(IV) complexed may vary between drops of different sizes.

Fog and cloudwater samples in the study were typically collected at 0.5-2 hour intervals depending on cloud liquid water content. At typical atmospheric conditions time scales of S(IV) depletion through oxidation and complexation are on the order of seconds (see Figure 3.14). Time scales of formaldehyde depletion by complexation are on the order of seconds, except at very low pH ($\text{pH} < 3$) where the complexation of formaldehyde with S(IV) is slow so that formaldehyde depletion may occur over a time scale comparable to the sampling periods. Therefore the measured S(IV) and formaldehyde concentrations should be considered as residual material remaining after cloud/fog drops were separated from their environments.

Concentrations of the different species in the small and large drop size fractions collected by the size-fractionating CASCC are summarized in Table 3.1. Measured total S(IV) represents the sum of free S(IV), formaldehyde-complexed S(IV) (HMS) and other aldehyde-S(IV) complexes possibly present in cloud/fogwater; measured total formaldehyde represents the sum of free (HCHO and $\text{CH}_2(\text{OH})_2$) and S(IV)-complexed formaldehyde (HMS).

Table 3.1. Chemical compositions of cloud/fogwater collected by the size-fractionating CASCC.

Sampling site	Local time	Hydrogen peroxide (μM)		Total S(IV) (μM)		HMS (μM)		
		Small drops	Large drops	Small drops	Large drops	Small drops	Large drops	
La Jolla Pk., CA 07/01/1993	00:50-01:50	12.8	16.4	0.9	ND*	1	0.5	
	01:56-02:29	15.3	17.6	1	0.6	1.1	0.5	
	02:31-03:34	15.2	16.6	0.9	ND	1.2	ND	
	03:38-04:05	13.7	14.3	1.4	ND	0.9	0.5	
	04:06-05:20	17.1	18.3	1	0.5	1	0.8	
	05:26-05:46	23.7	25	0.7	ND	0.8	0.5	
07/05/1993	21:48-23:23	40.5	41.4	4.4	2.6	3	2.3	
	01:03-02:04	55.8	61.4	4.6	2.4	3.4	2.4	
	02:31-03:36	66.6	71.8	5.4	2.7	4.1	2.4	
	04:04-05:18	56	51.7	5.8	1.7	3.7	1.8	
Angola Pk., OR 07/14/1993 07/15/1993	09:57-11:01	6.7	13.8	7.8	0.8	4.9	0.8	
	11:11-13:05	18.6	28.7	1.4	0.6	1.2	0.7	
	17:55-18:56	23.8	40	ND	ND	1.5	ND	
	19:40-23:12	16.6	29.5	0.5	ND	0.6	0.5	
Mt. Mitchell, NC 08/20/1993 08/22/1993	23:56-00:15	54.3	55.8	0.9	1.2	1.1	0.7	
	00:25-02:55	81.2	67.4	0.8	0.8	0.7	-	
	03:05-05:15	63.3	56.4	1.1	0.9	1.1	0.9	
	05:25-06:40	44.1	43	1.3	1.6	1.1	0.9	
	06:50-07:13	30.8	-	ND	0.8	0.5	-	
	19:36-22:00 22:05-22:30 22:37-23:24 23:29-23:42 23:47-00:55 01:00-01:20	19:36-22:00	103.2	86.5	0.9	1.2	0.7	-
		22:05-22:30	69.3	57	1.3	2	0.9	-
		22:37-23:24	64.9	66.9	1	0.5	0.5	0.8
		23:29-23:42	-	-	0.4	1.3	0.6	-
		23:47-00:55	75.6	66.2	0.9	2.2	0.5	1.4
		01:00-01:20	75	-	0.8	-	0.5	-
	01:24-02:15 02:20-02:50 02:55-03:31 03:36-03:57 04:02-04:55	01:24-02:15	56.9	53.7	1.9	3	0.9	2.1
		02:20-02:50	43.9	39.7	1	1.8	0.8	ND
		02:55-03:31	21.6	16	0.9	1	0.9	0.7
		03:36-03:57	11.8	8	1	1	1.2	0.9
		04:02-04:55	11.8	15.5	0.8	0.6	ND	0.6
Whiteface Mt., NY 09/18/1993		23:01-00:50	13.6	20.3	4.5	0.8	3.9	0.9
	01:06-02:10	-	12	-	1.4	1.7	1.7	
	02:30-03:55	12.8	13.2	ND	ND	ND	ND	
	04:20-06:05	4.4	4.1	ND	ND	ND	ND	
Bakersfield, CA 01/15/1993	02:50-07:00	1.4	0.3	28.3	2	29.8	6.5	
	07:45-09:45	0.7	3.7	68.2	1.1	37.8	0.5	
	09:50-10:10	-	21.3	-	1.6	-	1.8	
	10:10-11:20	-	24.2	-	1.1	-	3.1	

* ND - Not detected; ** - Sample not available

Table 3.1. (continued) Chemical compositions of cloud/fogwater collected by the size-fractionating CASCC.

Sampling site	Local time	pH		Formaldehyde (μM)		
		Small drops	Large drops	Small drops	Large drops	
La Jolla Pk., CA 07/01/1993	00:50-01:50	3.33	3.9	18.4	11.1	
	01:56-02:29	3.46	3.64	17.6	9.3	
	02:31-03:34	3.54	3.76	16	9.4	
	03:38-04:05	3.82	3.75	16.5	8.6	
	04:06-05:20	3.45	3.57	16.3	10.9	
	05:26-05:46	3.33	3.35	17.4	14.8	
	07/05/1993	21:48-23:23	3.03	3.12	28.2	18.2
		01:03-02:04	2.99	3.23	22	15
		02:31-03:36	2.99	3.2	27.5	16.8
		04:04-05:18	2.92	3.17	29.9	20.8
Angola Pk., OR 07/14/1993	09:57-11:01	5.23	4.84	8.6	4.4	
	11:11-13:05	4.92	4.66	10.4	5.1	
	07/15/1993	17:55-18:56	6.03	4.76	21.8	6.4
		19:40-23:12	5.45	5.01	9	5.5
Mt. Mitchell, NC 08/20/1993	23:56-00:15	2.99	3.15	20.2	15.5	
	00:25-02:55	2.99	3.09	22.5	-	
	03:05-05:15	3.12	3.19	18.4	14.5	
	05:25-06:40	3.21	3.28	17.9	13.2	
	06:50-07:13	3.16	3.23	19.8	-	
	08/22/1993	19:36-22:00	2.44	2.72	36.1	-
		22:05-22:30	2.58	2.96	26.1	19.5
		22:37-23:24	2.67	2.98	26.7	-
		23:29-23:42	2.57	2.8	25.9	-
		23:47-00:55	2.5	2.72	26.5	22.1
		01:00-01:20	2.54	2.75	27.4	-
		01:24-02:15	2.44	2.69	26.5	23.6
		02:20-02:50	2.58	2.88	25.8	23.8
	02:55-03:31	2.72	2.94	26.8	31.4	
	03:36-03:57	2.69	3.11	34.5	16.8	
	04:02-04:55	2.7	3	31.7	-	
Whiteface Mt., NY 09/18/1993	23:01-00:50	5.08	4.61	13	13.8	
	01:06-02:10	4.32	4.49	9.2	6.2	
	02:30-03:55	4.23	4.6	9.9	5.7	
	04:20-06:05	4.55	4.69	4.9	4.5	
Bakersfield, CA 01/15/1993	02:50-07:00	5.89	6.48	133.8	82.4	
	07:45-09:45	6.4	6.67	183.3	118.4	
	09:50-10:10	6.21	6.91	162.5	97.4	
	10:10-11:20	6.1	6.76	175.6	111.5	

Significantly higher total S(IV) concentrations were associated with small drops in the stratus clouds at La Jolla Pk., California, Angora Pk., Oregon and in the winter fog at Bakersfield, California. Higher HMS concentrations were also associated with small drops during these cloud and fog events. Higher concentrations of HMS in small drops might result from small cloud condensation nuclei (CCN) containing HMS (Munger et al., 1989); small drops might also favor formation of HMS at conditions of high pH and formaldehyde concentrations. At Mt. Mitchell, North Carolina, on the other hand, the differences of total S(IV) concentrations between the small and large drops are not significant and in some samples slightly higher total S(IV) were found in the large drops.

Total formaldehyde concentrations are much higher than HMS concentrations. Ratios of total formaldehyde to HMS range from 4 to 90 for the different cloud/fog events, indicating the existence of substantial free formaldehyde. The free formaldehyde ranges from 75 - 99% of the total formaldehyde for the different cloud/fog events.

Total formaldehyde concentrations were almost exclusively enriched in the small drops. Gas-aqueous equilibrium calculations show that aqueous formaldehyde concentrations should be in equilibrium with gaseous formaldehyde concentrations (Appendix F). Consequently, it is difficult to explain why formaldehyde concentrations are observed to vary as a function of drop size in the cases discussed here when only free formaldehyde is considered. Inclusion of S(IV)-complexed formaldehyde (HMS) could not account for the size dependence, since HMS contributes only a small part of the total formaldehyde. Investigation of other products of formaldehyde reaction in the drops might be helpful for explaining the drop size dependence. Formaldehyde has been observed to react with

nitrogen-containing compounds, including NH_3 , in the aqueous phase (Walker, 1964; Hoffmann and Calvert, 1985).

HMS concentrations are typically close to the total S(IV) concentrations in the samples (Figure 3.2), indicating that most residual S(IV) is present as HMS. This result is consistent with the presence of free formaldehyde and H_2O_2 in the clouds. Once sulfur dioxide is dissolved into droplets, it can be oxidized to S(VI) or react with formaldehyde to form HMS. In many situations this occurs quickly enough so that little free S(IV) remains by the time the samples are collected and preserved. For some of the samples in Figure 3.2 HMS concentrations are slightly higher than total S(IV) concentrations, but these differences are generally within the analytical error. The 95% confidence limits for 1.0 and 5.0 $\mu\text{mole/l}$ standard analyses are $1.0 \pm 0.2 \mu\text{mole/l}$ and $5.0 \pm 0.6 \mu\text{mole/l}$ respectively.

3.1.3. Hydrogen peroxide

Hydrogen peroxide data collected during the cloud events at different sites can be grouped into three categories based on their aqueous hydrogen peroxide concentration levels (Figure 3.3). Group one contains clouds with very high aqueous hydrogen peroxide concentrations, including coastal stratus clouds at La Jolla Pk, California and frontal/orographic clouds at Mt. Mitchell, North Carolina. Group two includes clouds with medium hydrogen peroxide concentrations, including coastal stratus clouds at Angora Pk, Oregon and frontal/orographic clouds at Whiteface Mt., New York. The last group is the radiation fogs in the San Joaquin Valley of California, with the lowest hydrogen peroxide concentrations. Interestingly, cloudwater pH values can also be grouped into similar sample

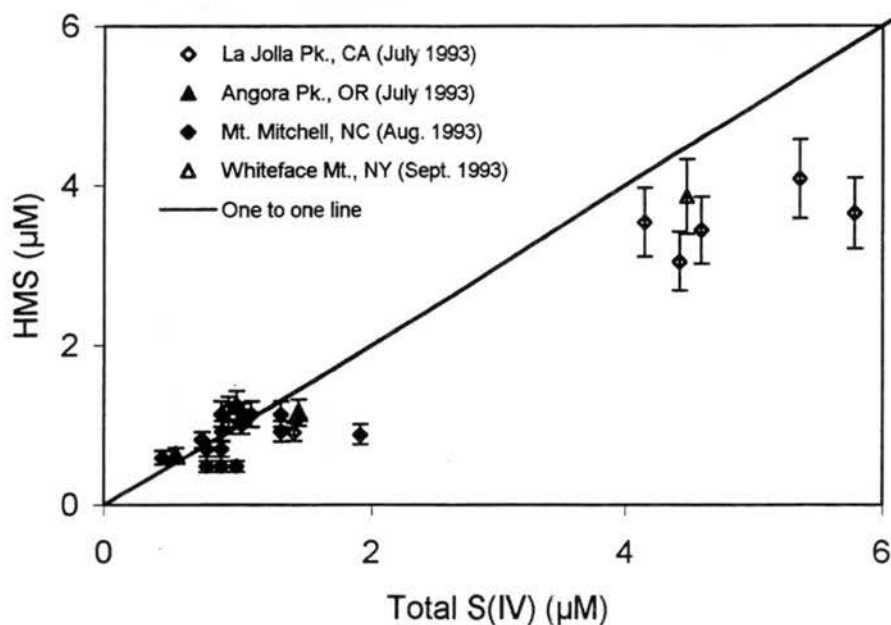
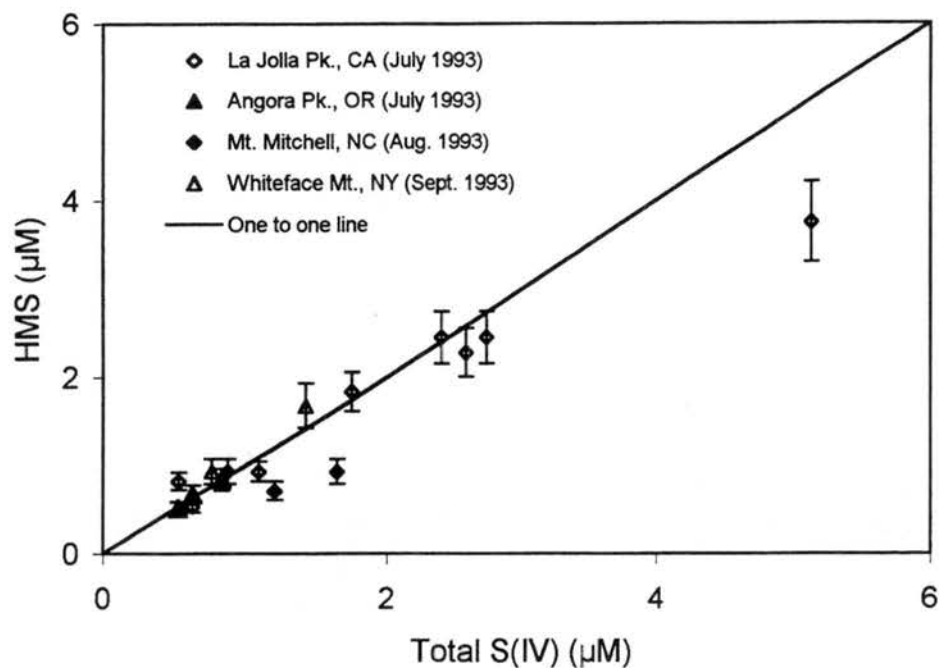


Figure 3.2. Comparison of total S(IV) and HMS concentrations in cloudwater collected by the sf-CASCC at several locations. The top panel represents concentrations in large drops and the bottom panel represents concentrations in small drops. The errors are calculated based on three standard deviations from analysis of standard solution.

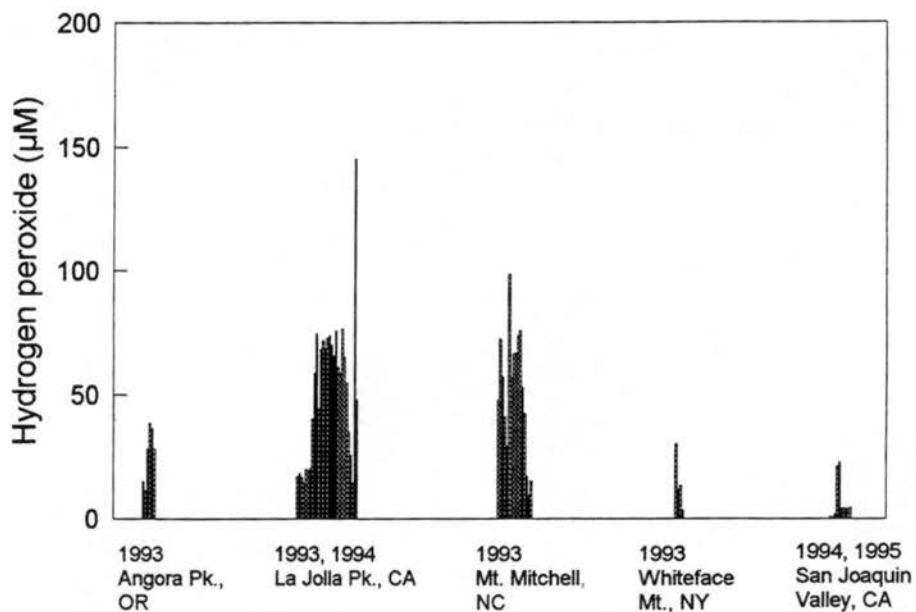


Figure 3.3. Aqueous hydrogen peroxide concentrations in bulk cloudwater collected by a CASC2 which collects drops with diameters larger than $3.5 \mu\text{m}$. Each bar in the graph represents the concentration of cloudwater collected during one sample period in the cloud events.

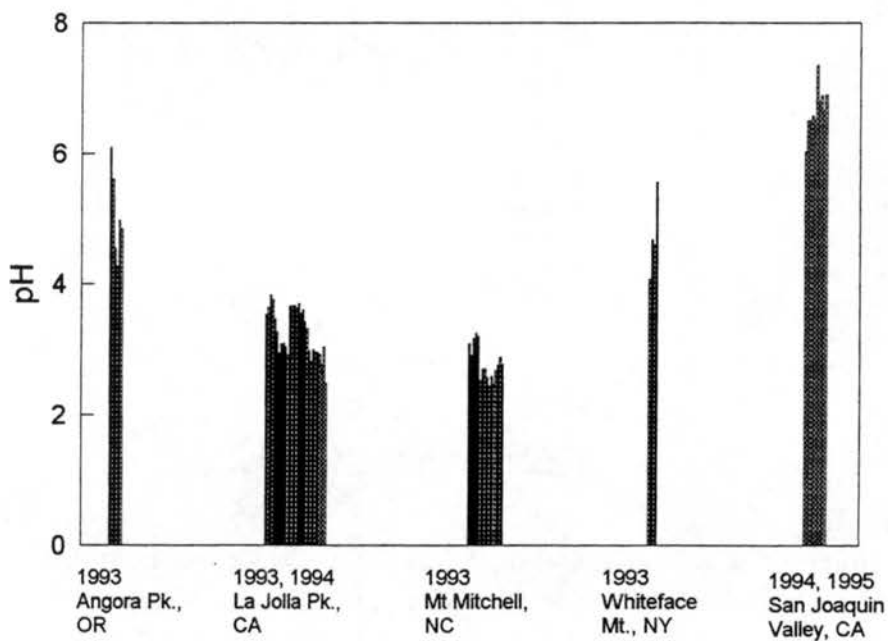


Figure 3.4. Corresponding pH values for the bulk cloud samples in Figure 3.3.

sets with a negative correlation between the hydrogen peroxide concentration and pH. Clouds/fogs in this data set having the highest aqueous H_2O_2 concentrations contain the lowest cloud pH and vice versa (Figures 3.3 and 3.4).

From the measured hydrogen peroxide concentrations and pH values of cloudwater at the different locations, preliminary results can be drawn with respect to the importance of S(IV) oxidation by H_2O_2 . Very high H_2O_2 concentrations and low cloud pH values ($\text{pH} < 4$), during the cloud events at La Jolla Pk., CA and Mt. Mitchell, NC, suggest that S(IV) oxidation by H_2O_2 is the dominant oxidation pathway. In contrast, fogwater in California's San Joaquin Valley collected on 1/15/94 had very low aqueous H_2O_2 concentrations and high pH values ($\text{pH} > 6$), indicating that S(IV) oxidation by oxidants other than H_2O_2 is important. During the cloud interception events at Angora Pk., OR and Whiteface Mt., NY, relatively high aqueous H_2O_2 concentrations and cloudwater pH ($4 < \text{pH} < 6$) suggest that S(IV) oxidation through several pathways (H_2O_2 , O_3 and O_2 with trace metal catalysis) can all be important.

Kinetic calculations of aqueous S(IV) depletion through oxidation by H_2O_2 show that the characteristic time for the S(IV) oxidation is on the order of seconds. Fast reaction between free S(IV) and H_2O_2 excludes coexistence of the two species. Field measurements show a strong negative correlation between aqueous S(IV) and H_2O_2 concentrations in most of the cloud samples (Figure 3.5). When a significant amount of H_2O_2 was present in cloudwater, little S(IV) was detected. In contrast, cloudwater with very low H_2O_2 concentrations possessed significant amounts of total S(IV) and even free S(IV).

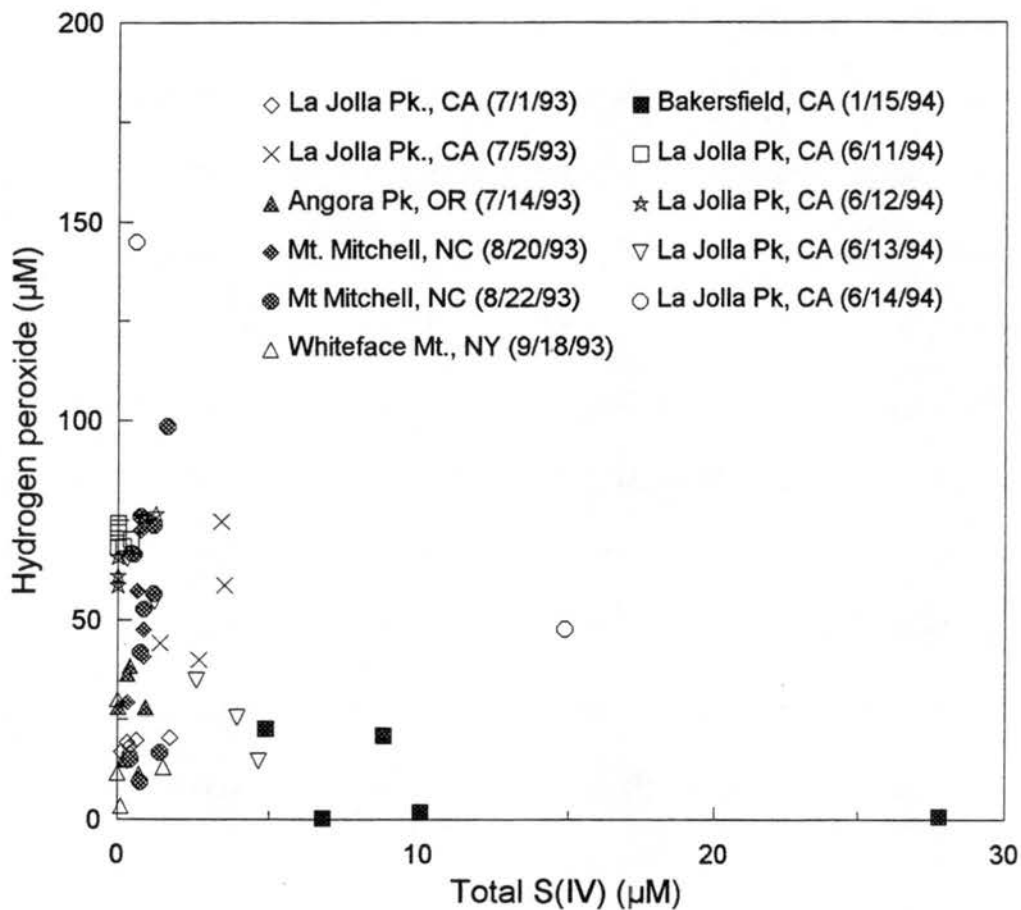
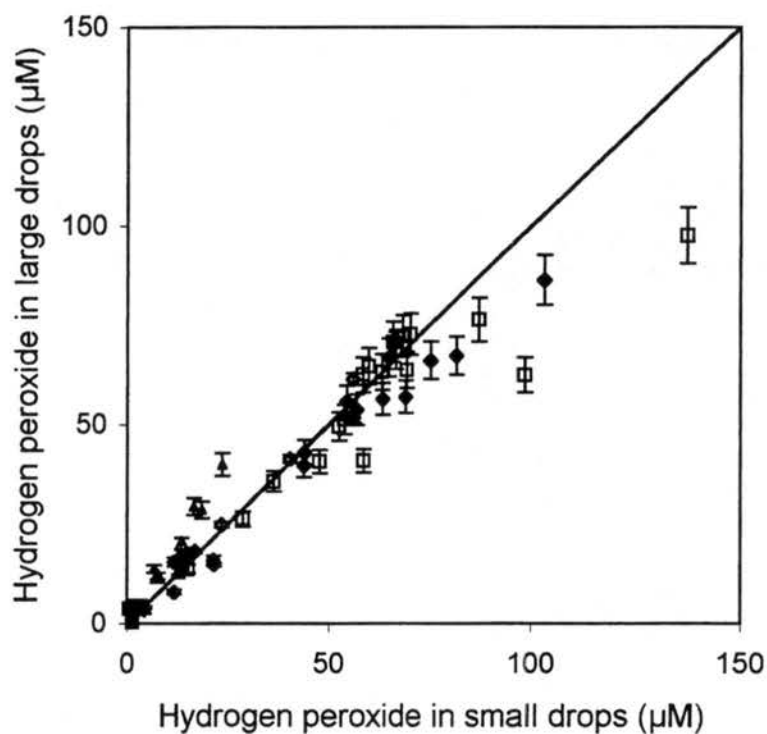


Figure 3.5. Comparison of total S(IV) and hydrogen peroxide concentrations in bulk cloudwater collected by the CASCC2 at several locations.

oxidation. H_2O_2 concentrations in two drop size fractions were compared. No obvious pattern of drop size-dependence of H_2O_2 concentrations was observed. In some cloud/fog samples slightly higher concentrations were found in large drops, while an opposite trend was found in other samples (Figure 3.6). Use of average cloud drop composition to predict the sulfur oxidation rate via the H_2O_2 pathway may not generate large error, since the rate of S(IV) oxidation by H_2O_2 is not dependent on pH over a relevant pH range for atmospheric water and is linear with respect to the H_2O_2 concentration.



- | | |
|--------------------------|---------------------------|
| ◇ La Jolla Pk., CA 07/93 | ▲ Angora Pk., OR 07/93 |
| ◆ Mt. Mitchell, NC 08/93 | △ Whiteface Mt., NY 09/93 |
| ■ Bakersfield, CA 01/94 | □ La Jolla Pk., CA 06/94 |
| × KWR, CA 12/95 | — One to one line |

Figure 3.6. Comparison of hydrogen peroxide concentrations in small and large drops collected at several locations. The small drop fraction includes drops with diameters between 4 and 23 μm , while the large drop fraction contains drops with diameters larger than 23 μm . The errors are calculated based on three standard deviations from analysis of standard solutions.

3.1.4. Iron and manganese

Figures 3.7 and 3.8 illustrate total iron and manganese concentrations in small and large cloud/fog drop fractions. Most of our measurements show that higher total iron and manganese concentrations are associated with large drops, although an opposite trend is present in San Joaquin Valley fog samples and Oregon coastal cloud samples. The differences in concentrations between most large and small drop fractions are significant compared to the analytical standard deviations. For example, eight of nine sample pairs from frontal clouds sampled at Mt. Mitchell, North Carolina and five of seven coastal stratus cloud samples collected at La Jolla Peak, California contained significantly (99% confidence level) higher concentrations of total iron in large drops than were found in small drops.

The observed drop size dependence of trace metal concentrations is consistent with our expectation, based on the fact that trace metals are predominantly found in coarse particles from crustal sources in non-urban areas. Higher concentrations of total iron and manganese associated with small drops at the urban Bakersfield site may reflect the prevalence of local industrial sources for these species. This hypothesis cannot explain, however, the preferential enrichment of iron and manganese in small drops in the clean clouds sampled on the Oregon coast, although long-distance transport of transition metal containing aerosols to the site might be important in this case. Zhuang et al. (1992) measured total Fe in atmospheric aerosol samples collected at several Pacific island stations and aerosols collected from an urban area near the Chinese loess plateau. They found that although the total Fe concentrations in aerosols from the urban area were about 800-900 times greater than total Fe concentrations in remote marine aerosols, the volume-weighted mean Fe/Al ratios in both

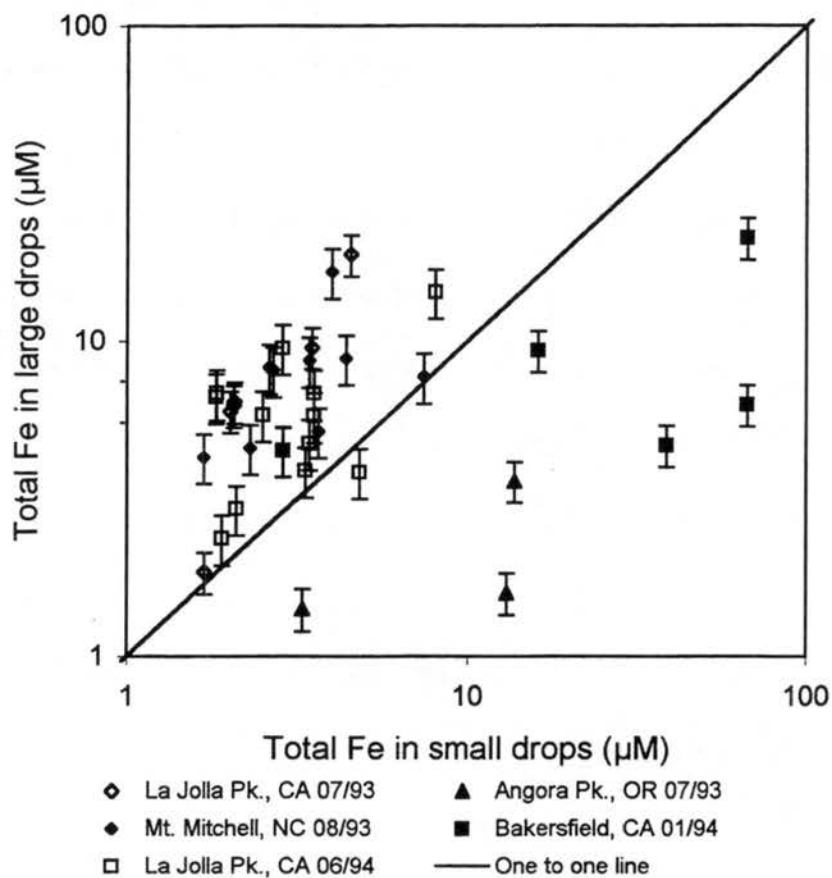


Figure 3.7. Total iron concentrations in small and large drop fractions at several locations. Small drop fraction includes drops with diameters between 4 and 23 μm , while large drop fraction contains drops with diameters larger than 23 μm . The errors are calculated based on three standard deviations from replicates of sample analysis.

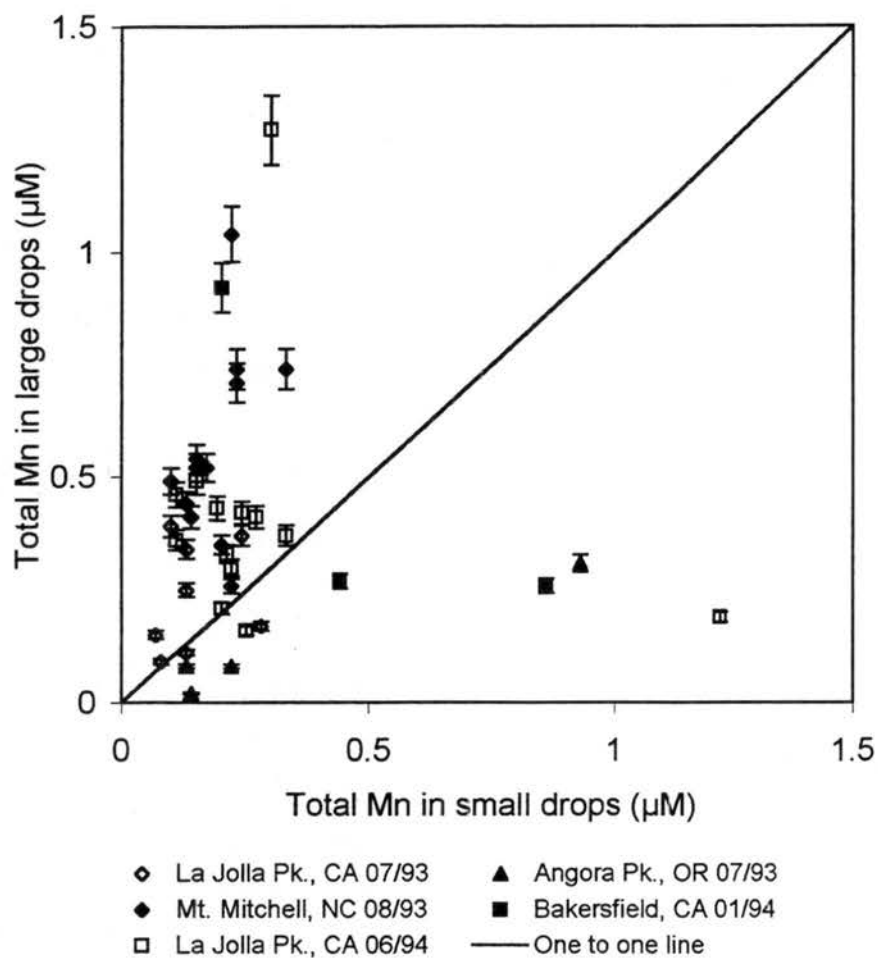


Figure 3.8. Total manganese concentrations in small and large drop fractions at several locations. The cloud collector used is the same as in Figure 3.7. The errors are calculated based on three standard deviations from analysis of standard solutions.

types of aerosols were almost identical. Their results suggested that a long range transport of atmospheric iron from Asia to the central North Pacific region might be an important source of iron in the marine aerosol.

3.1.5. Iron speciation

Both iron and manganese are present in the cloud/fogwater at concentrations high enough to synergistically catalyze S(IV) oxidation. While manganese should exist almost entirely as dissolved Mn(II) in atmospheric liquid water, iron can be present as Fe(II) or Fe(III) and exist as undissolved forms at high pH. Iron containing particles could catalyze S(IV) oxidation at the solid-liquid interface (Faust and Hoffmann, 1985). It is clear that dissolved Fe(III) possesses a catalytic effect toward S(IV) autooxidation, while Fe(II) does not appear to catalyze the reaction.

Iron speciation was also measured on-site for some San Joaquin Valley fog samples collected in 1995 and 1996. Table 3.2 lists concentrations of dissolved Fe(II) and Fe(III) and ratios of Fe(III) to total dissolved Fe in the small and large fog drop fractions for these samples. As for total iron, substantially higher dissolved iron concentrations were associated with small drops, in which the fractions of Fe(III) ranged from 0.88 to 0.93. Hence, most dissolved iron is present as Fe(III) in small drops. In large drops both Fe(III) and Fe(II) concentrations were found to be very low. Fe(III) concentrations were generally below the detection limit. Therefore, fractions of Fe(III) in large drops are not reported here. The submicromolar concentrations of Fe(II) measured in small and large drop fractions were close to the blanks, therefore, the reported fractions of Fe(III) should be considered as lower limits.

While only submicromolar Fe(II) concentrations existed in both small and large drop fractions, surprisingly high Fe(III) concentrations (up to 9 micromolar) were detected in small fog drops. The observed pH range for the fogwater samples was 6.57 - 7.52. From the thermodynamic point of view, at the high fogwater pH ferric ion and its hydroxo complexes are not expected to account for such high dissolved Fe(III) concentrations. To exclude dissolution of particulate Fe(III) during analysis, fogwater samples were filtered through 0.45 μm pore size filters before analysis. No significant differences in Fe(III) concentrations were observed between filtered and unfiltered samples (Table 3.3), suggesting that as high as nine micromolar dissolved Fe(III) can be found in atmospheric water with high pH, where it might exist as various complexed forms.

Table 3.2. Fe(III) and Fe(II) concentrations in the San Joaquin Valley fog droplets

Location and date	Local time	Fe(III) (μM)		Fe(II) (μM)		Fraction of Fe(III)	
		Small drops	Large drops	Small drops	Large drops	Small drops	Large drops
KWR	02:44-06:24	$9.0 \pm 1.9^*$	ND**	0.7 ± 0.5	0.3 ± 0.2	0.93	-
01/01/96	06:24-09:53	4.8 ± 1.9	ND	0.5 ± 0.3	ND	0.9	-
	09:53-11:44	5.2 ± 2.0	ND	0.7 ± 0.5	0.3 ± 0.2	0.88	-
KWR	00:00-05:12	6.2 ± 2.4	ND	0.7 ± 0.5	0.3 ± 0.2	0.9	-
01/02/96	05:12-09:10	6.5 ± 2.5	ND	0.9 ± 0.7	0.5 ± 0.3	0.88	-

* The errors are calculated based on three standard deviations from analysis of standard solutions.

** ND- Not Detectable, the detection limits for both Fe(III) and Fe(II) are $0.3 \mu\text{M}$.

Table 3.3. Fe(III) concentrations in filtered and unfiltered fogwater samples (μM)

Sample Name	Unfiltered	Filtered
KWR 01/01/96 Small drops #1	$9.0 \pm 1.9^*$	8.6 ± 1.3
KWR 01/01/96 Small drops #2	4.8 ± 1.9	5.2 ± 2.0
KWR 01/01/96 Small drops #3	5.2 ± 2.0	5.2 ± 2.0
KWR 01/02/96 Small drops #1	6.2 ± 2.4	6.8 ± 2.6
KWR 01/02/96 Small drops #2	6.5 ± 2.5	6.0 ± 2.3

* The errors are calculated based on three standard deviations from analysis of standard solutions.

3.2. Drop size dependence of S(IV) oxidation

Chemical heterogeneity across the cloud drop size spectrum has been observed for a variety of cloud types. Since S(IV) oxidation rates are functions of drop acidity, aqueous H_2O_2 and catalyst concentrations, the chemical heterogeneity may result in different S(IV) oxidation rates in drops of diverse sizes. Figures 3.10 to 3.13 compare the S(IV) oxidation rates, through different oxidation pathways, in small and large drops for the cloud events at several locations. The calculations are based on the chemical compositions, including H^+ , H_2O_2 , total Fe and total Mn, measured in simultaneously collected small and large drop fractions. The small drop fraction includes drops with diameters between 4 and 23 μm , while the large drop fraction contains drops larger than 23 μm . The assumptions made for gaseous SO_2 and O_3 concentrations are listed in Table 3.4.

Table 3.4. Gaseous SO_2 and O_3 concentrations used in the calculations

Site	P_{SO_2} (ppbv)	P_{O_3} (ppbv)
Bakersfield, CA 01/94	5	7
Mt. Mitchell, NC 08/93	5	50
Angora Pk., OR 07/93	5	30
La Jolla Pk., CA 07/93	5	50
La Jolla Pk., CA 06/94	5	50
Whiteface Mt., NY 09/93	5	50

Note: Gas-liquid equilibria for SO_2 and O_3 were assumed in the calculations.

The rate of S(IV) oxidation by H₂O₂ (given by Equation (3.2) and Figure 3.9) is not a function of hydrogen ion concentration in the pH range observed.

$$-d[S(IV)]/dt = kK_{a1}H_{SO_2}P_{SO_2}[H_2O_2]/(1+K[H^+]) \quad (3.1)$$

$$-d[S(IV)]/dt \cong kK_{a1}H_{SO_2}P_{SO_2}[H_2O_2] \quad @ \text{ pH} > 2.0 \quad (3.2)$$

where k ($7.45 \times 10^7 \text{ M}^{-2}\text{sec}^{-1}$ at 25°C) and K (13 M^{-1} at 25°C) are the reaction constants, K_{a1} is the first dissociation equilibrium constant of SO₂, and H_{SO_2} and P_{SO_2} are the Henry's law coefficient and partial pressure of SO₂ respectively. Drop size dependence of the S(IV) oxidation rate is therefore governed by the size dependence of H₂O₂ concentrations. Only slight differences in H₂O₂ concentrations between the small and large drop fractions were observed for most sampling periods. Since the characteristic time of H₂O₂ depletion by oxidation of S(IV) was estimated based on Equation (1.19) to be 40 minutes at 283 K and at 1 ppb gas partial pressure of SO₂, the time scale is comparable to the sampling periods. Therefore the measured H₂O₂ concentration represents residual H₂O₂ that was left in the collected sample when it was preserved. Based on the measured H₂O₂ concentrations in the small and large drop fractions, only slight differences in S(IV) oxidation by H₂O₂ are present (Figure 3.10). Ratios of the oxidation rates of large to small drops range from 0.6 - 1.6 for all the sampling periods except for the highly polluted Bakersfield fogwater, where larger H₂O₂ concentration differences between small and large drops were observed and the ratios range from 0.2 - 4.5. Generally slightly higher rates of S(IV) oxidation by H₂O₂ were found in small drops in the clouds of Mt. Mitchell, NC, and an opposite size-dependent trend was observed

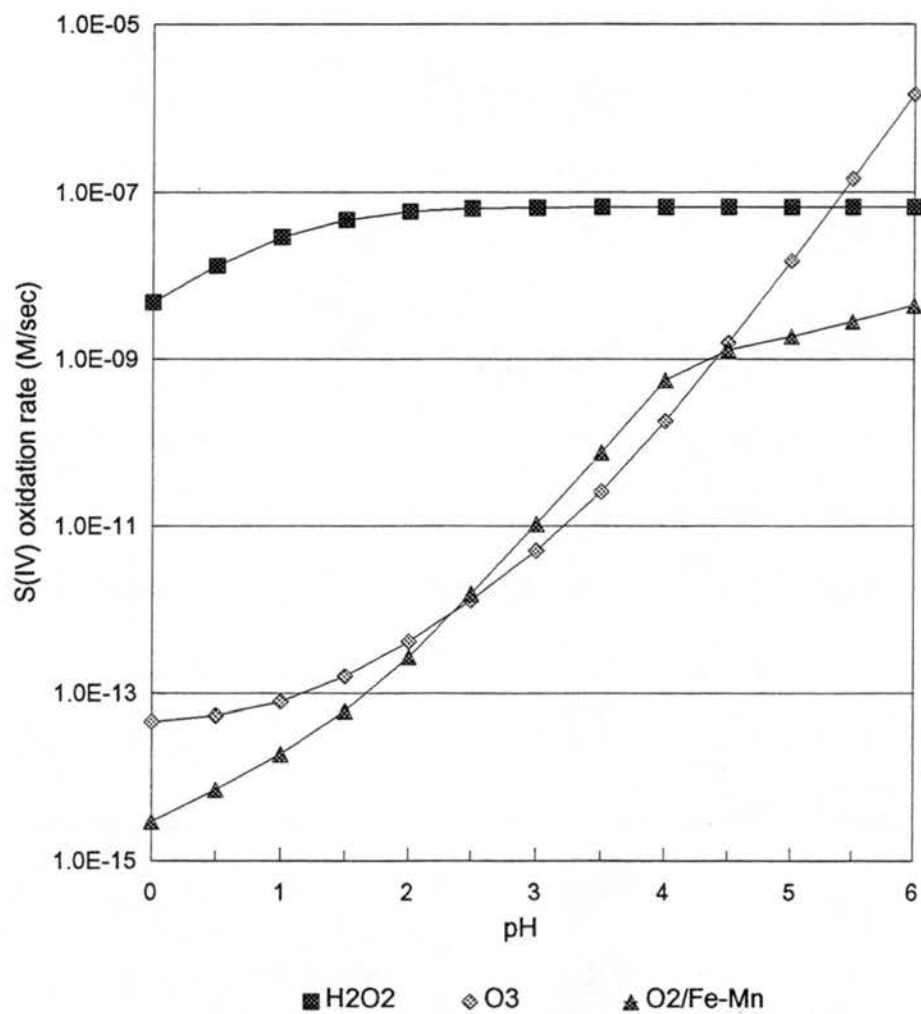
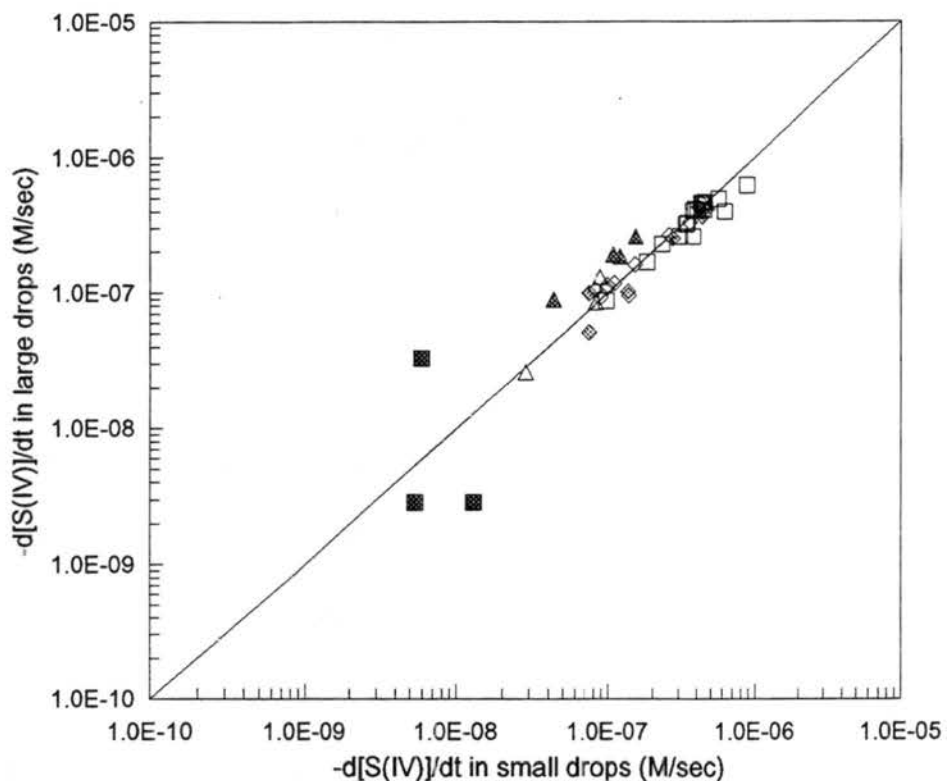


Figure 3.9. Dependence of the oxidation rates for the different paths on pH.
Conditions assumed are: P(SO₂) = 1 ppb; P(O₃) = 40 ppb; [H₂O₂] = 50 μM;
[Fe(III)] = 1 μM; [Mn(II)] = 0.2 μM; T = 283 K.



- Bakersfield, CA 01/1994 ◇ La Jolla Pk., CA 07/1993
- ◆ Mt. Mitchell, NC 08/1993 △ Whiteface Mt., NY 09/1993
- ▲ Angora Pk., OR 07/1993 - One to one line
- La Jolla Pk., CA 06/1994

Figure 3.10. Rates of S(IV) oxidation by hydrogen peroxide in cloud/fog drops of small and large drop fractions collected by the sf-CASCC at various locations. The small drop fraction includes drops with diameters between 4 and 23 μm , while the large drop fraction contains drops larger than 23 μm .

in Oregon clouds. No obvious pattern of a drop size-dependence of S(IV) oxidation by H₂O₂ was found in the clouds of La Jolla Pk., CA, Whiteface Mountain, NY, and in the fog of Bakersfield, CA.

The rate of S(IV) oxidation by ozone is a strong function of drop acidity (Equation (3.3) and Figure 3.9).

$$-d[S(IV)]/dt = (k_0 + k_1 K_{a1}/[H^+] + k_2 K_{a1} K_{a2}/[H^+]^2) P_{SO_2} H_{SO_2} P_{O_3} H_{O_3} \quad (3.3)$$

where k_0 , k_1 , and k_2 are the reaction rate constants for ozone oxidation of SO₂·H₂O, HSO₃⁻ and SO₃²⁻ respectively. K_{a1} and K_{a2} are the first and second dissociation constants of SO₂ respectively. P and H represent the gas partial pressure and Henry's law coefficient. High pH cloud drops can sustain high solubility of SO₂ and rapid S(IV) oxidation by ozone. Therefore any drop size dependence of acidity can result in variations in S(IV) oxidation by ozone among drops of diverse sizes. The observations of the dependence of cloudwater pH on drop size reveal that the large drop fraction tends to have higher pH than the small drop fraction, although in less polluted clouds the reverse is sometimes observed. Calculations of S(IV) oxidation rates by O₃ based on the measured pH values in the small and large drops suggest that the rates tend to be higher in the large drops (Figure 3.11). The drop size dependence of oxidation rates is the same as that of pH. Ratios of the oxidation rates of large to small drops can be as high as 60 in the fog at Bakersfield, CA. In the clouds of Angora Pk., OR, however, a substantially higher oxidation rate is predicted in the small drops for some sampling periods, when the small drop pH values are higher than the pH values measured in large drops.

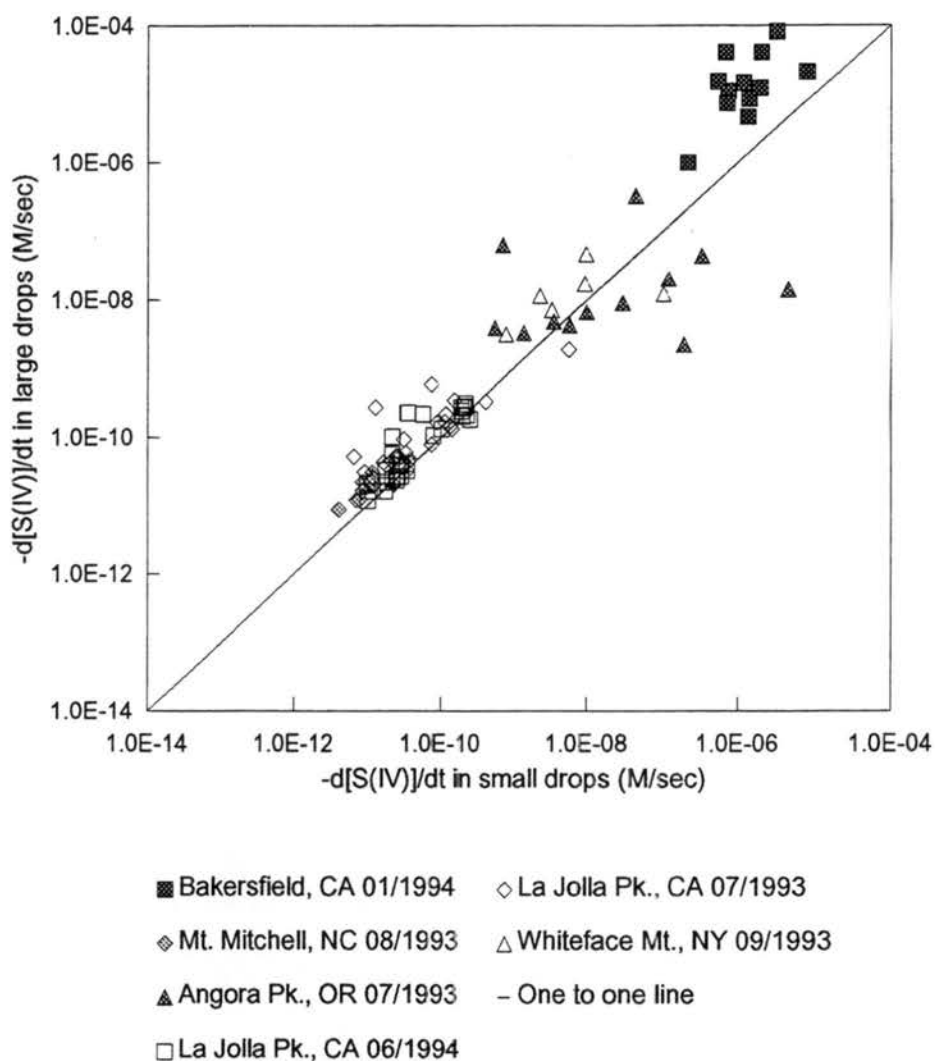


Figure 3.11. Rates of S(IV) oxidation by ozone in cloud/fog drops of small and large drop fractions collected by the sf-CASCC at various locations. A measured ozone concentration of 7 ppb was used in the Bakersfield fog. An ozone concentration of 30 ppb was assumed for the clouds at Angora Pk., Oregon, and 50 ppb was assumed for the clouds at other sites.

The rate of S(IV) autooxidation in the presence of Fe(III) and Mn(II) is a function of both cloud drop pH and trace metal concentrations (Equations (3.4) and (3.5))

$$\text{pH} \leq 4.2$$

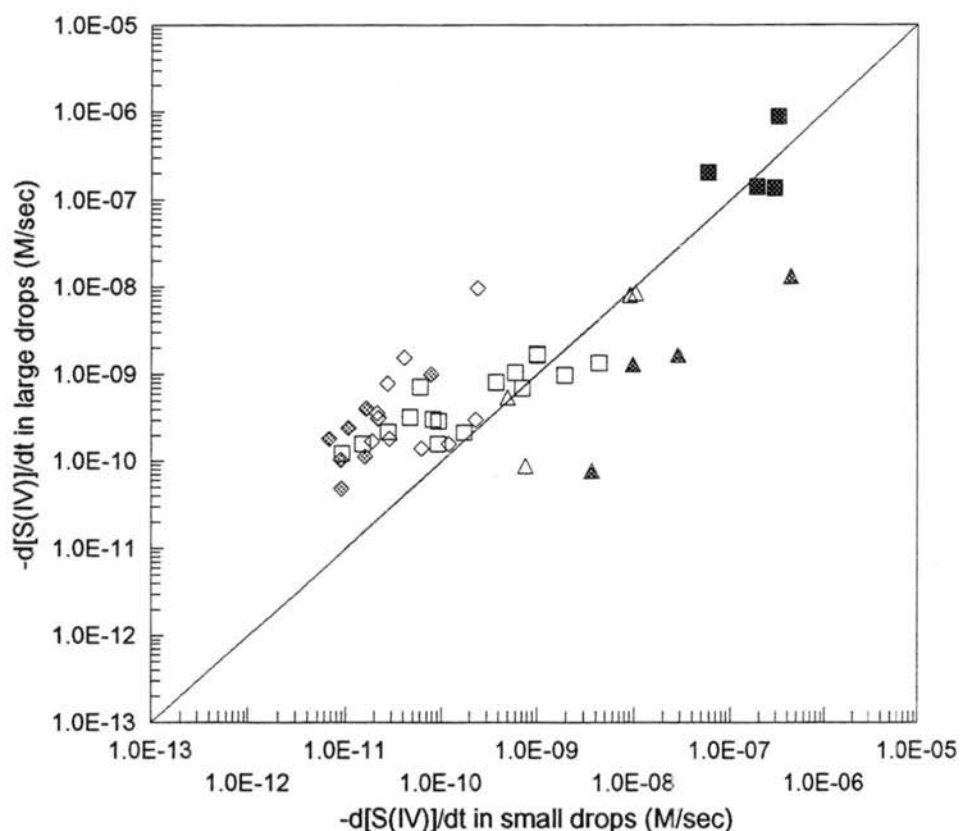
$$-d[\text{S(IV)}]/dt = k_s' [\text{H}^+]^{-0.74} [\text{Fe(III)}][\text{Mn(II)}](1 + K_{a1}/[\text{H}^+] + K_{a1}K_{a2}/[\text{H}^+]^2)P_{\text{SO}_2}H_{\text{SO}_2} \quad (3.4)$$

$$\text{pH} \geq 4.2$$

$$-d[\text{S(IV)}]/dt = k_s'' [\text{H}^+]^{0.67} [\text{Fe(III)}][\text{Mn(II)}](1 + K_{a1}/[\text{H}^+] + K_{a1}K_{a2}/[\text{H}^+]^2)P_{\text{SO}_2}H_{\text{SO}_2} \quad (3.5)$$

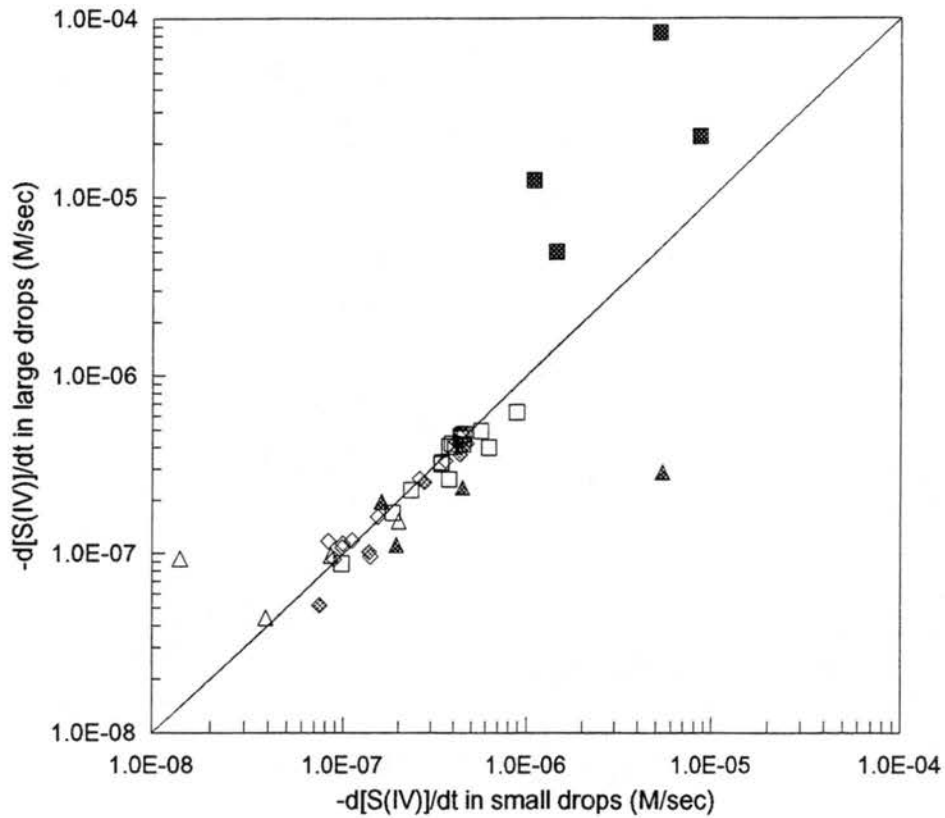
where k_s' and k_s'' are reaction rate constants. High pH and metal concentrations support fast S(IV) autooxidation. For the cloud periods at La Jolla Pk., CA and Mt. Mitchell, NC, both pH and trace metal concentrations were higher in the large drop fraction. The covariance of the two parameters with drop size appears to result in larger differences in S(IV) autooxidation rate than those from S(IV) oxidation by ozone (Figure 3.12). The covariance is also evidenced in the Oregon clouds, but with both higher pH and metal concentrations in the small drops. In the Bakersfield fog, however, the fog drops with higher pH were associated with lower metal concentrations. The inverse correlation of these two parameters reduces the effect of chemical heterogeneity in each individual parameter on S(IV) autooxidation.

Figure 3.13 compares total S(IV) oxidation rates through all three oxidation paths between small and large drop fractions. While substantial differences in the total S(IV) oxidation between the small and large drops are generally predicted in Bakersfield fog, large differences may also be found in some of the sampling periods in Angora Pk., OR and Whiteface Mt., NY. By comparing the S(IV) oxidation rates among the three paths in the clouds and fog at various locations (Figure 3.10 - 3.12) it is clear that when S(IV) oxidation



- Bakersfield, CA 01/1994 ◇ La Jolla Pk., CA 07/1993
- ◆ Mt. Mitchell, NC 08/1993 △ Whiteface Mt., NY 09/1993
- ▲ Angora Pk., OR 07/1993 - One to one line
- La Jolla Pk., CA 06/1994

Figure 3.12. Rates of S(IV) autooxidation catalyzed by both Fe(III) and Mn(II) in cloud/fog drops of small and large drop fractions collected by the sf-CASCC at various locations. The fraction of total Fe assumed to exist as soluble Fe(III) was taken as 25% and soluble Mn(II) was taken as 100% of total Mn for all the samples.



- Bakersfield, CA 01/1994 ◇ La Jolla Pk., CA 07/1993
- ◇ Mt. Mitchell, NC 08/1993 △ Whiteface Mt., NY 09/1993
- ▲ Angora Pk., OR 07/1993 - One to one line
- La Jolla Pk., CA 06/1994

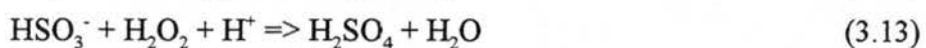
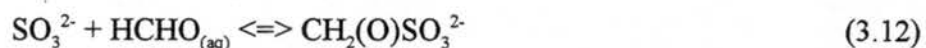
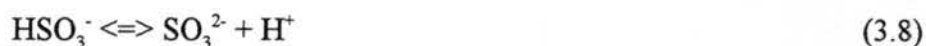
Figure 3.13. Total S(IV) oxidation rates in cloud/fog drops of small and large drop fractions collected by the sf-CASCC at various locations. Assumptions in the calculation are the same as in Figure 3.11 and Figure 3.12.

by ozone and/or autooxidation dominate, substantial differences in S(IV) oxidation rate between the small and large drops can be expected. When S(IV) oxidation by H_2O_2 dominates little difference in S(IV) oxidation rates between drops of the two size fractions is predicted.

3.3. Field observations of S(IV) complexation with formaldehyde and its competition with S(IV) oxidation

3.3.1. S(IV) complexation and oxidation

In comparing the relative importance of S(IV) complexation and oxidation, the major reactions considered here are S(IV) ionization, complexation with formaldehyde and oxidation by H_2O_2 , O_3 and autooxidation catalyzed by trace metals (Equations (3.6) - (3.17)). Rates of S(IV) complexation and oxidation are highly dependent on cloud pH and on formaldehyde and oxidant concentrations. We will examine conditions under which S(IV) complexation with formaldehyde is competitive with rates of S(IV) oxidation, focusing mainly on effects of pH. For comparing the rate of the S(IV) complexation to the oxidation rates, we employ characteristic times of free S(IV) depletion for the individual reactions (Equations (3.11) - (3.17)).





The reaction between free S(IV) and formaldehyde is believed to occur predominantly between HCHO and HSO_3^- or SO_3^{2-} (Equations (3.11) and (3.12)). Therefore, the overall S(IV) complexation rate can be expressed as

$$-d[\text{S(IV)}]/dt = k_1[\text{S(IV)}]\alpha_1[\text{HCHO}] + k_2[\text{S(IV)}]\alpha_2[\text{HCHO}] \quad (3.18)$$

The characteristic time of free S(IV) depletion through complexation can be expressed as:

$$\tau_1 = 1/([\text{HCHO}](k_1\alpha_1 + k_2\alpha_2)) \quad (3.19)$$

where k_1 and k_2 are the rate constants for complexation of HCHO with HSO_3^- and SO_3^{2-} respectively, α_1 and α_2 represent the fractions of total free S(IV) present as HSO_3^- and SO_3^{2-} , and HCHO does not include its hydrated form $\text{CH}_2(\text{OH})_2$. The values of α_1 and α_2 vary with pH. The expression for τ_1 assumes constant pH and formaldehyde concentrations. Although this assumption does not strictly hold over entire cloud events, the results obtained are adequate for purposes of discussion.

S(IV) oxidation through the H_2O_2 pathway is believed to involve mainly bisulfite (Seinfeld, 1986). The S(IV) depletion rate can be expressed as:

$$-d[\text{S(IV)}]/dt = k[\text{H}^+][\text{H}_2\text{O}_2][\text{S(IV)}]\alpha_1/(1+K[\text{H}^+]) \quad (3.20)$$

The characteristic time of free S(IV) depletion through this pathway

$$\tau_2 = (1+K[H^+])/(k[H^+][H_2O_2]\alpha_1) \quad (3.21)$$

is also obtained by assuming the pH and H₂O₂ concentrations in the cloudwater are constant.

S(IV) oxidation by O₃ is believed to occur for all the free S(IV) species (Hoffmann, 1986). The overall free S(IV) depletion rate due to ozone can be expressed as

$$-d[S(IV)]/dt = (k_0\alpha_0 + k_1\alpha_1 + k_2\alpha_2)[S(IV)][O_3] \quad (3.22)$$

where k₀, k₁ and k₂ are the reaction rate constants for SO₂·H₂O, HSO₃⁻ and SO₃²⁻ respectively.

The characteristic time for S(IV) depletion

$$\tau_3 = 1/([O_3](k_0\alpha_0 + k_1\alpha_1 + k_2\alpha_2)) \quad (3.23)$$

is once again obtained by assuming constant pH and ozone concentrations.

S(IV) autooxidation catalyzed by Fe(III) and Mn(II) follows two kinetic paths due to the different pH dependence in low and high pH regions (Ibusuki and Takeuchi, 1987).

At 2.6 ≤ pH ≤ 4.2

$$-d[S(IV)]/dt = k'_s[H^+]^{-0.74}[Fe(III)][Mn(II)][S(IV)] \quad (3.24)$$

At 4.2 ≤ pH ≤ 6.5

$$-d[S(IV)]/dt = k''_s[H^+]^{0.67}[Fe(III)][Mn(II)][S(IV)] \quad (3.25)$$

The characteristic time of S(IV) depletion through this pathway is obtained at constant pH and metal concentrations.

At $2.6 \leq \text{pH} \leq 4.2$

$$\tau_4 = 1 / (k'_s [\text{H}^+]^{-0.74} [\text{Fe(III)}][\text{Mn(II)}]) \quad (3.26)$$

At $4.2 \leq \text{pH} \leq 6.5$

$$\tau_4 = 1 / (k'_s [\text{H}^+]^{0.67} [\text{Fe(III)}][\text{Mn(II)}]) \quad (3.27)$$

We see from the above characteristic time expressions that they are all functions of cloud pH as well as formaldehyde, oxidant, or catalyst concentrations. The characteristic times of S(IV) depletion through complexation and oxidation are compared in Figure 3.14 for relevant ranges of HCHO, oxidant and trace metal concentrations, and pH. The concentration ranges selected for formaldehyde, H₂O₂ and trace metals are representative of our measurements. Dissolved Fe(III) concentrations were assumed to be 25% of the total Fe, and dissolved Mn(II) was assumed to be 100% of the total Mn. Ozone concentrations were not measured. Therefore, a range of concentrations is chosen to represent values typically observed in clean to moderately polluted atmospheres: 10 - 100 ppb. Equilibrium and reaction rate constants used in the calculations are listed in Tables 3.5 and 3.6. From the graph we see when pH increases, the characteristic times for free S(IV) depletion resulting from reactions with HCHO and O₃ decrease, but the characteristic time for depletion via reaction with H₂O₂ increases. The characteristic times of S(IV) depletion via autooxidation reach a minimum value at pH 4.0 due to the highest reaction rate at this pH. When pH is less than 4, the

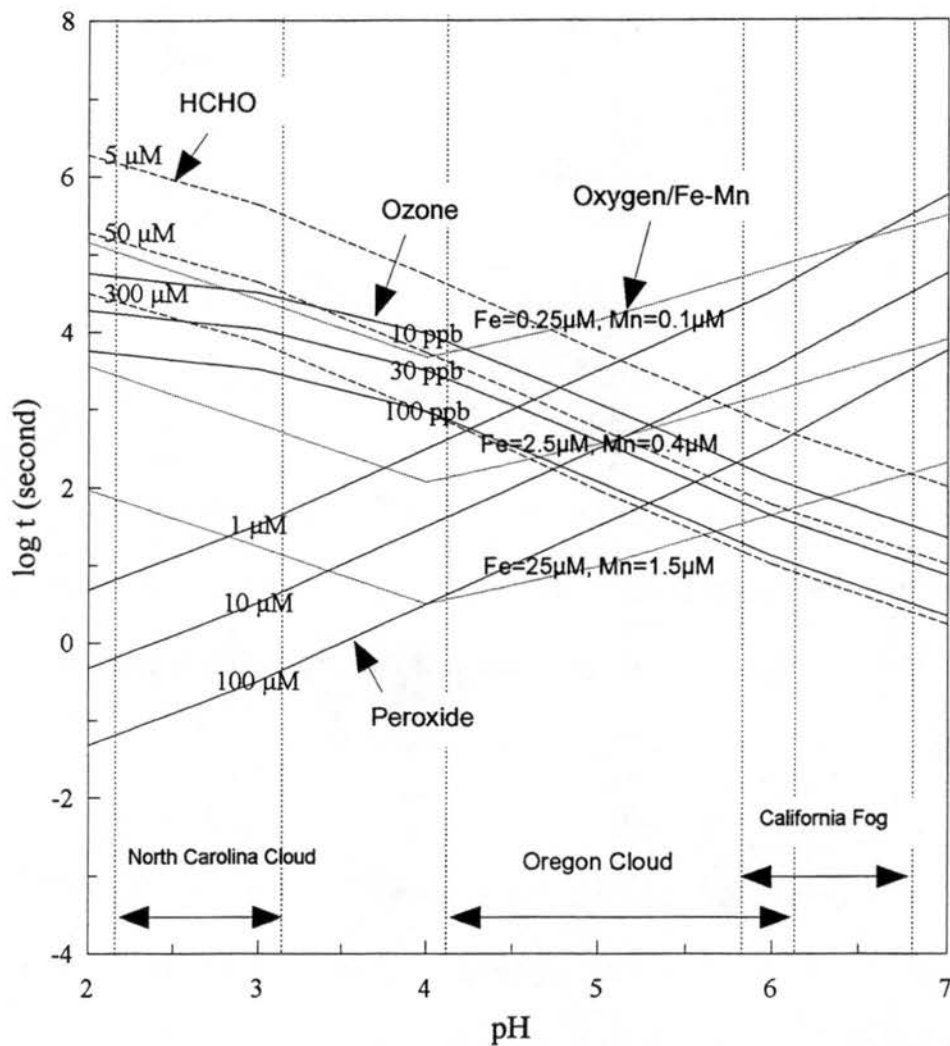


Figure 3.14. A comparison of the characteristic times for S(IV) complexation and oxidation. Three oxidation pathways are included. The vertical dashed lines indicate the pH ranges of the cloud events. Temperature was 283 K.

characteristic times for free S(IV) depletion through reactions with HCHO and O₃ are orders of magnitude longer than the characteristic time for reaction with H₂O₂. However S(IV) autooxidation in the presence of high metal concentrations may compete with oxidation by H₂O₂.

Table 3.5. Thermodynamic data: Henry's law and aqueous-phase equilibrium constants

Reaction	ΔH_{298}^0 (kJmol ⁻¹)	K (Matm ⁻¹ or M ⁿ)		
		5 °C	10 °C	25 °C
(1) H ₂ O <=> H ⁺ + OH ⁻	55.8	2.00E-15	3.00E-15	1.00E-14
(2) SO ₂ (g) + H ₂ O <=> SO ₂ H ₂ O	-26.13	2.65E+00	2.17E+00	1.24E+00
(3) SO ₂ H ₂ O <=> HSO ₃ ⁻ + H ⁺	-16.2	2.11E-02	1.87E-02	1.32E-02
(4) HSO ₃ ⁻ <=> SO ₃ ²⁻ + H ⁺	-11.8	9.00E-08	8.3E-08	6.42E-08
(5) NH ₃ (g) + H ₂ O <=> NH ₃ H ₂ O	-34.15	1.59E+02	1.22E+02	5.89E+01
(6) NH ₄ ⁺ <=> NH ₃ + H ⁺	-52.04	2.60E-09	1.80E-09	5.75E-10
(7) CO ₂ (g) + H ₂ O <=> CO ₂ H ₂ O	-20.27	6.12E-02	5.24E-02	3.40E-02
(8) CO ₂ H ₂ O <=> HCO ₃ ⁻ + H ⁺	7.64	3.40E-07	3.60E-07	4.28E-07
(9) HCO ₃ ⁻ <=> CO ₃ ²⁻ + H ⁺	14.86	3.00E-11	3.40E-11	4.69E-11
(10) HCHO + H ₂ O <=> CH ₂ (OH) ₂	-33.4	4.80E+03	3.72E+03	1.82E+03
(11) HCHO + HSO ₃ ⁻ <=> CH ₂ (OH)SO ₃ ⁻	-51.41	3.30E+05	2.20E+05	7.50E+04
(12) H ₂ O ₂ (g) <=> H ₂ O ₂ (aq)	-60.6	4.11E+05	2.59E+05	7.08E+04
(13) O ₃ (g) <=> O ₃ (aq)	-19.86	1.70E-02	1.40E-02	9.40E-03

Sources: (1), (2), (4), (6), (7), (10), (11), (12), (13) from Hoffmann and Calvert (1985); (5), (8), (9) from Seinfeld (1986); (3) from Jacob (1986).

Table 3.6. Kinetic data of S(IV) related reactions

Reaction	Activation Energy (kJmole ⁻¹)	k (M ⁿ s ⁻¹)		
		5 °C	10 °C	25 °C
(1) SO ₂ ·H ₂ O + O ₃ → SO ₄ ²⁻ + O ₂ + 2H ⁺				2.40E+04
(2) HSO ₃ ⁻ + O ₃ → SO ₄ ²⁻ + O ₂ + H ⁺	46	9.70E+04	1.40E+05	3.70E+05
(3) SO ₃ ²⁻ + O ₃ → SO ₄ ²⁻ + O ₂	43.9	4.20E+08	5.90E+08	1.50E+09
(4) HSO ₃ ⁻ + H ₂ O ₂ + H ⁺ → H ₂ SO ₄ + H ₂ O	39.5	2.37E+07	3.20E+07	7.45E+07
(5) S(IV) + 1/2O ₂ (Fe ³⁺ , Mn ²⁺) → S(VI)	70.1	5.45E+06	9.31E+06	3.72E+07*
		@ pH < 4.2	@ pH < 4.2	@ pH < 4.2
		3.7E+12	6.3E+12	2.51E+13*
		@ pH > 4.2	@ pH > 4.2	@ pH > 4.2
(6) HSO ₃ ⁻ + HCHO → HMS	24.7	3.86E+02	4.66E+02	7.90E+02
(7) SO ₃ ²⁻ + HCHO → HMS	20	1.38E+07	1.61E+07	2.48E+07
(8) HMS + OH ⁻ → HSO ₃ ⁻ + HCHO				3.60E+03

* The rate constants were determined at 23.8 °C.

Sources: (1), (2), (3) and (4) from Hoffmann and Calvert (1985); (5) from Ibusuki and Takeuchi (1987); (6) and (7) from Boyce and Hoffmann (1984); (8) from Munger et al. (1986)

When the cloudwater pH is less than 4, the time scale for depletion of free S(IV) via HMS formation is so long that this complexation reaction exerts no influence on rates of S(IV) oxidation. However, when the pH is greater than 5, free S(IV) depletion through reaction with HCHO can be competitive with oxidation by H₂O₂, O₃ and O₂/Fe-Mn (Figure 3.14). When the pH is larger than 6, reactions of S(IV) with HCHO, O₃ and O₂/Fe-Mn become more important than reaction with H₂O₂ over most of the concentration ranges we considered. In this pH region HMS formation and S(IV) oxidation by O₃ and autooxidation can occur at similar rates if the aqueous phase formaldehyde concentration is high.

Whether HMS formation can inhibit S(IV) oxidation is a matter of interest. Inhibition can occur if the S(IV) complexation rate is comparable to (or greater than) the S(IV) oxidation rate and the rate of SO₂ mass transport into the drop limits the rate of S(IV)

oxidation. Under these conditions HMS formation is rapid enough to reduce the concentration of free S(IV) available for oxidation in the cloud droplets. Figure 3.14 indicates that the S(IV) complexation rate begins to exceed the S(IV) oxidation rate when drop pH exceeds approximately 5, depending on chemical composition. Schwartz (1988) examined SO₂ mass transport limitations for oxidation by ozone and predicted that gaseous diffusion of SO₂ to the drop surface limits the rate of oxidation within the drops only at high pH (e.g., pH greater than approximately 6 for 30 μm drops in the presence of 30 ppbv gaseous ozone). This suggests HMS formation is most likely to limit rates of in-cloud S(IV) oxidation at pH > 6 and given the pH dependence on size, the effect is more likely to be important in large, rather than small drops.

3.3.2. Case studies on the relative importance of reactions of S(IV) with H₂O₂, O₃ and HCHO

Three cloud events with very different acidities were selected for further analysis. Cloudwater sampled on August 20, 1993 at Mt. Mitchell, North Carolina, exhibited a pH range during the event from 2.99 to 3.28. Cloudwater sampled on July 14, 1993 at Angora Pk., Oregon, had pH values ranging from 4.21 to 5.23. Fogwater sampled on January 15, 1994 at Bakersfield, California, exhibited a pH range from 5.89 to 6.91. The chemical compositions of the small ($4 < d < 23 \mu\text{m}$) and large ($d > 23 \mu\text{m}$) drops for the three events are listed in Table 3.1.

The August 20, 1993 cloudwater from Mt. Mitchell, North Carolina exhibited low pH (2.99 - 3.28) and high H₂O₂ concentrations (31 - 82 μM). For these conditions the characteristic time of S(IV) oxidation by H₂O₂ is very short, while the characteristic time of

HMS formation is relatively long (Figure 3.14). Consequently, dissolved free S(IV) is expected to be quickly oxidized by H_2O_2 leaving no free S(IV) in the cloud drop samples; both total S(IV) and HMS concentrations are expected to be very low. This is consistent with the observations reported in Table 3.1. Although limitations to mass transport of SO_2 into the cloud drops, if present, could affect the rate of HMS formation, mass transport limitation appears unlikely for this pH range (Schwartz, 1988). At these low pH values, however, the rate of HMS formation is limited by the intrinsically slow rate of reaction and the low SO_2 solubility. In fact, little HMS was present in the samples from this event. Small changes in drop pH, formaldehyde concentration or oxidant concentration will not affect the relative importance of S(IV) oxidation and complexation in this pH range. Therefore, little difference is expected between small and large drops despite their different compositions. This expectation is again consistent with our observations.

In the July 14, 1993 Angora Pk. samples the cloud pH ranged from 4.66 to 5.23. The concentration ranges of other chemical species are formaldehyde 4 - 10 μM , peroxides 7 - 29 μM , Fe(III) 0.2 - 3.2 μM , and Mn(II) 0.05 - 0.2 μM . In this pH regime the relative importance of S(IV) complexation and oxidation is more complicated than in the low pH region. It is sensitive to cloud pH as well as to concentrations of formaldehyde, oxidants and catalysts. Since these parameters vary with drop size, variations in the relative importance of S(IV) complexation and oxidation may occur as a function of drop size. The relevant characteristic times can be compared for the small and large drops by reference to Figure 3.14. The characteristic times for free S(IV) consumption as a result of HMS formation are longer than the corresponding characteristic times for depletion by oxidation by H_2O_2 (or by O_3 or

$O_2/Fe-Mn$) for both the large and the small drops. As in the Mt. Mitchell clouds, mass transfer of SO_2 into the drops is not expected to limit S(IV) reaction. While the pH in both the large and small drops is low enough to prevent rapid production of HMS, formation of HMS is more likely in the small drops than in the large due to their higher HCHO concentrations and high pH. Measurements of HMS in the cloud samples are consistent with this expectation: HMS concentrations are low in both drop size fractions but are higher in the small drops than in the large (Table 3.1).

In contrast to the former two cases, S(IV) depletion through oxidation by H_2O_2 during the January 15, 1994 fog event at Bakersfield, California appears less important due to high pH (5.9 - 6.9) and low H_2O_2 (0.3 - 24 μM) concentrations. At the high pH values and formaldehyde concentrations (82 - 183 μM) observed, HMS formation becomes much more rapid (Figure 3.14) and competitive with oxidation by O_3 and autooxidation at the measured ozone (6 - 10 ppb) (Maxwell, 1994) and catalyst concentrations (Fe(III) 1.2 - 16.6 μM and Mn(II) 0.2 - 0.9 μM). Indeed, in contrast to the two previous cases, significant concentrations of HMS (up to 38 μM) were measured in the Bakersfield fog samples (see Table 3.1). As described above for high pH samples, S(IV) oxidation by O_3 is expected to be limited by the rate of SO_2 diffusion to the drop surface. If the HCHO concentrations are high enough, therefore, complexation of free S(IV) by HCHO might be rapid enough to further reduce rates of S(IV) oxidation.

Variations in the chemical composition of the fog drops across the drop size distribution suggest the relative importance of S(IV) complexation and oxidation could also vary with drop size. The small drops in the Bakersfield fog had lower pH and higher

formaldehyde concentrations than the large drops (see Table 3.1). Increased pH and increased formaldehyde concentrations both enhance rates of HMS formation. In the samples collected in this event HMS concentrations were several times higher in the small drops than in the large drops. This could result from reduced HMS formation rates in the large drops associated with decreased free S(IV) concentrations. Free S(IV) concentrations are expected to be reduced in the large drops due to the enhanced rate of S(IV) oxidation at the higher pH found in these drops coupled with the limit to sulfur mass transport into the drops posed by gas phase diffusion at high pH and large drop size.

3.4. Enhancement of S(IV) oxidation in chemically heterogeneous clouds

3.4.1. Effect of cloud chemical heterogeneity on S(IV) oxidation by H₂O₂

There is general agreement that the rate of S(IV) oxidation by H₂O₂ follows the kinetics (Hoffmann and Edwards, 1975):

$$-d[\text{S(IV)}]/dt = k[\text{H}_2\text{O}_2][\text{H}^+][\text{HSO}_3^-]/(1+K[\text{H}^+]) \quad (3.28)$$

where k and K are constants. Study of mass transport limitation to the rate of in-cloud oxidation of SO₂ by H₂O₂ reveals that SO₂ is unlikely to be limited by mass transport processes for typical cloud conditions (Schwartz, 1988). Therefore aqueous SO₂ can be considered in equilibrium with gaseous SO₂, and the rate expression can be rewritten as:

$$-d[\text{S(IV)}]/dt = kK_{a1}P_{\text{SO}_2}H_{\text{SO}_2}[\text{H}_2\text{O}_2]/(1+K[\text{H}^+]) \quad (3.29)$$

where k and K are the reaction constants, P_{SO_2} and H_{SO_2} are the atmospheric partial pressure and Henry's law coefficient for SO₂ respectively, and K_{a1} is the first dissociation equilibrium constant for dissolved SO₂. The result is that the S(IV) oxidation rate is linear with respect to the H₂O₂ concentration and is not a function of the hydrogen ion concentration at pH > 2.0, the pH range for most atmospheric waters. Therefore the liquid water volume-weighted average S(IV) oxidation rate in a cloud with distinct drop compositions should equal the rate of S(IV) oxidation predicted using the liquid water volume-weighted average cloud drop

composition. Hence, cloud chemical heterogeneity should not influence the rate of in-cloud S(IV) oxidation by H_2O_2 .

3.4.2. Effect of cloud chemical heterogeneity on S(IV) oxidation by ozone

Our investigations of cloud/fog droplet chemical heterogeneity reveal that differences in chemical composition exist between drops of two independent size ranges. While changes in hydrogen peroxide concentrations with drop size are not significant, variations in drop acidity and trace metals, S(IV) and formaldehyde concentrations are generally significant. Variations in droplet acidity are expected to affect the oxidation rate of S(IV) in clouds through the pH sensitive oxidation pathways (e.g., O_3 and O_2 catalyzed by Fe(III) and Mn(II)). Due to the nonlinear dependence of the S(IV) oxidation rate on acidity for the ozone pathway (Equation (3.30)), use of the average cloud composition can lead to significant underprediction of the sulfate production rate.

$$-\frac{d[S(IV)]}{dt} = \left(k_0 + \frac{k_1 K_{a1}}{[H^+]} + \frac{k_2 K_{a1} K_{a2}}{[H^+]^2}\right) P_{SO_2} H_{SO_2} P_{O_3} H_{O_3} \quad (3.30)$$

k_0 , k_1 and k_2 are the reaction rate constants, K_{a1} and K_{a2} are the first and second dissociation equilibrium constants for dissolved SO_2 , P and H represent the partial pressure and Henry's law coefficient of gaseous species respectively.

In order to quantify the effect of the chemical heterogeneity on rates of S(IV) oxidation, calculations of enhancement of S(IV) oxidation by O_3 resulting from observed acidity variations were made for 105 cloudwater samples from numerous locations. In the

calculations clouds are treated to be composed of two chemically distinct droplet size classes and the rate of S(IV) oxidation in the cloud is calculated as the liquid-water-content weighted average rate of drops of the two size classes. The rate of S(IV) oxidation in the chemically heterogeneous cloud is then compared to that predicted using the averaged (again, weighted by liquid water content) cloud drop composition. The liquid-water-content weighted average acidity is calculated by assuming H^+ is conserved upon mixing, i.e., no buffer effect upon mixing (Appendix G). Figure 3.15 depicts the results as a frequency distribution of samples with various ranges of oxidation rate enhancement. The oxidation rate enhancement factor is obtained by dividing the average rate of S(IV) oxidation in a cloud with two distinct drop compositions by the rate of oxidation predicted using the average cloud drop composition. Approximately 67% of the samples considered were calculated to experience less than 20% enhancement in the oxidation rate due to the presence of two chemically distinct drop populations. Approximately 26% of the samples were calculated to experience enhancements between 30% and 100%, with the remaining samples experiencing enhancement in excess of 100%. Clouds with calculated S(IV) oxidation enhancement exceeding 50% were sampled at every location except Mt. Mitchell and covered a pH range nearly as wide as present in the entire data set. The enhancement factors increase in magnitude when the differences in pH between drops of two size classes are large (Figure 3.16).

3.4.3. Effect of chemical heterogeneity on S(IV) autooxidation catalyzed by trace metals

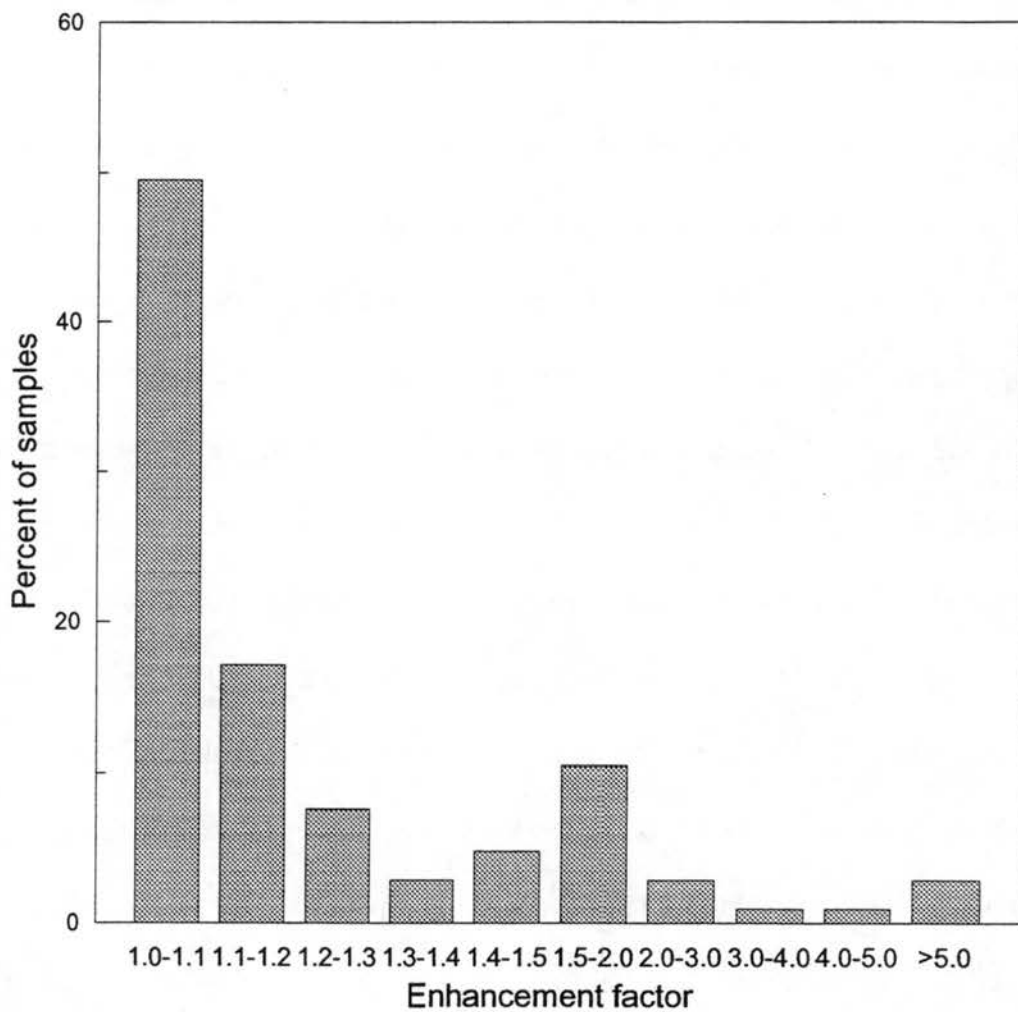


Figure 3.15. Calculated enhancement of sulfur oxidation by ozone due to the presence of chemical heterogeneity within the cloud. The data are presented as a frequency distribution of samples with various ranges of oxidation rate enhancement. Oxidation rates are calculated using the expression of Hoffmann (1986).

Past kinetic studies have revealed that rates of trace metal catalyzed S(IV) autooxidation are functions of S(IV), catalyst and hydrogen ion concentrations (Conklin and Hoffmann, 1988; Hoffmann and Calvert, 1985; Hoffmann and Jacob, 1984; Ibusuki and Takeuchi, 1987; Martin, 1984; Martin et al., 1991). Although the published rate laws are not entirely consistent with each other, especially at high pH, there is general agreement that the S(IV) oxidation rate is nonlinear with respect to the hydrogen ion concentration. As a result of this nonlinear dependence, use of the average hydrogen ion concentration, in a cloud or fog with variations in hydrogen ion concentrations across the drop size spectrum, to predict the S(IV) oxidation rate can result in a significant error. The error may be particularly severe if average catalyst concentrations are also used in clouds or fogs where droplet pH and catalyst concentrations covary. This effect can be magnified even further when iron and manganese concentrations covary due to their large synergistic effect on S(IV) autooxidation described above (Ibusuki and Takeuchi, 1987).

The effects of variations in droplet pH and catalyst concentrations on S(IV) autooxidation rates were determined for 38 fog and cloud sampling periods in this study. The periods included are those for which sample volume, pH, iron, and manganese concentrations were measured in simultaneously collected large and small drop fractions. Oxidation enhancement factors were obtained by dividing the liquid-water-content-weighted average S(IV) autooxidation rate in a cloud with two distinct, measured drop compositions by the rate of oxidation predicted using the liquid water volume-weighted average cloud drop composition for each pair of large and small cloud drop fractions. The calculations were made for four catalytic pathways: catalysis by (1) Fe(III) only, (2) Mn(II) only, (3) Fe(III) and

Mn(II) acting independently, and (4) Fe(III) and Mn(II) acting together (i.e., including the synergistic effects). Rate expressions from Ibusuki and Takeuchi (1987) were used for the four oxidation paths. Iron speciation was not measured in small and large drop fractions collected at the sites other than California's San Joaquin Valley. It is expected that fractions of Fe(III) in cloudwater are dependent on cloudwater pH, other chemical species concentrations, photochemical properties and the total iron (Graedel and Mandich, 1986). For the purpose of this study it is assumed that the fraction of dissolved iron represents 50% of the total iron and Fe³⁺ comprises 50% of the dissolved iron. Soluble Mn(II) was assumed to comprise 100% of the total Mn.

Figure 3.17 depicts frequency distributions of samples with various ranges of oxidation rate enhancement for the four catalytic pathways considered. The frequency distributions are similar for the first three catalytic pathways, where iron and manganese act as independent catalysts. Note that negatively correlated pH and metal catalyst concentrations result in net suppression of the S(IV) oxidation rate in approximately 20% of the samples, while positively correlated values of these two parameters result in enhancements larger than 30% in approximately 25% of the samples. The frequency distributions change substantially when Fe(III) and Mn(II) are considered to act synergistically to catalyze S(IV) autooxidation. Approximately 50% of the samples are calculated to experience oxidation rate enhancement of 30% or more for the synergistic pathway, while only about 10% of the samples are calculated to experience net suppression of S(IV) autooxidation. It is not surprising that the oxidation rate enhancement is most significant for the synergistic pathway, since the S(IV) oxidation rate is highly sensitive to the product of Fe(III) and Mn(II) concentrations for this pathway,

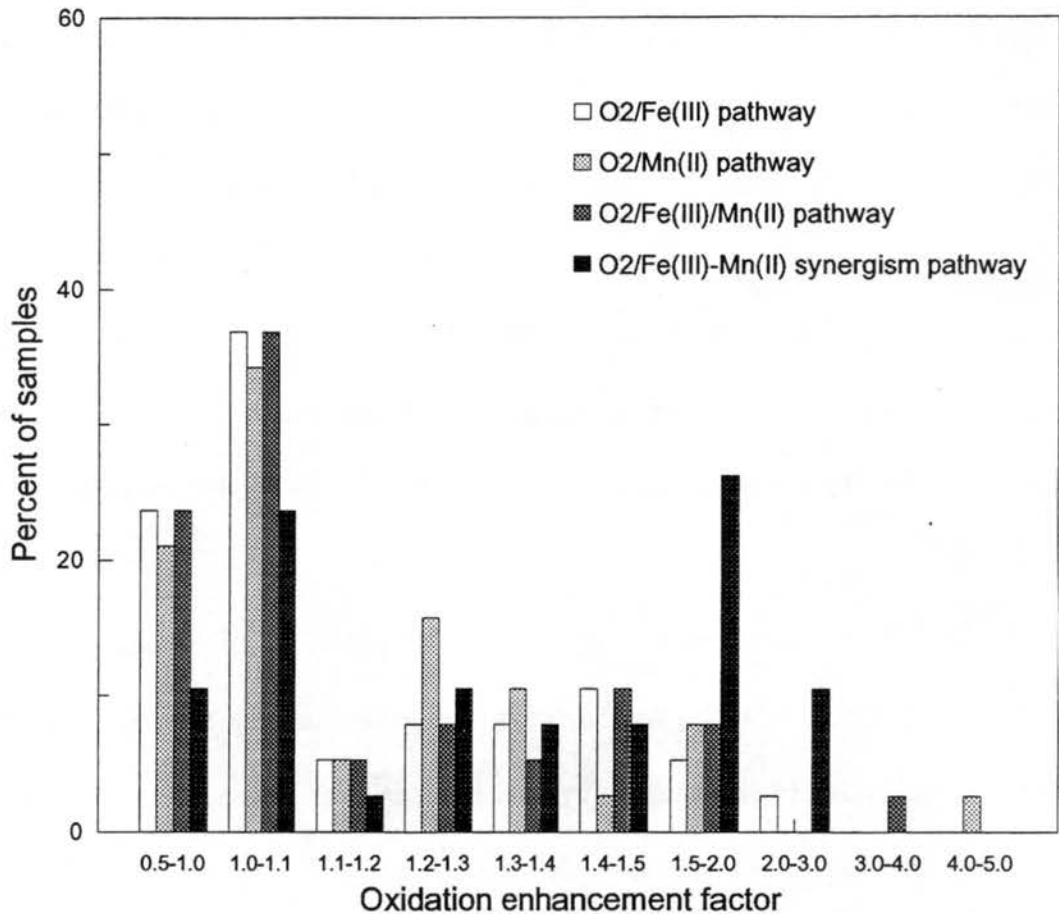
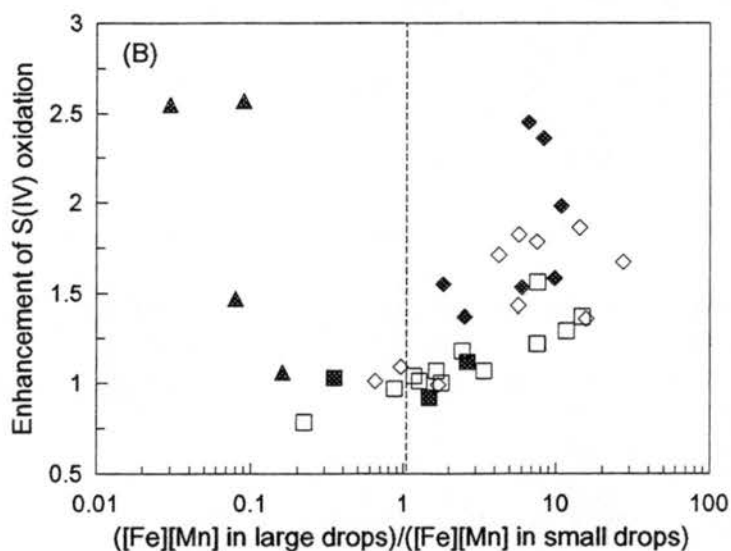
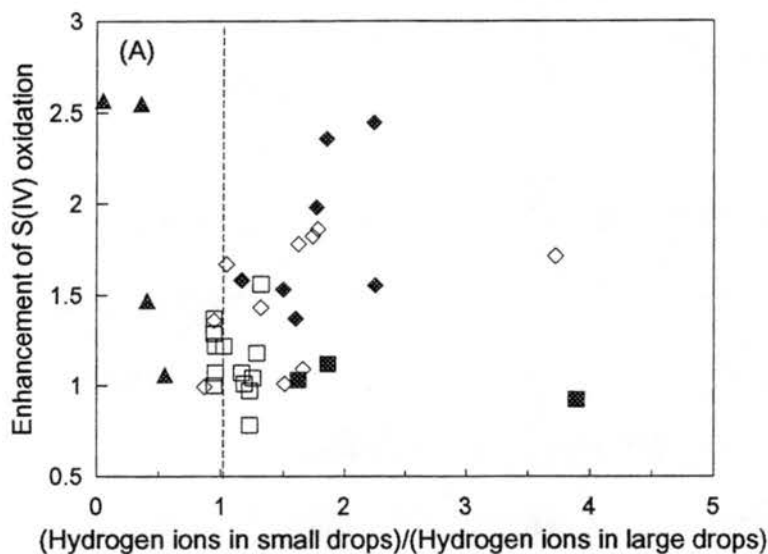


Figure 3.17. Calculated enhancement of sulfur oxidation for different catalyzed S(IV) autooxidation pathways due to the presence of chemical heterogeneity within the clouds. Cloud samples of small and large drop fractions were collected at several locations including La Jolla Pk., California and Angora Pk., Oregon coastal stratus clouds, Mt Mitchell, North Carolina frontal clouds and Bakersfield, California radiation fogs. The data are presented as a frequency distribution of samples with various ranges of oxidation rate enhancement. For the purpose of these calculations, the fraction of total Fe assumed to exist as soluble Fe(III) was taken as 25% and soluble Mn(II) was taken as 100% of total Mn for all samples. Rate expressions from Ibusuki and Takeuchi (1987) were used in the calculations.

and we usually observed concentrations of these species to covary across the drop size spectrum.

Figure 3.18 depicts relationships between the enhancements in S(IV) oxidation and the ratios of H^+ and $[Fe][Mn]$ in small drops to those in large drops. It shows that the enhancements tend to increase as the small and large drop compositions diverge. Large enhancements in the S(IV) oxidation rate through the Fe(III) and Mn(II) synergistic catalysis pathway were calculated for the coastal stratus clouds at Angora Pk., OR and La Jolla Pk., CA, and in the frontal clouds at Mt. Mitchell, NC, where we observed strong covariance of Fe, Mn and pH between small and large drops. For some of the samples at La Jolla Pk., CA and in the San Joaquin Valley the enhancements were not significant, either because the size dependence of pH and catalysts were insignificant, or because the effects of negatively correlated pH and metal concentrations canceled each other. It is also noted that for a few samples at La Jolla Pk., CA suppression of oxidation was observed due largely to the negatively correlated pH and metal concentrations.

Enhancement factors for aqueous phase S(IV) oxidation by ozone were reported for clouds and fogs collected at these sites in the previous section and by Collett et al. (1994). Variations in droplet acidity as a function of drop size were found to significantly enhance S(IV) oxidation by ozone. In order to facilitate comparison, frequency distributions of oxidation enhancement factors for the particular samples examined in this study are shown for the ozone pathway and for the synergistic metal-catalyzed autooxidation pathway in Figure 3.19. The metal catalyzed pathway shows a much larger range of effects than is predicted for the ozone pathway. Chemical heterogeneity among the droplet populations always leads to



- Bakersfield, CA (January 1994) □ La Jolla Pk., CA (June 1994)
- ◆ Mt. Mitchell, NC (August 1993) ◇ La Jolla Pk., CA (July 1993)
- ▲ Angora Pk., OR (July 1993)

Figure 3.18. Calculated enhancement of sulfur oxidation for the Fe(III)-Mn(II) synergistic catalysis pathway as functions of chemical heterogeneity within the clouds. (A) enhancement of S(IV) oxidation as a function of the ratio of hydrogen ions in small drops to hydrogen ions in large drops. (B) enhancement of S(IV) oxidation as a function of the ratio of [Fe][Mn] in large drops to [Fe][Mn] in small drops.

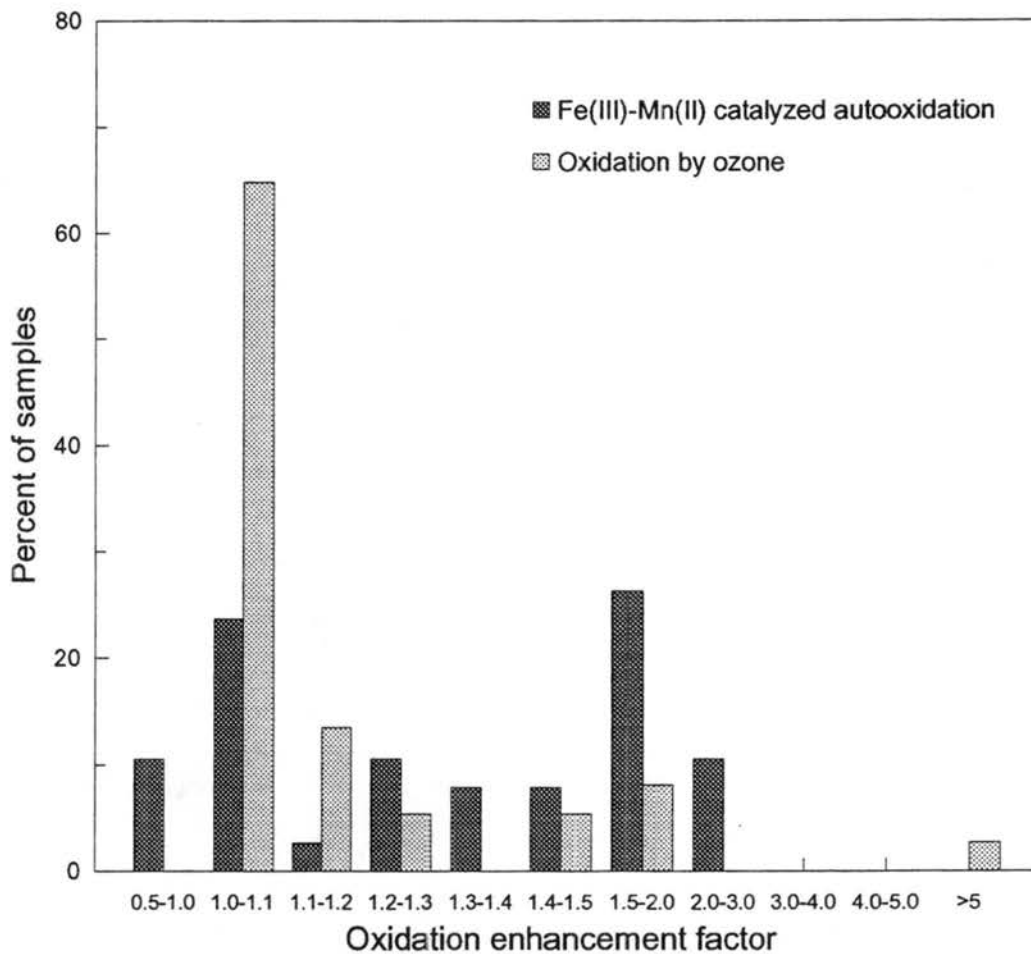


Figure 3.19. Calculated enhancement of S(IV) oxidation for ozone and Fe(III)-Mn(II) synergistic catalysis pathways due to the presence of chemical heterogeneity within the clouds. Thirty-eight samples from various locations were included in the calculations. The assumptions in the calculations were the same as in Figure 3.17.

oxidation rate enhancement for the ozone pathway, whereas oxidation rate suppression is possible in the metal catalyzed pathway when higher than average catalyst concentrations are found in drops that are more acidic than average. On the other hand, when higher than average catalyst concentrations are associated with relatively basic drops, autooxidation rate enhancement is greater than the enhancement in the ozone based oxidation, which comes from the non-uniform pH effect alone.

These observations suggest that chemical heterogeneity among real cloud and fog drop populations can significantly enhance S(IV) autooxidation relative to rates we might predict based on average cloud or fog drop composition. The effect of chemical heterogeneity on S(IV) autooxidation will be significant in terms of its effect on total aqueous phase sulfate production only if autooxidation is competitive with other S(IV) oxidation pathways including oxidation by hydrogen peroxide or ozone. This is most likely to occur (1) in regions where hydrogen peroxide concentrations are low relative to sulfur dioxide concentrations, (2) after hydrogen peroxide has been depleted through reaction, or (3) in cases where the droplet pH is high enough to support rapid metal-catalyzed S(IV) autooxidation. Of course, given the significant impact chemical heterogeneity among droplet populations can have on S(IV) autooxidation rates, determining which pathways are competitive in a given situation may require some knowledge about the chemical heterogeneity present.

3.4.4. Enhancement of S(IV) oxidation by the non-uniform distribution of chemical species in cloud and fog drop populations

It has been demonstrated that a significant chemical heterogeneity is present in a variety of cloud types and in a variety of environments. Although the chemical heterogeneity has little influence on S(IV) oxidation by H_2O_2 , it can significantly enhance in-cloud S(IV) oxidation by ozone and trace metal catalyzed S(IV) autooxidation. Therefore it is expected when S(IV) oxidation by H_2O_2 dominates the total S(IV) oxidation, the chemical heterogeneity will have little influence on S(IV) oxidation. When S(IV) oxidation by ozone and S(IV) autooxidation dominate, the presence of chemical heterogeneity will typically enhance the total S(IV) oxidation in a cloud.

With all three oxidation paths taken into account, enhancements in S(IV) oxidation due to the measured chemical heterogeneity were calculated for 43 fog and cloud sampling periods. The sampling periods were from various types of clouds and fog. Cloud/fogwater chemical composition of small and large drop fractions were from the measurements with assumptions made for fractions of dissolved Fe(III) and Mn(II). Gas partial pressures of ozone at Bakersfield, California were taken from measurements by the California Air Resources Board (Maxwell, 1994). Gas partial pressures of ozone at other sites were assumed to be typical values observed in clean to moderately polluted atmospheres. From Figure 3.20 we see that about 84 percent of the samples are calculated to experience little enhancement in S(IV) oxidation, due to the dominance of the H_2O_2 path. Approximately 9 percent of the samples are

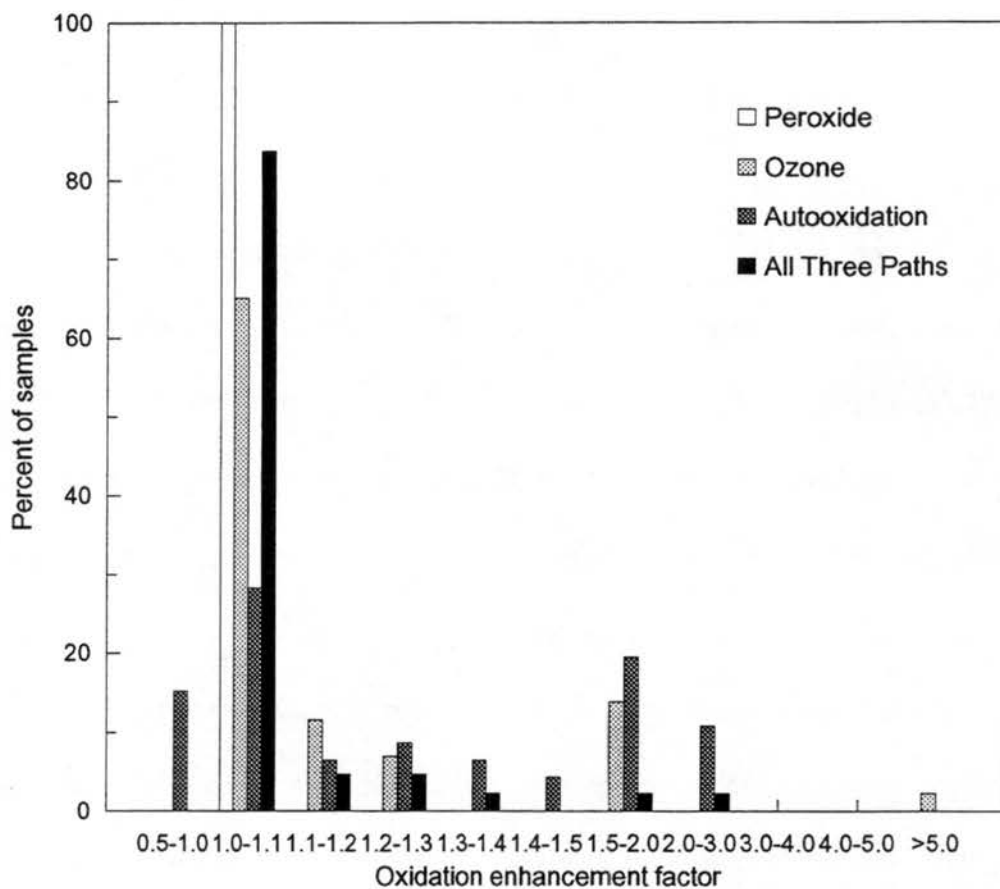


Figure 3.20. Comparison of S(IV) oxidation enhancement factors among the different oxidation paths. The calculations were based on 43 sample pairs of small and large drop fractions from a variety of cloud types and a variety of environments.

calculated to experience oxidation rate enhancement between 10 and 30%, while 7 percent of the samples are calculated to experience oxidation rate enhancement of 30% or more.

The enhancement factors are higher when the cloud and fog water pH are high enough to support rapid S(IV) oxidation by ozone and S(IV) autooxidation (Table 3.7). In the winter radiation fog at Bakersfield, California, S(IV) oxidation by ozone is the dominant oxidation path. Therefore variations in fog pH with drop size can have a significant influence on the S(IV) oxidation rate. In coastal stratus clouds at Angora Pk., Oregon and frontal clouds at Whiteface Mountain, New York S(IV) oxidation by H_2O_2 and O_3 dominated and S(IV) autooxidation in the presence of both Fe(III) and Mn(II) may contribute considerably to the total S(IV) oxidation. Variations in cloud pH and the trace metal concentrations may also significantly enhance the in-cloud S(IV) oxidation. Coastal stratus clouds collected at La Jolla Pk., California and frontal clouds measured at Mt. Mitchell, North Carolina, on the other hand, had very low cloud pH ($\text{pH} < 4.0$), and S(IV) oxidation by H_2O_2 is the dominant oxidation path. The observed chemical heterogeneity has little influence on S(IV) oxidation in these clouds.

Of course there are some uncertainties associated with the calculations in terms of gaseous ozone and H_2O_2 concentrations and fractions of dissolved Fe(III). The uncertainties may result in changes of the fractions of S(IV) oxidized through the different paths and, thus changes in oxidation enhancement factors. The influence of the uncertainties is expected to be greater for the clouds at Angora Pk. and Whiteface Mountain than for the clouds and fog measured at the other sites, since no single oxidation path dominates in the Angora and

Table 3.7. Fractions of S(IV) oxidation through the different paths and enhancement in S(IV) oxidation rate

Site	Sample	pH Small Drop	pH Large Drop	% Peroxide	% Ozone	% Autooxidation	Enhancement
Bakersfield, CA	1/15/94 #1	5.89	6.48	0.0	91.8	8.1	1.65
	1/15/94 #2	6.41	6.62	0.1	99.0	0.9	1.10
	1/16/94 #1	6.02	6.29	0.1	95.5	4.4	1.36
Mt. Mitchell, NC	8/22/93 #2B	2.58	2.93	100.0	0.0	0.1	1.00
	8/22/93 #3	2.67	2.94	100.0	0.0	0.0	1.00
	8/22/93 #4	2.50	2.70	100.0	0.0	0.0	1.00
	8/22/93 #5B	2.58	2.83	100.0	0.0	0.0	1.00
	8/22/93 #6	2.72	2.90	99.9	0.0	0.1	1.00
	8/22/93 #6B	2.69	3.04	99.8	0.0	0.1	1.00
Angora Pk., OR	7/14/93 #2	5.23	4.84	55.5	37.4	7.1	1.21
	7/14/93 #3	4.92	4.66	77.5	17.0	5.5	1.02
	7/15/93 #1	6.03	4.76	30.9	62.2	7.0	2.80
	7/15/93 #2	5.45	5.01	67.1	32.7	0.2	1.14
LaJolla Pk., CA	6/11/94 #1	3.61	3.62	99.7	0.1	0.3	1.00
	6/11/94 #2	3.60	3.70	99.8	0.1	0.2	1.00
	6/11/94 #2B	3.64	3.73	99.4	0.1	0.5	1.00
	6/11/94 #3	3.60	3.67	99.8	0.1	0.1	1.00
	6/11/94 #3B	3.63	3.71	99.7	0.1	0.3	1.00
	6/11/94 #4	3.65	3.63	99.6	0.1	0.3	1.00
	6/12/94 #1	3.62	3.70	99.7	0.1	0.2	1.00
	6/12/94 #1B	3.42	3.50	99.9	0.0	0.1	1.00
	6/12/94 #2	3.35	3.44	99.9	0.0	0.1	1.00
	6/12/94 #3	3.01	3.12	100.0	0.0	0.0	1.00
	6/13/94 #1	3.02	3.12	100.0	0.0	0.0	1.00
	6/13/94 #1B	3.02	3.00	100.0	0.0	0.0	1.00
	6/13/94 #2	2.97	2.95	100.0	0.0	0.0	1.00
	6/13/94 #2B	2.98	2.99	99.9	0.0	0.1	1.00
	6/13/94 #3	2.84	2.82	99.9	0.0	0.1	1.00
	6/14/94 #1	3.09	3.07	100.0	0.0	0.0	1.00
6/14/94 #2	2.70	2.82	100.0	0.0	0.0	1.00	
LaJolla Pk., CA	7/02/93 #1	3.33	3.90	92.0	0.5	7.5	1.03
	7/02/93 #1B	3.46	3.64	99.6	0.2	0.3	1.00
	7/02/93 #2	3.54	3.76	99.6	0.3	0.1	1.00
	7/02/93 #2B	3.81	3.75	99.5	0.4	0.2	1.00
	7/02/93 #3	3.45	3.57	99.8	0.1	0.1	1.00
	7/02/93 #3B	3.33	3.35	99.8	0.1	0.2	1.00
	7/02/93 #4	3.08	3.06	99.9	0.0	0.1	1.00
	7/05/93 #1	3.03	3.12	100.0	0.0	0.0	1.00
	7/06/93 #4	2.99	3.20	100.0	0.0	0.0	1.00
	7/06/93 #5	2.92	3.17	99.7	0.0	0.3	1.00
Whiteface Mt., NY	9/19/93 #1	5.08	4.61	53.8	41.5	4.7	1.20
	9/19/93 #3	4.23	4.60	91.8	7.6	0.6	1.03
	9/19/93 #4	4.55	4.69	63.7	35.6	0.7	1.02

Note: Ozone partial pressure of 7 ppb for Bakersfield, 30 ppb for Angora Pk., and 50 ppb for other sites were used. Dissolved Fe(III) was assumed to represent 25% of the total Fe, and dissolved Mn(II) comprises 100% of the total Mn.

Whiteface clouds. The influence of the uncertainties will be discussed in the next section for the clouds at Angora Pk., Oregon.

3.5. Case studies of S(IV) oxidation in chemically heterogeneous clouds/fog

3.5.1. The radiation fog in California's San Joaquin Valley

3.5.1.1. Fogwater chemical heterogeneity and enhancements in S(IV) oxidation rates

The chemical composition of fogwater collected by the size-fractionating CASCC and the CASCC2 are shown in Figure 3.21. The size-fractionating CASCC collects drops of two disparate size ranges, one with diameters between 4 and 23 μm and another with diameters larger than 23 μm . The CASCC2 collects all drops with diameters larger than 3.5 μm . The fogwater at Bakersfield was characterized by high pH values, ranging from 6 to 7, largely because high concentrations of atmospheric ammonia provided high acid neutralization capacities. The drop size dependent pattern of pH shows that lower pH values were associated with small drops ($4 < d < 23 \mu\text{m}$), which is consistent with the observations of enrichment of nitrate and sulfate concentrations in the small drop fraction at the site (Bator and Collett, 1997). The hydrogen peroxide concentrations in the fogwater were very low during the night hours, ranging from 0.3 to 1.4 $\mu\text{mole/l}$, and increased significantly after sunrise. This suggests that photochemical activities in the gas and aqueous phase are responsible for the aqueous H_2O_2 concentrations. Total iron concentrations in the fogwater were higher than concentrations typically found in cloudwater (1 - 10 μM); and the drop size dependent pattern shows higher concentrations in the small drops than in the large drops. Both the concentration levels and the drop size dependence pattern reflect that in addition to crustal sources industrial activities may also contribute significantly to the fogwater iron.

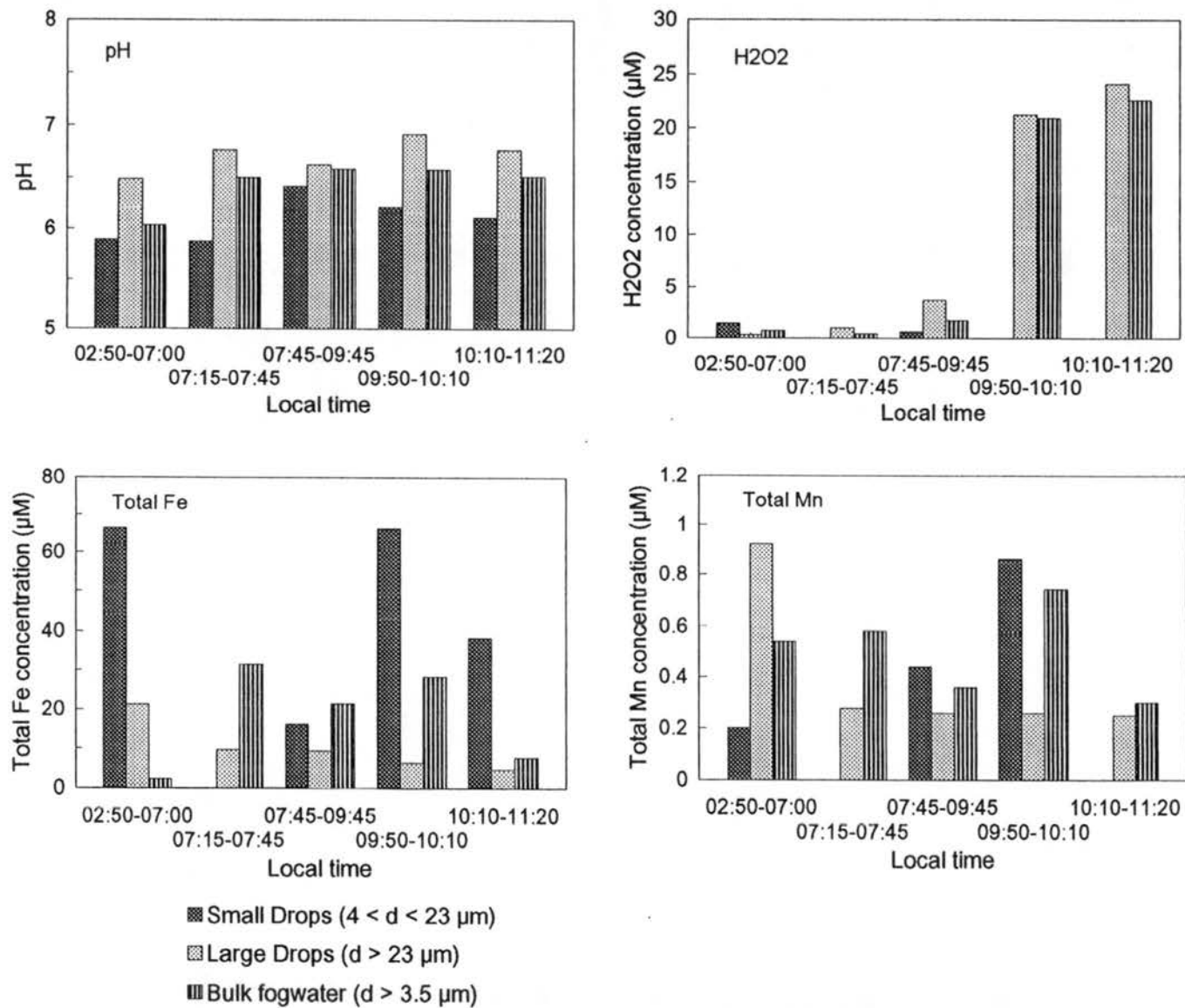


Figure 3.21. Chemical composition of fog drops collected by the size-fractionating CASCC at Bakersfield, CA 1/15/1994. The bulk fogwater was collected by the CASCC2.

Rates of S(IV) oxidation in fogs are largely dependent on chemical concentrations of fog drops and the composition of the ambient environment. Using the measured chemical compositions of small and large drops and the ambient sulfur dioxide and ozone concentrations, we calculated S(IV) oxidation rates and percentages of S(IV) oxidation through different oxidation pathways, in the fog drops of two disparate size ranges. The gas phase ozone concentration of 7 ppbv was selected to represent an average value during the fog event (Maxwell, 1994). The sulfur dioxide concentration of 0.07 ppbv was the measured value during the sampling period. It is assumed that during the fog event atmospheric sulfur dioxide and ozone were in equilibrium with their aqueous concentrations. The results show that the total S(IV) oxidation rate ranges from 1.7×10^{-7} - 1.2×10^{-6} Msec⁻¹ in the large drops and 1.5×10^{-8} - 1.2×10^{-7} Msec⁻¹ in the small drops (Figure 3.22). Figure 3.22 also shows the percentages of S(IV) oxidation through three different pathways, namely hydrogen peroxide, ozone, and trace metal catalyzed autooxidation. From the graph we can see that the fractions of S(IV) oxidation by H₂O₂ were always less than one percent. Therefore S(IV) oxidation by H₂O₂ was unimportant for this fog event. This is because, (1) the H₂O₂ concentrations were low; and (2) the fogwater pH values were high enough to support rapid S(IV) oxidation through other pathways. S(IV) oxidation by ozone is a dominant pathway in both small and large drops. S(IV) oxidation by oxygen catalyzed by trace metals, however, had significant contributions (29%) to the sulfate production in the small drops due to the high trace metals concentrations.

S(IV) oxidation by ozone and trace metal catalyzed autooxidation are highly dependent on aqueous pH and concentrations of catalysts. Variations of these chemical

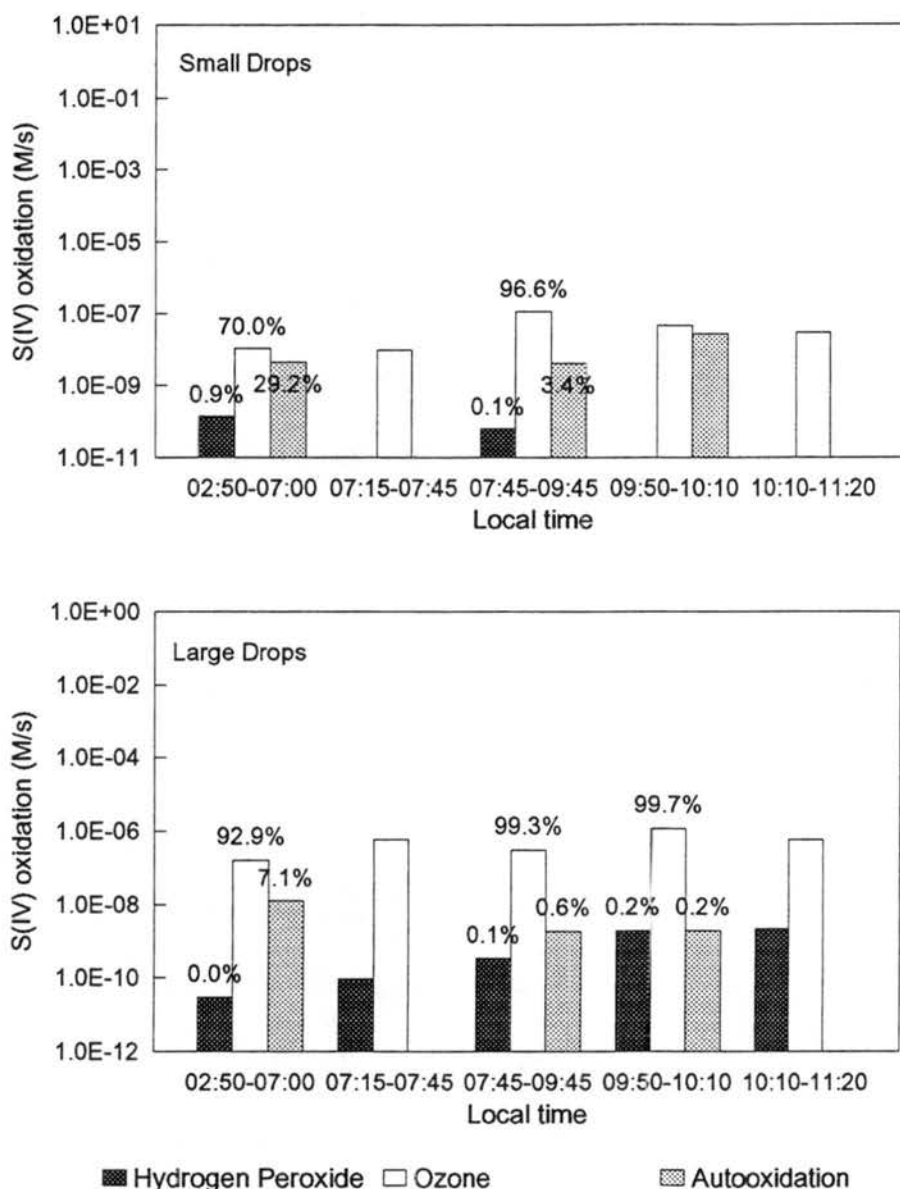


Figure 3.22. S(IV) oxidation rate by different pathways for the fog event of January 15, 1994 (02:50 a.m. - 11:20 a.m.) at Bakersfield, CA. Gas phase concentrations of ozone and sulfur dioxide were held constant at 7 ppbv and 0.07 ppbv, respectively. Fogwater hydrogen peroxide, pH and total Fe and Mn concentrations were taken from the measurements. Dissolved Fe(III) concentrations were assumed to be 25% of the total Fe, and dissolved Mn(II) was assumed to be 100% of the total Mn. The ambient temperature was 278 K. The top and bottom panels represent the percentages of S(IV) oxidation in small and large drops respectively. The numbers above the bars represent percentages of S(IV) oxidation by the different pathways.

species across the drop size spectrum can result in substantial differences in the oxidation rates among drops of diverse sizes. Consequently using average chemical compositions to calculate rates of aqueous S(IV) oxidation may cause large errors. Figure 3.23 compares the calculated S(IV) oxidation rates in the small drops, large drops, and bulk fogwater and liquid water volume-weighted S(IV) oxidation rates of small and large drops. Again, the oxidation rates in bulk fogwater were calculated using liquid water volume-weighted chemical compositions of small and large drops. From the fog samples we have all the information of pH and trace metals concentrations for small and large drops. It is found that S(IV) oxidation rates are generally higher in the large drops. Since the dominant S(IV) oxidation pathway during this fog event is the ozone pathway, variation of pH with drop size is the governing factor in determining the size dependence of oxidation rate. Accordingly, the S(IV) oxidation proceeded faster in the large drops due to their higher pH values, and more sulfate was produced in the large drops due to the higher S(IV) oxidation rates and their larger liquid water volume fractions. The existence of a small volume fraction of acidic small drops, however, could significantly lower the bulk fogwater pH so that the calculated S(IV) oxidation rates in bulk fogwater are lower than the volume-weighted oxidation rates of small and large drops. The resulting enhancements in S(IV) oxidation rates due to the chemical heterogeneity ranged from 10 to 65 percent for the different fog periods.

The real fog is expected to contain more than two independent drop compositions. Chemical composition is expected to vary across the drop size spectrum and probably even differs among drops of the same size. Therefore the real fog is expected to experience greater

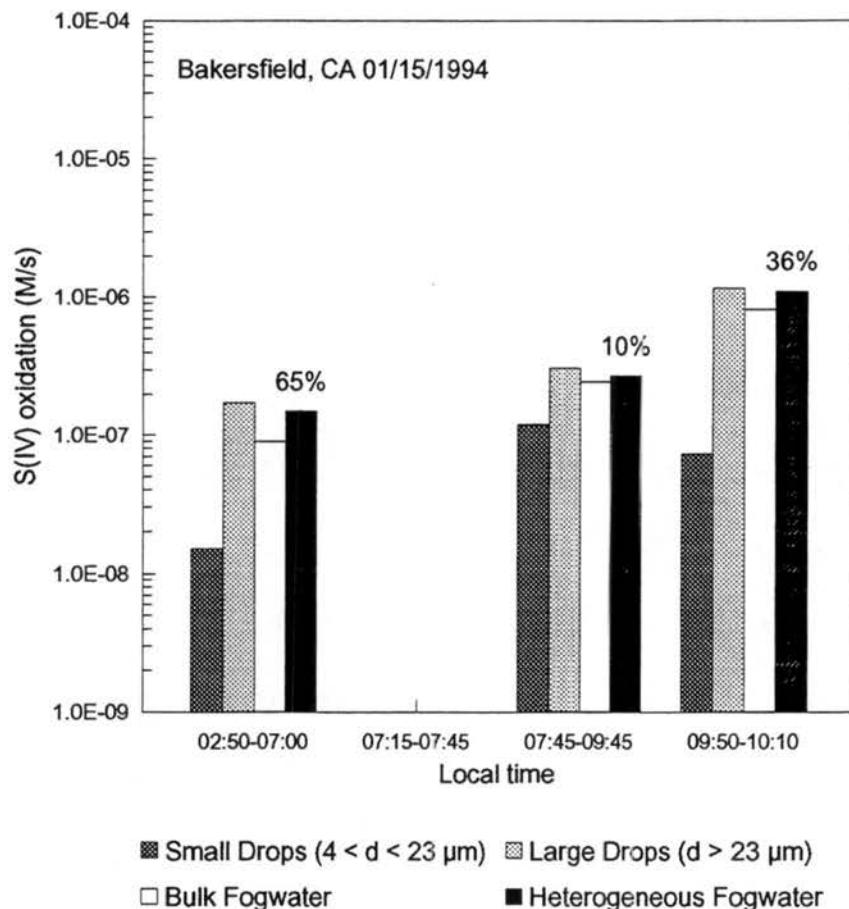


Figure 3.23. Calculated sulfur oxidation rates in small and large drop fractions and in bulk fogwater with averaged fog drop compositions. The net oxidation rate labeled 'Heterogeneous Fogwater' was calculated as a liquid-water-content weighted average of the rates associated with the two drop compositions. The numbers above the bars represent the enhancements of sulfur oxidation due to the presence of chemical heterogeneity within the fog. The chemical compositions of ambient air and fog drops are the same as those in Figure 3.22. The ambient temperature was 278 K.

enhancements in S(IV) oxidation rate than those calculated from drop populations of two size fractions.

3.5.1.2. Comparison of enhancements in S(IV) oxidation rates obtained from the two-stage size-fractionating CASCC and the three-stage size-fractionating IESL

The IESL cloud collector was also used simultaneously to sample fog drops of three independent size fractions during the fog event of January 15, 1994. The size cuts for the three stages of the IESL were 3, 10 and 20 μm respectively. Figure 3.24 shows the pH values of the fog drops collected by the sf-CASCC and IESL. The pH values obtained from both collectors indicate that fog drop pH increases with drop diameter. Using the pH values we calculated the S(IV) oxidation rates in the drop populations of different size fractions and oxidation rates in bulk fogwater with liquid water volume-weighted chemical composition. The rates in the bulk fogwater are then compared to the liquid water volume-weighted rates of the small and large drops to get enhancements in S(IV) oxidation rates. Again it is assumed that gas-liquid equilibria for sulfur dioxide and ozone are maintained.

Enhancements in S(IV) oxidation rates, due to the chemical heterogeneity obtained from the sf-CASCC and the IESL data are compared in Figure 3.25. The oxidation rates in Figure 3.25 are calculated for the ozone pathway only, since trace metal concentrations of the IESL samples are not available. Results obtained for the ozone pathway should represent the overall S(IV) oxidation rate reasonably well for this fog event since oxidation by ozone is the dominant oxidation pathway. From Figure 3.25 we see that the enhancements in S(IV)

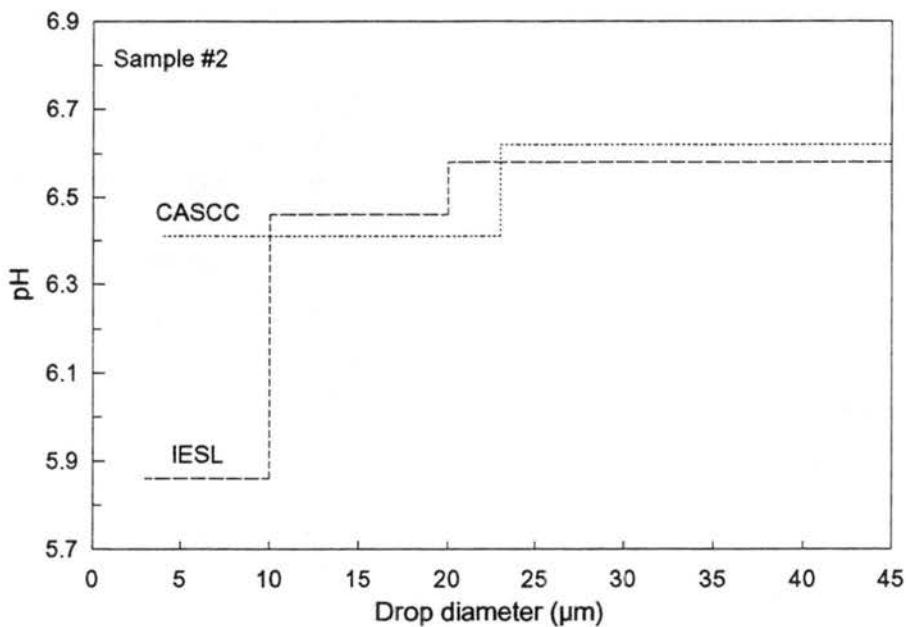
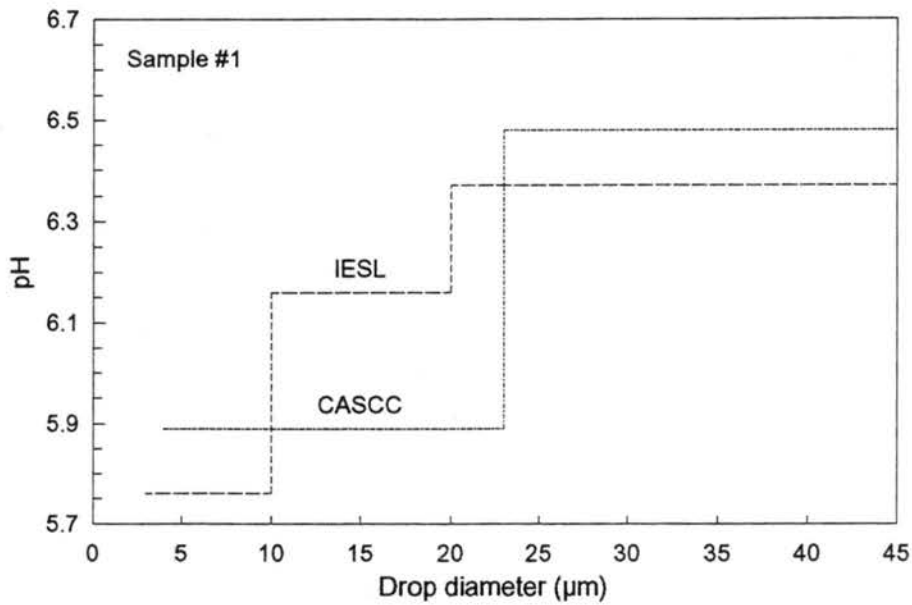


Figure 3.24. Fogwater pH values as functions of drop size for IESL and sf-CASCC samples. The IESL impactor has cut sizes of 3, 10, and 20 μm . The sf-CASCC has cut sizes of 4 and 23 μm . The top panel represents sample #1 collected from 02:50 a.m. to 07:00 a.m. on 01/15/94 at Bakersfield, CA. The bottom panel represents samples #2 collected from 07:45 - 09:45 a.m. on 01/15/94 at Bakersfield, CA.

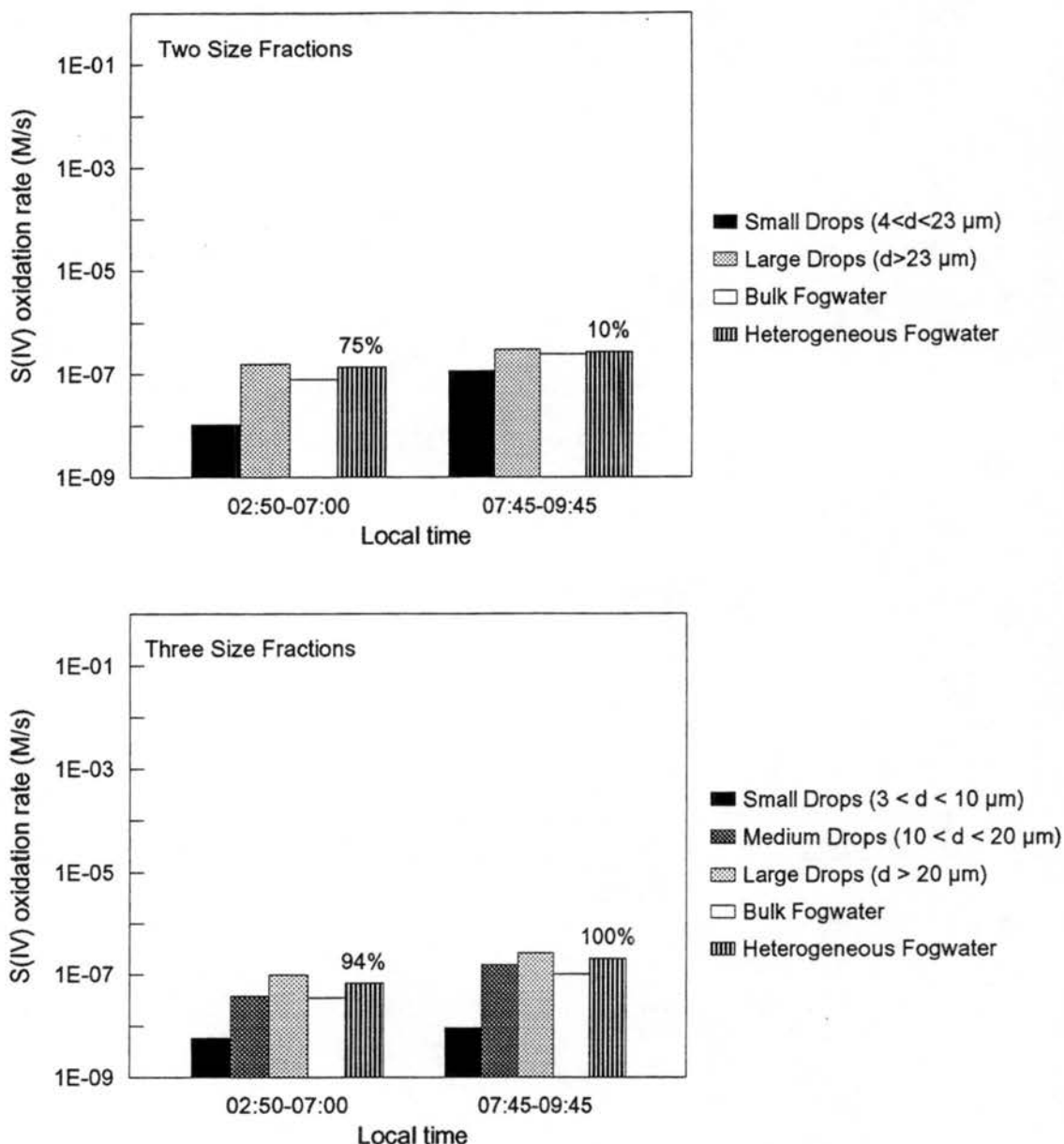


Figure 3.25. The S(IV) oxidation rates in size-fractionated drops and bulk fogwater. The oxidation rate in heterogeneous fogwater is the volume-weighted average rate of the independent drop size fractions. The numbers above the bars represent the enhancements of sulfur oxidation due to the presence of chemical heterogeneity within the fog. The top panel represents the oxidation rates in size-fractionated fogwater collected by the sf-CASCC (two size fractions), and the bottom panel represents the oxidation rates in size-fractionated fogwater collected by the IESL (three size fractions). Only the ozone pathway was considered in the calculation. Fogwater was collected at Bakersfield, CA on January 15, 1994. Gas phase ozone and sulfur dioxide concentrations were 7 ppbv and 0.07 ppbv respectively.

oxidation rates are much higher when the fogwater is divided into three size fractions.

Whereas the enhancements calculated for the two independent size fractions collected with the sf-CASCC are 75 and 10 percent for the two fog periods respectively, the enhancements are 94 and 100 percent, respectively, when the three size fractions collected with the IESL impactor are considered.

While the liquid water volume-weighted (bulk) fogwater pH values calculated from the sf-CASCC data are 6.48 and 6.62 for the two sampling periods respectively, the bulk fogwater pH values calculated from the IESL data are 6.37 and 6.38. It is noted that the bulk fogwater pH values calculated from the sf-CASCC data are higher than those calculated from the IESL data. Consequently, the higher bulk fogwater pH values from the sf-CASCC data resulted in higher bulk S(IV) oxidation rates than the bulk rates calculated from the IESL data. Theoretically, if a chemical species is conservative, its liquid water volume-weighted concentration is not dependent on where the drop cut sizes are and how many size fractions the fog water is cut. However the calculations show that the bulk fogwater pH values obtained from the two fogwater collectors are significantly different from each other. Additionally the calculated bulk fogwater pH are not always equal to the bulk fogwater pH values measured in the CASCC2 bulk fog samples, which were 6.03 and 6.58 for the two sampling period respectively. Comparison between the calculated bulk pH from the sf-CASCC and the measured bulk pH by the CASCC2 for other sampling periods is shown in Figure 3.26. The differences between the calculated and measured pH values are substantial for some samples. Several reasons could account for these observations. First, hydrogen ion is not a conservative species. Mixing of drops of different size fractions could result in chemical

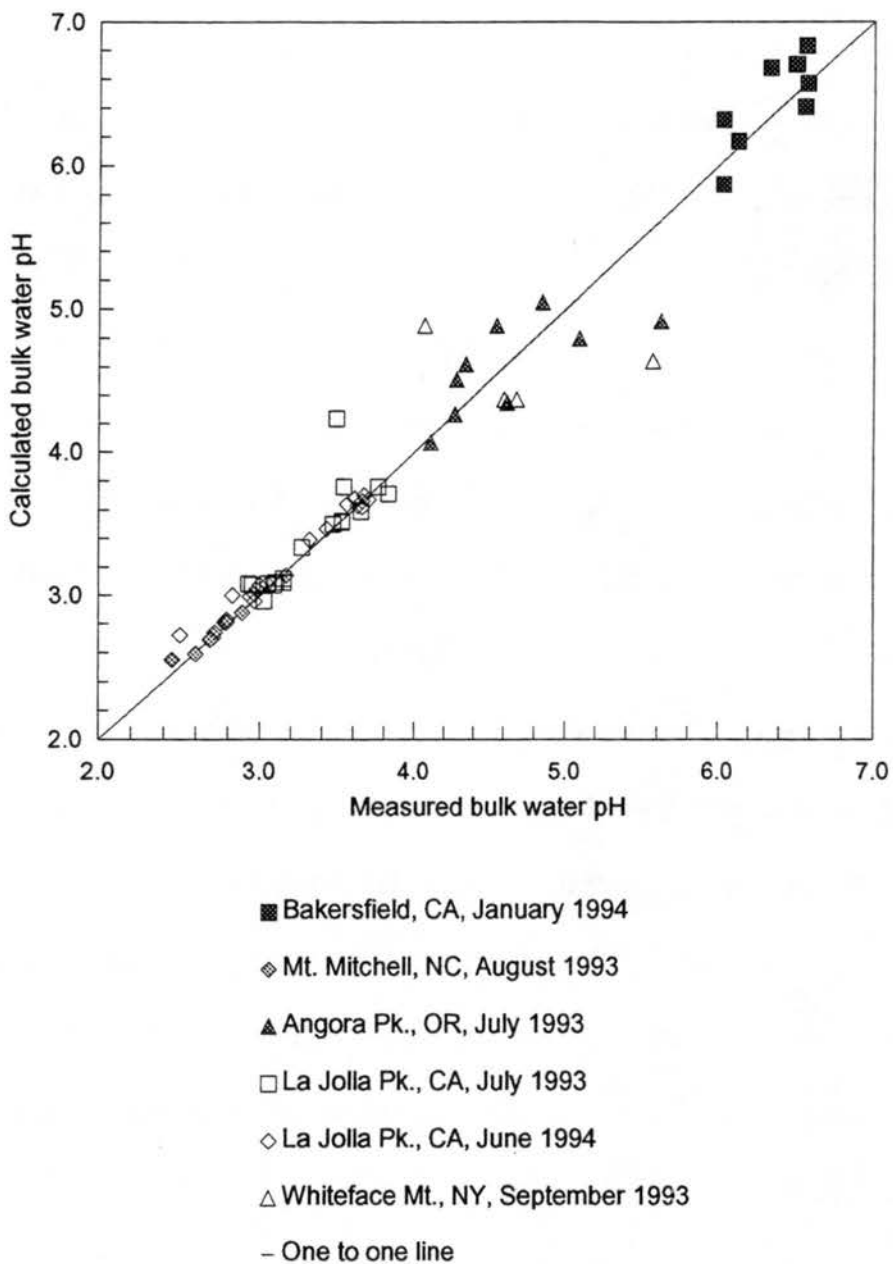


Figure 3.26. Comparison of bulk cloud/fog pH values calculated from the sf-CASCC samples and measured in the CASCC2 bulk fog samples.

reactions either consuming or producing hydrogen ions (Perdue and Beck, 1988). Second, the different fogwater collectors have different efficiencies in collecting drops of certain sizes. Since chemical concentrations in fog drops vary with drop size, the bulk water chemical concentrations obtained either by liquid water volume-weighting or by measurement represent only part of the fog drop size spectrum, not the whole size spectrum. Therefore even for conservative chemical species the bulk fogwater chemical concentrations obtained by different collectors may vary to some degree. Third, evaporation of collected water in some collectors and stages is possible. The IESL is more prone to evaporation since collected water is not separated from the air stream.

The above reasons may explain why the bulk water pH values calculated from the sf-CASCC are different from the bulk water pH calculated from the IESL collector. For the calculations in Figure 3.25 the liquid water volume-weighted average pH values instead of the measured bulk water pH were used to exclude differences in collection efficiencies between the collectors.

It is also noted that, although the enhancements calculated from the three size fractionated (IESL) fog samples are higher than those from the two size fractionated (sf-CASCC) samples, the volume-weighted S(IV) oxidation rates from the IESL data are lower than those from the sf-CASCC data. This is because (1) the size cut of large drops is higher for the sf-CASCC than for the IESL, which resulted in higher pH values and hence higher oxidation rates in the large drops of the sf-CASCC than determined in the large drops of the IESL impactor; (2) the volume fractions of large drops sampled by the sf-CASCC are much higher than those sampled by the IESL impactor. Since the large drops dominate S(IV)

oxidation in the fog, the volume-weighted S(IV) oxidation rates are faster from the sf-CASCC data than those from the IESL data.

In this high pH environment, where fog drop pH increases with drop size, S(IV) oxidation rates will also increase rapidly with drop size. Accurate estimation of the overall S(IV) oxidation rate requires greater information about pH variations with drop size, particularly at the larger drop sizes.

Here we examine the influence of more size cuts on the enhancements in oxidation rate. Since the pH value of each size fraction of the IESL represents an average pH of drops of various sizes within that size range, we divide each size fraction of the IESL into two sub-fractions to estimate the influence on oxidation enhancement. First we divide the large drop fraction ($d > 20 \mu\text{m}$) of the IESL impactor into two sub-fractions, one with diameters between 20 and 23 μm and one with diameters larger than 23 μm . The liquid water volume of the two sub-classes is calculated based on the drop size distribution measured by a Particle Measurement Systems CSASP-100-HV drop sizing probe. The pH of drops larger than 23 μm was set to 6.48, matching the pH value measured in large drops ($d > 23 \mu\text{m}$) from the sf-CASCC. The pH of drops with $20 < d < 23 \mu\text{m}$ can then be calculated so that the average pH of the two sub-fractions is the same as that of the large drop fraction of the IESL. Figure 3.27 shows the pH values of the simulated four drop size fractions, together with the calculated rates of S(IV) oxidation by ozone for the four size fractions and the enhancements in oxidation due to the chemical heterogeneity. Compared to the enhancements of 94% and 100% calculated from the three size fractions of the IESL (Figure 3.25) the enhancements are

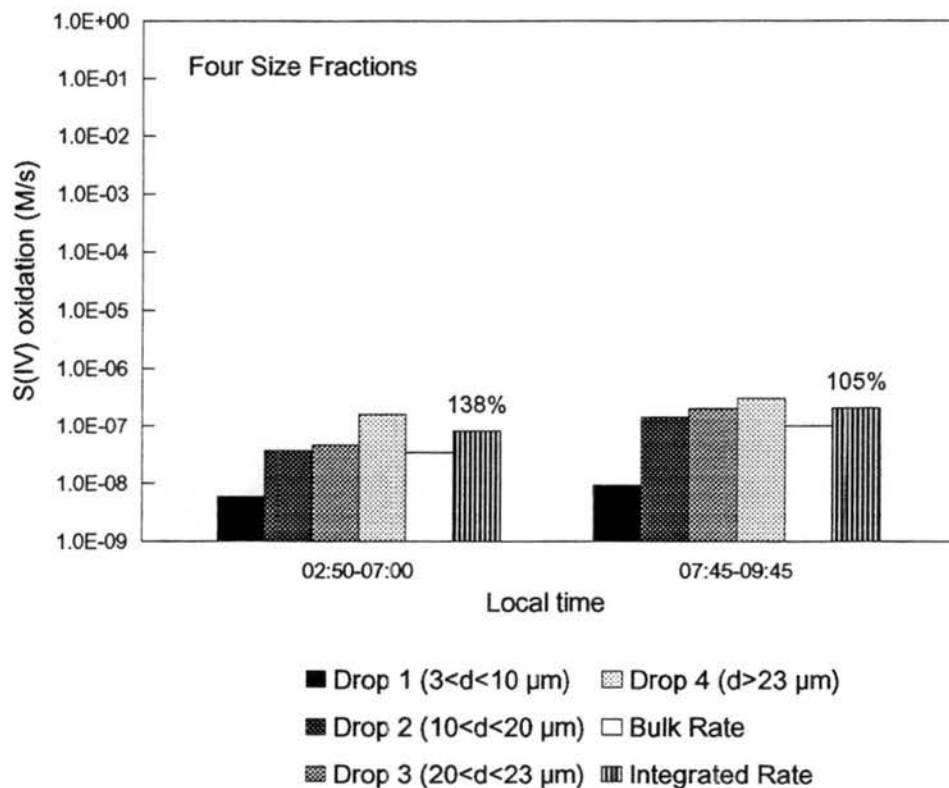
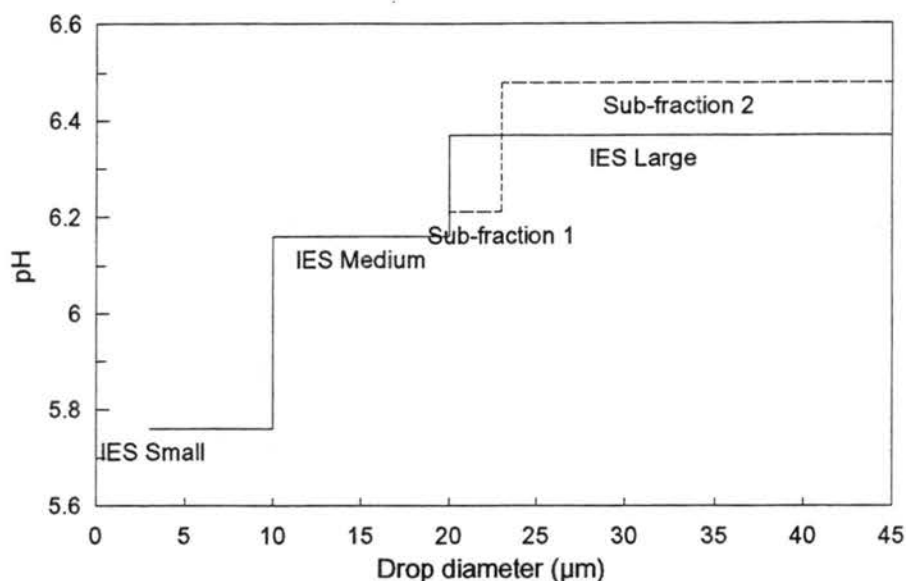


Figure 3.27. S(IV) oxidation rates in drops of the four size fractions derived from the IESL impactor. The large size drops of the IESL impactor were divided into two sub-fractions with hypothetical compositions (see text). The top panel shows the pH values of the four size fractions for sample #1 (02:50 - 07:00 a.m.) on January 15, 1994 at Bakersfield, CA. The integrated rate is the volume-weighted average rate calculated from the individual rates of the four independent drop size fractions.

138% and 105% for the two fog periods respectively when the large fraction from the IESL impactor is divided into two sub-fractions.

We have seen that as more size fractions are considered S(IV) oxidation enhancement increases. However, even if the fog is cut into the same number of drop size fractions, enhancements in oxidation rates may depend on the cut sizes selected. Using the same example as above, we examine the oxidation enhancements for the fog of four size fractions where we divide the medium drop size fraction from the IESL impactor into two sub-fractions, one with diameters between 10 and 15 μm and one with diameters between 15 and 20 μm . Again the liquid water volumes of the two sub-classes are calculated based on the measured drop size distribution. The liquid water volume-weighted average hydrogen ion concentration of the two sub-fractions is the same as that of the medium fraction of the IESL. The ratio of H^+ concentrations of the two sub-fractions is set to be an average of the ratio of the H^+ in small drops to the H^+ in the medium drop size fraction and the ratio of the H^+ in medium drops to the H^+ in the large drop size fraction. Figure 3.28 shows the pH values of the simulated four drop size fractions, together with calculated rates of S(IV) oxidation by ozone for the four size fractions and the enhancements in oxidation due to the chemical heterogeneity. From the graph we see that, for the first sampling period, although the enhancement is somewhat higher than those calculated from the three size-fractionated fog (Figure 3.25), the enhancements are lower than the case where the large drop fraction of the IESL was divided into two sub-fractions (Figure 3.27). For the second sampling period, the enhancement is higher than the case where the large drop fraction of the IESL was divided into two sub-fractions. This is because the pH in one of the sub-fractions is the highest among

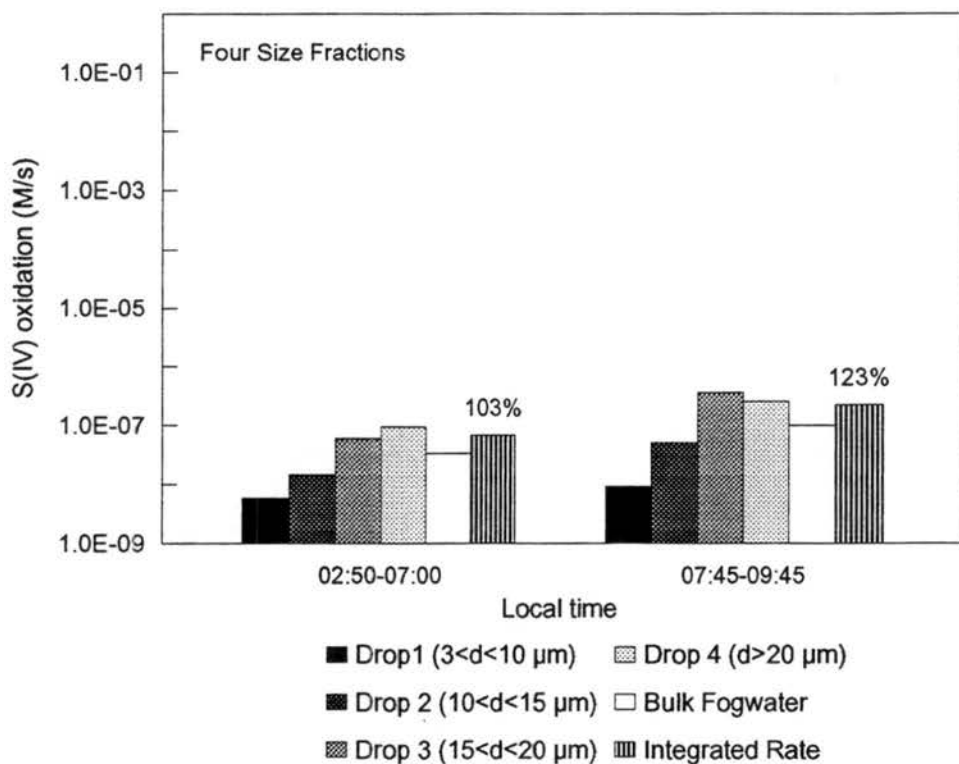
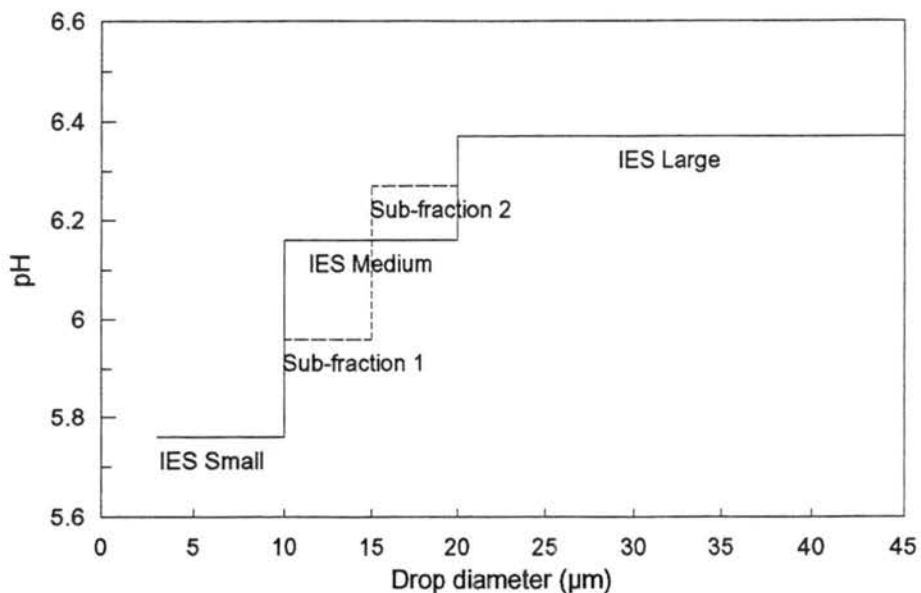


Figure 3.28. S(IV) oxidation rates in drops of the four size fractions derived from the IESL. The medium size drops of the IESL impactor were divided into two sub-fractions. The top panel shows the pH values of the four size fractions for sample #1 (02:50 - 07:00 a.m.) on 1/15/94 at Bakersfield, CA.

the four size fractions. For these two sampling periods the enhancement is greater when more size cuts are in the size range with high pH. Therefore, in order to more accurately estimate S(IV) oxidation rates in chemically heterogeneous clouds and fog, more size cuts are needed especially in size ranges with high pH.

Up to present we have been examining the enhancements in S(IV) oxidation rates due to the chemical heterogeneity. The existence of chemical heterogeneity permits faster oxidation of sulfur dioxide. As S(IV) is oxidized sulfuric acid is produced leading to acidification of the fog drops. The acidification of drops with higher pH is more rapid than that of drops with lower pH due simply to the logarithmic definition of pH. Therefore as S(IV) oxidation proceeds, chemical heterogeneity in drop pH may decrease. Drop acidification quickly depresses S(IV) oxidation by ozone and can also significantly alter rates of trace metal catalyzed S(IV) autooxidation. However, fogwater may contain acid buffering materials that neutralize the produced sulfuric acid and slow down the acidification. In addition to internal buffering agents that may exist in fogwater, uptake of atmospheric ammonia can also neutralize produced acidity and help keep fog drop pH high for a longer time.

3.5.1.3 Fogwater acid buffer capacity and its effect on enhancements in sulfate production

One mechanism counteracting the tendency for droplets to acidify is uptake of gaseous ammonia, in those environments where excess ammonia exists in the gas phase. This is a well recognized phenomenon which has been included in many model studies of aqueous phase sulfate production. Less well recognized is the possibility that a significant acid buffer capacity can exist within the droplets themselves. Jacob et al. (1986) considered fogwater alkalinity, which they defined as the deficiency of aqueous phase H^+ with respect to the reference system of neutralized fogwater species and calculated as

$$[ALK] = [HCOO^-] + [CH_3COO^-] + [CH_3CH_2COO^-] + [CH_3CH(OH)COO^-] + [HCO_3^-] + [NH_3(aq)] + [OH^-] - [H^+] \quad (3.31)$$

Facchini et al. (1992) have also examined fogwater acidity (equivalent to negative alkalinity) while Liljestrand (1985) has considered acid buffering associated with proton exchange in solution and uptake of soluble gases. In all of these cases, the species considered have been mainly restricted to the NH_3 - HNO_3 - H_2SO_4 system, with addition of soil dust and sea salt components, the carbonate system, low molecular weight organic acids, and S(IV)-aldehyde complexes.

Despite the appeal of modeling cloud and fogwater as a relatively simple system, there is increasing evidence that its composition may be much more complex than is typically considered. Organic compounds, for example, appear to contribute significantly to atmospheric water drop compositions in many environments (Capel et al., 1990; Leuenberger

et al., 1988; Munger et al., 1989; Tremp, 1992); some organic compounds are likely to contribute to fog acid buffering capacities. In order to test whether actual fogwater possesses a significant internal capability to buffer acid addition or production, we have conducted acid titrations of several fog samples collected in the San Joaquin Valley of California. We have found that these samples often contain significant acid buffer capacity at high pH that cannot be accounted for by chemical species normally considered.

Acid titration curves for fog samples collected on January 15, 1994 in Bakersfield, California are shown in Figure 3.29. These fog samples were highly polluted, with nitrate concentrations exceeding 3,000 microequivalents/l (μN) in each sample and sulfate concentrations in excess of 400 μN . The high sample pH is the result of locally abundant ammonia. The deviations of the acid titration curves from a simple exponential decay, which would be expected for an unbuffered sample where each unit of hydrogen ion added increases the sample's hydrogen ion concentration by an equal amount, indicate that something within the sample is consuming protons, thereby buffering the sample from such rapid acidification. The curve shapes suggest that this buffering occurs most effectively at relatively high pH (around pH 6 to 7). The titration curves also demonstrate that sufficient acid buffer capacity is present to permit several hundred micromolar hydrogen ion to be added before the drop pH decreases to a value of 5. In contrast only 10 micromolar hydrogen ion is needed to decrease the pH of deionized water to a value of 5. Since the sulfate production rate at high pH increases strongly with increasing pH, this suggests that much more sulfuric acid could be produced in the strongly buffered fog samples than in fogwater with no internal acid buffer capacity.

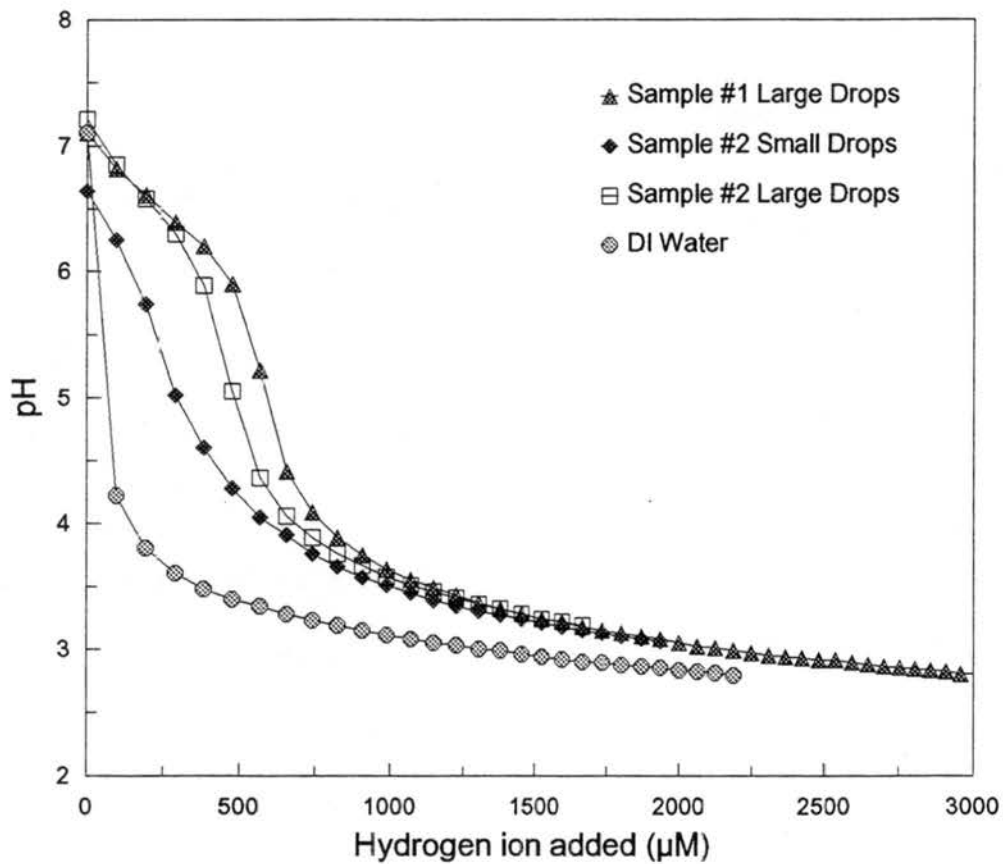


Figure 3.29. Acid titration curves for fog samples collected with the sf-CASCC at Bakersfield, CA on 1/15/94.

Fog samples collected in Bakersfield on December 10, 1995 were moderately polluted, with nitrate and sulfate concentrations varying mostly between a few hundred and several hundred micronormal during the course of the morning. Any acidity that might have been present within the fog was again observed to be neutralized during most periods, with the exception of a period in the early morning where increased sulfur concentrations corresponded with a decline in fog pH toward pH 5. This period of acidification was brief, however, and fog pH rose again in the subsequent two hours. Acid titration curves for four samples collected during this event are shown in Figure 3.30. Three of the four titration curves (samples 2, 4, and 8) are similar in shape to those corresponding to the 1994 Bakersfield samples. Significant buffering is evident once again at relatively high pH values in the range of pH 6 to 7. It is notable, however, that the total buffer capacity present in these samples is much less than was observed in the 1994 samples. The amount of acid required to acidify the 1995 fog samples to pH 5 is of the order of only 10% of the amount required to similarly acidify the 1994 samples. The third titration curve in Figure 3.30, representing acid titration of sample 6, which was collected during the period of fog acidification, exhibits an exponential decay of pH with added hydrogen ion, suggesting little additional buffer capacity remained in this sample.

In order to quantitatively compare acid buffering among fog samples we define an acid buffer intensity (β) as the unit increase of acid needed per unit pH decrease in the fog.

$$\beta = - dC_a/dpH \quad (3.32)$$

This definition is commonly used in aquatic chemistry (see e.g., Stumm and Morgan, 1996). Clearly the value of β will vary with pH as a sample containing internal acid buffer capacity is

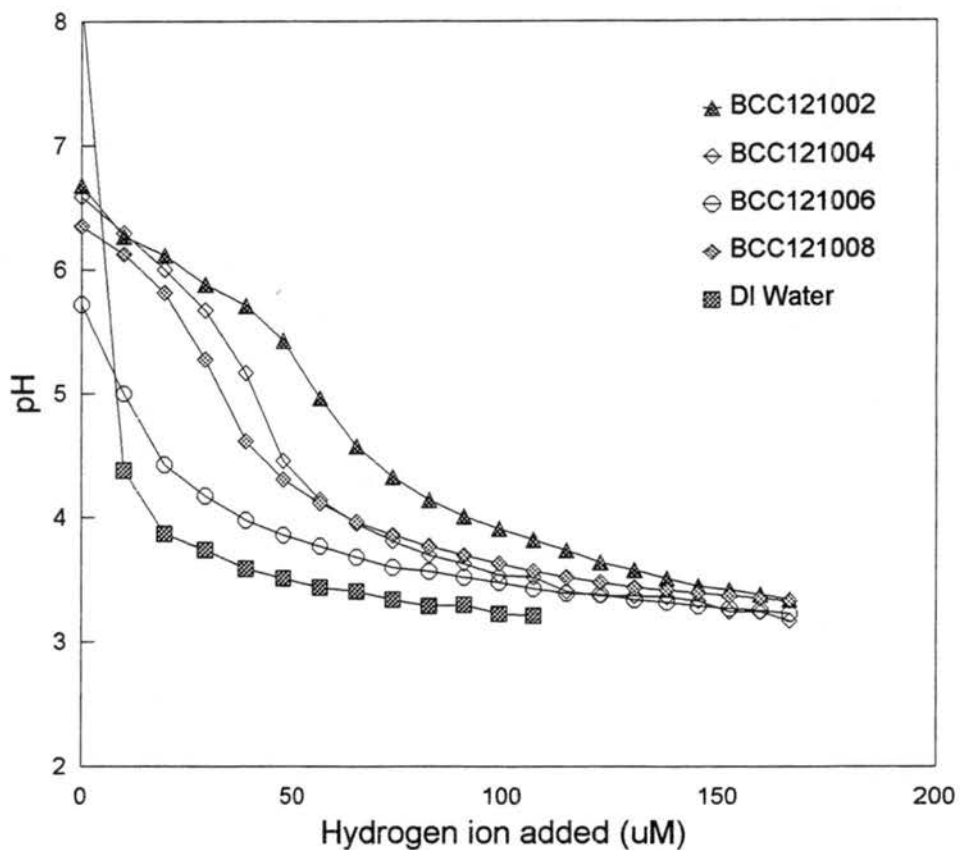


Figure 3.30. Acid titration curves for four bulk fog samples collected with a CASCC2 at Bakersfield, CA on December 10, 1995. Samples were collected at one hour intervals and numbered sequentially. For clarity curves are included for only four of the eight hourly samples collected.

titrated. For example, the buffer intensity due to a specific species will rise and then fall as the pH approaches and passes the pK_a of that species. β values can be calculated at any pH from measured acid titration curves.

In Figure 3.31 we compare initial buffer intensities for titrated San Joaquin Valley fog samples collected at the various sites and during different events. β values for deionized water are also shown for comparison. The highest initial acid buffer intensities (the initial β values) were observed during the highly polluted Bakersfield fog event of January 15, 1994. For this event, and the December 10, 1995 Bakersfield event, we see that the initial acid buffer intensity increases strongly with initial sample pH above 6, suggesting that the compound or compounds responsible for much of the buffering exhibit their greatest effect at a pH above 6.

These observations are reinforced by an analysis of how buffer intensity varies with pH during the course of acid titrations of individual samples. Values of β as a function of pH are plotted in Figure 3.32 for three samples from the January 15, 1994 Bakersfield fog event. Once again, little buffering is evident below pH 6, with a dramatic increase in buffer intensity above pH 6, peaking between pH 6.5 and 7. The maximum buffer intensity should occur at the pK_a of the weak acid or base responsible for the buffering (Stumm and Morgan, 1996), suggesting that the pK_a of the agent responsible for the acid buffering in these samples is probably between 6.5 and 7. Of course it may be an oversimplification to assume that a single chemical compound is responsible for the buffering. The presence of multiple buffering compounds with a range of relevant pK_a 's could make unraveling their identity a very complex task.

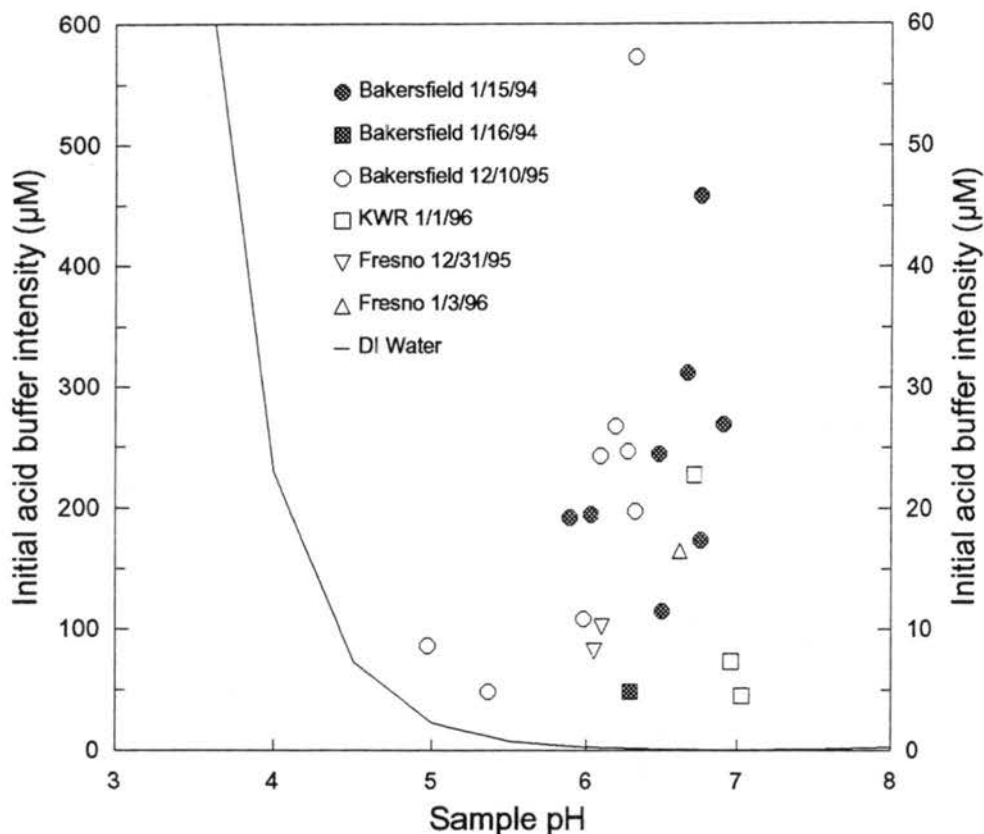


Figure 3.31. Acid buffer intensities of fog samples measured at pH values observed immediately after collection in the field. Two scales have been used to better illustrate dependence of buffer intensity on fogwater pH. Samples from 1994 are plotted against the left y-axis; samples from 1995 and 1996 are plotted against the right y-axis. The line representing the buffer intensity of deionized water is shown plotted against the left y-axis. Note that the deionized water buffer intensity increases at low pH due to the logarithmic definition of pH.

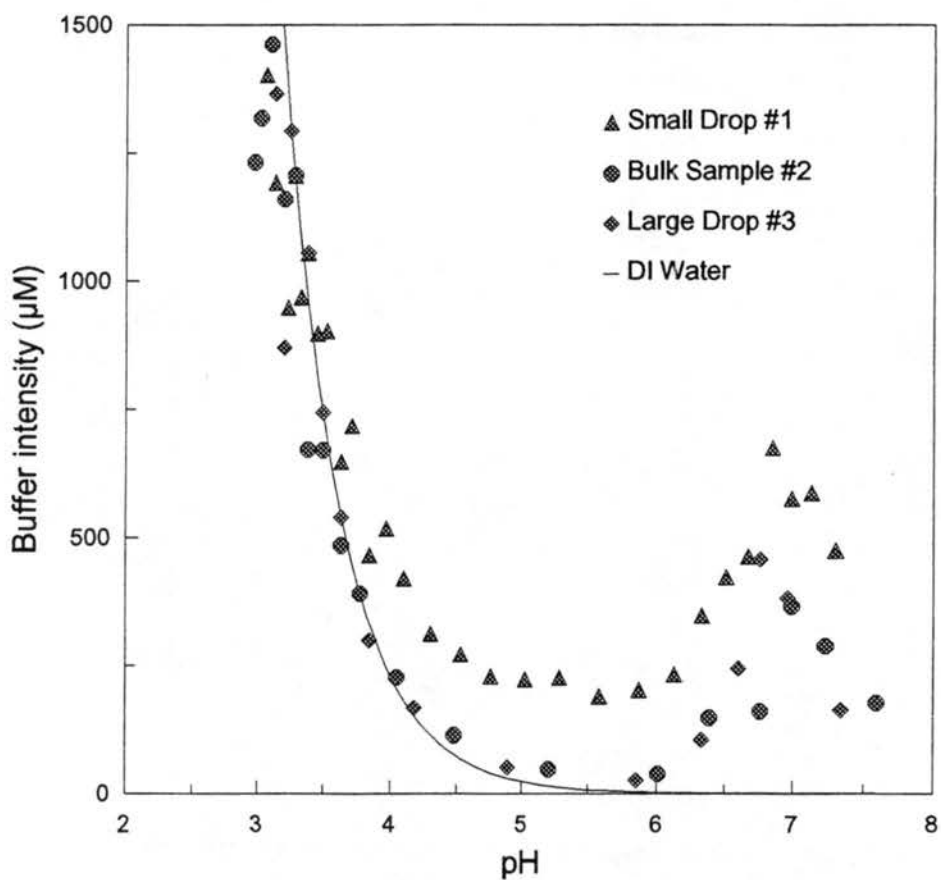


Figure 3.32. Acid buffer intensities measured as a function pH during acid titration of three fog samples collected at Bakersfield, California on January 15, 1994.

Given the information available here, however, it seems safe to rule out most common atmospheric carboxylic acids (e.g., formic acid, acetic acid, oxalic acid) as contributors, since they exhibit pK_a 's well below 6. We have also examined some highly buffered samples for phosphate (pK_{a2} for phosphoric acid is 7.2 at 25 °C), which was found only in trace quantities. Measurements of free S(IV) concentrations in solution also revealed that concentrations were too low for the protonation of sulfite (forming bisulfite, $pK_a = 7.2$ at 25 °C) to account for the observed buffering. Ammonium ($pK_a = 9.23$ at 25 °C) concentrations were usually high in Bakersfield fogwater, thus it may contribute some fogwater acid buffer capacity. Protonation of bicarbonate and carbonate ($pK_{a1} = 6.37$; $pK_{a2} = 10.33$ at 25 °C) may also contribute to total acid buffer capacities. We calculated contributions of $CO_3^{2-}/HCO_3^-/H_2CO_3$ and $NH_{3(aq)}/NH_4^+$ systems to the β for the Bakersfield fog samples collected in 1994 and 1995 (Table 3.8). The acid buffer capacities from $CO_3^{2-}/HCO_3^-/H_2CO_3$ and $NH_{3(aq)}/NH_4^+$ systems are calculated according to Equations (3.33) and (3.34).

$$\beta_{CO_2} = 2.3 (\alpha_{H_2CO_3} \alpha_{HCO_3^-} C_{T,CO_3} + \alpha_{HCO_3^-} \alpha_{CO_3^{2-}} C_{T,CO_3}) \quad (3.33)$$

$$\beta_{NH_3} = 2.3 \alpha_{NH_4^+} \alpha_{NH_3} C_{T,NH_3} \quad (3.34)$$

where α represents the mole fraction of the chemical species, C_{T,CO_3} represents the total concentration of carbonate species ($H_2CO_3 + HCO_3^- + CO_3^{2-}$), and C_{T,NH_3} represents the total concentration of ammonium species ($NH_4^+ + NH_{3(aq)}$). Total ammonium concentrations are taken from our measurements.

Table 3.8. Contributions of various chemical components to the initial acid buffer intensities at the sample pH

Location and date	Sample name	Sample pH	Initial β (μM)	$P_{\text{CO}_2} = 360 \text{ ppm, } T = 293 \text{ K}$					$P_{\text{CO}_2} = 500 \text{ ppm, } T = 278 \text{ K}$				
				β_{CO_2} (μM)	β_{NH_3} (μM)	% CO_2	% NH_3	% CO_2 and NH_3	β_{CO_2} (μM)	β_{NH_3} (μM)	% CO_2	% NH_3	% CO_2 and NH_3
Bakersfield, CA 1/15/94	Large #1	6.48	244.5	17.8	19.2	7.3	7.8	15.1	35.7	59.9	14.6	24.5	39.1
	Small #1	5.89	192.6	7.8	20.2	4	10.5	14.5	14.7	63.7	7.6	33.1	40.7
	Large #1B	6.76	174.3	22.7	19.7	13	11.3	24.3	46.6	60.9	26.7	34.9	61.6
	Large #2	6.62	312.2	21.2	17.1	6.8	5.5	12.3	43.2	53.1	13.8	17	30.8
	Small #2	6.41	166	16.3	55.9	9.8	33.7	43.5	32.4	175	19.5	105.4	124.9
	Large #2B	6.91	269.4	24.9	36	9.2	13.4	22.6	51.7	110.5	19.2	41	60.2
	Large #3	6.76	458.4	22.7	29.7	4.9	6.5	11.4	46.6	91.9	10.2	20	30.2
	Bulk #1	6.03	195.3	9.8	14.9	5	7.6	12.6	18.8	46.8	9.6	23.9	33.5
	Bulk #2	6.58	114.9	18.2	33.2	15.8	28.9	44.7	36.5	103.6	31.7	90.2	121.9
Bakersfield, CA 1/16/94	Large #1	6.29	48.4	14.3	8.5	29.6	17.5	47.1	28.1	26.6	58	55	113
Bakersfield, CA 12/10/95	Bulk #1	6.32	57.2	14.9	4.9	26	8.6	34.6	29.2	15.5	51.1	27	78.1
	Bulk #2	6.19	26.7	12.5	4.4	46.8	16.4	63.2	24.3	13.8	46.8	51.6	98.4
	Bulk #3	6.32	19.8	14.9	4.3	75	21.9	96.9	29.2	13.6	147.6	68.7	216.3
	Bulk #4	6.27	24.7	13.9	3.5	56.4	14.2	70.6	27.3	11	110.5	44.6	155.1
	Bulk #5	5.98	10.8	9	2.9	83.4	26.6	110	17.3	9.1	83.4	83.9	167.3
	Bulk #6	4.97	8.6	1.2	0.4	13.7	4.9	18.6	2.2	1.3	25.1	15.5	40.6
	Bulk #7	6.09	24.3	10.8	2.8	44.4	11.5	55.9	20.8	8.8	85.4	36.1	121.5
	Bulk #8	5.36	4.8	2.8	0.5	57.2	11.2	68.4	5.1	1.7	105.5	35.5	141

The contributions of CO_2 and NH_3 to the initial acid buffer intensity are calculated for two conditions. One is a CO_2 partial pressure of 360 ppm and a temperature of 293 K, close to the conditions where acid titrations were measured. The second is a CO_2 partial pressure of 500 ppm (representative of high CO_2 concentrations measured in stagnant conditions at a busy urban intersection during morning rush hour, per Doug Lawson, Colorado State University, personal communication) and a temperature of 278 K, to account for severe pollution when fogwater was sampled. These latter conditions are chosen to represent an upper limit of the buffering contributions of NH_3 and CO_2 . Real contributions were almost certainly less than this case represents, since CO_2 concentrations tend to decline rapidly due to dispersion away from source areas and dissolved CO_2 was probably outgassed from samples as they were warmed during the titration process.

At the background CO_2 concentration and high temperature the acid buffer intensities from $\text{CO}_3^{2-}/\text{HCO}_3^-/\text{H}_2\text{CO}_3$ and $\text{NH}_{3(\text{aq})}/\text{NH}_4^+$ systems together contribute at most about 44 percent of the measured buffer intensity for the highly polluted fog samples collected on January 15, 1994 in Bakersfield, California. However, for the moderately polluted fog samples collected in Bakersfield on December 10, 1995, contributions of $\text{CO}_3^{2-}/\text{HCO}_3^-/\text{H}_2\text{CO}_3$ and $\text{NH}_{3(\text{aq})}/\text{NH}_4^+$ systems can be as high as 100 percent with many around 60 percent. For the cold, severe pollution conditions, CO_2 and NH_3 account for 100 percent of the observed buffer intensity in some samples, but still are insufficient to account for the buffering intensity observations in many samples from January 15, 1994. The calculated buffering contributions using the cold, polluted case assumptions represent much more than 100 percent of the observed buffering in several of the December 10, 1995 samples, but are still below the

measured buffering in other samples from this event. Actual contributions of NH_3 and the carbonate species to the buffering are almost certainly less than calculated for the high CO_2 case. Yet even with these upper limit calculations, the observed buffering in several samples can not be accounted for by ammonia, bicarbonate, and carbonate. Apparently, other species must be present to add to the internal buffering capacity of the drops.

A further clue about the source of the buffering can be obtained by comparing acid titration curves for small and large fog drop fractions. Figure 3.33 depicts acid titration curves for large and small fog drop fractions collected at the rural KWR site on January 1, 1996. Although the initial pH of the large drops is higher than the small drop pH during both time periods illustrated, the crossover of the large and small drop acid titration curves in both cases indicates that greater total buffer capacity is present in the small fog drops, i.e., more added acid is eventually neutralized by the small drop fraction. Analysis of large and small fog and cloud drop fractions collected at a variety of sites with the size fractionating CASCC typically reveals small drops to be enriched in secondary, accumulation mode aerosol species (e.g., sulfate, nitrate, and ammonium) while large drops are preferentially enriched in coarse, primary aerosol species (e.g., soil dust and sea salt species) (Bator and Collett, 1997). We have found the small drops are often enriched in total organic carbon relative to the large drops as well. Taken together, these observations suggest that the buffering may be associated with accumulation mode aerosol rather than coarse aerosol, although it is also possible that the buffer agent is a soluble gaseous species absorbed by the drops. A variety of organic compounds appear to be candidates for the buffering. These include several nitrated phenols

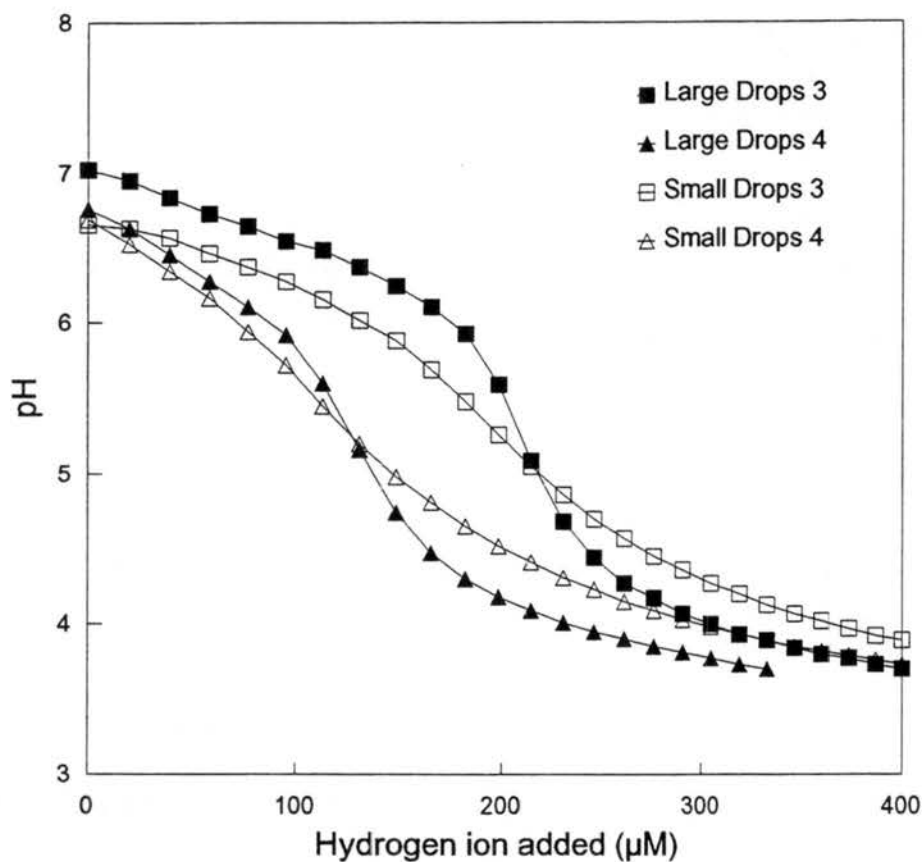


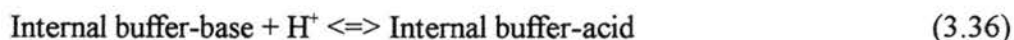
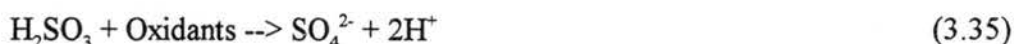
Figure 3.33. Acid titration curves for small ($4 < d < 23 \mu\text{m}$) and large ($d > 23 \mu\text{m}$) drop fractions collected with the size fractionating CASCC at a rural site near the Kern Wildlife Refuge in California's San Joaquin Valley on January 1, 1996.

which have pK_a 's in the pH range where the buffering appears strongest and which have been found in urban fog at a number of locations (Trempe, 1992).

The presence of significant buffer capacity within fog drops and atmospheric basic gases provide important mechanisms for absorbing hydrogen ions released in the drops as a result of sulfuric acid production, meaning fog pH could remain high for a longer time in a well buffered system. Consequently, the S(IV) oxidation rate may be enhanced, especially for those oxidation pathways effective at high pH. If rates of the pH sensitive pathways remain elevated for some time, they may play a greater role in total S(IV) oxidation than is typically expected.

A simple simulation was conducted to compare changes of pH and S(IV) oxidation rates over time for the small and large drops, with and without acid buffering. Three S(IV) oxidation pathways were considered: oxidation by H_2O_2 , by O_3 and autooxidation catalyzed by the simultaneous presence of Fe(III) and Mn(II). Rate laws for these oxidation pathways can be found in section 3.3.1. Fog chemical compositions for the simulation were based on our measurements of the highly buffered January 15, 1994 Bakersfield fog, with assumptions made as to the fraction of total Fe and Mn present in catalytic form. The fogwater chemical composition was held constant at $1.5 \mu M H_2O_2$, $16.6 \mu M Fe(III)$, and $0.2 \mu M Mn(II)$ for the small drops with initial pH of 5.89 and at $0.3 \mu M H_2O_2$, $5.3 \mu M Fe(III)$, and $0.9 \mu M Mn(II)$ for the large drops with initial pH of 6.48. The sulfur dioxide gas phase partial pressure was maintained at 0.07 ppbv (measured value during the sampling period) and the partial pressure of ozone in the gas phase was fixed at 7.0 ppbv (the average value during the fog event). Fogwater acidity produced due to S(IV) oxidation was buffered by internal weak acids and

external NH_3 . The contribution of carbonate species to acid buffer intensity is included in the internal buffer intensity. Further dissolution of gaseous CO_2 can not provide additional buffering capacity since dissociation of aqueous CO_2 to bicarbonate/carbonate, the effective buffer species, is associated with production of hydrogen ion. Internal acid buffering was selected to match that observed in the titrated fog samples (or set to zero). The NH_3 partial pressure was held constant at 5 ppbv to provide external buffering. The aqueous ammonia concentration was held at equilibrium with the gaseous ammonia during the process of buffering. The chemical processes of acid production and internal and external buffering are expressed in Equations (3.35) - (3.38).



A schematic diagram for the modeling approach is shown in Figure 3.34. The model allows one to investigate changes of the rates of S(IV) oxidation with time and to calculate amounts of sulfate produced over time. Calculations of S(IV) oxidation rates will assume aqueous $\text{SO}_2\text{H}_2\text{O}$ and O_3 concentrations are in equilibrium with the gas phase. Hydrogen ion concentration changes during cloud events will be governed by S(IV) oxidation, internal acid buffer intensities and uptake of atmospheric ammonia. The mathematical equations employed in the model simulation are listed in Figure 3.35.

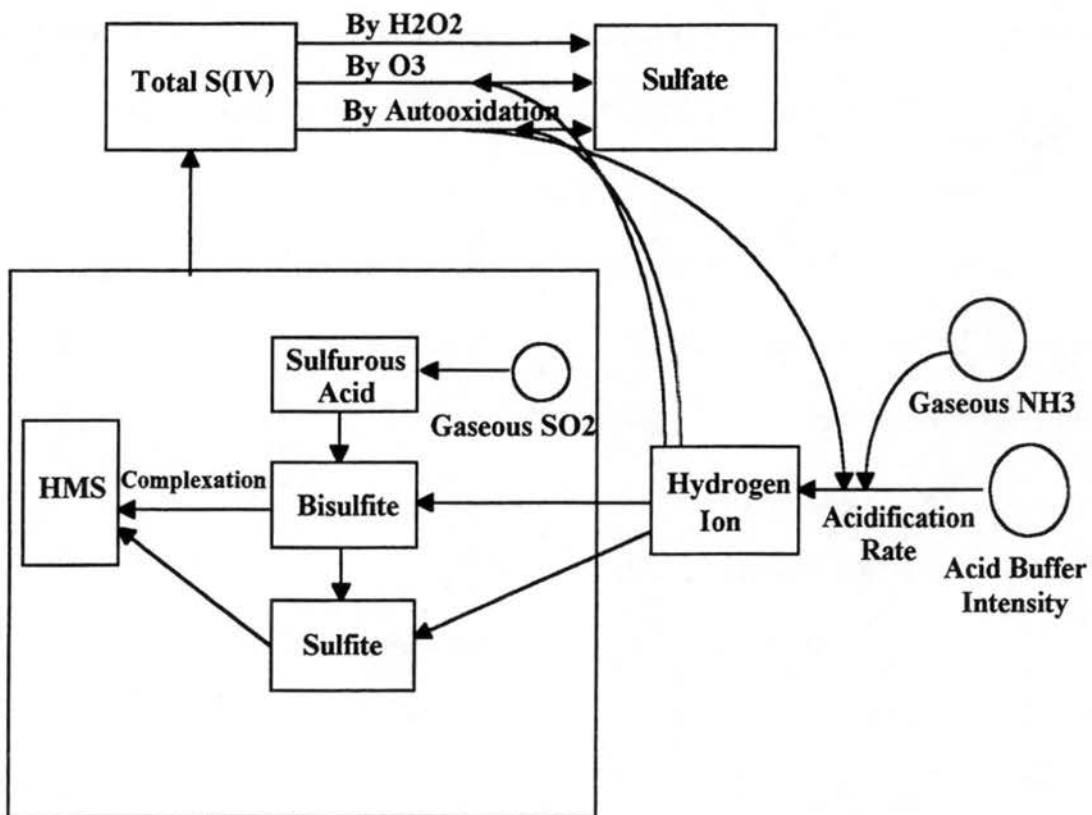


Figure 3.34. Diagram of the model simulation.

- [Sulfate](t) = [Sulfate](t - dt) + (Rate of S(IV) Oxidation by H₂O₂ + Rate of S(IV) Oxidation by O₂\Fe(III)\Mn(II) + Rate of S(IV) Oxidation by O₃) * dt
- Initial [Sulfate] = 0
- Rate of S(IV) Oxidation by H₂O₂ = k[H⁺][H₂O₂][S(IV)]α₁/(1+K[H⁺])
- Rate of S(IV) Oxidation by O₂\Fe(III)-Mn(II) = K_s[H⁺]^{-0.74}[Fe(III)][Mn(II)][S(IV)]
@ pH ≤ 4.2
- Rate of S(IV) Oxidation by O₂\Fe(III)-Mn(II) = K_s"[H⁺]^{0.67}[Fe(III)][Mn(II)][S(IV)]
@ pH ≥ 4.2
- Rate of S(IV) Oxidation by O₃ = (k₀a₀ + k₁a₁ + k₂a₂)[S(IV)][O₃]
- [H₂O₂] = Constant
- [O₃] = P_{O₃} * H_{O₃}
- [SO₂H₂O] = P_{SO₂} * H_{SO₂}
- Free [S(IV)] = [SO₂H₂O] + [HSO₃⁻] + [SO₃²⁻]
- [Total Sulfur (IV)] = [SO₂H₂O] + [HSO₃⁻] + [SO₃²⁻] + [HMS]
- [HMS](t) = [HMS](t - dt) + (Complexation Rate) * dt
- Initial [HMS] = 0
- Complexation Rate = k₁[S(IV)]a₁[HCHO] + k₂[S(IV)]a₂[HCHO]
- [H⁺](t) = [H⁺](t - dt) + (d[H⁺]/dt) * dt
- Initial [H⁺] = 10^(- Initial pH value)
- Rate of [H⁺] Change = 2*(Rate of S(IV) Oxidation by H₂O₂ + Rate of S(IV) Oxidation by O₃ + Rate of S(IV) Oxidation by O₂\Fe(III)-Mn(II))/Acid Buffering Capacity - (Rate of Gaseous NH₃ Uptake)
- Acid Buffer Intensity = GRAPH(pH)

Figure 3.35. Mathematical equations employed in the simulation.

By definition the internal buffer intensity (β) is the number of units of added acid needed per unit pH decrease ($-dC_A/dpH$). It can be converted to a modified buffer intensity (β') defined as the unit increase of acid needed per unit hydrogen ion increase ($dC_A/d[H^+]$). Since increase of acid in the simulation is due to production of sulfate, every molecule of sulfate production can generate two molecules of hydrogen ion. β' is equivalent to two times the number of units of sulfate produced per unit of hydrogen ion increase (Equation (3.39)).

$$\beta' = \frac{dC_A}{d[H^+]} = \frac{2d[S(VT)]}{d[H^+]} \quad (3.39)$$

The relationship between β and β' is

$$\beta' = \frac{1}{2.3[H^+]} \beta \quad (3.40)$$

Therefore the acidification rate of fog drops ($d[H^+]/dt$) in the presence of internal buffering is

$$\frac{d[H^+]}{dt} = \frac{2d[S(IV)]}{dt} \frac{d[H^+]}{2d[S(VT)]} = \frac{2d[S(VT)]}{dt} \frac{1}{\beta'} \quad (3.41)$$

where $d[S(IV)]/dt$ is the sulfur oxidation rate. Since every mole of SO_2 oxidation will produce two moles of hydrogen ions, the sulfur oxidation rate is multiplied by two to get the acid production rate.

In the presence of gaseous NH_3 a part of the acid produced above will be neutralized by absorbed NH_3 . If the neutralization rate by NH_3 is x and x is fast enough compared to the sulfate production rate, then the final acidification rate would be

$$\frac{d[H^+]}{dt} = \frac{2d[S(IV)]}{dt} \frac{1}{\beta'} - x \quad (3.42)$$

where β' is the modified buffer intensity excluding buffer from NH_3 . X can be obtained by an equilibrium consideration between aqueous NH_3 and NH_4^+ . At any time Equation (3.43) must be satisfied.

$$\frac{[H^+]_t}{[NH_4^+]_t} = \frac{K_a}{[NH_3]_{aq}} \quad (3.43)$$

where K_a is the dissociation constant of NH_4^+ . After a small time increment the amount of hydrogen ion neutralized by NH_3 has to equal the amount of NH_4^+ produced due to acid neutralization and therefore Equation (3.45) must be satisfied.

$$\frac{[H^+]_{t+dt}}{[NH_4^+]_{t+dt}} = \frac{K_a}{[NH_3]_{aq}} \quad (3.44)$$

$$\frac{[H^+]_{t+dt}}{[NH_4^+]_{t+dt}} = \frac{[H^+]_t + 2 \frac{d[S(IV)]}{dt} \frac{1}{\beta'} dt - xdt}{[NH_4^+]_t + xdt} \quad (3.45)$$

where the term $\frac{2d[S(IV)]}{dt} \frac{1}{\beta'} dt$ is the acid produced after considering the internal buffer except NH_3 ; the term xdt is the amount of acid neutralized by NH_3 . Therefore we have

$$\frac{[H^+]_t + \frac{2d[S(VT)]}{dt} \frac{1}{\beta'} dt - xdt}{[NH_4^+]_t + xdt} = \frac{K_a}{[NH_3]_{aq}} \quad (3.46)$$

or, equivalently,

$$[H^+]_t [NH_3]_{aq} + \frac{2d[S(VT)]}{dt} \frac{1}{\beta'} [NH_3]_{aq} dt - x [NH_3]_{aq} dt = K_a [NH_4^+]_t + K_a x dt \quad (3.47)$$

Recalling that $[H^+]_t [NH_3]_{aq} = K_a [NH_4^+]_t$, this becomes

$$\frac{2d[S(VT)]}{dt} \frac{1}{\beta'} [NH_3]_{aq} - x [NH_3]_{aq} = K_a x \quad (3.48)$$

so that

$$x = \frac{\frac{2d[S(VT)]}{dt} \frac{1}{\beta'} [NH_3]_{aq}}{[NH_3]_{aq} + K_a} \quad (3.49)$$

noting that

$$[NH_3]_{aq} = P_{NH_3} H_{NH_3} \quad (3.50)$$

where P_{NH_3} and H_{NH_3} are the partial pressure and Henry's law coefficient of NH_3 , respectively.

So that

$$x = \frac{\frac{2d[S(VT)]}{dt} \frac{1}{\beta'} P_{NH_3} H_{NH_3}}{P_{NH_3} H_{NH_3} + K_a} \quad (3.51)$$

Substituting Equation (3.51) into Equation (3.42) gives the acidification rate

$$\frac{d[H^+]}{dt} = \frac{2d[S(IV)]}{dt} \frac{1}{\beta} \frac{K_a}{K_a + P_{NH_3} H_{NH_3}} \quad (3.52)$$

Figure 3.36 depicts the fog pH and oxidation rates predicted by the simulation in the case with no acid buffering, with external NH_3 buffering only and with both internal and external buffering. S(IV) oxidation by H_2O_2 is always unimportant compared to S(IV) oxidation by O_3 and/or autooxidation in the three cases. Therefore the oxidation rates by H_2O_2 are not plotted in Figure 3.36. In the case of no acid buffering (Figure 3.36 (1a) and (2a)), The pH values decrease 1.62 and 2.30 units for small and large drops respectively over the four hour simulation. The chemical heterogeneity in pH between drops of diverse sizes diminishes in ten minutes. The fast acidification results in a decrease of the rate of S(IV) oxidation by ozone by four orders of magnitude. The trace metal catalyzed S(IV) autooxidation becomes predominant in ten minutes. Therefore the chemical heterogeneity in Fe(III) and Mn(II) plays an important role in enhancement of sulfate production. Table 3.9 presents the sulfate concentrations produced over the four hour simulation and enhancement factors of sulfate production due to the presence of chemical heterogeneity. Because of association of high catalyst concentrations with low pH drops, the sulfate production is suppressed by 14% due to the presence of chemical heterogeneity in the no buffer case.

When external NH_3 buffering is included, the pH drop is much smaller and the chemical heterogeneity in pH remains longer compared to the no buffer case. Both S(IV) oxidation by ozone and autooxidation are important oxidation pathways.

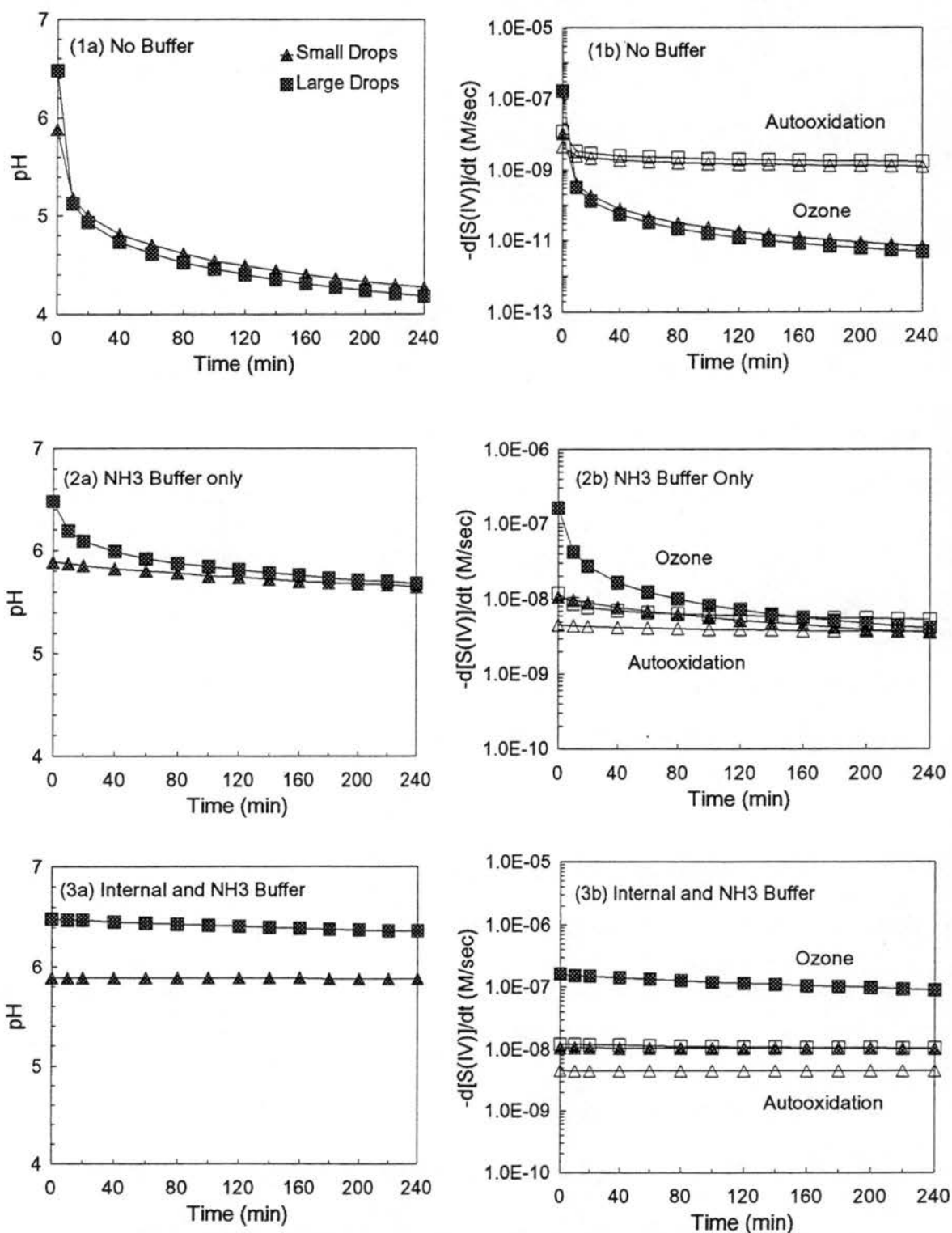


Figure 3.36. (1a) - (3a) Profile of pH versus time. (1b) - (3b) Profile of S(IV) oxidation by ozone and S(IV) autooxidation versus time. Filled squares and triangles refer to the ozone pathway and open squares and triangles refer to the autooxidation path. The simulation temperature was 278 K; partial pressures of sulfur dioxide, ozone and ammonia were 0.07, 7.0 and 5.0 ppbv, respectively.

Table 3.9. Effects of external and internal buffering on sulfate production over the four hour simulation. $f_{\text{Small Drops}} = 0.15$, $f_{\text{Large Drops}} = 0.85$, LWC = 0.06 g/m³ and T = 278 K.

	No buffer	External NH ₃ buffer	External and internal buffer
Sulfate production in small drops (μM)	26	140	220
Sulfate production in large drops (μM)	33	270	1860
Overall sulfate production in homogeneous fog (μg/m ³)	2.2	15.6	71.8
Overall sulfate production in heterogeneous fog (μg/m ³)	1.9	15.0	96.9
Enhancement of sulfate production	0.86	0.96	1.35

Consequently, the rates of the S(IV) oxidation are higher and the decrease in sulfate production due to the chemical heterogeneity of pH, Fe and Mn is only 4%. When both external NH₃ and internal buffering are included, only a slight drop in pH is predicted and the chemical heterogeneity in pH between small and large drops remains throughout the four hour simulation. The enhancement in sulfate production due to the chemical heterogeneity is 35%. With both external and internal buffering the overall sulfate production increases about 50 times compared to the no buffer case and 6.5 times compared to the external NH₃ buffer case. The consequences of the internal buffering, therefore, are (1) the fog pH remains nearly steady, despite the fact that sulfuric acid production is greater, as a result of maintaining a high rate of S(IV) oxidation by ozone; (2) the chemical heterogeneity between small and large drops remains nearly as in the initial state after a four hour simulation; (3) sulfate production is enhanced due to the chemical heterogeneity whereas some suppression of sulfate production is expected from the chemical heterogeneity when internal buffering is ignored. The findings

presented here suggest that internal acid buffering at high pH may help to sustain high sulfate production rates in large drops that might otherwise drop off rapidly as the drops acidify due to sulfuric acid production. The internal acid buffering may also help to maintain chemical heterogeneity among the fog drop population throughout the fog event. Therefore using bulk fogwater chemical composition to predict sulfate production may generate large errors.

3.5.2. Coastal stratus clouds at Angora Pk., Oregon

3.5.2.1. Cloud water chemical heterogeneity and enhancements in S(IV) oxidation rates

Coastal stratus clouds were sampled in July 1993 at Angora Pk., a remote site on the northern Oregon coast. The size-fractionating CASCC and CASCC2 were used to sample drops of two size classes and bulk cloudwater respectively.

The liquid water content and the chemical compositions of the cloud drops of two size fractions and the bulk water are shown in Figure 3.37. The liquid water contents were obtained from measurements of the cloudwater collection rates and the formulas by Demoz et al. (1996).

The cloud pH ranged from 4.34 to 6.03. Whereas S(IV) oxidation by hydrogen peroxide is an important oxidation pathway, ozone and metal catalyzed oxidation may also contribute significantly to the total S(IV) oxidation in this pH range. S(IV) oxidation through ozone and metal catalyzed pathways are strong functions of cloud acidity and catalyst concentrations. Presence of cloud chemical heterogeneity in these parameters, therefore, is expected to enhance the in-cloud S(IV) oxidation rate.

The chemical heterogeneity was evidenced by measurements of the chemical compositions of two drop size classes (Figure 3.37). The small drops were associated with lower acidity and peroxide concentrations and higher trace metals concentrations compared to the large drops. The chemical heterogeneity indicates that S(IV) oxidation by ozone and autooxidation catalyzed by trace metals may contribute important portions to total S(IV) oxidation in the small drops. Table 3.10 compares percentages of total S(IV) oxidation

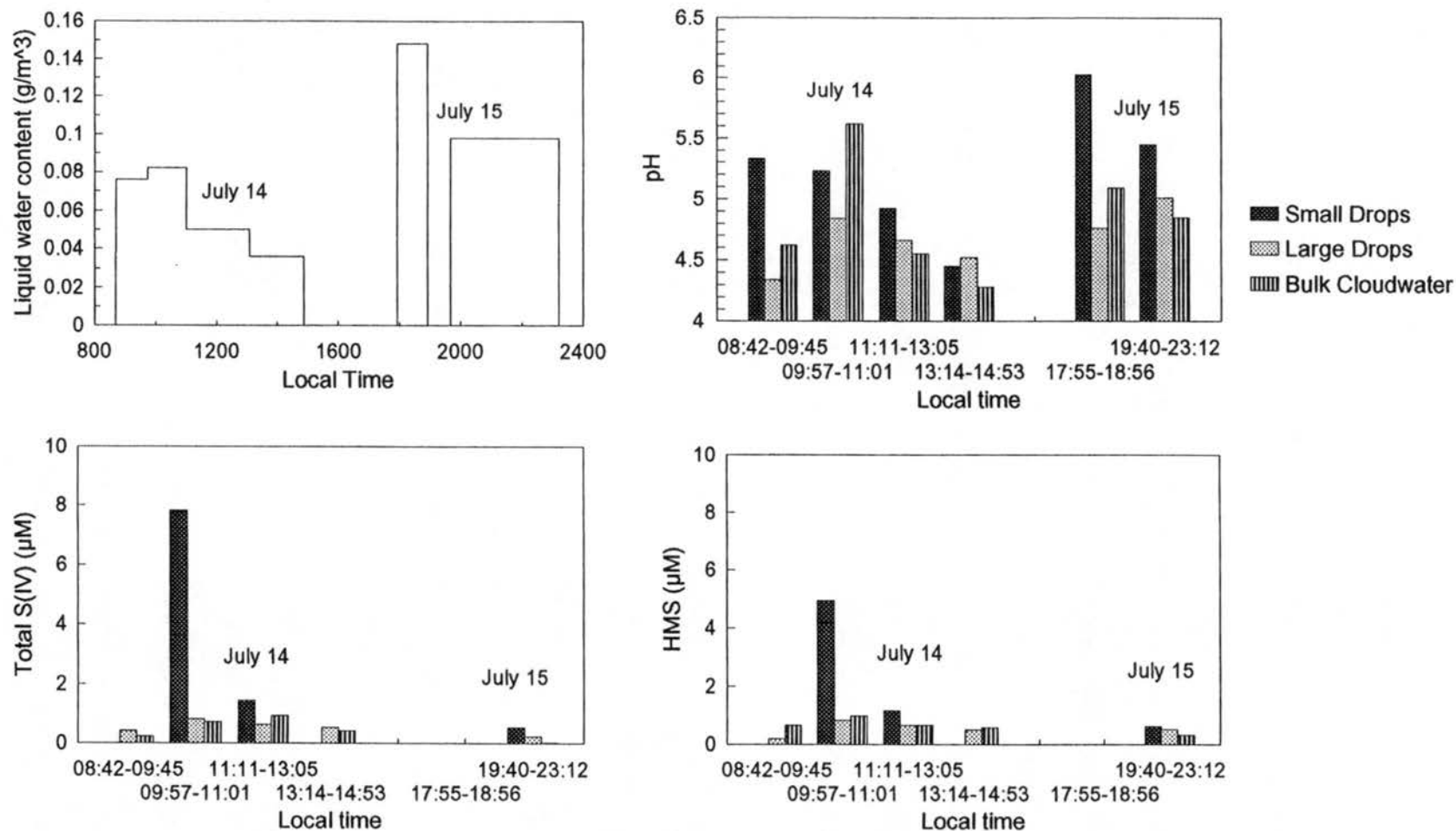


Figure 3.37. The liquid water contents and chemical compositions of clouds at Angora Pk., Oregon, July 14-15, 1993. The small and large drops were collected by the sf-CASCC and the bulk cloudwater was collected by the CASCC2.

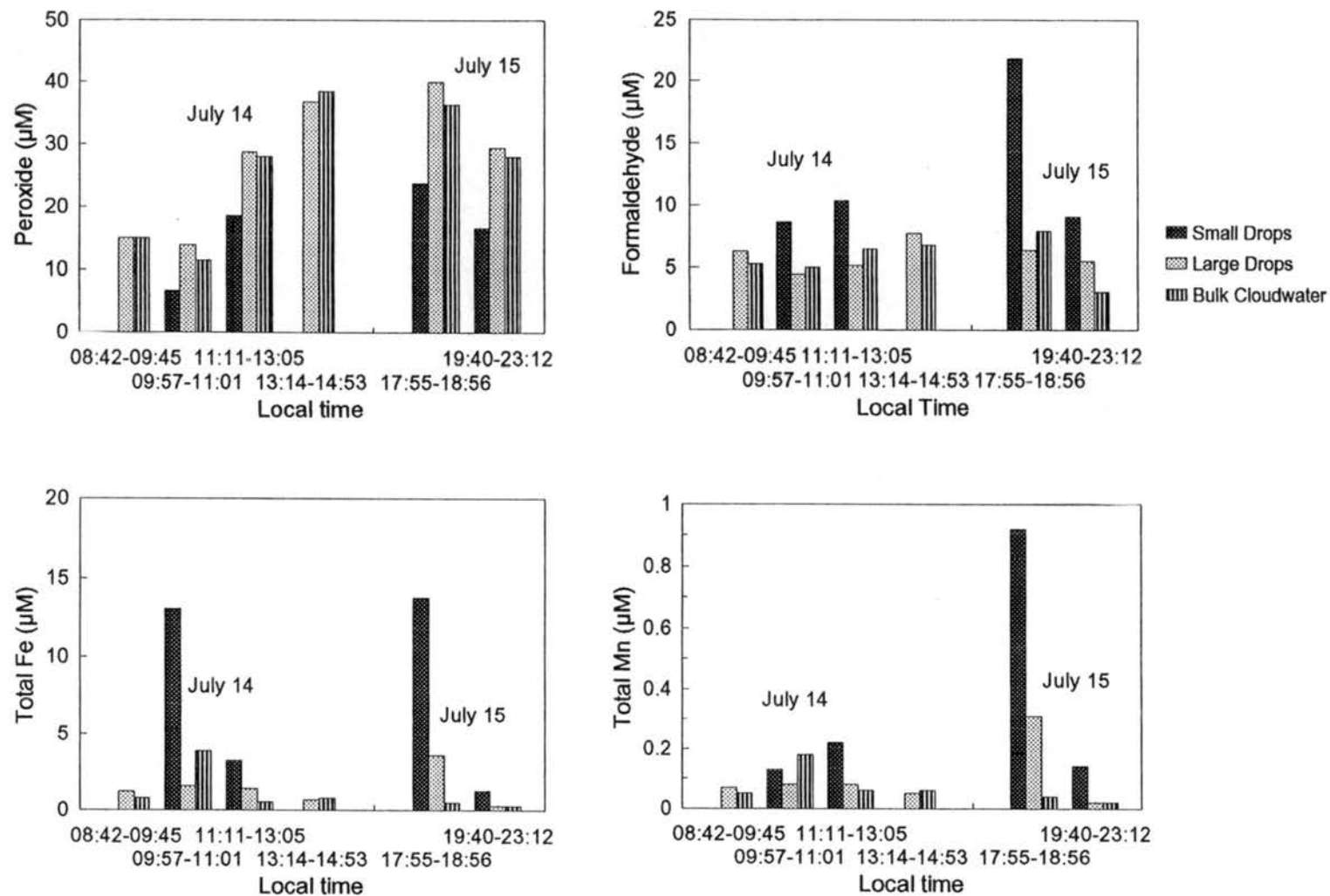


Figure 3.37 (continued). Chemical compositions of clouds at Angora Pk., Oregon, July 14-15, 1993. The small and large drops were collected by the sf-CASCC and the bulk cloudwater was collected by the CASCC2.

through peroxide, ozone and trace metal catalyzed pathways for the cloud events of July 14 and 15, 1993. An ozone concentration of 30 ppbv is used to represent a value typically observed in clean atmospheres. Hydrogen ion, peroxide and trace metal concentrations are from our measurements. It is assumed that the fraction of dissolved iron comprises 50% of the total iron and Fe^{3+} comprises 50% of the dissolved iron. Soluble Mn^{2+} is assumed to comprise 100% of the total Mn. Rate laws for S(IV) oxidation can be found in section 3.3.1. Temperature is 10 °C.

Table 3.10. Contributions of different S(IV) oxidation pathways in the small and large drops; $P_{\text{O}_3} = 30$ ppb, $f_{\text{Fe(Mn)}} = 0.25$.

Date	Local time	Small drops			Large drops		
		% H_2O_2	% O_3	% $\text{O}_2/\text{Fe-Mn}$	% H_2O_2	% O_3	% $\text{O}_2/\text{Fe-Mn}$
07/14/1993	09:57-11:01	22.4	62.9	14.6	79.9	18.6	1.5
	11:11-13:05	75.3	18.6	6.1	94.6	4.7	0.7
07/15/1993	17:55-18:56	2.9	89.1	8	90.3	5	4.7
	19:40-23:12	24.2	75	0.8	81	19	0

While S(IV) oxidation by peroxide was the dominant oxidation pathway (80% - 95%) in the large drops, peroxide in the small drops, on the other hand, only contributed 3% to 75% of the total S(IV) oxidation. S(IV) oxidation by ozone and autooxidation catalyzed by Fe^{3+} and Mn^{2+} together contributed large portions of the total S(IV) oxidation in three of the four small drop samples. All three S(IV) oxidation pathways played important roles in oxidizing S(IV) in the small drops.

Due to the cloud chemical heterogeneity it is expected that contributions of the different oxidation paths to the total S(IV) oxidation may differ depending on whether the

clouds are treated as being comprised of chemically homogeneous or heterogeneous drops. In the chemically homogeneous clouds the oxidation rate is calculated based on a volume-weighted average chemical composition of small and large drops. In the chemically heterogeneous clouds the S(IV) oxidation rate through the different oxidation paths is the volume-weighted oxidation rate of small and large drops. From Table 3.11 we see that ozone and trace metals play more important roles in S(IV) oxidation when the clouds are treated as being comprised of a chemically heterogeneous drop population.

Table 3.11. Contributions of different S(IV) oxidation pathways in chemically homogeneous and heterogeneous clouds; $P_{O_3} = 30$ ppb, $f_{Fe/Mn} = 0.25$.

Date	Local time	Homogeneous clouds			Heterogeneous clouds		
		% H ₂ O ₂	% O ₃	% O ₂ /Fe-Mn	% H ₂ O ₂	% O ₃	% O ₂ /Fe-Mn
07/14/1993	09:57-11:01	67.2	27	5.8	55.5	37.4	7.1
	11:11-13:05	78.8	16	5.2	77.5	17	5.5
07/15/1993	17:55-18:56	86.4	6.1	7.4	30.8	62.2	7
	19:40-23:12	76.6	23.3	0.1	67.1	32.7	0.2

As stated above oxidation of S(IV) by ozone and S(IV) autooxidation played important roles in the cloud events. Variations of pH and catalyst concentrations as a function of drop size can result in various S(IV) oxidation rates in small and large drops. Calculations of total S(IV) oxidation rates in the small and large drops and in the bulk cloudwater and the chemically heterogeneous clouds are shown in Table 3.12. Assumptions were made as for the calculations in Table 3.10 in terms of the ozone concentration and the fractions of dissolved Fe³⁺. Generally the total oxidation rates are higher in the small drops due to their higher pH and catalyst concentrations, except in the second time period of July 14 when the peroxide

pathway dominates the S(IV) oxidation and the large drops sustain a higher oxidation rate. The enhancements in S(IV) oxidation due to the chemical heterogeneity range from 1.02 to 2.80 in the cloud event of July 14 and 15, 1993. Larger enhancements are predicted when oxidation by peroxide contributes less to the total S(IV) oxidation and variations in cloud pH and trace metal concentrations between small and large drops were large. The decrease in enhancement with time in an event was due to rapid acidification of small drops and a decrease in catalyst concentrations in small drops.

Table 3.12. Total S(IV) oxidation rates in the clouds of Angora Pk., Oregon (M/sec); $P_{SO_2} = 5$ ppb, $P_{O_3} = 30$ ppb, $f_{Fe(III)} = 0.25$

Date	Local time	Small drops	Large drops	Bulk water	Volume weighted	Enhancements
07/14/1993	09:57-11:01	1.94E-07	1.12E-07	1.13E-07	1.37E-07	1.21
	11:11-13:05	1.60E-07	1.97E-07	1.61E-07	1.64E-07	1.02
07/15/1993	17:55-18:56	5.39E-06	2.88E-07	2.88E-07	8.07E-07	2.8
	19:40-23:12	4.46E-07	2.37E-07	2.34E-07	2.67E-07	1.14

Uncertainties in the ozone concentration can result in uncertainties in the contributions of ozone to the total S(IV) oxidation. Table 3.13 compares the contributions of S(IV) oxidation by ozone as gaseous ozone is assumed to be 30 ppb and 10 ppb. When the gaseous ozone concentration decreases the contributions of ozone to the overall S(IV) oxidation decrease. While the contributions of S(IV) autooxidation catalyzed by trace metals do not change substantially with ozone concentration change, the contributions of H_2O_2 increase considerably as the ozone concentration decreases. Consequently smaller enhancements of S(IV) oxidation were predicted due to the intensified S(IV) oxidation by H_2O_2 .

Table 3.13. Influence of the ozone concentration on contributions of the different S(IV) oxidation paths in the chemically heterogeneous cloud

Date	Local time	30 ppb O ₃				10 ppb O ₃			
		% H ₂ O ₂	% O ₃	% O ₂ /Fe-Mn	Enhance- ment	% H ₂ O ₂	% O ₃	% O ₂ /Fe-Mn	Enhance- ment
07/14/93	09:57-11:01	55.5	37.4	7.1	1.21	73.9	16.6	9.4	1.11
	11:11-13:05	77.5	17	5.5	1.02	87.4	6.4	6.2	1.01
07/15/93	17:55-18:56	30.8	62.2	7	2.8	52.7	35.4	11.9	1.71
	19:40-23:12	67.1	32.7	0.2	1.14	85.8	13.9	0.3	1.06

We have seen that S(IV) autooxidation catalyzed by both iron and manganese may contribute 7 percent of the total S(IV) oxidation in the chemically heterogeneous clouds. It has been assumed that effective catalyst Fe³⁺ species comprise 25% of the measured total iron. Uncertainties in the fraction of dissolved Fe³⁺ can influence the importance of the trace metal catalyzed S(IV) oxidation path. If the fraction of dissolved Fe³⁺ increases from 25% to 50%, the S(IV) autooxidation path may contribute up to 13 percent (Table 3.14). Although S(IV) autooxidation contributes larger fractions when the dissolved Fe³⁺ increases from 25% to 50%, the enhancements in S(IV) oxidation do not change considerably. This is because the contributions of S(IV) oxidation by H₂O₂ do not decrease substantially. Secondly, the effect of an increase in contributions of S(IV) autooxidation and a decrease in contributions of S(IV) oxidation by O₃ on enhancement of S(IV) oxidation canceled each other.

Uncertainties in the fraction of dissolved Fe³⁺ result from the presence of inorganic and organic ligands and from in-cloud photochemical activities. While the presence of inorganic and organic ligands will increase the solubility of iron, photochemical activity will influence the speciation of iron between Fe(II) and Fe(III) (Faust, 1994).

Table 3.14. Influence of the catalytically active iron fraction on contributions of the different S(IV) oxidation paths in the chemically heterogeneous clouds

Date	Local time	25% of total Fe as Fe ³⁺				50% of total Fe as Fe ³⁺			
		% H ₂ O ₂	% O ₃	% O ₂ /Fe-Mn	Enhancement	% H ₂ O ₂	% O ₃	% O ₂ /Fe-Mn	Enhancement
07/14/93	09:57-11:01	55.5	37.4	7.1	1.21	51.8	34.9	13.2	1.23
	11:11-13:05	77.5	17	5.5	1.02	73.5	16.1	10.4	1.02
07/15/93	17:55-18:56	30.8	62.2	7	2.8	28.8	58.1	13	2.79
	19:40-23:12	67.1	32.7	0.2	1.14	66.9	32.6	0.4	1.14

Dissolution of iron can also be photoassisted (Pehkonen et al., 1993; Sulzberger et al., 1994). Studies on photochemical reactions of Fe(III) species in authentic cloud waters have shown that Fe(II) and Fe(III) undergo rapid cycling via photochemical reactions (Sedlak and Hoigne, 1993; Zuo, 1992). Therefore concentrations of Fe(II) and Fe(III) are expected to be in a dynamic equilibrium at daytime.

The cloud event of July 14, 1993 occurred at daytime. It is expected that photochemical activity may have influenced S(IV) oxidation. Although Fe speciation was not measured on site, simple photochemical experiments using the Oregon cloud samples and prepared Fe(III) complex solutions were conducted in the laboratory in order to study possible effects of photochemical reactions on S(IV) oxidation.

3.5.2.2. Photochemical reactions in the authentic cloud water and prepared solutions and their influence on S(IV) oxidation

It has been demonstrated that Fe(III) can initiate photochemical reactions in cloud waters leading to formation of important oxidants, including $\cdot\text{OH}$, HO_2/O_2^- and H_2O_2 (Allen

and Faust, 1994; Faust and Zepp, 1993; Graedel et al., 1985; Siefert et al., 1996; Zuo and Hoigne, 1992; 1993;). The photochemical reactions can influence oxidation of S(IV) through the formation of oxidants and by affecting the speciation of iron. One of the important Fe(III) species involved in photochemical reactions is Fe(III)-polycarboxylates. Polycarboxylates are common constituents in atmospheric aerosols and water (Grosjean et al., 1978; Likens et al., 1983; Satsumabayashi et al., 1990), and measured Fe concentrations in atmospheric water are often comparable in magnitude with polycarboxylate concentrations. It has been shown that photochemistry of Fe(III)-polycarboxylate complexes is a potentially important source of Fe(II) and oxidants $\cdot\text{OH}$, HO_2/O_2^- and H_2O_2 in cloudwater (Pehkonen et al., 1993; Zuo and Hoigne, 1992).

Absorption spectra of small and large cloud drop samples from July 14, 1993 Oregon coastal stratus cloud were measured between 280 and 600 nm (Figure 3.38). The absorption spectra have overlap regions with the sunlight spectrum at wavelengths greater than 300 nm. The absorption spectra demonstrate that the cloud water contains light-absorbing substances or functional groups. This UV-light absorption can initiate photochemical reactions.

Preliminary photochemical experiments were carried out at indoor and outdoor environments at Colorado State University in Fort Collins, Colorado. Indoor photochemical experiments were conducted in a quartz cuvette with dimensions of 1.0-cm L x 0.5-cm W x 4.5-cm H. Authentic cloud waters were irradiated with 313 nm light from a xenon lamp in a Shimadzu RF-1510 spectrofluorophotometer. Concentrations of Fe^{2+} , Fe^{3+} , H_2O_2 and pH were measured before and after irradiation. In the indoor photochemical experiments the small drop fraction of Oregon cloud sample #2 from July 14, 1993 was used. After the cloud water was

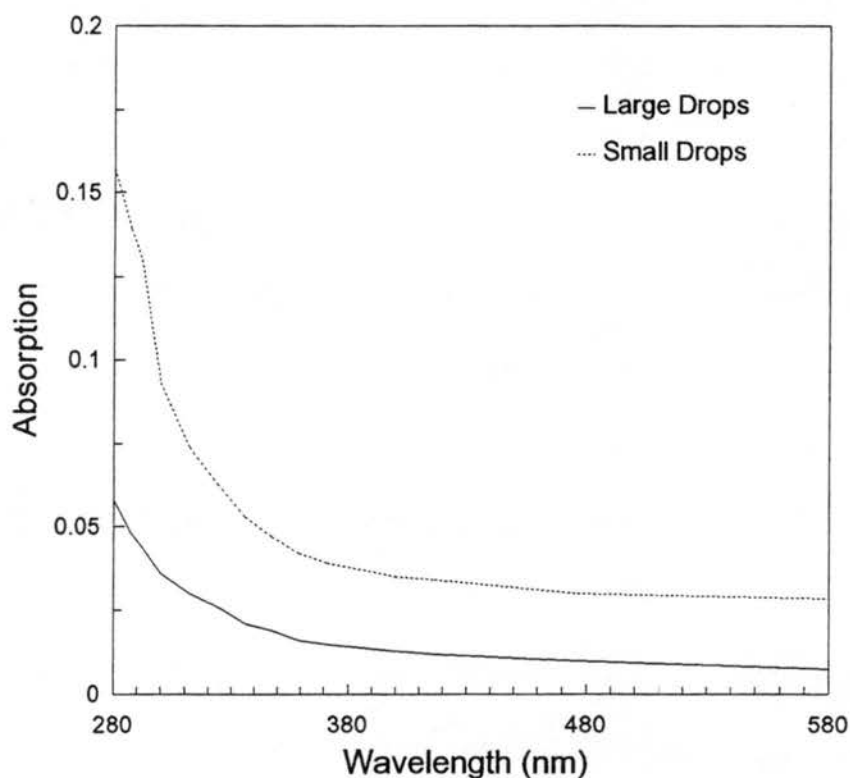


Figure 3.38. Ultraviolet-visible absorption spectra of filtered (0.45 μm) cloud samples measured by a Hitachi U-2000 UV/VIS spectrophotometer with 1.0 cm path length. The spectra have been adjusted by subtracting the spectrum of water. The cloud samples were collected from coastal stratus clouds at Angora Pk., Oregon on July 14, 1993. The small drop sample represents drops with diameters between 4 and 23 μm , while the large drop sample primarily contains drops with diameters larger than 23 μm .

irradiated for 12 minutes with 313 nm light, we observed a pH increase from 7.10 to 7.23. H_2O_2 concentrations increased from an average value of 0.17 ($\sigma = 0.01$) to 0.28 ($\sigma = 0.05$) μM , and Fe^{2+} concentrations increased from an average value of 1.58 ($\sigma = 0.09$) to 1.94 ($\sigma = 0.08$) μM (Figure 3.39). The fraction of Fe(III) decreases from 88% to 85%. The large range of peroxide concentrations observed after irradiation is not due to analytical errors but instability of H_2O_2 immediately after the irradiation. The H_2O_2 concentrations decreased with time after irradiation until about 10 minutes when a stabilized H_2O_2 concentration was reached. Although only monochromatic light was used in the indoor experiments and the light intensity might be much smaller than the sunlight, the results suggest that photochemical reactions could occur if the cloud water is exposed to sunlight.

In the outdoor photochemical experiment, again, the Oregon cloud sample #2 was used. The cloudwater, in a quartz cuvette (1.0-cm L x 0.5-cm W x 4.5-cm H), was first stabilized outdoor in a dark environment shielded from light and then exposed to February noon sunlight (February 14, 1995). Several tenths of a unit pH increase were observed for the samples of small and large drop fractions after exposure to sunlight for less than 20 minutes (Figure 3.40). The pH values dropped when the samples were placed in the dark again. The experiment was repeated in July noon sunlight (July 17/1995). Again several tenths of a unit pH increase were observed. At the end of irradiation an aliquot of the water was removed from the sample of large drop fraction for Fe^{2+} analysis. The Fe^{2+} concentration increased from 0.36 ($\sigma = 0.08$) to 1.46 ($\sigma = 0.06$) μM . The fraction of Fe(III) decreases from 78% to 9%. The results suggest that photochemical reactions could be accompanied by pH and Fe speciation changes.

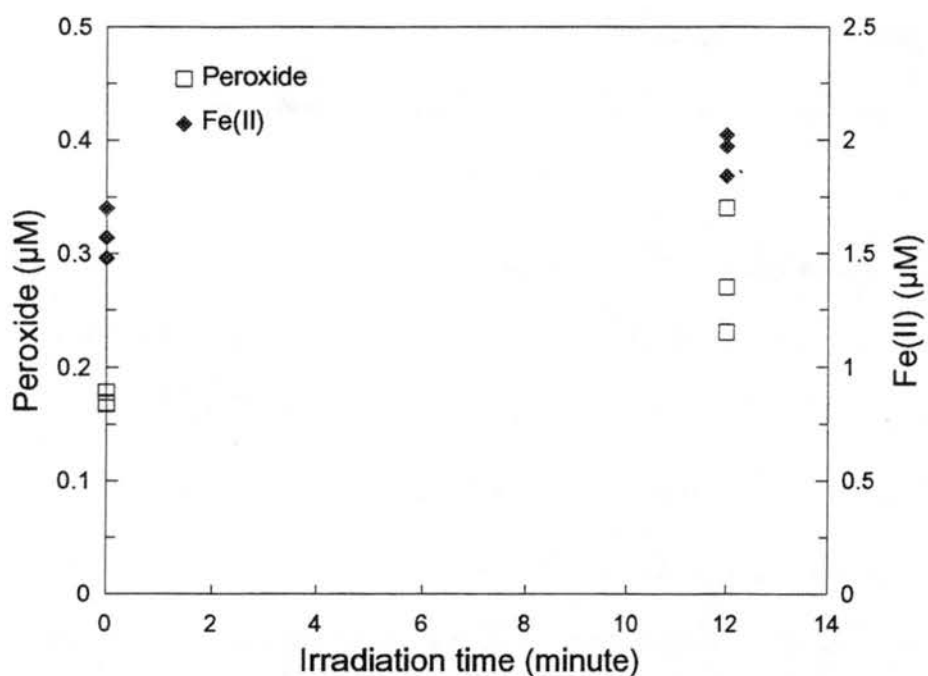
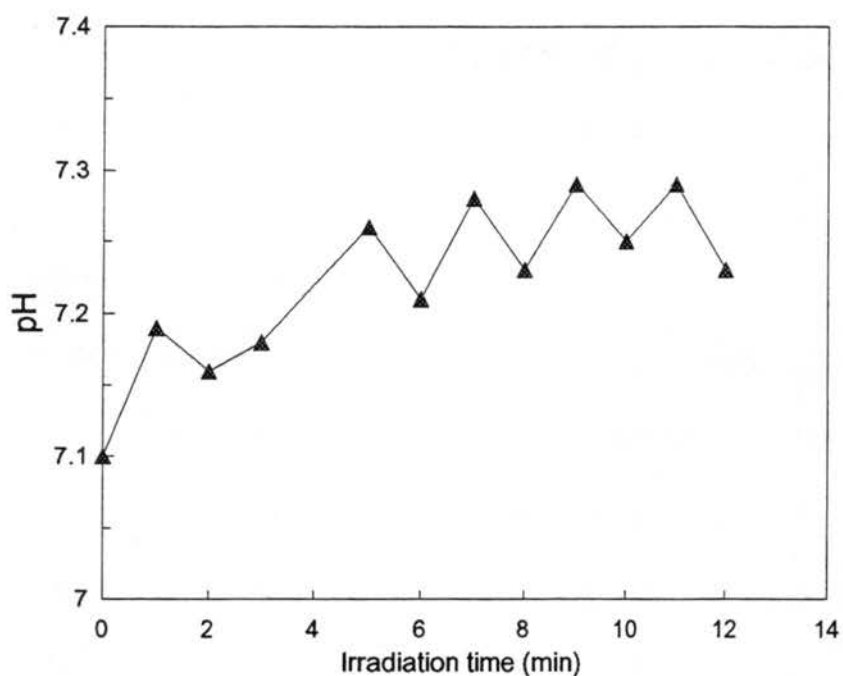


Figure 3.39. Change of chemical composition of an authentic cloud water after irradiation with 313 nm light. Three replicates were made for each measurement of peroxide and Fe(II). The cloud samples was the small drop fraction collected during local time 09:57 - 11:01 a.m. from the coastal stratus cloud at Angora Pk., Oregon on July 14, 1993.

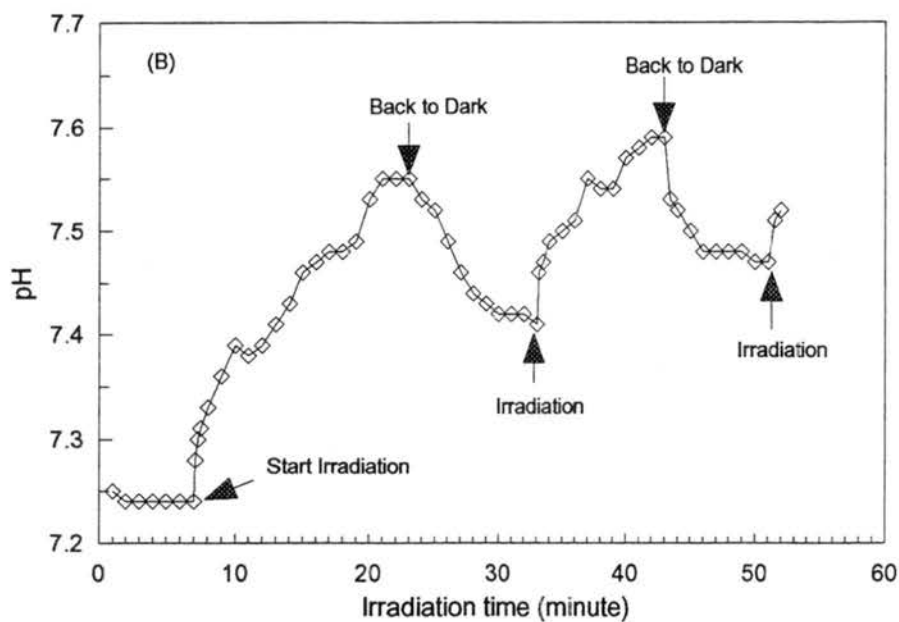
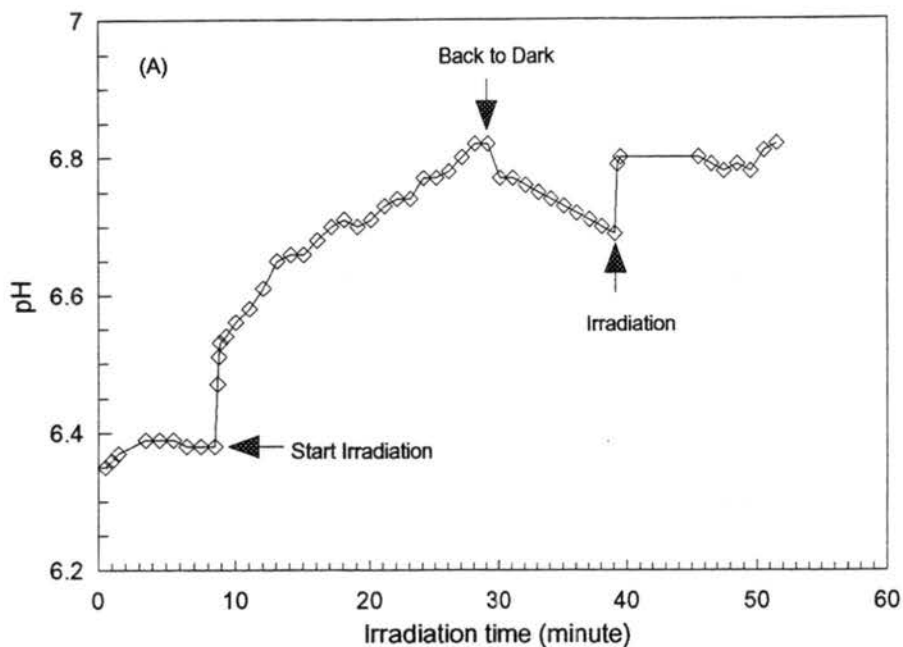
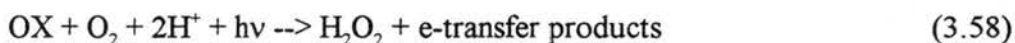


Figure 3.40. Cloudwater pH change during irradiation with February sunlight (February 14, 1995). The cloudwater samples of small and large drop fractions were collected from coastal stratus clouds at Angora Pk., Oregon during 09:57 - 11:01 a.m. on July 14, 1993. (A) a sample from the large drop fraction, [Fe] = 1.6 μ M. (B) a sample from the small drop fraction, [Fe] = 13 μ M.

One mechanism that has been proposed for photoformation of H₂O₂ coupling with Fe speciation change is photolysis of Fe(III)-oxalate (Zuo, 1992) (Equations (3.53) - (3.57)).



A net reaction can be written as:



It has been demonstrated that the rate of H₂O₂ photoformation increases with oxalate and Fe(III) concentrations. A photostationary Fe(II) concentration can be established within minutes of exposure to September noon sunlight, suggesting that the photochemical/chemical cycling time for Fe(III)-Fe(II)-Fe(III) is of the order of minutes.

However, influence of the photoredox reactions on aqueous acidity has not been studied due to the use of buffered media. It is noted from the net reaction of Fe(III)-oxalate photolysis that production of one molecule of H₂O₂ can result in consumption of one molecule of oxalate and two molecules of hydrogen ions. Therefore we might expect that total hydrogen ion consumed is proportional to the oxalate concentration.

To test this hypothesis preliminary experiments were conducted in July sunlight. The solutions for photolysis were comprised of ferric chloride and different concentrations of oxalic acid. Fe(III)-oxalate solutions (20 ml) were irradiated simultaneously in July sunlight from 10:30 to 11:00 am on July 21, 1995 at Colorado State University in Fort Collins, Colorado. The ambient temperature was 32-35 °C. Figure 3.41 depicts the change of solution pH with the sunlight exposure time. It shows that the solution pH can increase several tenths of a unit upon exposure to sunlight for several minutes. This result suggests that photolysis of Fe(III)-polycarboxylates in clouds may considerably increase cloudwater pH if no significant hydrogen ion buffering materials exist.

After exposure to sunlight for 20 minutes aliquots of the solutions were removed for H₂O₂ analysis and Fe speciation. Figure 3.42 shows experimental results for total hydrogen ion consumption, H₂O₂ formation and fraction of Fe³⁺ as functions of initial oxalate concentration. The ratio of hydrogen ion consumption to initial oxalate concentration is 1.3, which is less than the theoretically predicted value of 2.0. Production of superoxide radical (Equation (3.55)) probably faces competition from other reactions, for example the reduction of Fe(III) by oxalate radical (Equation (3.59))



The competition may result in reduced production of superoxide radical, a precursor of H₂O₂ and therefore reduced consumption of hydrogen ions.

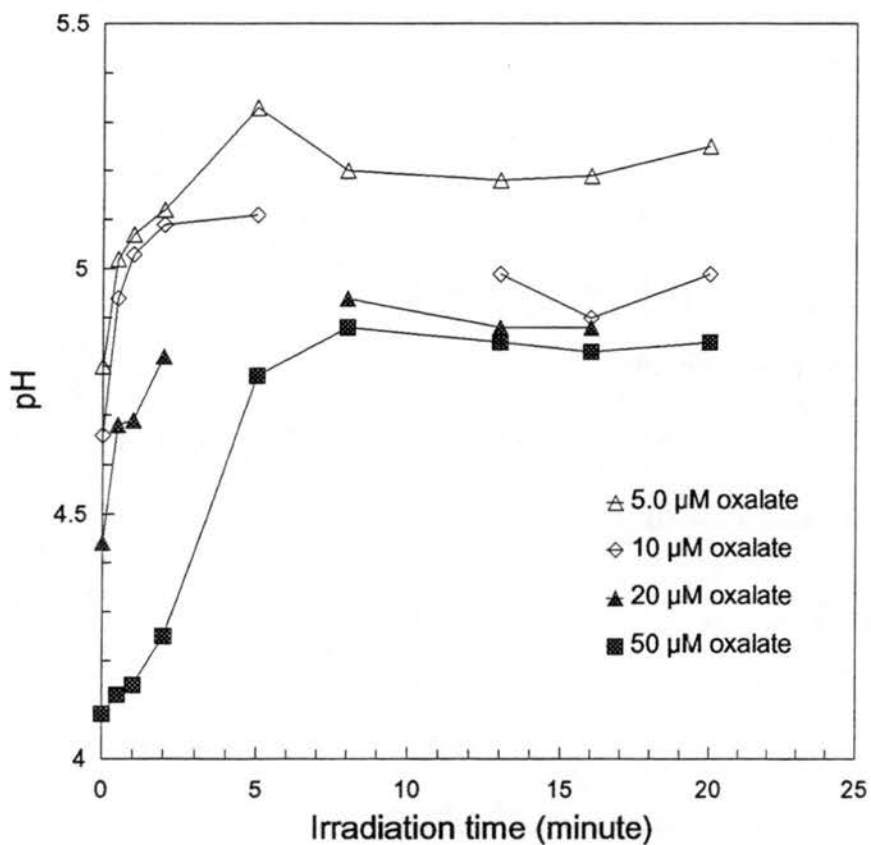


Figure 3.41. Change of pH in the Fe(III)-oxalate solutions illuminated with July sunlight. The Fe(III)-oxalate solutions have identical initial Fe(III) concentrations ($[\text{Fe(III)}] = 5.0 \mu\text{M}$) and different oxalate concentrations. The solution pH values were first stabilized in the dark before the solutions were exposed to sunlight.

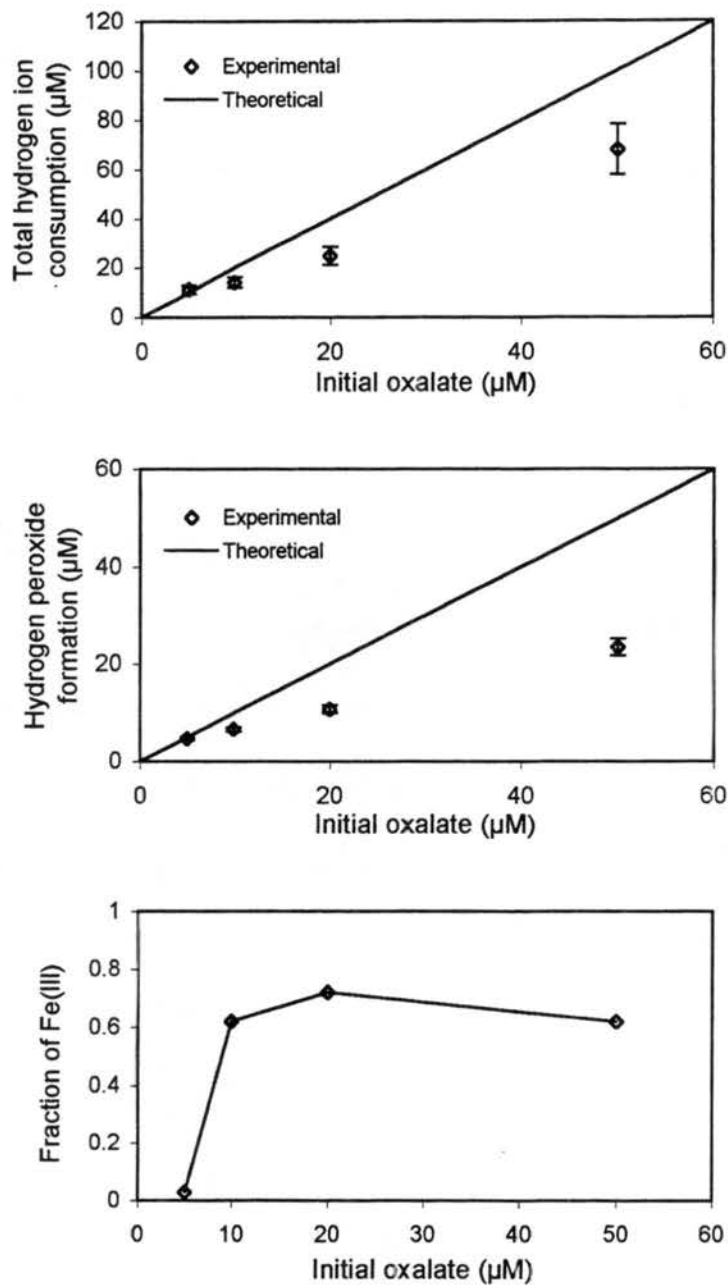
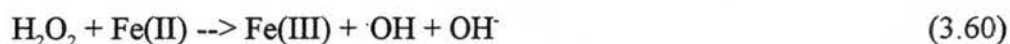


Figure 3.42. Total hydrogen ion consumption, hydrogen peroxide formation and fraction of Fe(III) as functions of initial oxalate concentration. All four solutions with different initial oxalate concentrations were illuminated simultaneously at 10:35 am on July 21, 1995 in Ft. Collins, Colorado. The initial Fe(III) concentrations were 5.0 μM in all the solutions. The errors are calculated based on three standard deviations from sample analysis.

The ratio of H_2O_2 formation to initial oxalate concentration is 0.42, which is less than theoretically predicted value 1.0. The ratio, however, is very close to the value of 0.45 measured by Zuo and Hoigne (1992). Reduced H_2O_2 production could be caused by the competition reaction stated above and Fenton's reaction (Equation (3.60)).



The relationship between the fraction of Fe(III) and the initial oxalate concentration shows that Fe(III) increases with initial oxalate concentration when total Fe is fixed. Higher oxalate concentrations may result in higher radical levels during irradiation. Photoreduced Fe(II) can be reoxidized to Fe(III) by the radicals. At high initial oxalate concentrations Fe(II) could also be reoxidized to Fe(III) by high levels of photoproducted H_2O_2 . The results suggest that in atmospheric conditions speciation of Fe will depend on concentration levels of photo-active species, for example polycarboxylates. Of course in-cloud conditions of light-screening and light-scattering are also important factors in determining the cycling between Fe(III) and Fe(II).

In summary photochemical reactions of Fe(III) species have several important implications for S(IV) oxidation. First, production of H_2O_2 provides another source of oxidants in clouds for S(IV) oxidation. Higher Fe concentrations in cloud drops may result in higher H_2O_2 production rates. Therefore any cloud drop size dependence of total Fe concentrations could produce a size dependence of in-cloud H_2O_2 production. Second, photochemical consumption of hydrogen ions could act as an 'acid buffer' to neutralize sulfuric

acid produced through S(IV) oxidation, and thereby enhance the importance of pH sensitive S(IV) oxidation pathways. The acid buffer effect is expected to vary among drops of different size due to the drop size dependence of iron, and possibly polycarboxylate concentrations.

CHAPTER 4. CONCLUSIONS

Field measurements of chemical composition in cloud/fog drops of diverse sizes reveal that differences in chemical composition exist between drops of two size fractions. The size-dependent chemical composition at various locations is summarized in Table 4.1. Small drops ($4 < d < 23 \mu\text{m}$) tend to be more acidic than the large drops ($d > 23 \mu\text{m}$) in most cases, although in less polluted clouds the reverse is sometimes observed. No obvious pattern of drop size-dependence of hydrogen peroxide concentrations was observed. Significantly higher total iron and total manganese concentrations are associated with large drops in most clouds sampled, except in California's San Joaquin Valley fog and in Oregon's coastal stratus clouds, where the opposite trend is present. Iron speciation for San Joaquin Valley fog samples shows that most dissolved Fe in the small drops exists as Fe(III). Total formaldehyde concentrations, including free formaldehyde and formaldehyde complexed with bisulfite as HMS, are almost exclusively enriched in the small drop fraction. When high hydrogen peroxide concentrations exist in clouds, no free S(IV) can be detected due to the rapid reaction between S(IV) and H_2O_2 . However S(IV) can be detected in the form of HMS, a complex between S(IV) and formaldehyde; HMS concentrations are usually higher in the small drop fraction.

The chemical heterogeneity across the drop size spectrum is expected to affect S(IV) oxidation and complexation rates in drops of diverse sizes. While S(IV) oxidation by H_2O_2 does not vary substantially with drop size at most sampling sites, S(IV) oxidation by ozone and autooxidation catalyzed by trace metals vary with drop size due to the size dependent pH and trace metal concentrations. Higher rates of S(IV) oxidation by ozone in the large drop

Table 4.1. Summary of the size-dependent cloud/fog chemical composition at various locations

Site	Typically enriched in large drops ($d > 23 \mu\text{m}$)	Typically enriched in small drops ($4 < d < 23 \mu\text{m}$)	No preference
San Joaquin Valley, CA 01/94 and 12/95	H_2O_2	H^+ , Total S(IV), HMS, HCHO, Total Fe, Fe^{3+} , Total Mn	
Mt. Mitchell, NC 08/93	Total S(IV), HMS, Total Fe, Total Mn	H^+ , H_2O_2 , HCHO	
Angora Pk., OR 07/93	H^+ , H_2O_2	Total S(IV), HMS, HCHO, Total Fe, Total Mn	
La Jolla Pk., CA 07/93	Total Fe, Total Mn	H^+ , Total S(IV), HMS, HCHO	H_2O_2
La Jolla Pk., CA 06/94	Total Fe	H^+ , H_2O_2 , HCHO	
Whiteface Mt., NY 09/93	H_2O_2	H^+ , Total S(IV), HMS, HCHO, Total Fe	

fraction are predicted at most sampling sites. S(IV) autooxidation in the presence of Fe and Mn tends to be rapid in large drops in Mt. Mitchell and La Jolla Pk. clouds, whereas small drops sustain higher rates in Angora Pk. clouds. S(IV) complexation with formaldehyde is of interest since the reaction may compete with S(IV) oxidation under certain conditions, and the reaction product may provide a S(IV) reservoir. The complexation becomes important when cloud pH is higher than 5. The competition between S(IV) oxidation and complexation can vary with drop size, since they are all functions of cloud pH as well as formaldehyde or oxidant concentrations.

Given the presence of chemical heterogeneity in cloud/fog drop populations use of average chemical composition to predict in-cloud S(IV) oxidation rate may generate errors. Errors are smallest when pH is low and abundant H_2O_2 is present, since S(IV) oxidation by H_2O_2 is not a function of cloud acidity and is a linear function of aqueous H_2O_2 concentrations. Errors in predicting S(IV) oxidation rates based on average chemical composition can be large for the ozone and autooxidation pathways. Therefore the effects of chemical heterogeneity on in-cloud S(IV) oxidation rates will largely depend on relative contributions of the different paths to S(IV) oxidation.

With all three oxidation paths taken into account, enhancements in S(IV) oxidation rates due to chemical heterogeneity were studied in a variety of cloud types and in a variety of environments. About 84 percent of the samples are calculated to experience little enhancement in S(IV) oxidation, due to the dominance of the H_2O_2 path. Approximately 9 percent of the samples are calculated to experience oxidation rate enhancement between 10 and 30%, while 7 percent of the samples are to experience oxidation rate enhancement of 30% or more.

In summer clouds at La Jolla Pk., California and Mt. Mitchell, North Carolina high aqueous H_2O_2 concentrations are coupled with low cloud pH ($\text{pH} < 4$). S(IV) oxidation by H_2O_2 is the dominant oxidation path in these cases. Therefore observed cloud chemical heterogeneity has little influence on the overall S(IV) oxidation rate in these clouds. On the other hand, the effects of chemical heterogeneity on enhancement in S(IV) oxidation rates appear to be strong in winter radiation fogs in California's San Joaquin Valley, where aqueous H_2O_2 concentrations are low and pH is high. Enhancement in S(IV) oxidation is also substantial in summer clouds at Angora Pk., Oregon and at Whiteface Mountain, New York,

when cloud pH values are high enough ($\text{pH} > 5$) to support rapid S(IV) oxidation by ozone and trace metal catalyzed S(IV) autooxidation.

We expected real clouds to contain more than two chemically distinct drop populations, a hypothesis supported by preliminary studies using a cloud sampler that samples three independent drop size fractions. In addition to variations in pH as a function of drop size, it is unlikely that all drops of the same size will have the same acidity. A wider distribution of drop compositions can support even faster sulfur oxidation rates. Effects of chemical heterogeneity of fogs with four drop size fractions on additional oxidation rate enhancement were tested for the Bakersfield fog. Results show that more chemically distinct drop fractions, especially in the drop populations with high pH, may result in enhancement up to 138%, whereas the calculated enhancement is 93% from the chemical heterogeneity measured in three fog drop size fractions.

Field measurements show that chemical heterogeneity is not only present at the beginning of cloud/fog events but can be maintained throughout the events. For example, in high pH fog events at Bakersfield, California, variations in pH among drops of diverse sizes are expected to decrease as S(IV) oxidation proceeds, resulting from sulfuric acid production. However, the expected decrease in chemical heterogeneity of pH was not observed in the fog event. High acid buffering capacity was measured in these highly polluted fog samples. Acid buffering agents other than traditionally considered aqueous ammonia, carbonate species and carboxylates, contributed significantly to the acid buffer intensity. Simulations of S(IV) oxidation based on the fogwater chemical composition at Bakersfield show that the presence of high acid buffering capacity prevents the fog drop pH from rapidly decreasing. As a result

variations in pH among drops of different sizes are maintained throughout a four hour simulation. The internal buffering played important roles in enhancement of sulfate production. The total sulfate production in the chemically heterogeneous fog with both internal buffering and external ammonia buffering increases 6.5 times compared to the sulfate production in the fog with external ammonia buffering alone. When both external ammonia buffering and internal buffering are included, due to the maintenance of chemical heterogeneity among the drop population, the total sulfate production during a four hour simulation increases 35 percent relative to the sulfate production calculated using the average chemical composition.

The effect of chemical heterogeneity on in-cloud S(IV) oxidation will depend on relative contributions of the different S(IV) oxidation pathways. Uncertainties exist about the contributions of the different oxidation paths in this study due to the assumptions made for ozone concentrations and fractions of total Fe and total Mn present as dissolved Fe(III) and dissolved Mn(II). The uncertainties are smallest for the Bakersfield fog since ozone concentrations were measured. The uncertainties are also small for the clouds at Mt. Mitchell, NC and at La Jolla Pk., CA, since S(IV) oxidation by H_2O_2 is the dominant oxidation pathway. Uncertainties of the relative contributions of the different oxidation pathways can be reduced in future as more Fe speciation data becomes available.

CHAPTER 5. RECOMMENDATIONS FOR FUTURE WORK

The study revealed that significant chemical heterogeneity is present in clouds of various types in various environments. The chemical heterogeneity can substantially enhance in-cloud S(IV) oxidation rates under certain conditions. More sulfate can be produced due to the chemical heterogeneity. To verify the enhancement in sulfate production due to chemical heterogeneity, calculated sulfate production due to aqueous S(IV) oxidation in chemically heterogeneous clouds/fog can be compared to measurements of sulfate concentration changes before, during and after cloud/fog events. Three approaches can be used in comparing calculated sulfate production to field measurements. First, one can compare measured sulfate concentrations in successive cloud/fog water samples after correcting sulfate concentration changes for physical processing, e.g. condensation, evaporation and deposition (Equation (5.1)) (Jacob et al., 1984)

$$[S(VT)]_2 L_2 = ([S(VT)]_1 L_1 + \int_1^2 \frac{d[S(VT)]}{dt} L_t dt)(1 - r) \quad (5.1)$$

where L is the liquid water content of clouds/fog and r is the correction factor for physical processing. If it is assumed that L and r also control concentration changes of conservative species in successive cloud/fog water samples, then:

$$[T]_2 L_2 = [T]_1 L_1 (1 - r) \quad (5.2)$$

where T represents a conservative quantity defined as the sum of the equivalent concentrations of all components A_i in solution minus sulfate and its counter-ion (Equation (5.3))

$$[T] = \sum_{i=1}^n [A_i] - 2[S(VT)] \quad (5.3)$$

One can relate calculated sulfate production rates with measured sulfate concentration changes by substituting Equation (5.2) into Equation (5.1):

$$\int_{t_1}^{t_2} \frac{d[S(VT)]}{dt} L_t dt = L_{t1} ([S(VT)]_{t2} \frac{T_{t1}}{T_{t2}} - [S(VT)]_{t1}) \quad (5.4)$$

When applying this method the successive cloud/fog water samples need to be from the same air mass. Therefore, the approach may be applicable to the fog in California's San Joaquin Valley where winter radiation fog is often associated with severe stagnation episodes. Accurate estimation of the correction factor r needs complete characterization of cloud and fog water chemical composition. Ionic balances are a good indicator for complete analysis of cloud and fog water chemical components.

The second method to quantify in-cloud sulfate production is using a tracer technique (Husain, 1989). Cloud sulfate is generally derived from aerosol scavenging and in-cloud S(IV) oxidation (Equation (5.5))

$$[SO_4^{2-}]_{\text{cloud}} L = \alpha (SO_4^{2-})_{\text{aa}} + [SO_4^{2-}]_{\text{ox}} L \quad (5.5)$$

where $[\text{SO}_4^{2-}]_{\text{cloud}}$ represents the sulfate concentration in cloudwater, $(\text{SO}_4^{2-})_{\text{aa}}$ represent the pre-cloud ambient concentration of sulfate aerosols, $[\text{SO}_4^{2-}]_{\text{ox}}$ represents the concentration of sulfate formed from S(IV) oxidation, L is the liquid water content of the cloud, and α is the scavenging coefficient for ambient sulfate aerosols. The amount of sulfate scavenged into the cloud can be tracked by a trace element which possesses a similar behavior upon cloud formation. Trace elements Se, As, and Sb can be selected since these elements are primarily derived from gas to particle conversion processes related to high-temperature combustion, and they are also present in the accumulation mode. The relationship between the concentration of a trace element in cloudwater and in ambient aerosols is, using Se as an example,

$$[\text{Se}]_{\text{cloud}} L = \beta (\text{Se})_{\text{aa}} \quad (5.6)$$

where $[\text{Se}]_{\text{cloud}}$ represents the Se concentration in cloudwater, $(\text{Se})_{\text{aa}}$ represent the pre-cloud ambient concentration of Se aerosols, and β represents the scavenging coefficient of the tracer. Therefore the amount of sulfate produced can be obtained from Equations (5.5) and (5.6)

$$[\text{SO}_4^{2-}]_{\text{ox}} = ([\text{SO}_4^{2-}]_{\text{cloud}} / [\text{Se}]_{\text{cloud}} - \alpha / \beta (\text{SO}_4^{2-})_{\text{aa}}) / (\text{Se})_{\text{aa}} [\text{Se}]_{\text{cloud}} \quad (5.7)$$

If α/β is known, in-cloud sulfate production can be obtained by measuring in-cloud and pre-cloud concentrations of sulfate and Se. Again it is critical that the pre-cloud and in-cloud chemical compositions are measured for the same air mass.

The third method to compare the calculated sulfate production to the field measurements is using the change of atmospheric sulfate aerosol levels before and after cloud/fog events. Air mass changes and sulfate deposition also need to be considered in this approach.

Accurate estimation of in-cloud S(IV) oxidation rates requires information about chemical heterogeneity of more than two size fractions. While limited data on variations of cloud pH among three size-fractionated drops are available, very few data exist for iron and manganese. Calculations of enhancement in S(IV) oxidation obtained from the hypothetical four size-fractionated fogwater samples indicated that more size fractions can support greater oxidation enhancement. However the chemical heterogeneity among drops of more than three size-fractions needs to be verified by field measurements.

Accurate estimation of in-cloud sulfate production needs simultaneous measurements of atmospheric sulfur dioxide, ozone, and H_2O_2 concentrations. Iron speciation is also important, especially in daytime clouds/fog where a substantial amount of Fe(II) could be present. These parameters should be measured in future field campaigns examining chemically heterogeneous clouds or fogs.

HMS, the complexation product of S(IV) with formaldehyde, has been detected in various types of clouds. It can be oxidized by hydroxyl radical to form sulfate. Its contribution to sulfate production especially in daytime clouds and fog needs to be addressed.

Chemical components or functional groups that contributed the majority of the acid buffer intensities in the highly polluted fogwater at Bakersfield, California remain unknown at this point. Organic compounds appear to be candidates for the buffering. More work is needed to identify these buffering agents and assess their role in sulfate production in the San Joaquin Valley and elsewhere.

By obtaining this additional information we will be able to evaluate more accurately the roles clouds and fog play in promoting sulfate production in the atmosphere. The knowledge gained will also provide explicit information for modeling cloud chemistry as clouds and fog act as processors of atmospheric aerosols and trace gases.

REFERENCES

- Adeyuy Y. G., Cho S-Y, Tsay R-P and Carmichael G. R. (1984) Importance of formaldehyde in cloud chemistry. *Atmos. Environ.* **18**, 2413-2420.
- Allen J. M. and Faust B. C. (1994) Aqueous-phase photochemical formation of peroxy radicals and singlet molecular oxygen in cloud water samples from across the United States, in *Aquatic and Surface Photochemistry* edited by Helz, Zepp, R. G. and Crosby, Lewis Publications.
- Anastasio C., Faust B. C. and Allen J. M. (1994) Aqueous phase photochemical formation of hydrogen peroxide in authentic cloud waters. *J. Geophys. Res.* **99**, D4:8231-8248.
- Ayers G. P. and Larson T. V. (1990) Numerical study of droplet size dependent chemistry in oceanic, wintertime stratus cloud at southern mid-latitudes. *J. Atmos. Chem.* **11**, 143-167.
- Bator A. and Collett J. L., Jr. (1997) Cloud chemistry varies with drop size. *J. Geophys. Res.* submitted.
- Behra P. and Sigg L. (1990) Evidence for redox cycling of iron in atmospheric water droplets. *Nature* **344**:29, 419-421.
- Bell R. P. (1966) The reversible hydration of carbonyl compounds. *Adv. Phy. Org. Chem.* **4**, 1-29.
- Berglund J., Fronaeus S. and Elding L. I. (1993) Kinetics and mechanism for manganese-catalyzed oxidation of sulfur (IV) by oxygen in aqueous solution. *Inorg. Chem.* **32**, 4527-4538.

- Berglund J. and Elding L. I. (1995) Manganese-catalysed autoxidation of dissolved sulfur dioxide in the atmospheric aqueous phase. *Atmos. Environ.* **29**, 1379-1391.
- Botha C. F., Hahn J., Pienaar J. J. and Eldik R. V. (1994) Kinetics and mechanism of the oxidation of sulfur (IV) by ozone in aqueous solutions. *Atmos. Environ.* **28**, 3207-3212.
- Bott A and Carmichael G. R. (1993) Multiphase chemistry in a microphysical radiation fog model - A numerical study. *Atmos. Environ.* **27A**, 503-522.
- Bower K. N., Hill T. A., Coe H. and Choularton T. W. (1991) SO₂ oxidation in an entraining cloud model with explicit microphysics. *Atmos. Environ.* **25A**, 2401-2418.
- Boyce S. D. and Hoffmann M. R. (1984) Kinetics and mechanism of the formation of hydroxymethanesulfonic acid at low pH. *J. Phys. Chem.* **88**, 4740-4746.
- Brimblecombe P. and Spedding D. J. (1974) The reaction order of the metal ion catalysed oxidation of sulfur dioxide in aqueous phase. *Chemosphere* No.1, 29-32.
- Calvert J. G., Lazrus A., Kok G. L., Heikes B. G., Walega J. G., Lind J. and Cantrell C. A. (1985) Chemical mechanisms of acid generation in the troposphere. *Nature* **317**:5, 27-35.
- Capel P. D., Gunde R., Zurcher F. and Giger W. (1990) Carbon speciation and surface tension of fog. *Environ. Sci. Technol.* **24**, 722-727.
- Chameides W. L. (1984) The photochemistry of a remote marine stratiform cloud. *J. Geophys. Res.* **89**, 4739-4755.

- Collett J. L., Jr., Oberholzer B. and Staehelin J. (1993) Cloud chemistry at Mt. Rigi, Switzerland: dependence on droplet size and relationship to precipitation chemistry. *Atmos. Environ.* **27A**, 33-42.
- Collett J. L., Jr., Bator A., Rao X. and Demoz B. (1994) Acidity variations across the cloud drop size spectrum and their influence on rates of atmospheric sulfate production. *Geophys. Res. Lett.* **21**, 2393-2396.
- Collett J. L., Jr., Iovinelli R. and Demoz B. B. (1995) A three-stage cloud impactor for size-resolved measurement of cloud drop chemistry. *Atmos. Environ.* **29**, 1145-1154.
- Conklin M. H. and Hoffmann M. R. (1988) Metal iron-sulfur (IV) chemistry. 3. Thermodynamics and kinetics of transient iron (III)-sulfur (IV) complexes. *Environ. Sci. Technol.* **22**, 899-907.
- Dasgupta P. K., Decesare K. and Ullrey J. C. (1980) Determination of atmospheric sulfur dioxide without tetrachloromercurate (II) and the mechanism of the Schiff reaction. *Anal. Chem.* **52**, 1912-1922.
- Demoz B. B., Collett J. L., Jr. and Daube B. C., Jr. (1996) On the Caltech Active Strand Cloudwater Collectors. *Atmos. Res.* **41**, 47-60.
- Dong S. and Dasgupta P. K. (1987) Fast fluorometric flow injection analysis of formaldehyde in atmospheric water. *Environ. Sci. Technol.* **21**, 581-588.
- Erel Y., Pehkonen S. O. and Hoffmann M. R. (1993) Redox chemistry of iron in fog and stratus clouds. *J. Geophys. Res.* **98**:D10, 18423-18434.

- Erickson R. E., Yates L. M., Clark R. L. and McEwen D. (1977) The reaction of sulfur dioxide with ozone in water and its possible atmospheric significance. *Atmos. Environ.* **11**, 813-817.
- Espenson J. H. and Taube H. (1965) Tracer experiments with ozone as oxidizing agent in aqueous solution. *Inorg. Chem.* **4**, 704-709.
- Facchini M. C., Fuzzi S., Kessel M., Wobrock W., Jaeschke W., Arends B. G., Mols J. J., Berner A., Solly I., Kruisz C., Reischl G., Pahl S., Hallberg A., Ogren J. A., Fierlinger-Oberlinninger H., Marzorati A. and Schell D. (1992) The chemistry of sulfur and nitrogen species in a fog system: A multiphase approach. *Tellus* **44B**, 505-521.
- Facchini M. C., Fuzzi S., Lind J. A., Fierlinger-Oberlinninger H., Kalina M., Puxbaum H., Winiwarter W., Arends B. G., Wobrock W., Jaeschke W., Berner A. and Kruisz C. (1992) Phase-partitioning and chemical reactions of low molecular weight organic compounds in fog. *Tellus* **44B**, 533-544.
- Faust B. and Hoffmann M. R. (1985) Photo-assisted oxidation of S(IV) by oxygen in aqueous hematite ($\alpha\text{-Fe}_2\text{O}_3$) suspensions. American Chemical Society, 189th National Meeting, Miami, FL.
- Faust B. C. and Hoigne J. (1990) Photolysis of Fe(III)-hydroxy complexes as sources of OH radicals in clouds, fog and rain. *Atmos. Environ.* **24A**, 79-89.
- Faust B. C. and Zepp R. G. (1993) Photochemistry of aqueous iron (III)-polycarboxylate complexes: roles in the chemistry of atmospheric and surface waters. *Environ. Sci. Technol.* **27**, 2517-2522.

- Faust B. C. (1994) A review of the photochemical redox reactions of iron (III) species in atmospheric, oceanic, and surface waters: influences on geochemical cycles and oxidant formation, in *Aquatic and Surface Photochemistry*, Helz, G., Zepp, R and Crosby, D. Ed., Lewis Publishers, Boca Raton, FL., Chapter 1, pp. 3-36.
- Fuzzi S. (1978) Study of iron (III) catalysed sulfur dioxide oxidation in aqueous solution over a wide range of pH. *Atmos. Environ.* **12**, 1439-1442.
- Graedel T. E., Weschler C. J. and Mandich M. L. (1985) Influence of transition metal complexes on atmospheric droplet acidity. *Nature* **317**, 240-242.
- Graedel T. E. and Mandich M. L. (1986) Kinetics model studies of atmospheric droplet chemistry 2. homogeneous transition metal chemistry in raindrops. *J. Geophys. Res.* **91**, 5205-5221.
- Grgic I., Hudnik V., Bizjak M. and Levec J. (1992) Aqueous S(IV) oxidation - II. Synergistic effects of some metal ions. *Atmos. Environ.* **26A**, 571-577.
- Grosjean D., Van Cauwenberghe K., Schmid J. P., Kelley P. E. and Pitts J. N., Jr. (1978) Identification of C₃ - C₁₀ aliphatic dicarboxylic acids in airborne particulate matter. *Environ. Sci. Technol.* **12**, 313-317.
- Hegg D. A. and Larson T. V. (1990) The effects of microphysical parameterization on model predictions of sulfate production in clouds. *Tellus* **42B**, 272-284.
- Hegg D. A., Yuen P. and Larson T. V. (1992) Modeling the effects of heterogeneous cloud chemistry on the marine particle distribution. *J. Geophys. Res.* **97**, 12927-12933.
- Hillamo R. E., Kerminen V. M., Maenhaut W., Jaffrezo J. L., Balachandran S. and Davidson C. I. (1993) Size distributions of atmospheric trace elements at Dye 3, Greenland - I.

- distribution characteristics and dry deposition velocities. *Atmos. Environ.* **27A**, 2787-2802.
- Hoffmann M. R. and Jacob D. J. (1984) Kinetics and mechanisms of the catalytic oxidation of dissolved sulfur dioxide in aqueous solutions: An application to nighttime fogwater chemistry, in "*SO₂, NO and NO₂ Oxidation Mechanisms: Atmospheric Consideration*". Edited by Jack G. Calvert, Butterworth, Boston.
- Hoffmann M. R. and Calvert J. G. (1985) Chemical Transformation Modules for Eulerian Acid Deposition Models, Volume II. The Aqueous-phase Chemistry. EPA/600/S3-85/036. June 1985.
- Hoffmann M. R. (1986) On the kinetics and mechanism of oxidation of aquated sulfur dioxide by ozone. *Atmos. Environ.* **20**, 1145-1154.
- Hoffmann P. A., Dedik A. N., Ensling J., Weinbruch S., Weber S., Sinner T., Gutlich P. and Ortner H. M. (1996) Speciation of iron in atmospheric aerosol samples. *J. Aerosol Sci.* **27**, 325-337.
- Hoigne J., Bader H., Haag W. R. and Staehelin J. (1985) Rate constants of reactions of ozone with organic and inorganic compounds in water - III. Inorganic compounds and radicals. *Water Res.* **19**, 993-1004.
- Hough A. M. (1987) A computer modeling study of the chemistry occurring during cloud formation over hills. *Atmos. Environ.* **21**, 1073-1095.
- Hough A. M. (1988) Atmospheric chemistry at Elevated sites- A discussion of the processes involved and the limits of current understanding, in *Acid Deposition at High Elevation Sites*. Edited by M. H. Unsworth and D. Fowler.

- Husain L. (1989) A technique for determining in-cloud formation of SO_4 . *Geophys. Res. Lett.* **16**, 57-60.
- Ibusuki T. and Takeuchi K. (1987) Sulfur dioxide oxidation by oxygen catalyzed by mixtures of manganese (II) and iron (III) in aqueous solutions at environmental reaction conditions. *Atmos. Environ.* **21**, 1555-1560.
- Jacob D. J. (1986) Chemistry of OH in remote clouds and its role in the production of formic acid and peroxymonosulfate. *J. Geophys. Res.* **91**, 9807-9826.
- Jacob D. J. and Hoffmann M. R. (1983) A dynamic model for the production of H^+ , NO_2^- and SO_4^{2-} in urban fog. *J. Geophys. Res.* **88**, 6611-6621.
- Jacob D. J., Waldman J. M., Munger J. W. and Hoffmann M. R. (1984) A field investigation of physical and chemical mechanisms affecting pollutant concentrations in fog droplets. *Tellus* **36B**, 272-285.
- Jacob D. J., Munger J. W., Waldman J. M. and Hoffmann M. R. (1986) The $\text{H}_2\text{SO}_4\text{-HNO}_3\text{-NH}_3$ system at high humidities and in fogs 1. Spatial and temporal patterns in the San Joaquin Valley of California. *J. Geophys. Res.* **91**, 1073-1088.
- Jacob D. J., Gottlieb E. W. and Prather M. J. (1989) Chemistry of a polluted boundary layer. *J. Geophys. Res.* **94D**, 12975-13002.
- Jaffrezo J. L., Hillamo R. E., Davidson C. I. and Maenhaut W. (1993) Size distributions of atmospheric trace elements at Dye 3, Greenland - II. sources and transport. *Atmos. Environ.* **27A**, 2803-2814.
- Kaufman Y. J. and Tanre D. (1994) Effect of variations in supersaturation on the formation of cloud condensation nuclei. *Nature* **369**, May 5, 45-48.

- Kelly T. J., Schwartz S. E. and Daum P. H. (1989) Detectability of acid producing reactions in natural clouds. *Atmos. Environ.* **23**, 569-583.
- Kleinman L. I. (1991) Seasonal dependence of boundary layer peroxide concentration: The low and high NO_x regimes. *J. Geophys. Res.* **96**, 20721-20733.
- Klemm O., Talbot R. W. and Klemm K. I. (1992) Sulfur dioxide in coastal New England fog. *Atmos. Environ.* **26A**, 2063-2075.
- Langner, J., Rodhe H., Crutzen P. J. and Zimmermann P. (1992) Anthropogenic influence on the distribution of tropospheric sulfate aerosol. *Nature* **359**, 712-716.
- Larson T. V., Horike N. R. and Harrison H. (1978) Oxidation of sulfur dioxide by oxygen and ozone in aqueous solution: kinetic study with significance to atmospheric rate processes. *Atmos. Environ.* **12**, 1597-1611.
- Lazrus A. L., Kok G. L., Gitlin S. N. and Lind J. A. (1985) Automated fluorometric method for hydrogen peroxide in atmospheric precipitation. *Anal. Chem.* **57**, 917-922.
- Lelieveld J. and Heintzenberg J. (1992) Sulfate cooling effect on climate through in-cloud oxidation of anthropogenic SO₂. *Science* **258**, 117-120.
- Leuenberger C., Czuczwa J., Heyerdahl E. and Giger W. (1988) Aliphatic and polycyclic aromatic hydrocarbons in urban rain, snow and fog. *Atmos. Environ.* **22**, 695-705.
- Likens G. E., Edgerton E. S. and Galloway J. N. (1983) The composition and deposition of organic carbon in precipitation. *Tellus* **35B**, 16-24.
- Liljestrand H. M. (1985) Average rainwater pH, concepts of atmospheric acidity, and buffering in open systems. *Atmos. Environ.* **19**, 487-499.

- Lin X. and Chameides W. L. (1991) Model studies of the impact of chemical inhomogeneity on SO₂ oxidation in warm stratiform clouds. *J. Atmos. Chem.* **13**, 109-129.
- Lodge J. P., Jr. (1989) *Methods of Air Sampling and Analysis*, 3rd ed., Lewis Publishers, Inc., Chelsea, MI., pp. 499-502.
- Maahs H. G. (1983a) Measurement of the oxidation rate of sulfur (IV) by ozone in aqueous solution and their relevance to sulfur dioxide conversion in nonurban tropospheric clouds. *Atmos. Environ.* **17**, 341-345.
- Maahs H. G. (1983b) Kinetics and mechanics of the oxidation of S(IV) by ozone in aqueous solution with particular reference to SO₂ conversion in nonurban tropospheric clouds. *J. Geophys. Res.* **88C**, 10721-10732.
- Martin L. R. (1984) Kinetic studies of sulfite oxidation in aqueous solution, in "*SO₂, NO and NO₂ Oxidation Mechanisms: Atmospheric Consideration*". Edited by Jack G. Calvert, Butterworth, Boston, pp. 63-100.
- Martin L. R. and Hill M. W. (1987) The effect of ionic strength on the manganese catalyzed oxidation of S(IV). *Atmos. Environ.* **21**, 2267-2270.
- Martin L. R., Hill M. W., Tai A. F. and Good T. W. (1991a) The iron catalyzed oxidation of sulfur (IV) in aqueous solution: differing effects of organics at high and low pH. *J. Geophys. Res.* **96**, 3085-3091.
- Martin L. R. and Good T. W. (1991b) Catalyzed oxidation of sulfur dioxide in solution: the iron-manganese synergism. *Atmos. Environ.* **25A**, 2395-2399.
- Maxwell R. (1994) California Air Resources Board, personal communication.

- Miller D. F., Lamb D. and Gertler A. W. (1987) SO₂ oxidation in cloud drops containing NaCl or sea salt as condensation nuclei. *Atmos. Environ.* **21**, 991-993.
- Munger J. W., Jacob D. J. and Hoffmann M. R. (1984) The occurrence of bisulfite-aldehyde addition products in fog- and cloudwater. *J Atmos. Chem.* **1**, 335-350.
- Munger J. W., Tiller C. and Hoffmann M. R. (1986) Identification of hydroxymethanesulfonate in fog water. *Science* **231**, 247-249.
- Munger J. W., Collett Jr., J. L., Daube Jr., B. and Hoffmann M. R. (1989a) Chemical composition of coastal stratus clouds: dependence on droplet size and distance from the coast. *Atmos. Environ.* **23**, 2305-2320.
- Munger J. W., Collett Jr., J. L., Daube Jr., B. C. and Hoffmann M. R. (1989b) Carboxylic acids and carbonyl compounds in southern California clouds and fogs. *Tellus* **41B**, 230-242.
- Noble C. A. and Prather K. A. (1996) Real-time measurement of correlated size and composition profiles of individual atmospheric aerosol particles. *Environ. Sci. Technol.* **30**, 2667-2680.
- Oberholzer B., Collett, Jr. J. L., Staehelin J. and Waldvogel A. (1992) In-cloud scavenging of gases and aerosols at a mountain site in central Switzerland. *J. Atmos. Chem.* **14**, 61-71.
- Ogren J. A. and Charlson R. J. (1992) Implications for models and measurements of chemical inhomogeneities among cloud droplets. *Tellus* **44B**, 208-225.
- Olson T. M. and Hoffmann M. R. (1989) Hydroxyalkylsulfonate formation: its role as a S(IV) reservoir in atmospheric water droplets. *Atmos. Environ.* **23**, 985-997.

- Pandis S. N. and Seinfeld J. H. (1990) Chemical composition differences in fog and cloud droplets of different sizes. *Atmos. Environ.* **24A**, 1957-1969.
- Pehkonen S. O., Erel Y. and Hoffmann M. R. (1992) Simultaneous spectrophotometric measurement of Fe(II) and Fe(III) in atmospheric water. *Environ. Sci. Technol.* **26**, 1731-1736.
- Pehkonen S. O., Siefert R., Erel Y., Webb S. and Hoffmann M. R. (1993) Photoreduction of iron oxyhydroxides in the presence of important atmospheric organic compounds. *Environ. Sci. Technol.* **27**, 2056-2062.
- Penkett S. A., Jones B. M., Brice K. A. and Eggleton A. E. (1979) The importance of atmospheric ozone and hydrogen peroxide in oxidizing sulfur dioxide in cloud and rainwater. *Atmos. Environ.* **13**, 123-137.
- Penner J. E., Charlson R. J., Hales J. M., Laulainen N. S., Leifer R., Novakov T., Ogren J., Radke L. F., Schwartz S. E. and Travis L. (1994) Quantifying and minimizing uncertainty of climate forcing by anthropogenic aerosols. *Bulletin of the American Meteorological Society* **75**:3, 375-400.
- Perdue E. M. and Beck K. C. (1988) Chemical consequences of mixing atmospheric droplets of varied pH. *J. Geophys. Res.* **93**, 691-698.
- Richards L. W., Anderson J. A., Blumenthal D. L., McDonald J. A. Kok G. L. and Lazrus A. L. (1983) Hydrogen peroxide and sulfur (IV) in Los Angeles cloudwater. *Atmos. Environ.* **17**, 911-914.
- Rao, X. and Collett J. L. (1995) Behavior of S(IV) and formaldehyde in chemically heterogeneous cloud, *Environ. Sci. Technol.* **29**, 1023-1031.

- Roelofs G. J. H. (1992) On the drop and aerosol size dependence of aqueous sulfate formation in a continental cumulus cloud. *Atmos. Environ.* **26A**, 2309-2321.
- Roelofs G. J. H. (1993) A cloud chemistry sensitivity study and comparison of explicit and bulk cloud performance. *Atmos. Environ.* **27A**, 2255-2264.
- Sakugawa H., Kaplan I. R., Tsai W. and Cohen Y. (1990) Atmospheric hydrogen peroxide. *Environ. Sci. Technol.* **24**, 1452-1462.
- Satsumabayashi H., Kurita H., Yokouchi Y. and Ueda H. (1990) Photochemical formation of particulate dicarboxylic acids under long-range transport in central Japan, *Atmos. Environ.* **24A**, 1443-1450.
- Schwartz S. E. (1986) Mass-transport considerations pertinent to aqueous phase reactions of gases in liquid-water clouds. In *Chemistry of Multiphase Atmospheric System*, Jaeschke W., Ed., Springer: New York, pp. 415-471.
- Schwartz S. E. (1987) Aqueous-phase reactions in clouds, in *The Chemistry of Acid Rain, Sources and Atmospheric Processes*. ACS Washington D.C.
- Schwartz S. E. (1988) Mass-transport limitation to the rate of in-cloud oxidation of SO₂: Re-examination in the light of new data. *Atmos. Environ.* **22**, 2491-2499.
- Sedlak D. L. and Hoigne J. (1993) The role of copper and oxalate in the redox cycling of iron in atmospheric waters. *Atmos. Environ.* **27A**, 2173-2185.
- Seidl W. (1989) Ionic concentrations and initial S(IV) oxidation rates in droplets during the condensational stage of cloud. *Tellus* **41B**, 32-50.
- Seinfeld J. H. *Atmospheric Chemistry and Physics of Air Pollution*, Wiley Interscience, New York, 1986, pp. 195-229.

- Siefert R. L., Webb S. M. and Hoffmann M. R. (1996) Determination of photochemically available iron in ambient aerosols. *J. Geophys. Res.* **101**, 14441-14449.
- Sievering H., Gorman E., Kim Y., Ley T., Seidle W. and Boatman J. (1994) Heterogeneous conversion contribution to the sulfate observed over Lake Michigan. *Atmos. Environ.* **28**, 367-370.
- Sinner T., Hoffmann P. and Ortner H. M. (1994) Determination of pH-value, redox-potential, transition metals concentration and Fe(II)- and Fe(III)-content in cloud water samples. *Beitr. Phys. Atmosph.* **67**, 353-357.
- Stumm W. and Morgan J. J. (1996) *Aquatic Chemistry*, 3rd Edition; Wiley Interscience: New York, pp. 134.
- Sulzberger B., Laubscher H. and Karametaxas G. (1994) Photoredox reactions at the surface of iron(III)(hydr)oxides, in *Aquatic and Surface Chemistry*, Helz, G., Zepp, R and Crosby, D. Ed., Lewis Publishers, Boca Raton, FL., Chapter 3, pp. 53-72.
- Twohy C. H., Austin P. H. and Charlson R. J. (1989) Chemical consequences of the initial diffusional growth of cloud droplets: a clean marine case. *Tellus* **41B**, 51-60.
- Tremp J. (1992) Sources and fate of nitrated phenols in the atmospheric environment; Ph.D. Dissertation, ETH-Zurich.
- Walker J. F. (1964) *Formaldehyde* 3rd Ed., Reinhold Publishing Corporation: New York, pp. 454.
- Warneck P. (1991) Chemical reactions in clouds. *Fresenius J. Anal. Chem.* **340**, 585-590.

- Weinstein-Lloyd J. and Schwartz S. E. (1991) Low-intensity radiolysis study of free radical reactions in cloudwater: H_2O_2 production and destruction. *Environ. Sci. Technol.* **25**, 791-800.
- Yuen P., Hegg D. A. and Larson T. V. (1994) The effects of in-cloud sulfate production on light-scattering properties of continental aerosol. *J. Applied Meteorology* **33**, 848-854.
- Zhuang G., Yi Z. and Duce R. A. (1992a) Chemistry of iron in marine aerosols, *Global Biogeochem. Cycles* **6:2**, 161-173.
- Zhuang G., Yi Z., Duce R. A. and Brown P. R. (1992b) Link between iron and sulphur cycles suggested by detection of Fe(II) in remote marine aerosols. *Nature* **355**, 537-539.
- Zhuang G., Yi Z. and Wallace G. T. (1995) Iron (II) in rainwater, snow, and surface seawater from a coastal environment. *Mar. Chem.* **50**, 41-50.
- Zuo Y. (1992) Photochemistry of iron(III)/iron(II) complexes in atmospheric liquid phases and its environmental significance, Ph.D. thesis, EHTZ No. 9727, Swiss Federal Institute of Technology, Zurich.
- Zuo Y. and Hoigne J. (1992) Formation of H_2O_2 and depletion of oxalic acid by photolysis of Fe(III)-oxalate complexes in atmospheric waters. *Environ. Sci. Technol.* **26**, 1014-1022.
- Zuo Y. and Hoigne J. (1993) Evidence of photochemical formation of H_2O_2 and oxidation of SO_2 in authentic fog water. *Science* **260**, 71-73, April, 1993.

APPENDICES

Appendix A. Sample preservation

- ◆ Always store the catalase solution and fluorescent solution at 0°C- 5°C
- ◆ Do the chemistry procedures for each blank sample exactly like the procedure for cloud samples given below
- ◆ Do a separate DI water blank for each cloud event
- ◆ Before each cloud event check activities of the enzyme solutions

For samples collected by the ETH impactor

Sample priority

1. pH Measurement: 20 µl sample
2. Major ion analysis by IC: 500 µl sample

1. pH Measurement

Place two polyethylene microcentrifuge vials into holder

Pipette 20 µl sample into each vial

Rinse the electrode with DI water

Place pH probe into the first vial, making sure it is in contact with sample

Remove the probe from the first vial and shake off excess solution

Place the probe into the second vial, making sure it is in contact with sample

Write down the pH on the project log sheet when the reading first stabilizes (3 seconds)

2. Major ion analysis by IC

Pipette 500 μ l sample into a polyethylene autosampler vial with Teflon-lined septum.

Label vial with sample name and letters "IC".

For samples collected by the IESL impactor

Sample priority

1. pH Measurement: 40 μ l sample
2. Major ion analysis by IC: 500 μ l
3. Total S(IV): 100 μ l
4. Peroxides: 100 μ l
5. Total formaldehyde: 100 μ l
6. HMS: 100 μ l
7. Total Fe/Mn: 100 μ l
8. Organic acids: 100 μ l
9. TOC (Bakersfield only)

1. pH measurement

Place two polyethylene microcentrifuge vials into holder

Pipette 20 μ l sample into each vial

Rinse the electrode with DI water

Place pH probe into the first vial, making sure it is in contact with sample

Remove the probe from the first vial and shake off excess solution

Place the probe into the second vial, making sure it is in contact with sample

Write down the pH on the project log sheet when the reading first stabilizes (after a few seconds)

2. Major ion analysis by IC

Pipette 500 μ l sample into a polyethylene autosampler vial with Teflon-lined septum.

Label vial with sample name and letters "IC".

3. Total S(IV)

Pipette 100 μ l sample into a 0.1 ml cone-shaped glass vial

Add 10 μ l S(IV) preservative solution

Add 10 μ l catalase solution

Close cap and mix completely

Label vial with sample name and "S(IV)"

4. Peroxides

Pipette 100 μ l sample into a 0.1 ml cone-shaped glass vial

Add 20 μ l conditioning reagent

Add 20 μ l fluorescent reagent

Close cap and mix completely

Label vial with sample name and "Peroxides"

5. Total formaldehyde

Pipette 100 μ l sample into a 0.1 ml cone-shaped glass vial

Add 10 μ l formaldehyde preservative solution

Close cap and mix completely

Label vial with sample name and "HCHO"

6. HMS

Pipette 100 μ l sample into a 0.1 ml cone-shaped glass vial

Add 10 μ l 1.0 mM H_2O_2 solution

Mix completely

Add 10 μ l catalase solution

Add 10 μ l S(IV) preservative solution

Close cap and mix completely

Label vial with sample name and "HMS"

7. Total Fe/Mn

Pipette 100 μ l sample into a 0.5 ml conical plastic micro vial

Add 10 μ l 9.7% HNO_3 solution

Close cap and mix completely

Label vial with sample name and "Metals"

8. Organic Acids

Pipette 5 μ l chloroform into a 0.1 ml cone-shaped glass vial

Fill the vial with sample

Close cap and mix completely

Label vial with sample name and "Org Acids"

For samples collected by CASCC collectors (CASCC2 and sf-CASCC)

Sample priority

1. pH Measurement: 60 μ l sample
2. Major ion analysis by IC: 500 μ l
3. Total S(IV): 1.0 ml
4. Peroxides: 1.0 ml
5. Total formaldehyde: 1.0 ml
6. HMS: 1.0 ml
7. Total Fe/Mn: 1.0 ml
8. Organic acids: 1.5 ml
9. TOC (Bakersfield only): 1.0 ml

1. pH measurement

Place two polyethylene microcentrifuge vials into holder

Pipette 20 μ l sample into each vial

Rinse the electrode with DI water

Place pH probe into the first vial, making sure it is in contact with sample

Remove the probe from the first vial and shake off excess solution

Place the probe into the second vial, making sure it is in contact with sample

Write down the pH on the project log sheet when the reading first stabilizes (after a few seconds)

2. Major ion analysis by IC

Pipette 500 μ l sample into a polyethylene autosampler vial with Teflon-lined septum.

Label vial with sample name and letters "IC".

3. Total S(IV)

Pipette 1.0 ml sample into a 1.5 ml glass vial with Teflon-lined septum

Add 100 μ l S(IV) preservative solution

Add 100 μ l catalase solution

Close cap and mix completely

Label vial with sample name and "S(IV)"

4. Peroxides

Pipette 1.0 ml sample into a 1.5 ml glass vial with Teflon-lined septum

Add 200 μ l conditioning reagent

Add 200 μ l fluorescent reagent

Close cap and mix completely

Label vial with sample name and "Peroxides"

5. Total formaldehyde

Pipette 1.0 ml sample into a 1.5 ml glass vial with Teflon-lined septum

Add 100 μ l formaldehyde preservative solution

Close cap and mix completely

Label vial with sample name and "HCHO"

6. HMS

Pipette 1.0 ml sample into a 1.5 ml glass vial with Teflon-lined septum

Add 100 μ l 1.0 mM H₂O₂ solution

Mix completely

Add 100 μ l catalase solution

Add 100 μ l S(IV) preservative solution

Close cap and mix completely

Label vial with sample name and "HMS"

7. Total Fe/Mn

Pipette 1.0 ml sample into a 1.2 ml cryovial

Add 100 μ l 9.7% HNO₃ solution

Close cap and mix completely

Label vial with sample name and "Metals"

8. Organic Acids

Pipette 50 μ l chloroform into a 1.0 ml glass vial

Fill the vial with sample

Close cap and mix completely

Label vial with sample name and "Org Acids"

9. TOC

Pipette 1.0 ml sample into a 1.0 ml glass vial

Close cap

Label vial with sample name and "TOC"

Methods of checking activities of enzyme solutions

1. Checking activity of peroxidase

Pipette 1.0 ml DI water into a 1.5 ml glass vial

Add 100 μ l 1.0 mM H₂O₂ solution

Add 200 μ l conditioning reagent

Add 200 μ l fluorescent reagent

Close cap and mix completely

Label with date and "Peroxidase Check"

2. Checking activity of catalase

Pipette 1.0 ml DI water into a 1.5 ml glass vial

Add 100 μ l 1.0 mM H_2O_2 solution

Add 100 μ l catalase solution

Mix completely

Add 200 μ l conditioning reagent

Add 200 μ l fluorescent reagent

Close cap and mix completely

Label with date and "Catalase Check"

Appendix B. Analyses of total S(IV) and HMS in cloudwater

1. Principle of analysis

S(IV) in cloud sample is preserved as HMS. During analysis HMS is first decomposed to HCHO and free S(IV) by adding strong base, and then free S(IV) and HCHO can react with acidic pararosaniline to form a purple compound, which can be measured spectrophotometrically. A mechanism for the color compound formation is recommended by Dasgupta (1980):



It takes 14 minutes from addition of the pararosaniline to achieve optimum color development.

2. Sample preservation

Since S(IV) in cloudwater can be readily oxidized by H_2O_2 , O_3 and O_2 in the presence of transition metals, sample should be preserved as soon as possible after collection. Preservation is accomplished by adding a preserving solution containing formaldehyde, CDTA (trans-1,2-Cyclohexylene-dinitrilo-tetraacetic acid) and sodium hydroxide. The method for preparing the S(IV) preserving solution is described below. The ratio of preservation solution to cloudwater is 1:15.

The principle of preservation is that S(IV) reacts rapidly with formaldehyde to form HMS (hydroxymethanesulfonate). HMS is stable in the preserved cloudwater samples since it is not easily oxidized. HMS formed in the preserved cloudwater can then be easily decomposed to free S(IV) before analysis. CDTA in the preservative solution prevents interference of trace metals in the S(IV) analysis. A catalase solution is also added to the samples to destroy any H₂O₂ in cloudwater, since aqueous oxidation of S(IV) by H₂O₂ is a very fast reaction and could interfere with the measurements. Preserved samples should be kept at 4 °C until analysis.

3. Preparation of the solutions for S(IV)/HMSA analysis

0.125 M NaOH solution

Dissolve 0.5 g NaOH in a 100 ml flask, dilute to 100 ml with DI water

S(IV) preservative solution

Pipette 1.0 ml 0.125 M NaOH solution into a 250 ml flask. Add 0.0275 g CDTA (trans-1,2-Cyclohexylenedinitrilo-tetraacetic acid, Fluka Chemika Company) and shake the solution until all solid is completely dissolved. Add 2.125 ml commercial formaldehyde solution (37%) and dilute to 250 ml with DI water.

Catalase solution

Dissolve 200 μl commercial catalase solution (105 mg protein/ml and activity of 58000 σ/mg , Sigma Company) to 50 ml deionized water (each σ unit of catalase can destroy 1 $\mu\text{mole H}_2\text{O}_2$).

PRA reagent (Pararosaniline, $\text{C}_{19}\text{H}_{19}\text{N}_2\text{O}$)

PRA stock solution:

Dissolve 0.25 g PRA (Fluka Chemika Company) in a 250 ml flask, add 20.625 ml concentrated HCl and dilute to 250 ml with deionized water. Because the PRA solid is hard to dissolve completely, the solution should be filtered through 1.0 μm pore size Nylon membrane filter after PRA solid is dissolved as much as possible.

PRA working solution:

Take 13.2 ml PRA stock solution, add 16 ml concentrated HCl and dilute to 100 ml with DI water.

2.5 M NaOH

Dissolve 10 g NaOH in a 100 ml flask and diluted to 100 ml with DI water.

S(IV) standard solution

S(IV) stock solution (5.0 mM):

Dissolve 0.0630 g Na_2SO_3 (Fisher Scientific) in DI water, add 6.5 ml S(IV) preservative solution and then dilute to 100 ml with DI water.

S(IV) standard solutions:

Add 20 μl S(IV) stock solution to a 100 ml volumetric flask, add 6.5 ml S(IV) preservative solution and dilute to 100 ml with DI water. Repeat with 40, 100, 200, and 400 μl of S(IV) stock solution to prepare the remaining standards. The S(IV) standard concentrations are 1.0, 2.0, 5.0, 10.0 and 20.0 μM respectively.

4. Analytical procedure

Instrument set-up parameters

Turn on the Hitachi U-2000 UV/VIS spectrophotometer, set up instrument parameters as the following, and let the instrument warm up for 15 minutes before any measurements are taken.

At the main menu select photometry and then press ENTER key

1. DATA MODE: select CONC using the number key, and then ENTER

2. TEST SETUP:	Sample num.	1
	WL (nm)	580
	Initial delay (s)	0
	HI limit	9999
	LO limit	-9999
	Unite label	μM

3. CURVE TYPE: 1ST order (press number 1 and enter)

4. NUM STDS: 5

5. CURVE MODE: New (select number 1 and enter)

6. CURVE DATA:	Std	Conc. (μM)
	1	1.0
	2	2.0
	3	5.0
	4	10.0
	5	20.0

7. TEST NAME: S(IV)

8. INSTR SETUP: Baseline System
 Response Speed Medium
 Lamp Change Default number
 UV and VIS Lamp VIS on
 UV off (depending on the
 wavelength you use)
 TEXT PRINT on or off

9. SAVE PARAMS: Select a number and then enter (Total 20 methods can be saved.

Be sure not to overwrite other person's methods, you can check the TEXT MENU from the Main Menu for the files already saved)

Once all the parameters are set, press FORWARD key. Now you are ready to make a calibration curve.

Standard calibration

When measuring absorbance, put the blank reference cuvette into the back holder and sample cuvette into the front holder. Calibration curves are made by measuring the standard solutions one by one.

Pipette 0.75 ml of standards 1,2,3,4,5, each into a 1.0 cm cuvette; Add 62 μ l 2.5 N NaOH solution to each and mix completely; Add 280 μ l PRA working solution to each and mix completely; Start timer and after 14 minutes measure absorbance of each standard.

At the same time, do a DI blank sample as follows:

Pipette 0.75 ml DI water into a 1.0 ml cuvette; Add 62 μ l 2.5 N NaOH solution and mixing completely; Add 280 μ l PRA working solution and mixing completely.

Sample measurement

Pipette 0.75 ml sample into a 1.0 cm cuvette; Add 62 μ l 2.5 N NaOH solution and mixing completely; Add 280 μ l PRA working solution and mixing completely; Start timer and at 14 minutes measure absorbance.

5. Quality control

Precision and accuracy

The results of repeat measurements for total S(IV) standards and HMS standards are in the following table:

Limit of detection (LOD)

The LOD is calculated as 3 times standard deviation (σ) of the blank. LOD is 0.25 μM for total S(IV) and 0.50 μM for HMS.

Table B.1. Analysis precision and accuracy for S(IV) and HMS

Sample name	Absorbance	Measured Concentration (μM)	Standard Deviation (μM)	Relative Standard Deviation	Accuracy
S(IV) standard #2 (1.0 μM)	0.006	1.20	0.047	4.7%	23%
	0.007	1.30			
	0.006	1.20			
S(IV) standard #3 (5.0 μM)	0.029	3.42	0.20	4.0%	26%
	0.034	3.90			
	0.032	3.71			
S(IV) standard #4 (10.0 μM)	0.104	10.65	0.55	5.5%	0.6%
	0.090	9.30			
	0.096	9.88			
S(IV) standard #5 (20.0 μM)	0.215	21.36	0.80	4.0%	7.8%
	0.228	22.61			
	0.208	20.68			
S(IV) standard #6 (50.0 μM)	0.547	53.37	2.30	4.6%	5.4%
	0.508	49.61			
	0.565	55.11			

6. Discussion

Effect of formaldehyde concentration on the S(IV) analysis

Formaldehyde affects color development and the method sensitivity. Formaldehyde is one of the reactants in the mechanism which produces the purple compound which is measured by the spectrophotometer. Therefore the amount of formaldehyde in samples can influence the speed of color development. The more formaldehyde added, the faster the color develops.

On the other hand, formaldehyde can also decrease method sensitivity by the way that it competes with pararosaniline to react with free S(IV). During this process HMS is first decomposed to free S(IV) and formaldehyde, then acidic pararosaniline is added to the sample for color development. As long as the sample is acidified, formaldehyde would have a chance to react with free S(IV) to form HMS. Consequently less S(IV) would react with pararosaniline and the method sensitivity would be decreased.

Because of these two opposite effects of formaldehyde on the color development, there should be an optimum amount of formaldehyde added which enhances color development but does not speed up the reaction between S(IV) and formaldehyde so much that it decreases sensitivity. This optimum amount of formaldehyde was determined by experiment. Results showed that the maximum sensitivity can be reached between 10 and 20 mM HCHO. At this concentration it takes 12 - 14 minutes for color development (Figures B.1 and B.2). Therefore the concentration of 20 mM formaldehyde is a good compromise between color development and sensitivity.

Interference of organic materials on the S(IV) analysis

Because the S(IV) analysis is based on color measurement, background color in cloud samples could interfere with the analysis by masking the S(IV) absorption. In most cloudwater samples, background color is due to organic materials; therefore, for samples with high organic content, the colorimetric method can cause errors in S(IV) analysis. If organic amines are also present, they could compete with pararosaniline for S(IV). This would reduce the color development and result in a negative interference.

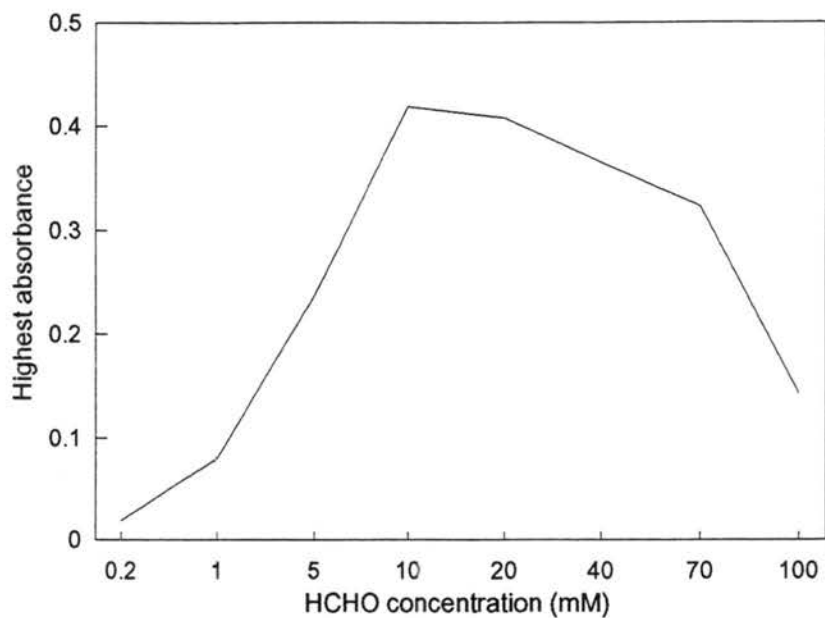


Figure B.1. Effect of formaldehyde concentration on method sensitivity

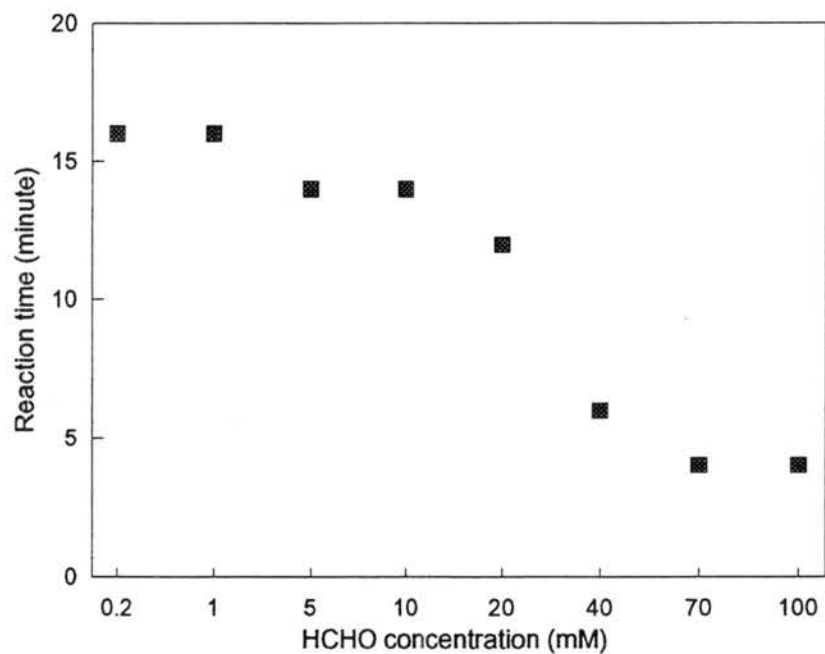


Figure B.2. Effect of formaldehyde concentration on color development.

Appendix C. Analysis of hydroperoxides in cloudwater

1. Principle of Analysis

The measurement of hydroperoxides using a fluorescence spectrophotometer measures both hydrogen peroxide and organic peroxides. Hydrogen peroxide can be reduced by a hydrogen donor molecule, such as *p*-hydroxyphenylacetic acid (POPHA), in the presence of peroxidase. A dimeric product can be formed and measured quantitatively by a fluorescence spectrophotometer (Lazrus et al., 1989). One molecular dimer is produced from one molecule of hydrogen peroxide. The hydrogen peroxide concentration in cloudwater can therefore be determined by measuring the dimer concentration. Hydrogen peroxide is very active chemically, however, requiring immediate analysis or preservation on site as soon as possible after cloudwater is taken from the collectors.

2. Sample preservation

Hydrogen peroxide in cloudwater is preserved on site by addition of *p*-hydroxyphenylacetic acid (POPHA) to form a stable dimer. The sample preservation is accomplished by adding 200 μ l conditioning reagent and 200 μ l fluorescent reagent to 1.0 ml cloudwater (or add conditioning and fluorescent reagents to cloud sample in a 1:5 ratio). The conditioning reagent contains potassium hydrogen phthalate (KHP), which acts as a buffer (pH = 5.5), and EDTA, which can also act as a buffer (pH = 5.5) and prevent interference by metal ions. Preparation of the conditioning and fluorescent reagents is as follows:

H₂O₂ conditioning reagent

7.147 g KHPthalate (Fluka)

Dissolved in 80 ml DI water and adjust to pH = 5.5 by 10 N NaOH
solution

0.028 g EDTA (Fluka)

Diluted to 100 ml with DI water

H₂O₂ fluorescent reagent

7.147 g KHPthalate (Fluka)

Dissolved in 80 ml DI water and adjust to pH = 5.5 by 10 N NaOH
solution

0.1218 g POPHA (Fluka)

0.0027 g Peroxidase (Sigma)

Diluted to 100 ml with DI water

3. Analysis procedure

Preparation of H₂O₂ stock solutions

H₂O₂ stock solution #1: Pipette 3.35 ml commercial 30% H₂O₂ solution into a clean 100 ml flask and dilute to 100 ml with DI water.

H₂O₂ stock solution #2: Pipette 500 µl of H₂O₂ stock solution #1 into a clean 100 ml flask and dilute to 100 ml with DI water.

Preparation of H₂O₂ standard solutions

Pipette 20, 50, 100, 200, 500, 1000, 2000 µl of H₂O₂ stock solution #2 into separate clean 100 ml flasks and dilute to 100 ml with DI water. Concentrations of the standard solutions are 0.34, 0.85, 1.70, 3.40, 8.50, 17.0 µM respectively.

Standard calibration and sample measurement

Turn on the Shimadzu RF-1501 spectrofluorometer power switch. After about 30 seconds warm up, turn the xenon light switch on. Select "Quantitative" mode at the main menu:

1. No. of standard	6
2. Ex wavelength (nm)	320
3. Em Wavelength (nm)	400
4. Unit	µM
5. No. of repetitions	1
6. Instrument params	
Ex band width (nm)	10
Em band width (nm)	10
Response (sec)	0.25
Sensitivity	High
Auto Shutter	ON

You can save your parameters here to one of the files. Press the Return key to go back to the "Quantitative" screen and press the F2 key to construct a calibration curve. Input

standard concentrations one by one as requested and select meas. mode. Make sure the fluorescent intensity showing up at the upper right corner of the screen is highlighted, which means that the shutter is closed. If it is not highlighted, press the Shutter key before opening the door of the sample compartment.

First, in order to re-zero instrument with reagent blank, load a clean cuvette as follows: Pipette 80 μl DI water into a 500 μl microcentrifuge vial, add 16 μl conditioning reagent, 16 μl fluorescent reagent and 16 μl 0.4 N NaOH solution, mix completely and transfer the solution to the fluorescence cuvette. Put the cuvette into the cuvette holder. Make sure that the unpolished side of the cuvette is facing toward the front of the instrument. Press the Shutter key to open the shutter door and then press the Auto Zero key to re-zero the instrument. Press the Shutter key again to close the shutter door.

Now you can construct the calibration curve with the H_2O_2 standard solutions. For each one follow the same procedure you followed for the reagent blank: 80 μl sample into a 500 μl microcentrifuge vial, add 16 μl conditioning reagent, 16 μl fluorescent reagent and 16 μl 0.4 N NaOH solution, mix completely and transfer the solution to the fluorescence cuvette. Measure the fluorescent intensity by pressing the Start key. Record the readings and the standard names in the lab notebook.

After the calibration curve is complete, press the F3 key to start sample measurements. Since the conditioning and fluorescent reagents have already been added to the cloud sample on site, you only need to add the NaOH solution before measuring: Pipette 112 μl preserved sample into cuvette, add 16 μl NaOH solution, mix it and measure fluorescent intensities as for the standard solutions. Record the readings and the sample names in the lab notebook.

4. Quality control

Analysis precision and accuracy

The results of repeat measurements of standard #3 and #5 are in the following table.

Table C.1. Analysis precision and accuracy for peroxides

Sample name	Fluorescence intensity	Measured concentration (μM)	Standard deviation (μM)	Relative standard deviation	Accuracy
Standard #3 (1.61 μM)	102	1.76			
	101	1.74			
	100	1.72			
	100	1.72			
	100	1.72			
	101	1.74			
	102	1.76			
	100	1.72			
	102	1.76			
	101	1.74	0.02	1.2%	8.1%
Standard #5 (8.05 μM)	411	8.4			
	414	8.46			
	415	8.49			
	418	8.55			
	418	8.55			
	409	8.36			
	416	8.51			
	422	8.64			
	423	8.66			
	389	7.93			
421	8.61	0.19	2.4%	5.2%	

Limit of detection (LOD)

The LOD is calculated as 3 times the standard deviation for standard #3, which is 0.06 μM .

5. Calibration of commercial H_2O_2 Solution

Principle of the calibration

H_2O_2 solution concentration can be calibrated using potassium iodide (Lodge, 1989). Hydrogen peroxide reacts with iodide to form iodine. The iodine produced reacts with iodide in solution to form I_3^- , which can be measured with the spectrophotometer. The reaction stoichiometry is as follows:



The H_2O_2 concentration in solution can be determined by the amount of I_3^- .

Solution preparation

1% KI in 0.1 M phosphate buffer:

13.6 g	KH_2PO_4 (EM Science)
58 μl	Concentrated H_3PO_4 (85%)
10.0 g	KI (Fisher Scientific)

Dilute to 1000 ml with DI water

I_3^- stock solution (5.0 mM):

3.2 g KI

0.1269 g Iodine (Fisher Scientific)

Dilute to 100 ml with DI water

Keep at room temperature for one day before use.

I_3^- standard solutions:

Pipette 50, 100, 200, 500, 1000 and 2000 μ l I_3^- stock solution into six 100 ml volumetric flasks and add 1% KI solution to the 100 ml line. The concentrations of the standard I_3^- are 2.5, 5.0, 10.0, 25, 50 and 100 μ M.

H_2O_2 stock solution #1:

3.35 ml Commercial H_2O_2 solution (~30%)

Dilute to 100 ml with DI water

H_2O_2 stock solution #2:

500 μ l H_2O_2 stock solution #1

Dilute to 100 ml with DI water

H_2O_2 calibration solution:

2.0 ml H_2O_2 stock solution #2

Add 1% KI solution to the 100 ml mark

I₃⁻ calibration curve and measurement of H₂O₂ calibration solution

Pipette 2.0 ml I₃⁻ standard solution into a cuvette and measure absorbance at 352 nm with 1% KI solution as the blank reference. Repeat for each standard. Pipette 2.0 ml H₂O₂ calibration solution and measure its absorbance and I₃⁻ concentration. Repeat the measurement three times and record the average.

Calculation of the concentration of commercial H₂O₂ solution

Nomenclature:

x: Percentage of H₂O₂ in the commercial H₂O₂ solution (%)

r: Density of the commercial H₂O₂ solution (r = 1.1)

y: Concentration of I₃⁻ in H₂O₂ calibration solution (μM)

M: Molar concentration of the commercial H₂O₂ solution (M)

N: Molar concentration of the H₂O₂ calibration solution (μM)

According to the reaction stoichiometry, one mole of H₂O₂ can produce one mole of I₃⁻.

Therefore the concentration of commercial H₂O₂ solution can be calculated as follows:

$$M = (x/100) * r * 1000/34 = 0.3235 * x$$

$$N = M * (3.35/100) * (0.5/100) * (2/100)$$

$$= 0.3235 * x * (3.35/100) * (0.5/100) * (2/100)$$

$$= 1.084 * x \text{ (}\mu\text{M)}$$

Since: N = y and y is known by measurement

Therefore: $1.084 * x = y$

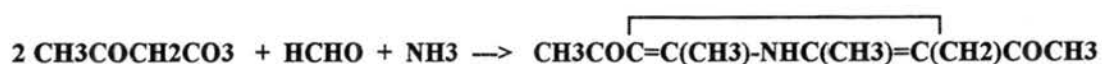
$$x = y/1.084$$

Appendix D. Analysis of formaldehyde in cloudwater

1. Principle of analysis

In the presence of small amounts of formaldehyde, 2,4-pentanedione and ammonia can react with formaldehyde quantitatively to form a fluorescent product

diacetyldihydrolutidine (DDL)



DDL can be measured with a fluorescence spectrophotometer. Since the amount of DDL produced equals the amount of formaldehyde present in solution (provided 2,4-pentanedione and ammonia are in excess) the formaldehyde concentration can be determined from the amount of DDL (Dong and Dasgupta, 1987).

2. Sample preservation

Formaldehyde can form a stable compound, HMS, in the presence of bisulfite. HMS can later be decomposed to formaldehyde to be analyzed. A formaldehyde preservation solution containing bisulfite is added on site. The volume ratio of preservation to sample is 1:10. Preparation of the HCHO preservation solution is as follows:

HCHO preservative solution (20 mM NaOH, 10 mM CDTA, 3 mM NaHSO₃)

0.08 g	NaOH
0.3644 g	CDTA (Fluka Scientific)

0.0294 g NaHSO₃ (Sigma Chemical Co.)

Dilute to 100 ml with DI water

The solution pH should be measured to ensure that it is approximately 4.8.

3. Analysis procedure

Solution preparation

HCHO stock solution (0.0206 M)

0.2765 g NaHMS (Aldrich)

10 ml HCHO preservation solution

Dilute to 100 ml with DI water

HCHO standard solution

Pipette 10, 20, 50, 100 and 200 μ l HCHO stock solution into five 100 ml flasks. Add 10 ml HCHO preservation solution and dilute to 100 ml with DI water. The standard concentrations are 2.06, 4.12, 10.30, 20.60 and 41.20 μ M.

HCHO reaction reagent (2.0 M NH₄Ac, 0.05 M Acetic Acid, 0.02 M

2,4-pentanedione)

15.418 g NH₄Ac (EM Science)

300 μ l Acetic Acid (Aldrich Chemical)

200 μ l 2,4-pentanedione (Aldrich Chemical)

Dilute to 100 ml with DI water

Na₄EDTA/NaOH solution (0.05 M Na₄EDTA, 0.1 M NaOH)

2.2612 g Na₄EDTA·4H₂O (Fluka)

0.4 g NaOH

Dilute to 100 ml with DI water

5.0 mM H₂O₂ solution

30 μl Commercial H₂O₂ solution (~30%)

Dilute to 100 ml with DI water

Set up instrument parameters

Turn on the Shimadzu RF-1501 spectrofluorophotometer power switch. After about 30 seconds warm up, turn the xenon light switch on. After the instrument self-checking is completed, select QUANTITATIVE mode at the main menu and input the following parameters:

No. of standard	5
Ex wavelength (nm)	412
Em Wavelength (nm)	510
Unit	μM
No. of repetitions	1
Instrument params	
Ex band width (nm)	10
Em band width (nm)	10

Response (sec)	0.25
Sensitivity	High
Auto Shutter	ON

Save your parameters to one of the file banks, then press the Return key to retain to the Quantitative screen and press the F2 key to do a calibration curve. Input standard concentrations one by one as requested and select meas. mode. Make sure the fluorescence intensity showing up at the upper right corner of the screen is highlighted, which means that the shutter is closed. If it is not highlighted, press the Shutter key before opening the door of the sample compartment. Now the instrument is ready to start the calibration.

Sample pre-treatment and measurement for standard solution and cloudwater

In order to re-zero the instrument with DI water and reagent blank, measure a DI blank first. Pipette 70 μl DI water into a 0.5 ml microcentrifuge vial, add 20 μl 5 mM H_2O_2 solution, 20 μl Na_4EDTA solution and 70 μl HCHO reaction reagent. Heat the solution at 80°C for exactly 2 minutes with the Temp-Blok Heater, then cool it at room temperature for exactly 8 minutes. Pipette 150 μl of the solution into the black fluorescence micro-cuvette and put the cuvette into the cuvette holder. Make sure that the unpolished side of the cuvette is facing the front of the instrument. Press the Shutter key (i.e. open the shutter door) and then press the Auto Zero key to re-zero the instrument. Press the Shutter key again to close the shutter door.

Now construct the calibration curve with the standard solutions, using the same steps given above for the DI water. Measure the fluorescence intensity by press the Start key. After the calibration curve is finished, press the F3 key to start sample measurements.

4. Analysis quality control

Precision and Accuracy

The results of repeat measurements of standard #2 and #4 are in Table D.1.

Limit of detection (LOD)

The LOD is determined as three times the standard deviation for DI blank, which is 0.4 μM .

Table D.1. Analysis precision and accuracy for formaldehyde

Sample name	Fluorescence intensity	Measured concentration (μM)	Standard deviation (μM)	Relative standard deviation	Accuracy
Standard #2 (4.12 μM)	41	4.26	0.5	12%	1.2%
	42	4.37			
	49	5.11			
	44	4.58			
	34	3.53			
	39	4.05			
	36	3.74			
	34	3.53			
	45	4.69			
	37	3.84			
Standard #4 (20.68 μM)	204	21.41	1.13	5.5%	11%
	213	22.36			
	227	23.83			
	231	24.24			

Appendix E. Analyses of Fe(II) and Fe(III) in cloudwater

1. Principle of Analysis

Dissolved Fe(II) and Fe(III) can both react with a chelating reagent, di-2-pyridyl ketone benzoylhydrazone (DPKBH). The complexed form of Fe(II), Fe(II)-DPKBH, has two absorption peaks at 377 nm and 660 nm, respectively, whereas the Fe(III)-DPKBH complex only has one absorption peak at 377 nm. Fe(II) can be quantified from its absorption at 660 nm and total Fe can be determined from the absorption at 377 nm. Therefore Fe(III) can be obtained by subtracting the amount Fe(II) from the total Fe (Pehkonen and Hoffmann, 1992).

The two oxidation states of Fe are interchangeable in cloudwater. Dynamic equilibrium between Fe(II) and Fe(III) depends on cloud conditions, for example types of oxidants present in cloudwater and solar irradiation intensity. Therefore Fe(II) and Fe(III) concentrations should be analyzed as quickly as possible after cloudwater is taken from collectors and should be finished within minutes.

2. Analysis procedure

Solution preparation

21 mM DPKBH solution: Dissolve 0.152 g DPKBH (synthesized in laboratory) into 25 ml ethanol.

4.2% NH₄AC buffer solution: Dissolve 4.2 g NH₄AC (EM Science) into 100 ml DI water.

1.0 M H_2SO_4 : Pipette 5.50 ml concentrated H_2SO_4 into a 100 ml flask and dilute to 100 ml with DI water.

Fe(II) stock solution #1:

Weigh 0.1961 g $\text{Fe}(\text{NH}_4)_2(\text{SO}_4)_2 \cdot 6\text{H}_2\text{O}$ (Department of Chemistry at CSU) into a 100 ml flask, add 80 ml DI water, adjust the solution pH to 2.0 with 1.0 M H_2SO_4 (~500 μl), dilute to 100 ml with DI water. For this solution and those immediately following, you want a final pH close to 2 to avoid precipitate formation. The amount of acid required here will suffice for adjusting pH of solutions below.

Fe(II) stock solution #2:

Pipette 5.0 ml Fe(II) stock solution #1 into a 100 ml flask, add 1.0 M H_2SO_4 to adjust solution pH to 2.0, dilute to 100 ml with DI water.

Fe(II) standard solutions:

Pipette 80, 200, 400, 800, 2000, 4000 μl Fe(II) stock solution #2 into six 100 ml flasks, add 1.0 M H_2SO_4 to adjust solution pH to 2.0 and dilute to 100 ml with DI water. Concentrations of the Fe(II) standard solutions are 0.2, 0.5, 1.0, 2.0, 5.0, 10.0 μM .

Fe(III) stock solution #1 (5.00 mM):

Weigh 0.1352 g $\text{FeCl}_3 \cdot 6\text{H}_2\text{O}$ (Mallinckrodt Specialty Chemicals Co, available at Dept. of Chem. at CSU) into a 100 ml flask, add 1.0 M H_2SO_4 to adjust solution pH to 2.0 and dilute to 100 ml with DI water.

Fe(III) stock solution #2 (0.25 mM):

Pipette 5.0 ml Fe(III) stock solution #1 into a 100 ml flask, add 1.0 M H₂SO₄ to adjust solution pH to 2.0 and dilute to 100 ml with DI water.

Fe(III) standard solutions:

Pipette 80, 200, 400, 800, 2000, 4000 µl Fe(III) stock solution #2 into six 100 ml flasks, add 1.0 M H₂SO₄ to adjust solution pH to 2.0 and dilute to 100 ml with DI water.

Concentrations of the Fe(III) standard solutions are 0.2, 0.5, 1.0, 2.0, 5.0, 10.0 µM.

Fe(II) standard calibration and sample measurement at 377 nm and 660 nm

Set up instrument parameters

Turn on the Hitachi U-2000 UV/VIS spectrophotometer, set up instrument parameters as follows, and let the instrument warm up for 15 minutes before any measurements are taken.

At the main menu select photometry and then press ENTER key

- | | |
|----------------|--|
| 1. DATA MODE: | select <u>ABS</u> using the number key, and then ENTER |
| 2. TEST SETUP: | Sample num. 1 |
| | WL (nm) 377 |
| | Initial delay (s) 0 |
| | HI limit 9999 |
| | LO limit -9999 |
| | Unite label µM |

- | | | |
|----------------|--------------------------------------|-------------------------|
| 3. CURVE TYPE | 1ST order (press number 1 and enter) | |
| 4. NUM STDS | 6 | |
| 5. CURVE MODE | New (select number 1 and enter) | |
| 6. CURVE DATA | Std | Conc. (μM) |
| | 1 | 0.2 |
| | 2 | 0.5 |
| | 3 | 1.0 |
| | 4 | 2.0 |
| | 5 | 5.0 |
| | 6 | 10.0 |
| 7. TEXT NAME | Fe(II) | |
| 8. INSTR SETUP | Baseline | System |
| | Response Speed | Medium |
| | Lamp Change | 340 nm |
| | VIS lamp | On |
| | UV | Off |
| | TEXT PRINT | On or Off |
| 9. SAVE PARAMS | Select a number and then enter | |

Once all the parameters are set, press the FORWARD key. Now you are ready to make a calibration curve.

Standard calibration and sample measurement

Pipette 120 μl ethanol into a 0.5 ml microcentrifuge vial, add 120 μl DI water, add 45 μl 21 mM DPKBH and 15 μl 4.2% NH_4Ac buffer solution. Mix the solution completely. Load DI blank into the 100 μL fluorescence quartz cuvette and put the cuvette into the back cuvette holder. Pipette 120 μl ethanol into a 0.5 ml microcentrifuge vial, add 120 μl standard solution, add 45 μl 21 mM DPKBH and 15 μl 4.2% NH_4Ac buffer solution. Mix the solution completely. Load the standard solution into the 50 μL UV/Vis quartz cuvette and put the cuvette into the front cuvette holder. Press the START key to measure absorbance at 377 nm and then press GO to λ key to change wavelength to 660 nm and measure absorbance again. Record the two absorbance readings at the two wavelengths.

NOTE: You must prepare separate calibration curves at 377 and 660 nm for Fe(II). Use the 660 nm curve to determine the sample Fe(II) concentration, then use the "inverted" 377 nm curve to transform the Fe(II) sample concentration into its absorbance at 377 nm (to subtract from total absorbance at 377 nm). It is easier to construct two calibration curves in Lotus 123 than to go through two calibrations on the spectrophotometer.

Fe(III) standard calibration and sample measurement

The instrument parameters are the same as for Fe(II) measurement except for measuring only at one wavelength 377 nm.

The Fe(III) concentration is determined subtracting the total absorbance at 377 nm from the absorbance from Fe(II) at 377 nm [determined as noted in NOTE above] using the Fe(III) calibration curve at 377 nm.

3. DPKBH Synthesis (Zatar et al., 1989; Garcia-Vargas et al., 1986)

Synthesis

Weight 0.921 g (0.005 mole) di-2-pyridyl ketone (Aldrich) and 0.6808 g (0.005 mole) benzoic hydrazide (Aldrich) into a 250 ml round flask, add 50 ml ethanol, add 50 μ l concentrated HCl and reflux for 60 minutes in a boiling water bath. The equipment set up is in Figure E.1.

Crystallization

After refluxing is complete, cool the solution at room temperature, add 150 ml DI water (the volume ratio of ethanol to DI water is 1:3), adjust solution pH to ~5.0 with several drops of 10 M NaOH. There will be white precipitation (DPKBH) coming out. Collect the precipitation with a Buchner funnel.

Re-crystallization

Transfer the precipitation into a 300 ml clean beaker. Add 200 ml ethanol-water solution (the volume ratio of ethanol to DI water is 1:3) and heat the solution until the

precipitation dissolve completely. Cool the solution at room temperature. Wait until DPKBH precipitate as complete as possible. Collect the crystal with a Buchner funnel.

Re-crystallize the crystal three times following the same procedure. Measure the melting point. The melting point range (onset and finish of melting) should be within 136-138 °C (literature value is 130-132° C, but we never get the same result).

Melting point measurement (Thiele tube technique)

Introduce crystal into a capillary tube. Invert the capillary tube and drop it through plastic tube from a height of 25 cm to "move" sample to bottom of capillary tube. Repeat until 2 mm of sample are in bottom of capillary tube.

Clamp Thiele tube to stand in fume hood. Fill Thiele tube with concentrated sulfuric acid to a height of 2 cm above upper opening. Suspend (with string or small clamp) thermometer in the Thiele tube so that center of metal thermometer tip is located at a height equal to center of upper Thiele tube opening. Lift thermometer and "attach" capillary to its side so that bottom of capillary is at the bottom of the thermometer tip (capillary will stick to wet thermometer). Put thermometer back into position in Thiele tube.

Using Bunsen burner, heat outer bend in Thiele tube arm until thermometer reading approaches desired melting value. Slow heating and watch for crystal to start melting (if you heat too fast past the melting point, you will not get an accurate reading for the melting point). Record temperature at which melting begins and temperature at which melting ends (a good heating rate will move from the start to the end of melting in approximately 5 seconds).

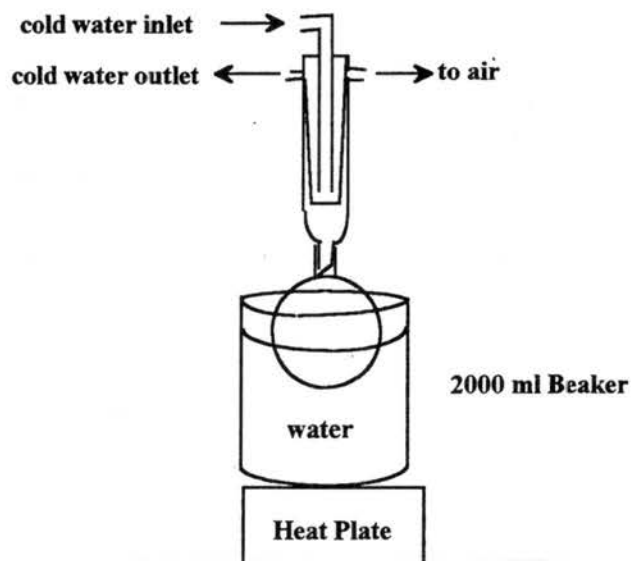


Figure E.1. Equipment set-up for DPKBH synthesis

Appendix F. Mass transport consideration for formaldehyde gas-liquid equilibrium

While equilibrium aqueous-phase concentrations of some gaseous species are affected by solution pH, variations in drop acidity across the drop size spectrum should not affect equilibrium formaldehyde concentrations. If equilibrium is not attained across the gas-water interface, however, differences in formaldehyde concentrations might occur as a function of drop size. The rates of several processes must be considered to determine whether the cloud drops are likely to attain equilibrium with gaseous formaldehyde. These include the rate of formaldehyde mass transport into the drop and the rates of chemical reaction (hydration and complexation) of formaldehyde within the drop. In addition, if the cloud drop is growing by condensation, the rate of growth is also important. In our samples, most of the formaldehyde in solution is not complexed as HMS, therefore we will ignore this process in considering rates of key steps affecting formaldehyde concentrations. Rates of the other processes have been studied as functions of drop size (Schwartz, 1986; Ogren, 1992; Bell, 1966). By comparing the rate of mass transfer with the rates of hydration and drop growth, we can determine whether aqueous formaldehyde concentrations should be in equilibrium with gaseous formaldehyde or whether they will be limited by the rate of mass transfer from the gas phase.

Mass transport of formaldehyde into the drop consists of three processes: gaseous diffusion to the drop surface, interfacial mass transport and aqueous diffusion throughout the drop. Expressions for the timescales of these processes are listed in Table F.1.

Table F.1. Characteristic times for droplet growth, formaldehyde mass transport and chemical reaction

Process	Characteristic time	Reference
Gas-phase diffusion	$\tau_{d,g} = \frac{r_d^2}{3D_g}$	(Schwartz, 1986)
Interfacial mass transport	$\tau_i = \frac{4r_d}{3v\alpha}$	(Schwartz, 1986)
Aqueous diffusion	$\tau_{d,a} = \frac{r_d^2}{\pi^2 D_a}$	(Schwartz, 1986)
Droplet growth	$\tau_{grow.} = \frac{\rho_w r_d^2}{3(n_w - n_{rw})q_w D_w}$	(Ogren and Charlson, 1992)
Hydration	$\tau_{hydr.} = \frac{1}{2000(k_0 + k_H[H^+] + k_{OH}[OH^-])}$	(Bell, 1966)

Nomenclature:

- α accommodation coefficient
- D_a aqueous diffusion coefficient
- D_g gas-phase diffusion coefficient
- D_w gas-phase diffusion coefficient of water molecule
- k_H acidic hydration constant
- k_0 neutral hydration constant of HCHO
- k_{OH} basic hydration constant
- n_{rw} gas-phase water molecule number concentration at droplet surface
- n_w gas-phase water molecule number concentration far from droplet
- q_w mass of a water molecule
- r_d droplet radius
- ρ_w density of water droplet
- v average molecular speed

A comparison among the timescales for the three mass transfer steps, drop growth and formaldehyde hydration is depicted in Figure F.1 as a function of drop size. For typical fog or cloud drops aqueous phase diffusion is likely to be the slowest portion of the mass transport. However, it is still much faster than rates of condensational drop growth, suggesting that formaldehyde transfer from the gas phase is fast enough to respond to aqueous phase formaldehyde dilution resulting from drop growth.

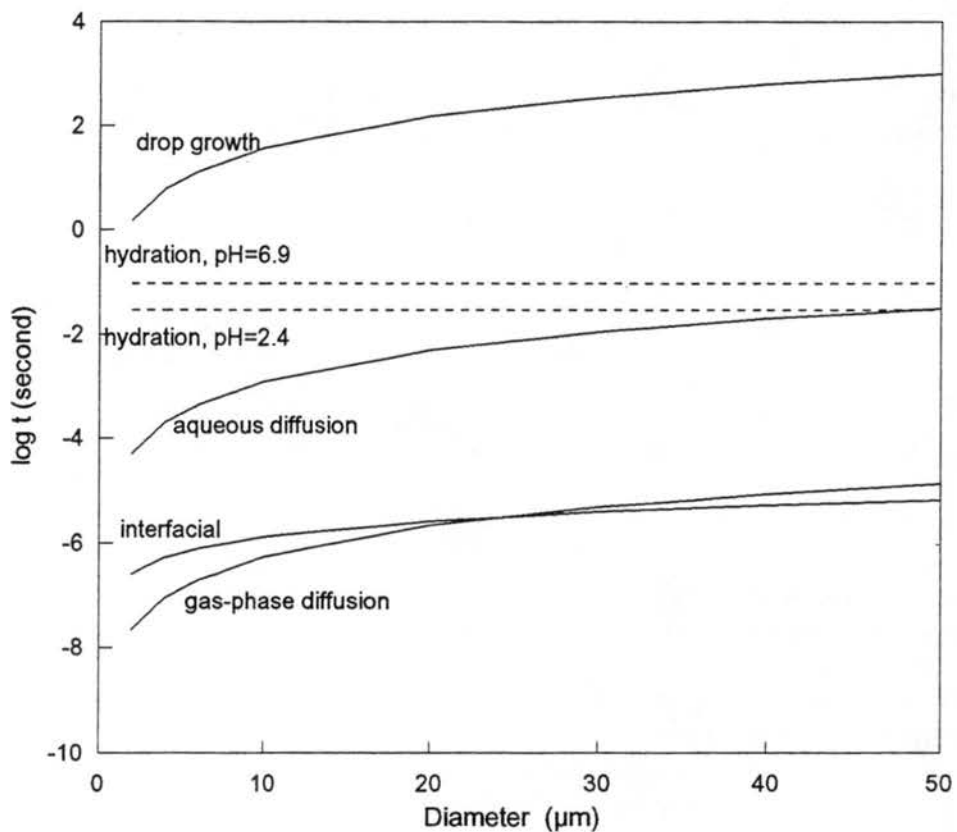


Figure F.1. A comparison of the characteristic times of droplet growth and formaldehyde hydration with those for formaldehyde mass transport processes. The calculations are based on the equations in Table F.1. Values of the constants in the equations are taken from the references cited in Table F.1. Hydration timescales are included for pH values of 2.4 and 6.9, representing the extreme pH values measured in the samples collected in this study.

The rate of formaldehyde mass transport into the drop must also be compared to the hydration rate to determine whether rapid hydration of formaldehyde can prevent attainment of gas-liquid equilibrium for some drop sizes. The characteristic time of HCHO hydration is a function of cloud pH (Table F.1). Since cloud pH generally varies with drop size (see Table 3.1 and Collett et al., 1994), the hydration characteristic time is probably an indirect function of drop size. Investigation of this relationship reveals a weak dependence on drop pH. Timescales for hydration at pH values of 2.4 and 6.9 (the extremes represented by the samples in our data set) are depicted in Figure F.1. The characteristic time for hydration is an order of magnitude longer than the characteristic time for mass transport in small drops (see Figure F.1). For large drops the mass transport timescale is still shorter than the hydration timescale except for very large, acidic drops where the timescales are similar. Apparently hydration occurs over a long enough timescale that mass transport of formaldehyde into the droplet should be capable of maintaining the aqueous formaldehyde concentration at equilibrium with respect to the gas phase.

Since mass transport of formaldehyde into cloud drops is faster than drop growth or chemical reaction of formaldehyde in the drops, we expect that aqueous formaldehyde concentrations should be in equilibrium with gaseous formaldehyde concentrations. Consequently, it is difficult to explain why formaldehyde concentrations are observed to vary as a function of drop size in the cases discussed here. Simultaneous measurements of formaldehyde concentrations in the drops and in the atmosphere are needed to test which, if any, of the drop sizes are truly at gas-liquid equilibrium. Investigation of other products of formaldehyde reaction in the drops might also be useful for explaining the drop

Appendix G. Calculation of liquid-water-content weighted average chemical composition

Nomenclature:

V_1 Volume of small drop fraction

V_2 Volume of large drop fraction

$[x]_1$ Chemical equivalent concentration of small drops

$[x]_2$ Chemical equivalent concentration of large drops

$[x]_{Avg}$ Average chemical equivalent concentration of small and large drops

K_w Ion product of water

If a chemical species is conservative the liquid-water- content weighted average concentration of small and large drops is calculated as (Equation (G.1))

$$[x]_{Avg} = \frac{[x]_1 V_1 + [x]_2 V_2}{V_1 + V_2} \quad (G.1)$$

The average concentrations of trace metals and H_2O_2 in section 3.4 are calculated based on Equation (G.1).

Hydrogen ion is not a conservative chemical species. The H^+ in one drop fraction may be buffered by the OH^- and/or other buffering compounds in the other fraction upon mixing. For the calculations in section 3.4 only the OH^- buffering effect was considered and it was assumed that no other buffering compounds are present.

Calculations of liquid-water-content weighted average H^+ are based on the charge balances in small, large and mixed bulk water (Equations (G.2) - (G.4))

$$[H^+]_1 + [Cations]_1 = [OH^-]_1 + [Anions]_1 \quad (G.2)$$

$$[H^+]_2 + [Cations]_2 = [OH^-]_2 + [Anions]_2 \quad (G.3)$$

$$[H^+]_{Avg} + [Cations]_{Avg} = [OH^-]_{Avg} + [Anions]_{Avg} \quad (G.4)$$

It is assumed that cations and anions other than H^+ and OH^- are conservative upon mixing, therefore average concentrations of the cations and anions are

$$[Cations]_{Avg} = \frac{[Cations]_1 V_1 + [Cations]_2 V_2}{V_1 + V_2} \quad (G.5)$$

$$[Anions]_{Avg} = \frac{[Anions]_1 V_1 + [Anions]_2 V_2}{V_1 + V_2} \quad (G.6)$$

or, equivalently,

$$[Cations]_{Avg} = \left(\frac{V_1}{V_1 + V_2}\right)[Cations]_1 + \left(\frac{V_2}{V_1 + V_2}\right)[Cations]_2 \quad (G.7)$$

$$[Anions]_{Avg} = \left(\frac{V_1}{V_1 + V_2}\right)[Anions]_1 + \left(\frac{V_2}{V_1 + V_2}\right)[Anions]_2 \quad (G.8)$$

Substituting Equations (G.7), (G.8) and the ion product of water into Equation (G.4) gives

$$[H^+]_{Avg} + \left(\frac{V_1}{V_1 + V_2}\right)[Cations]_1 + \left(\frac{V_2}{V_1 + V_2}\right)[Cations]_2 = \frac{K_w}{[H^+]_{Avg}} + \left(\frac{V_1}{V_1 + V_2}\right)[Anions]_1 + \left(\frac{V_2}{V_1 + V_2}\right)[Anions]_2 \quad (G.9)$$

Substituting Equations (G.2) and (G.3) into Equation (G.9) and rearranging gives

$$[H^+]_{Avg} - \frac{K_w}{[H^+]_{Avg}} = \left(\frac{V_1}{V_1+V_2}\right)\left([H^+]_1 - \frac{K_w}{[H^+]_1}\right) + \left(\frac{V_2}{V_1+V_2}\right)\left([H^+]_2 - \frac{K_w}{[H^+]_2}\right) \quad (G.10)$$

The average H^+ concentration, as a function of H^+ concentrations in small and large drop fractions, can be obtained by solving this second order equation.